GEOLOGICA ULTRAIECTINA

Mededelingen van de
Faculteit Aardwetenschappen
Universiteit Utrecht

No. 158

Sulphur geochemistry and sapropel formation

Syngenetic and diagenetic signals in eastern Mediterranean sediments

Hilde F. Passier

Sulphur geochemistry and sapropel formation

Syngenetic and diagenetic signals
in eastern Mediterranean sediments

Zwavelgeochemie en sapropeelvorming—syngenetische en diagenetische
signalen in sedimenten in de oostelijke Middellandse Zee

(met een samenvatting in het Nederlands)

PROEFSCHRIFT

TER VERKRIJGING VAN DE GRAAD VAN DOCTOR
AAN DE UNIVERSITEIT UTRECHT
OP GEZAG VAN DE RECTOR MAGNIFICUS, PROF. DR. H.O. VOORMA
INGEVOLGE HET BESLUIT VAN HET COLLEGE VAN DECANEN
IN HET OPENBAAR TE VERDEDIGEN
OP DONDERDAG 19 FEBRUARI 1998 DES MIDDAGS TE 14.30 UUR

DOOR

HILDE FRANÇOISE PASSIER

geboren op 18 februari 1971, te Bergen op Zoom

Promotor: Prof. Dr. C.H. van der Weijden
               Department of Geochemistry, Utrecht University,
               Utrecht, The Netherlands
Co-promotor: Dr. G.J. de Lange
               Department of Geochemistry, Utrecht University,
               Utrecht, The Netherlands

The wrecks dissolve above us; their dust drops down from afar –
Down to the dark, to the utter dark, where the blind white sea-snakes are.

(The Deep-Sea Cables, R. Kipling)

Voor Jeanne en Frans

Contents

Chapter 1

Introduction and summary

1.1 The modern Mediterranean Sea

The Mediterranean Sea (Fig. 1.1) is enclosed by the Eurasian and African continents, and it is connected with the Atlantic Ocean via the Strait of Gibraltar. The basin is divided into an eastern and a western basin by the sill in the Strait of Sicily. At present, evaporation exceeds precipitation and river runoff, whereby surface waters become denser and more saline. The negative water balance is compensated by the inflow of Atlantic waters at the surface. In the east, the surface water salinities have increased to such an extent, that the denser water is convected to greater depths. The dense saline deep waters flow out of the basin over the Sill of Gibraltar, resulting in the present-day anti-estuarine circulation pattern. The import of nutrient-depleted Atlantic surface waters and the export of nutrients in the saline deep water cause the eastern Mediterranean basin to be a nutrient-desert with low production of organic matter (OM) in the surface waters (e.g. Sarmiento et al., 1988; Béthoux, 1989).
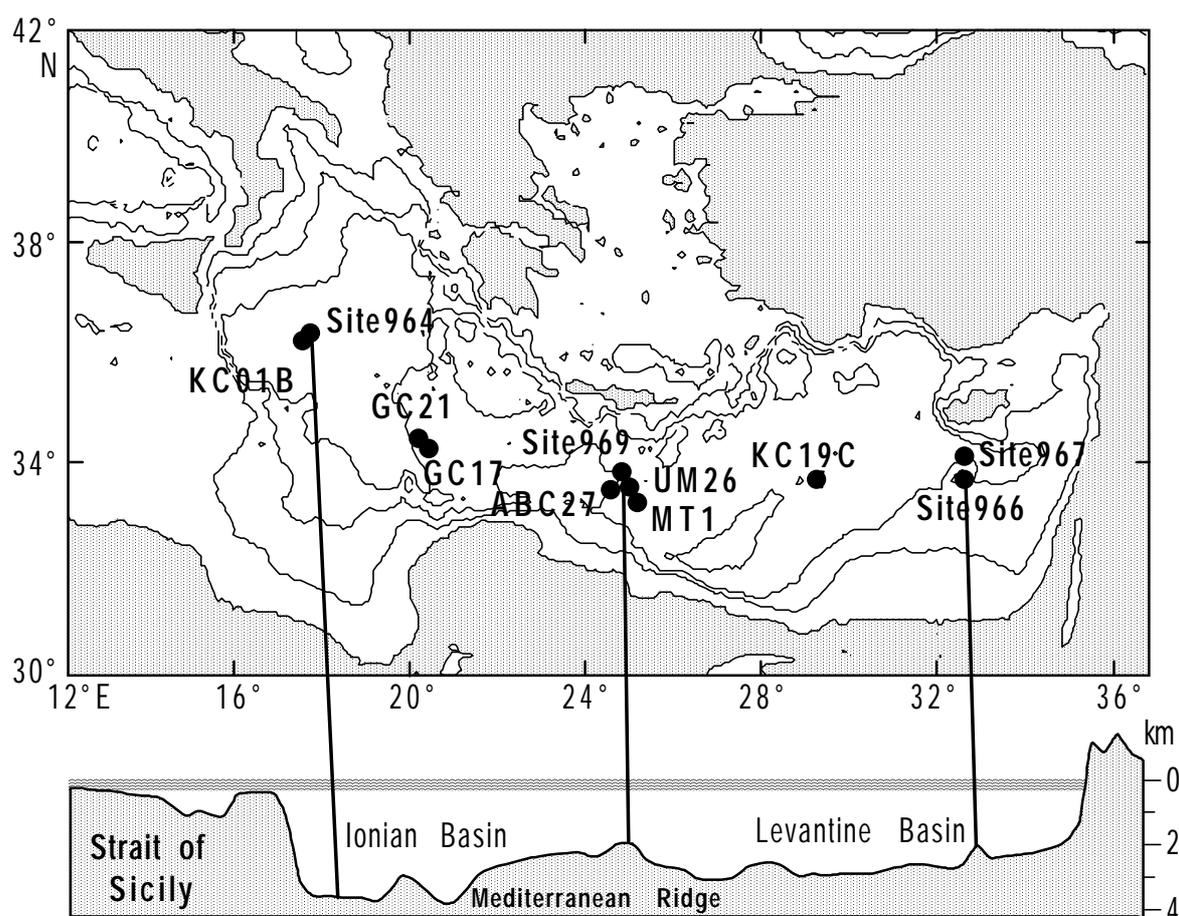

Figure 1.1 *Coring locations in the eastern Mediterranean Sea.*

1.2 Sapropels in the eastern Mediterranean

Presently deposited sediments at hemipelagic sites in the eastern Mediterranean contain less than half a weight percent of organic carbon, whereas the Neogene eastern Mediterranean sedimentary record is characterized by the cyclic occurrence of dark, distinct sediment layers with organic carbon contents ranging from a few to almost 30 weight percent. These organic-rich layers, called sapropels, are centimetres to decimetres thick, and they are embedded in light brown to grey hemipelagic sediments. The origin of sapropels is thought to be related to paleoclimatic changes in the Mediterranean area. They formed during humid climatic conditions at times of maximum Northern Hemisphere insolation by the Sun. The variations in insolation are mainly controlled by the precession cycle of the Earth's orbit, which has a period of about 21 thousand years (e.g. Hilgen, 1991; Lourens et al., 1992). The formation of sapropels has been widely discussed during the last decades. Their formation is thought to have been initiated by increased production of OM in the surface water that led to higher settling rates of OM on the seafloor and/or by enhanced OM preservation due to oxygen depletion in the bottomwaters. During insolation maxima, increased precipitation caused an elevated input of freshwater and nutrients to the eastern Mediterranean from the African and Eurasian continents. The additional input of nutrients increased the production of OM in the surface waters of the eastern Mediterranean. In addition, the input of freshwater and the overall change of the weather caused changes in the circulation pattern and anatomy of the water column in the eastern Mediterranean which probably influenced both the preservation and production of OM. One theory is that circulation in the basin became more sluggish resulting in anoxia and consequently enhancing preservation of OM on the seafloor. Another is that a change of the circulation pattern in the eastern Mediterranean basin caused upwelling of nutrient-rich waters and resulted in increased production. In addition, the input of freshwater may have resulted in the shoaling of the pycnocline, causing mixing of nutrients into the photic zone, which generated increased production of OM (e.g. Olausson, 1961; Rossignol-Strick et al., 1982; Rossignol-Strick et al., 1985; Rohling and Gieskes, 1989; Calvert et al., 1992).

1.3 A unique sediment alternation

The existence of sapropels is related to increased accumulation of OM on the bottom of the eastern Mediterranean. The accumulation of OM in marine sediments is closely related to early diagenetic processes. The most important of these processes is the decomposition of OM by bacteria, using a series of oxidants (oxygen, nitrate, manganese and iron (hydr)oxides, sulphate) (e.g. Froelich et al., 1979). In most organic-rich sediments, oxygen and nitrate are consumed by bacteria in the uppermost millimetres of the sediment. Deeper in the sediment other oxidants are used for the decomposition of OM. This consumption of oxidants results in the development of several redox zones in the sediment. Usually, sediments are progressively more reducing with depth, with a downward succession of oxic, suboxic and anoxic sediments. The sequence of alternating sapropels and organic-poor sediment layers in the eastern Mediterranean, however, provides a unique setting to study the diagenetic interactions between (anoxic) organic-rich layers on top of (sub)oxic organic-poor sediments and vice versa.

1.4 Sulphur in organic-rich sediments

One of the most important diagenetic processes in organic-rich marine sediments is decomposition of OM in bacterial sulphate reduction (e.g. Canfield, 1989; Mossmann et al., 1991; Calvert and Karlin, 1991). Bacterial sulphate reduction produces bisulphide (HS^-). Bisulphide can be partially oxidized or can react with OM and reactive metal species (e.g. Berner, 1984; Luther and Church, 1992). All these reactions may be bacterially mediated. The reaction of reduced sulphur with reactive dissolved iron and iron minerals, if available, results in the formation of iron sulphides. The most common iron sulphide is pyrite (FeS_2). The biogeochemical sulphur cycle is important for long-term control on oxygen and carbondioxide levels in the atmosphere. Pyrite burial and oxidation link the biogeochemical cycles of oxygen, carbon and sulphur, and these processes are, next to the burial and oxidation of OM, the most important processes in controlling the oxygen levels in the atmosphere (e.g. Berner and Canfield, 1989). Consequently, the sedimentary sulphur processes, especially pyrite formation, have been extensively studied. The properties of pyrite depend on its formation history, which is in turn closely related to the formation history of the sediments itself. The amount of pyrite formation in marine sediments is largely determined by the availability of sulphate, reactive iron and reactive OM during formation of the sediments (Berner, 1984). In addition, the specific microtexture of pyrite in marine sediments (either framboidal or euhedral; e.g. Sweeney and Kaplan, 1973; Raiswell, 1982; Wang and Morse, 1996; Wilkin and Barnes, 1996) and the isotopic composition of sulphur in pyrite (e.g. Goldhaber and Kaplan, 1974; Chambers and Trudinger, 1979; Raiswell, 1982; Canfield and Thamdrup, 1994) may reveal the environmental conditions during pyrite formation.

1.5 This thesis

In this thesis the sulphur geochemistry of eastern Mediterranean sediments is studied. The sediments discussed were recovered during the 1987 *ABC* cruise with R/V *Tyro* (core ABC27), the 1988 *BAMO-3* expedition of R/V *Bannock* (cores GC17 and GC21), the 1991 *Marflux* cruise with R/V *Marion Dufresne* (cores KC01B and KC19C), the 1993 *Marflux* cruise with R/V *Tyro* (core MT1), the 1994 *Palaeoflux* cruise with R/V *Urania* (core UM26) and ODP Leg 160 in 1995 (Sites 964, 966, 967, and 969) (Fig. 1.1).

Chapter 2 deals with the most eye-catching feature in the sedimentary sulphur chemistry around sapropels: apart from enrichments of solid phase sulphur and iron within sapropels, sulphur and iron are also enriched in a zone of decimetres thickness, directly below each organic-rich layer, where organic carbon is not enriched. The sulphur and iron enrichments reflect the presence of abundant pyrite (FeS_2). Stable sulphur isotopic compositions of bulk sediments show that the reduced sulphur within as well as below sapropels formed through bacterial sulphate reduction at or close to the sediment surface, i.e. during or shortly after sapropel deposition. Pyrite formation within the sapropels was iron-limited and consequently, bisulphide was able to migrate downwards. This resulted in pyrite formation below each sapropel by reaction of bisulphide with solid phase reactive iron and upward diffusing dissolved Fe(II). This downward sulphidisation mechanism allowed burial of twice as much sulphur in alternating organic-rich-

anoxic / organic-poor-suboxic sediments compared to homogeneous organic-rich-anoxic sediments.

In Chapter 3 the speciation of sulphur and contents of reactive iron in sediments with sapropels are discussed in detail. Pyrite is the dominant sulphur species within and immediately below each sapropel. Directly above sapropels, sulphur is hardly present in the solid phase, but occurs as porewater sulphate. Large scale formation of organic sulphur compounds occurred only in the most organic-rich sapropel that was investigated (maximum organic carbon content = 23.5 wt%). The presence of iron sulphides other than pyrite indicate that sulphate reduction probably still continues in this exceptionally organic-rich sapropel, whereas in other sapropels no sulphate reduction occurs at present.

Chapters 4 and 5 investigate detailed pyrite properties within and below sapropels, in order to gain further insight into the formation of pyrite and sapropels. The pyrite characteristics (contents, microtextures and isotopic compositions) were gouverned by the relative rates of bisulphide production and iron liberation and supply in the sapropels. These rates were both temporally and laterally variable during sapropel deposition. At times of relatively high sulphate reduction, bisulphide escaped from the sapropel and pyrite was formed in the underlying sediments. The sources of iron for pyrite formation comprised detrital reactive solid phase iron and diagenetically liberated dissolved $Fe(II)$ from sapropel-underlying sediments. In exceptionally organic-rich sapropels, input of dissolved $Fe(II)$ from the water column via iron sulphide formation in the water may have been important. Rapid pyrite formation at high saturation levels of iron and bisulphide resulted in the formation of framboidal pyrite within the sapropels, whereas directly below each sapropel slow euhedral pyrite formation at low saturation levels occurred. Stable sulphur isotopes in pyrite in sapropels are strongly enriched in the light sulphur isotope ^{32}S. Below the sapropels, sulphur isotopes are even more enriched in ^{32}S than within sapropels. This is a result of increased bisulphide reoxidation at times of relatively high bisulphide production, when bisulphide could escape from the sediment into the water column. The reoxidation may have effected up to 80% of the produced sulphide. The effect of extensive sulphide reoxidation on organic carbon burial efficiencies and paleoproductivity estimations are considered in Chapter 5. The enhanced accumulation of OM in sapropels appears to have been caused by both increased paleoproduction of OM in the surface waters and enhanced preservation of the OM after settling.

Chapter 6 explores the origin of sulphur in OM within and around sapropels by studying the stable sulphur isotopic compositions and sulphur to carbon ratios in the OM. The organic sulphur in the sediments is a mixture of sulphur derived from (1) inorganic reduced sulphur produced in microbial sulphate reduction, and (2) biosynthetic sulphur. The uptake of reduced sulphur into OM was most pronounced within the sapropels, where pyrite formation was iron-limited, so that reactive iron was no longer competing with OM for the uptake of reduced sulphur and dissolved sulphide concentrations increased.

In Chapter 7 results from organic geochemical analyses, trace metal chemistry and pyrite study in some exceptionally organic-rich Pliocene sapropels are integrated. These data prove that euxinic (sulphidic) water column conditions must have existed throughout the eastern Mediterranean basin over substantial periods of time during the formation of these sapropels.

Chapter 8 discusses the sediment chemistry and magnetic properties in a 19.6-metre-long core from an exceptional site in the abyssal eastern Mediterranean. This core contains a large number of sapropels which were used to construct a time frame for the sediment record at this site. The exceptional feature is that, in contrast with comparable sites, porewater contained sulphide down from a few metres below seafloor (mbsf). This sulphide was possibly produced by bacterial sulphate reduction combined with methane oxidation at a depth of about 17.5 mbsf. Upward migrating sulphide has pyritized all reactive iron up to a depth of 2 mbsf. As a consequence, the paleomagnetic signal of iron minerals has been destroyed, and no reliable paleomagnetic data can be obtained in the lower half of the core.

Summarizing, the work described in this thesis illustrates that chemical processes in marine sediments may be highly dynamic, especially when different redox systems are forced to coexist. This may happen when sediments with different OM contents are superimposed, as a result of periodically changing environmental conditions, or when processes in the subsurface, such as the input of methane, disturb the chemical system in the sediments. As a result of the redox imbalances, sediments may be chemically altered after deposition. On the one hand, this alteration can obscure and even destroy geological information stored in the sedimentary record. On the other hand, relicts of geochemical processes may reveal the paleoceanographic and diagenetic history of the sediments.

Chapter 2

Diagenetic pyritisation under eastern Mediterranean sapropels caused by downward sulphide diffusion

Abstract Recurrent organic-rich layers (sapropels) in eastern Mediterranean sediments are enriched in C_{org}, Fe and S. Sulphur and Fe are enriched in a zone immediately below the sapropels, whereas C_{org} is not. ^{34}S values of bulk sediments and simple mass-balance calculations indicate that SO_4^{2-} reduction has taken place in an open system, with all HS^- formed at, or close to, the sediment surface. Formation of pyrite in the sapropel was Fe-limited and consequently, excess HS^- was able to migrate downwards (downward sulphidisation). This resulted in the formation of pyrite below the sapropel by reaction of this HS^- with solid-phase ferric Fe and Fe^{2+} diffusing upwards from underlying sediments. The Fe^{2+} source probably includes Fe (hydr)oxide layers formed at former oxidation fronts above previously deposited and buried sapropels. This downward sulphidisation mechanism allows accumulation of twice as much S in alternating organic-rich-anoxic/ organic-poor-suboxic sediments compared to what is preserved in organic-rich anoxic sediments.

2.1 Introduction

Cyclic sediments are abundant in the sedimentary record and usually represent periodically changing environmental conditions. A variety of cyclic transitions in sediments have been reported, for example: oxic/ anoxic transitions (Cita et al., 1991), organic-rich/ organic-poor transitions (Pedersen, 1983; Mucci and Edenborn, 1992; Bertrand and Lallier-Vergès, 1993; Tribovillard et al., 1994), carbonate-rich/ carbonate-poor transitions (Bottrell and Raiswell, 1989), pelagic/ turbiditic transitions (Wilson et al., 1985; de Lange, 1986; de Lange et al., 1987; Jarvis and Higgs, 1987; Prahl et al., 1989), freshwater/ marine transitions (Ross et al., 1970; Boesen and Postma, 1988; Middelburg et al., 1990 and 1991), and combinations of these.

Each depositional environment is characterized by certain diagenetic conditions. The processes occurring in sediments accumulating at a steady state have been well studied (Berner, 1980). Less is known about the nonsteady-state diagenetic processes which occur during the transition from one depositional environment to another or at the interface between the two sediment types involved. Sedimentary cyclicity with two types of sediments implies that there are also two types of transitions. For example, in the case of alternating aerobic and anaerobic sediments, transitions may occur either from anaerobic to aerobic, or from aerobic to anaerobic conditions. Diagenetic processes at the interface between aerobic organic-poor sediments and underlying anaerobic organic-rich sediments have been described in detail during the last decade. One example is the formation of downward progressing oxidation fronts and burndown phenomena following deposition of organic-rich turbidites in the Madeira and Nares Abyssal

Plains (e.g. Colley et al., 1984; Wilson et al., 1985 and 1986; de Lange et al., 1987; Jarvis and Higgs, 1987; Prahl et al., 1989; Thomson et al., 1989 and 1993; van Os et al., 1993). Such downward oxidation fronts are initiated where downward oxidant fluxes (O_2 and NO_3^-) exceed upward reductant fluxes (Fe^{2+}, Mn^{2+} and NH_4^+).

Oxidation fronts have also been studied in sediments from the eastern Mediterranean, where the deposits consist of interbedded sequences of organic-poor hemipelagic and dark organic-rich sapropels or sapropelic layers (Buckley et al., 1974; Calvert, 1983; Murat and Got, 1987; de Lange et al., 1989). A sediment layer is defined as a sapropel when it is >1 cm thick and C_{org} is >2 wt%, or as sapropelic when the layer is similarly thick but contains 0.5 to 2 wt% C_{org} (Kidd et al., 1978), although this distinction is not always observed strictly. After deposition of a sapropel, a downward oxidation front develops, which results in oxidation of reduced C and S species in the top of the sapropel (de Lange et al., 1989; van Os et al., 1991; Pruysers et al., 1991 and 1993; Higgs et al., 1994; Thomson et al., 1995).

Although most geochemical studies of eastern Mediterranean sapropels have concentrated on the most recent transition from anaerobic organic-rich sediments to aerobic organic-poor sediments, the reverse transition also deserves attention. In this paper we describe results on one of the major processes occurring in and below sapropels, or sapropelic layers, deposited on top of 'normal' hemipelagic sediment. We discuss the development of a downward sulphidisation front and consequent Fe sulphide formation below organic-rich sediments.

2.2 Materials and methods

Four cores are discussed in this paper (Fig. 1.1). Gravity cores GC21 and GC17 were recovered during the 1988 *BAMO-3* expedition of R/V *Bannock*, and piston core ABC27 was recovered during the 87/3 *ABC* expedition of R/V *Tyro* to the eastern Mediterranean. Boxcore UM26 was recovered during the 1994 *Palaeoflux* cruise of R/V *Urania*.

Core GC21 (34°21.93'N, 20°02.09E, water depth 3250 m) and core GC17 (34°18.64'N, 20°06.76'E, water depth 3140 m) have been described in detail by van Os et al. (1991) and contain sapropels S5, S6, S7, S8 and S1, S5, S6, S7 and S8, respectively. Sedimentation rates for GC17 and GC21 were 1.3 cm kyr^{-1} during deposition of sediment in the interval from S8 to S5 and 1.5 cm kyr^{-1} for sapropel S1 in GC17 (after Cita, 1989).

Core ABC27 (33°22.7'N, 24°57.3'E, water depth 2180 m) was recovered south east of the Diapiric Belt Area in the eastern Mediterranean. The 394 cm core consists of Late Pleistocene to Holocene carbonate oozes with interbedded sapropels S1, S5, S6, S7, S8, and S9, and tephra layer Y_5. The intervals from S8 to S5, and S5 to the top of the core accumulated at respective rates of 1.68 cm kyr^{-1} and 0.78 cm kyr^{-1} (Erba, 1988).

After collection, cores GC17 and GC21 were split lengthwise, subsampled aboard ship, and stored at 4°C. Sampling was done within one week, using a bone spatula, at 1 mm resolution in the sapropel intervals and at 1 cm resolution elsewhere. Porewaters were obtained aboard ship by squeezing 10-15 cm^3 of wet sediment using manually-operated Teflon squeezers in the open air at a temperature of 15-20°C. Only major seawater element concentrations are considered reliable using this method. ABC27 was subsampled at Utrecht University in intervals of 0.2-2 cm two years after recovery.

The samples were dried for 24 hours at 105°C and ground in an agate mortar before dissolution in an $HClO_4$-HNO_3-HF acid mixture. The dried residue was dissolved in 1 M HCl for analysis of Fe, Al and S with an ARL 34000 inductively coupled plasma atomic emission spectrometer (ICP-AES). Analytical precision and accuracy were determined by replicate analyses of samples and by comparison with an international (SO-1) and in-house standard (MM 82). The relative standard deviations were better than 2% and the accuracy was better than 4%. Porewaters from cores GC21 and GC17 were analysed for total Na and S using ICP-AES, with a relative standard deviation of less than 6%. The C_{org} content in sapropel S7 in core GC17 was determined volumetrically following dry oxidation at 1000°C after prior removal of carbonate. Organic carbon contents in sapropels S1, S4, S5 and S6 in core GC17 and sapropels S6 and S7 in core GC21 were determined according to the method described by Nieuwenhuize et al. (1994), using a Fisons Instruments NA-1500 NCS-analyser. This method was proven to yield data consistent with those of the dry oxidation method (Nieuwenhuize et al., 1994). Bulk sediment samples for [34]S measurements were prepared by reducing inorganic S compounds to H_2S with Kiba reagent (Sn(II)-concentrated phosphoric acid). The H_2S generated was subsequently oxidized to SO_2 at 1000°C using V_2O_5. The isotopic composition of the SO_2 was measured with a Finnigan MAT 271/45 mass spectrometer equipped with a dual inlet system and a multicollector system. The [34]S data are reported in   relative to Canyon Diablo.

Table 2.1 *Porewater Na^+ and SO_4^{2-} analyses of cores GC17 and GC21.*

GC21			GC17		
depth (mbsf)	Na^+ (mM)	SO_4^{2-} (mM)	depth (mbsf)	Na^+ (mM)	SO_4^{2-} (mM)
0.10	4180	100.7	0.20	538	35.1
0.66	4037	94.5	0.56	549	31.7
0.98	4065	91.7	0.80	512	30.3
1.31	3921	87.6	1.30	508	29.2
1.65	3953	88.1	1.84	510	30.1
1.91	4125	85.3	2.15	489	29.1
2.15	4349	87.4	2.48	524	30.3
2.52	4133	74.7	2.91	520	31.9
3.12	3988	64.2	3.54	522	33.2
3.52	3866	59.1			
3.97	3863	55.6			

In order to study the nature of the sedimentary S enrichments in more detail, sediments from boxcore UM26 (33°23.6'N, 25°0.9'E, water depth 2160 m), which contains sapropel S1, were extracted for S-species. A subcore of UM26 was subsampled at a resolution of 0.5 to 1 cm aboard ship inside a N_2-filled glovebox and stored under N_2 in air-tight containers at 4°C. Total S was analysed by the above described method. Samples were dried at 40°C and washed with acetone for several hours to remove AVS, organic polysulphides and elemental S before pyrite extraction. Pyrite was extracted using a modification of the method of Zhabina and Volkov (1978), based on the reduction of FeS_2 to H_2S by oxidation of Cr^{2+} (Canfield et al., 1986; Cutter and Oatts, 1987; Luther, 1987; Henneke et al., 1991). Evolved H_2S was trapped as HS^- and analysed by square wave voltammetry (SWV) using a Princeton Applied Research Model 384B-4 polarographic analyser system equipped with a Model 303A static mercury drop electrode (SMDE). Furthermore, a sequential extraction procedure (Henneke, 1993), based on Francois (1987a and 1987b) and Ferdelman et al. (1991) was applied for elemental and low-molecular-weight organic S, organic polysulphides, and humic S compounds.

2.3 Results

The porewater SO_4^{2-} concentration found in the top of core GC21 is close to that found in the overlying brine (103.8 mM, de Lange et al., 1990) and gradually decreases with depth in the core (Table 2.1). The concentration remains well above that of normal seawater. The porewater SO_4^{2-} concentration in core GC17 is fairly constant, having values similar to those in Mediterranean seawater (32 mM). The gradient in core GC21 is caused by recent infiltration of brine and not by present-day SO_4^{2-} reduction, because other major elements, such as Na (Table 2.1), show corresponding gradients (van Os et al., 1991). Our porewater data are only used to correct S contents of sediment samples.

Sapropels and sapropelic layers are relatively rich in total S, total Fe and C_{org} (Figs. 2.1 and 2.2). Iron and S are also enriched below the sapropels, where C_{org} is not. Iron and S even show discrete maxima below sapropels S6, S7 and S8 in ABC27, S6 in GC21, and S6 and S7 in GC17.

Table 2.2 *Contents of S-species in boxcore UM26. The values are averages of n samples. S_{tot} are total S contents of the samples. S_{sum} = porewater S + elemental S + LMW organic S + organic polysulphide S + humic S + pyritic S. Percentages are relative to S_{sum}.*

position with respect to sapropel	n	S_{tot} (μmole gdry^{-1})	S_{sum} (μmole gdry^{-1})	percentage pyritic S	percentage porewater S	percentage humic S
above	3	57	41	2	75	23
within	5	340	338	82	11	7
below	8	250	262	85	8	6

Bulk sediment [34]S data for S7 in GC17 show a constant value of about -40 in the sapropel and in the S-enriched zone below the sapropel (Fig. 2.3). Above and below this horizon, bulk sediment [34]S values return to a base level of about +20 , reflecting the isotopic composition of porewater SO_4^{2-}. The distribution of porewater S, humic S, pyritic S and total S (S_{tot}) in sediment samples from boxcore UM26 is shown in Table 2.2. The sum of the various S fractions (S_{sum}) compares favourably with the independently determined total S content (S_{tot}). Elemental S, low-molecular-weight (LMW) organic S and organic polysulphides fractions were found to be less than 0.4 µmol g^{-1}. Pyritic S is by far the dominant S fraction in the sapropel and in the S-enriched zone below. Porewater S and humic S are present at all depths and dominate above the sapropel, where pyritic S is absent.
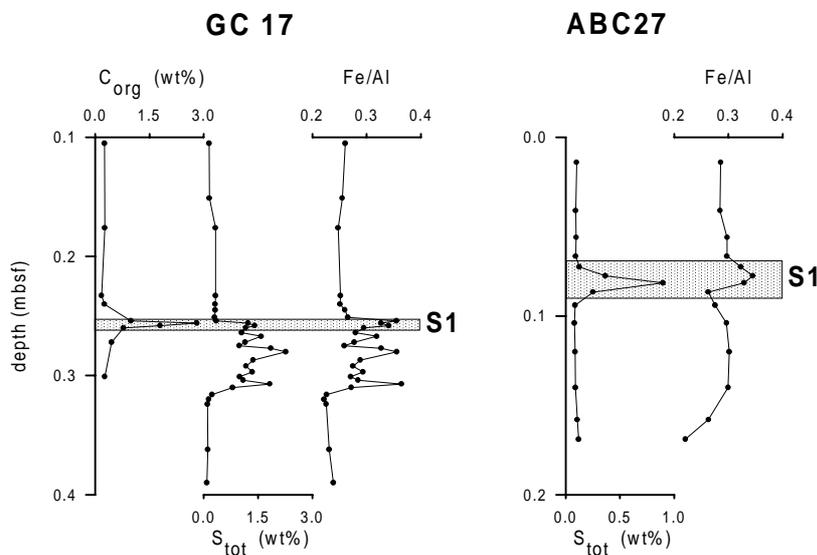

Figure 2.1 *Concentration vs. depth profiles of C_{org} and S_{tot} (total S contents of the samples, uncorrected for porewater S) and plot of Fe/Al vs. depth in sapropel S1 in core GC17 and in core ABC27 (mbsf: metres below seafloor). Iron concentrations in mol g^{-1} were divided by Al concentrations in mol g^{-1} to correct for closed sum effects due to carbonate dilution. The grey rectangles indicate stratigraphical positions of the sapropels visible in the cores.*

2.4 Discussion

Concentrations of S and C_{org} allow three zones of sediment to be distinguished, namely above, in and below sapropels. Sediments above, and far below a sapropel (i.e. above a previously deposited sapropel) are low in C_{org} and S. The S is mainly present in the form of residual porewater SO_4^{2-} and humic S (Table 2.2) and these samples have heavy bulk sediment [34]S values close to the value for seawater SO_4^{2-} (+20 , Fig. 2.3). Sapropel samples have high C_{org} and S contents; most of the S is present as pyrite (Table 2.2) and the samples have light bulk sediment [34]S values. Samples just below sapropels are low in C_{org}, yet rich in pyritic S and bulk sediment [34]S values are light (-40). This S enrichment is interpreted to be a diagenetic feature related to the downward diffusion of dissolved HS$^-$ to the horizon immediately below the sapropel and resulting pyrite formation.
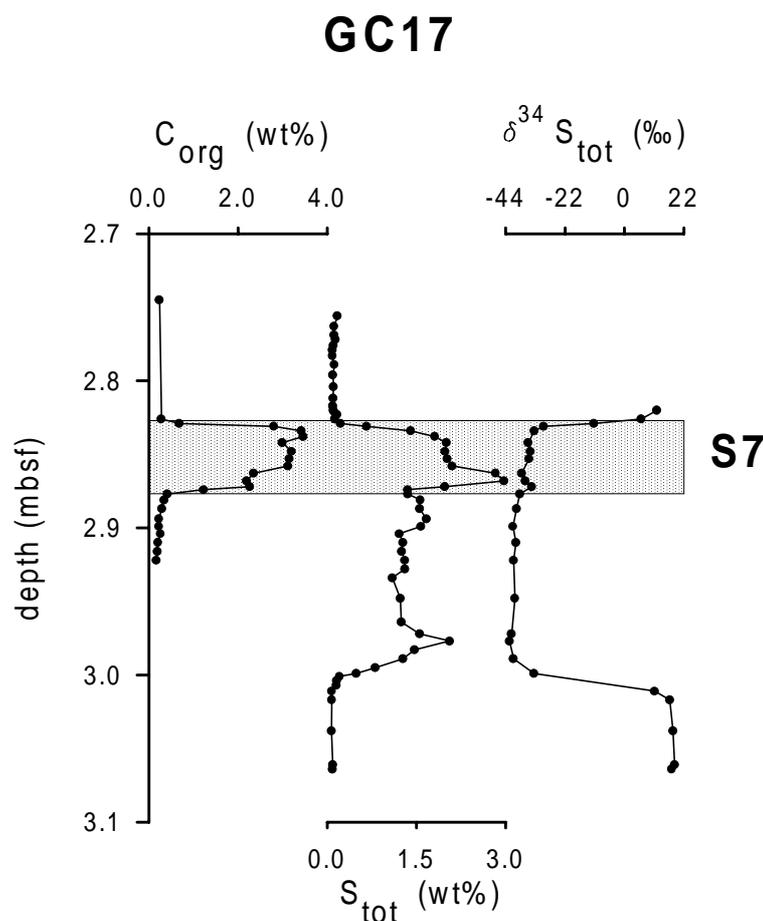
GC17

Figure 2.3 *Concentration vs. depth profiles of C_{org} and S_{tot} and plot of $^{34}S_{tot}$ vs. depth in sapropel S7 in core GC17 (mbsf: metres below seafloor). Iron concentrations in mol g^{-1} were divided by Al concentrations in mol g^{-1} to correct for closed sum effects due to carbonate dilution. The grey rectangles indicate stratigraphical positions of the sapropels visible in the cores.*

Downward sulphidisation fronts were studied experimentally by Berner (1969). Depending upon the relative amounts of reactive Fe and dissolved H_2S, he identified three scenarios; low-Fe-content, high-Fe-content and intermediate-Fe-content, the last being termed a Liesegang situation. In the low-Fe-content model, dissolved H_2S produced by SO_4^{2-}-reducing bacteria diffuses downward out of a C_{org}-rich layer until it reacts with immobile solid-phase reactive Fe to form Fe sulphides. In the high-Fe-content model Fe^{2+} migrates upward to the H_2S-rich organic layer, where Fe sulphides are formed subsequently. In the intermediate situation, dissolved H_2S migrates downward and Fe^{2+} migrates upward. Distinct Fe sulphide bands (Liesegang bands) are formed where the two species meet. In order to determine which of the

Table 2.3 *Values for the depth-integrated SO_4^{2-} reduction rate in sapropels (DSRR = $S_{int} \times$ /z), advective SO_4^{2-} flux into the sediment (J_{adv} = $C_{sulphate}$), diffusive SO_4^{2-} flux into the sediment (J_{diff} = DSRR - J_{adv}), openness of the sediment to receive SO_4^{2-} from the water column (=J_{diff}/(J_{diff} + J_{adv})), the estimated SO_4^{2-} gradient in the top of the sediment at times of sapropel formation ([SO_4^{2-}]/ x = J_{diff}/(- $D_{j,sed}$)) in sapropels of cores ABC27, GC17 and GC21.*

sapropel	DSRR (mmole cm^{-2} kyr^{-1})	J_{adv} (10^{-2} mmole cm^{-2} kyr^{-1})	J_{diff} (mmole cm^{-2} kyr^{-1})	openness (%)	[SO_4^{2-}]/ x (10^{-5} mmole cm^{-3} cm^{-1})
ABC27 S1	0.19	1.5	0.18	92	-0.20
ABC27 S5	2.7	3.8	2.6	99	-2.2
ABC27 S6	2.0	3.7	1.9	98	-1.7
ABC27 S7	2.5	3.7	2.5	99	-2.2
ABC27 S8	1.4	3.5	1.4	97	-1.3
ABC27 S9	0.95	3.0	0.92	97	-1.2
GC17 S1	5.8	2.6	5.8	100	-8.1
GC17 S5	1.5	2.9	1.5	98	-1.3
GC17 S6	1.1	2.9	1.1	97	-0.91
GC17 S7	2.3	2.9	2.3	99	-2.0
GC17 S8	0.68	2.6	0.65	96	-0.67
GC21 S5	0.78	2.5	0.76	97	-0.85
GC21 S6	1.3	2.5	1.3	98	-1.4
GC21 S7	2.4	2.8	2.4	99	-2.2

Berner (1969) scenarios applies to the sediments in the eastern Mediterranean, we will investigate the S and C_{org} budgets, as they might generate useful paleo-environmental insights.

Several stratigraphic positions in and below sapropelic layers are defined as follows: The top of the C_{org}-rich layer (sapropel) is position *0*, while the bottom of this layer is position *z*. Position *z* is also the top of the zone under the sapropel enriched in S. The lower boundary of this zone is position *l*. Using measured total S contents (S_{tot}, wt%), porosities ( ), a grain density ( ) of 2.55 g cm^{-3} and a molar weight for S (*M*) of 32.06 g mol^{-1}, depth-integrated S inventories can be calculated (S_{int}, mol cm^{-2}), via:

$$S_{int} \quad \int_o^l S \ dx \quad \int_o^l S_{tot} \ (\frac{(1 \quad)}{100 \ M}) \ dx.$$

This equation provides an estimate of the amount of SO_4^{2-} reduction that has taken place in the sapropel. Data used in the calculation include wt% S, corrected for porewater S in sapropels where such data were available (GC17 and GC21). In the S-rich horizon below sapropels corrections were made using base level values of S (porewater S and humic S). Corrections of S_{int} were on the order of 4 to 13%. The key assumption was made that S_{int} calculated in this way originates from the sapropel itself. From S_{int} (mol cm^{-2}), thicknesses of C_{org}-rich layers (z, cm) and sediment accumulation rates (, cm kyr^{-1}), depth-integrated SO_4^{2-} reduction rates (*DSRR*, mol cm^{-2} kyr^{-1}) are estimated via:

$$DSRR \quad \int_o^z SRR \quad \int_o^l S \ dx \times \frac{}{z} \ (S_{int}) \times \frac{}{z},$$

where *SRR* is the SO_4^{2-} reduction rate. Estimated depth-integrated rates of SO_4^{2-} reduction range from 0.19 to 5.8 mmol cm^{-2} kyr^{-1} (Table 2.3).

The depth-integrated SO_4^{2-} reduction-rate estimates are based on several assumptions. Firstly, a reduced S retention of 100% is assumed. Calculated S_{int} and *DSRR* values will therefore be underestimations if significant amounts of reduced S have been lost from the system. Secondly, any reduction in the thickness of the C_{org}-rich layer (z) due to oxidation of the sapropel following its formation (e.g. de Lange et al., 1989; Pruysers et al., 1991 and 1993) is neglected. Downward-progressing oxidation fronts may decrease the amount of reduced S retained in the sediment and hence S_{int}. This loss of S is not proportional to the decrease in thickness however, because part of the HS$^-$ originating from the sapropel is believed to have migrated below the sapropel. Accordingly, the calculated depth-integrated SO_4^{2-} reduction rates may be overestimated. Finally, we have assumed that there is no significant detrital reduced S or bottomwater HS$^-$ input so that all reduced S has been produced in the sediment.

Depth-integrated SO_4^{2-} reduction rates comprise advective as well as diffusive fluxes of SO_4^{2-}. Assuming no compaction, advective SO_4^{2-} fluxes (J_{adv}, mol cm^{-2} kyr^{-1}) can be calculated from porosity ( ), sediment accumulation rate (, cm) and concentration of SO_4^{2-} in average Mediterranean seawater ($C_{sulphate}$, mol cm^{-3}):

$$J_{adv} \qquad C_{sulphate}.$$

The fluxes have positive values, because they are directed from the water column into the sediment. $C_{sulphate}$ in present-day Mediterranean seawater is 3.2×10^{-5} mol cm^{-3}. The diffusive flux can then be obtained by difference:

$$J_{diff} \quad DSRR \quad J_{adv}.$$

Advective and diffusive fluxes of SO_4^{2-} estimated in this way range from 1.5×10^{-5} to 3.8×10^{-5} and 1.8×10^{-4} to 5.8×10^{-3} mol cm^{-2} kyr^{-1} respectively (Table 2.3). Based on these calculated diffusive SO_4^{2-} fluxes, it is possible to derive paleo-SO_4^{2-}-gradients from

$$J_{diff} = -D_{j,sed} \; (\frac{[SO_4^{2-}]}{x}),$$

where $D_{j,sed}$ is the diffusion coefficient for interstitial solution in sediments, which is calculated according to Li and Gregory (1974). For sediments with a porosity 0.7, such as the sediments discussed here, the diffusion coefficient for interstitial solution in sediment is estimated by

$$D_{j,sed} = D_j^0 \; ,$$

where D_j^0 is the diffusion coefficient of ions at infinite dilution (7.82×10^{-6} cm^2 s^{-1} for SO$_4^{2-}$ at 13°C, the ambient bottomwater temperature). Derived paleo-SO$_4^{2-}$-gradients range from -1.3×10^{-8} to -2.2×10^{-8} (with one exception of -2.0×10^{-9} for S1) mol cm^{-3} cm^{-1} in ABC27, -6.7×10^{-9} to -2.0×10^{-8} (with one exception of -8.1×10^{-8} for S1) mol cm^{-3} cm^{-1} in GC17, and -8.5×10^{-9} to -2.2×10^{-8} mol cm^{-3} cm^{-1} in GC21 (Table 2.3). The exceptions are probably caused by total burndown and partial burndown of sapropel S1 in ABC27 and GC17, respectively. In the former case estimation of the thickness of the C$_{org}$-rich and S-rich layers is faulty, because there is no C$_{org}$ layer left and only a thin S-rich layer. Consequently, SO$_4^{2-}$ reduction rates and SO$_4^{2-}$ gradients are underestimated. In sapropel S1 in GC17, underestimation of the original sapropel thickness leads to overestimations of SO$_4^{2-}$ reduction rates and SO$_4^{2-}$ gradients. These gradients might be slight overestimates because present-day porosities (0.6) were used to derive SO$_4^{2-}$ gradients near the sediment surface, where porosities may be somewhat higher (up to 0.8 in surface sediments in recent sediments from the eastern Mediterranean).

These paleo-SO$_4^{2-}$-gradients can be compared with those observed in modern environments. Berner (1978) made a compilation of SO$_4^{2-}$ gradients in marine sediments covering a range of sediment accumulation rates. He proposed a linear relationship between the initial SO$_4^{2-}$ gradient and the sediment accumulation rate:

$$-B = (\frac{c}{x})_0 \; ,$$

where $B = 1$ if the $(c/x)_0$ is expressed in mmol l^{-1} cm^{-1} and in cm yr^{-1}. From this relationship and an accumulation rate of about 1 cm kyr^{-1}, an initial SO$_4^{2-}$ gradient of about -1×10^{-9} mol cm^{-3} cm^{-1} would be expected. The estimated paleo-gradients calculated here are up to twenty times higher than this expected value. This relationship between sediment accumulation rate and initial SO$_4^{2-}$ gradient might not always be valid for environments that receive a high flux of organic matter however, such as sapropels and sediments underlying upwelling areas. In these environments higher initial SO$_4^{2-}$ gradients are observed. Pedersen and Shimmield (1991) reported a linear relationship between sediment accumulation rate and the initial SO$_4^{2-}$ gradient in Peru Margin sediment resulting in gradients twice as high as the values resulting from the relationship formulated by Berner (1978). Froelich et al. (1988) presented data for Peru

Continental Margin sediments with an initial SO_4^{2-} gradient of about 1.4×10^{-8} mol cm^{-3} cm^{-1} at a site with a sediment accumulation rate of 1.7 cm kyr^{-1}. Similarly, Canfield (1989) reported that SO_4^{2-} reduction rates in euxinic Black Sea sediments are about ten times higher than in pelagic (oxic) sediments with similar rates of sediment deposition. Accordingly, in spite of the assumptions made, the order of magnitude of the estimated paleo-SO_4^{2-}-gradients in the eastern Mediterranean is not inconsistent with observations for recent anoxic systems receiving high organic matter fluxes. Moreover, our depth-integrated SO_4^{2-} reduction rates fall within the envelope of data compiled by Canfield (1989) in the form of a *DSRR* vs. burial rate plot.

Depth-integrated amounts of S (S_{int} [mol cm^{-2}]), depth-integrated SO_4^{2-} reduction rates (*DSRR* [mol cm^{-2} kyr^{-1}]) and depth-integrated amounts of C_{org} (C_{int} [mol cm^{-2}]) can be used to obtain depth-integrated C_{org} oxidation rates (*DCOR* [mol cm^{-2} kyr^{-1}]) and burial efficiencies (*BE*) for C_{org} in sapropelic layers. On the basis of the generalized SO_4^{2-} reduction reaction:

$$2CH_2O + SO_4^{2-} \rightarrow H_2S + 2HCO_3^- ,$$
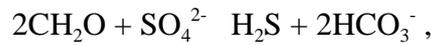
the depth-integrated C_{org} oxidation rate is calculated:

$$DCOR = 2 \times DSRR.$$

DCOR values range from 2.3 to 12 mmol cm^{-2} kyr^{-1} (Table 2.4). The amount of buried C_{org} (C_{int}) is obtained by integrating the amount of C_{org} present in the sapropel:

$$C_{int} = \int_o^z C_{org}\, dx.$$

The burial efficiency can be calculated using:

$$BE = \left(\frac{C_{int}}{2 S_{int} + C_{int}}\right) \times 100\%.$$

This approach is based on the assumption that all organic matter mineralisation took place by SO_4^{2-} reduction. Estimated burial efficiencies range from 20 to 46% in core GC17 and 37 to 45% in core GC21 (Table 2.4).

Canfield (1989 and 1994) reports burial efficiencies of 13-78% for euxinic and semi-euxinic sediments. Although Canfield (1989 and 1994) reports no actual data at a sediment accumulation rate of 1.3-1.5 cm kyr^{-1} (the range that applies to the sediments discussed here), burial efficiencies of 20-46% fit into the extrapolated data field in the plot of sediment burial rate vs. burial efficiency. Moreover, calculated *DCOR* values plot at the lower boundary of the extrapolated data fields given by Canfield (1989) in plots of C_{org} oxidation rates vs. sediment burial rates. This is a further indication that properties of the reconstructed paleo-SO_4^{2-}-reducing-environment in eastern Mediterranean sapropels are not inconsistent with those in comparable

recent sedimentary environments, which implies that the reduced S in and below the sapropels calculated as S_{int}, could have been formed initially within the sapropel itself.

Table 2.4 *Values for the depth-integrated C_{org} oxidation rate in sapropels, resulting from SO_4^{2-} reduction (DCOR = 2 × DSRR), the burial efficiency for C_{org} in sapropels (BE = C_{int} /(2 × S_{int} + C_{int})), the downward HS⁻ flux at the time of sapropel formation ($J_{sulphide}$ = $S_{int\,below\,sap}$ × /z), the porewater concentration of HS⁻ in the sapropel at times of its formation ($[HS^-]_{sap}$ = (x × $J_{sulphide}$)/($D_{j,sed}$) + $[HS^-]_{pyrite}$), the enhanced S-storage (= DSRR / (DSRR - $J_{sulphide}$)).*

sapropel	*DCOR* mmole cm⁻² kyr⁻¹	*BE* %	*J*$_{sulphide}$ 10⁻¹ mmole cm⁻² kyr⁻¹	[HS-]$_{sap}$ 10⁻⁵ mmole ml⁻¹	enhanced S-storage
ABC27 S1			0.48	0.030	1.3
ABC27 S5			8.1	8.9	1.4
ABC27 S6			3.9	2.5	1.2
ABC27 S7			6.3	3.2	1.3
ABC27 S8			1.9	0.68	1.2
ABC27 S9			0.67	0.14	1.1
GC17 S1	12	20	26	4.8	1.8
GC17 S5	3.1	33	6.6	5.9	1.8
GC17 S6	2.3	46	2.9	2.0	1.3
GC17 S7	4.6	34	10	5.4	1.8
GC17 S8					1.0
GC21 S5			1.9	2.2	1.3
GC21 S6	2.6	45	2.5	1.4	1.2
GC21 S7	4.8	37	9.3	1.5	1.6

2.4.1 Sulphur source and mobility

The ^{34}S characteristics of S in and below the sapropels are consistent with formation of H_2S within the sapropel. The H_2S produced during bacterial reduction of SO_4^{2-} is depleted in ^{34}S relative to ^{32}S. Maximum isotopic fractionations of 40-70 between SO_4^{2-} and reduced S have been observed (e.g. Goldhaber and Kaplan, 1974; Chambers and Trudinger, 1979). A large fractionation occurs if SO_4^{2-} is abundantly available, yielding relatively light ^{34}S values. Relatively little fractionation occurs when SO_4^{2-} is limiting, yielding ^{34}S values in H_2S that are not as light. Bulk sediment ^{34}S values in sapropel S7 in GC17, and in the S-rich horizon below are about -40 (Fig. 2.3), while Mediterranean seawater has a ^{34}S value of 20.6 (de Lange et al.,1990). This means that the reduced S was produced with a fractionation of about 60 . This large discrimination of ^{34}S relative to ^{32}S implies that SO_4^{2-} reduction took place in an

environment where SO_4^{2-} was plentiful. Thus, H_2S formation has occurred either in the uppermost centimetres of sediment, or in the bottomwater, or both.

Additionally, the ratio of diffusive to total fluxes, $(J_{diff})/(J_{diff} + J_{adv})$, can be used to determine whether the system has been open to receive SO_4^{2-} from the overlying water. The calculated ratios, 92-100% (Table 2.3), reveal that this has been the case. The sediment accumulation rate is low enough to allow large amounts of SO_4^{2-} to diffuse into the sediment, to form H_2S.

The observed isotopic signature of S could also be explained by diffusion of HS^- from the water column into the sediments if bottomwaters were euxinic, rather than formation of HS^- in the sediment itself. However, during sapropel deposition diffusion of HS^- into the sediment is unlikely. Even in the Black Sea (Lyons and Berner, 1992) and the Cariaco Trench (Scranton et al., 1987) diffusion of HS^- occurs from porewaters to the overlying water column. Furthermore, diffusion of HS^- into the sediment before sapropel deposition is not likely either, because the pre-sapropel deposits contain only small amounts of organic matter and bottomwater was likely to have been well oxygenated. Therefore, the source of downward diffusing HS^- must be in the sapropel itself.

From the integrated amount of S found in the S-enriched zone below a sapropel corrected for base-level wt% S ($S_{int\ below\ sap}$), and using the sediment accumulation rate ( ) and the thickness of a sapropel (z), the average downward HS^- flux ($J_{sulphide}$) during sapropel formation can be calculated:

$$J_{sulphide} \quad S_{int\ below\ sap} \times \frac{}{z}.$$

The assumption is made that all excess HS^- has migrated down during sapropel deposition. Estimated depth-integrated HS^- fluxes range from 6.7×10^{-5} to 1.0×10^{-3} mol cm^{-2} kyr^{-1}, with exceptions of 4.8×10^{-5} and 2.6×10^{-3} mol cm^{-2} kyr^{-1} for sapropels S1 in ABC27 and GC17 respectively (Table 2.4). Pruysers et al. (1993) reported upward Fe^{2+} fluxes in the range of 10^{-4} to 10^{-3} mol cm^{-2}kyr^{-1} for recent eastern Mediterranean sediments. Fe^{2+} fluxes therefore are on the same magnitude as the computed downward HS^- fluxes. If we consider the upward Fe^{2+} fluxes from sapropel S1 to be reasonable estimates for the upward Fe^{2+} fluxes towards newly forming sapropels, the amount of upward diffusing Fe^{2+} is sufficient to form Fe sulphides via reaction with HS^- migrating downward from an overlying sapropel.

From the downward HS^- flux ($J_{sulphide}$) and a mean diffusion path length, the porewater concentration of HS^- in the sapropel at the time of its formation can be calculated:

$$[HS^-]_{sap} \quad (\frac{J_{sulphide}}{D_{j,sed}} \times x) \quad [HS^-]_{pyrite}.$$

The D_j° for HS^- is 13.7×10^{-6} cm^2 s^{-1} at the ambient bottomwater temperature of 13°C, $D_{j,sed}$ is estimated according to Li and Gregory (1974) as explained above for SO_4^{2-}; x is half the

thickness of the sapropel and S-enriched zone below the sapropel ($= \frac{1}{2} \times l$);   is the porosity; $[HS^-]_{pyrite}$ is the equilibrium concentration of HS^- in the presence of pyrite, about 1×10^{-7} mol l^{-1} (Berner, 1969). Estimated $[HS^-]_{sap}$ values range from 1.4×10^{-9} to 8.9×10^{-8} mol cm^{-3}, with one exception of 3.0×10^{-10} mol cm^{-3} for sapropel S1 in ABC27 (Table 2.4). These values are consistent with observations in modern euxinic sediments (Raiswell, 1993) and are all higher than the value for an Fe-dominated sediment, which is about 10^{-10} mol cm^{-3} HS^-, as defined by Berner (1969). These first-order estimates for paleo-HS^--levels within sapropels provide an additional indication that the environment in the sapropels must have been HS^--dominated and Fe^{2+}-limited. Preliminary data on 1 N HCl (20 h) extractable Fe are consistent with Fe limitation during sapropel formation, because sapropel and above-sapropel sediments contain about 60 and 250 µmol g^{-1} Fe respectively.

The patterns of total S and total Fe contents below sapropels can be partitioned into two groups. Iron and S content maxima are observed below some sapropels (S6 and S7 in GC17, S6 in GC21, S6, S7 and S8 in ABC27) whereas below other sapropels (S5 in GC17, S5 in GC21, S5 and S9 in ABC27) there is merely a broad zone of Fe and S enrichments (Fig. 2.2). These two
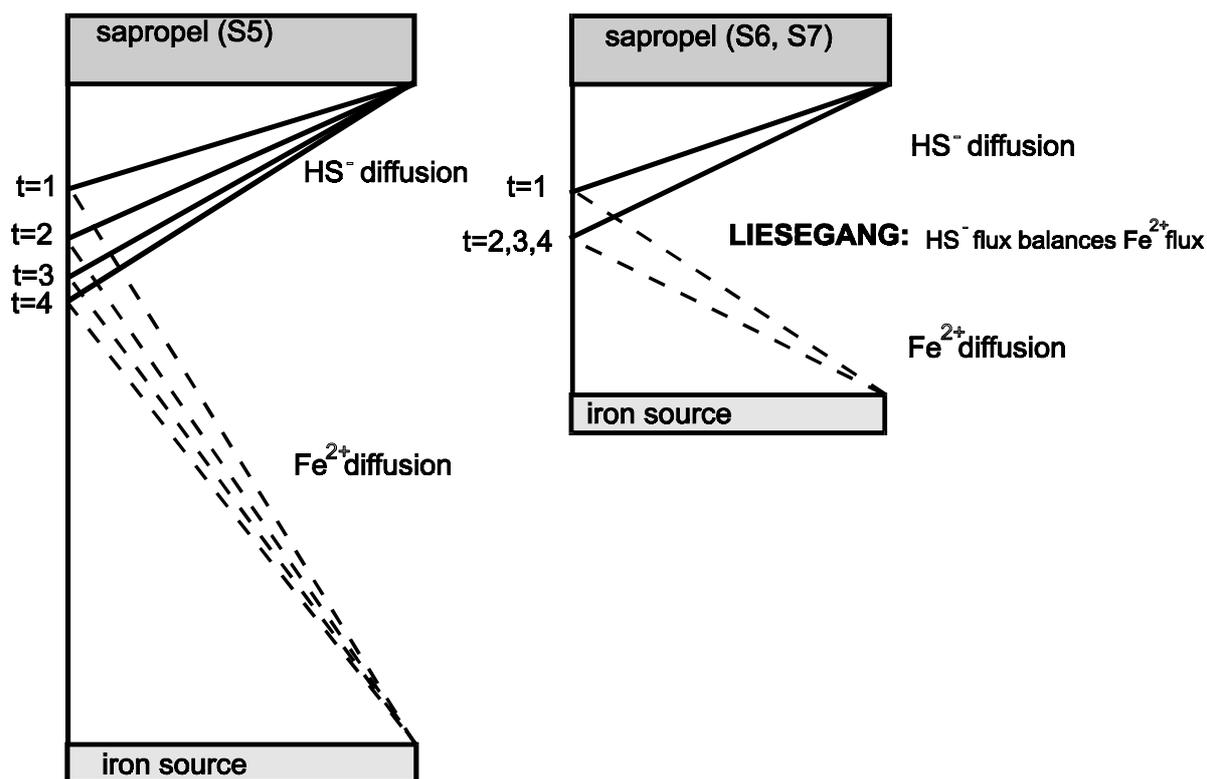

Figure 2.4 *Schematic model for iron sulphide formation below sapropels. Two situations are distinguished, one in which the system remains HS⁻ dominated and another one in which the Fe source is located closer to the sapropel and Liesegang phenomena occur. Note that all gradients have been normalized, so that differences in diffusion constants for Fe and HS⁻ and stoichiometric ratios for iron sulphides formed are not important. The relative magnitudes of the fluxes are indicated by the slopes of the diffusion-lines.*

types of enrichments are consistent with a scenario in which initially all downward sulphidisation fronts will be HS^- dominated and migrate downwards, and where an Fe source is present in the underlying sediments (Fig. 2.4). Most of the Fe is probably liberated from the Fe (hydr)oxide layer above the previously deposited sapropel, the remaining amount of Fe being derived from the intercalated marl oozes between sapropels. As the front moves down, the HS^- flux decreases and the Fe^{2+} flux increases. The magnitude of the Fe^{2+} flux meeting the HS^- flux increases with depth, i.e., time, because the front is progressively situated closer to the underlying sapropel and thus closer to the Fe source. An intermediate situation may evolve in which a Liesegang band develops at the bottom of the S-enriched zone. At this stratigraphic position both fluxes are balanced and the front penetration comes to a standstill. In situations where the underlying sapropel is relatively close, the Fe sulphide formation in Liesegang bands is the most intense (e.g. sapropels S6 and S7). In situations where an underlying sapropel is much deeper relative to the sapropel that creates a downwards sulphidisation front, such as below sapropel S5, the system remains HS^- dominated over the entire period of SO_4^{2-} reduction in the younger sapropel. In this case no distinct peaks of S and Fe are observed at the bottom of the S-enriched zone (Fig. 2.4).

2.4.2 C/S/Fe relationships

In slowly-accumulating marine sediments, pyrite formation can be limited by the availability of SO_4^{2-}, or the amount and lability of organic matter, or the concentration and reactivity of Fe minerals (Berner, 1984). Relationships between C_{org}, S and Fe can be used to characterize pyrite formation and/or the paleo-environments of ancient rocks (Berner and Raiswell, 1983; Raiswell and Berner, 1985; Raiswell et al., 1988; Middelburg, 1991; Leventhal, 1995). These relationships are usually presented in the form of S and degree of pyritisation (*DOP*, see definition below) vs. C_{org} plots. For sapropels S6 and S7 in GC21, S5, S6 and S7 in GC17, plots of S_{tot} (wt%) and DOP_T (based on contents in mol cm^{-3}, see definition below) vs. C_{org} are shown in Figs. 2.5 and 2.6. These sapropels were selected because the most extensive datasets are available for these intervals. The samples have been divided into three groups on the basis of DOP_T values and sample position with respect to the sapropel, namely upper sapropel, sapropel and below sapropel. The parameter *DOP* was proposed by Berner (1970), and defined as:

$$DOP = \frac{pyrite\ iron}{pyrite\ iron + reactive\ iron}.$$

Here *DOP* is calculated from total S and total Fe values as follows:

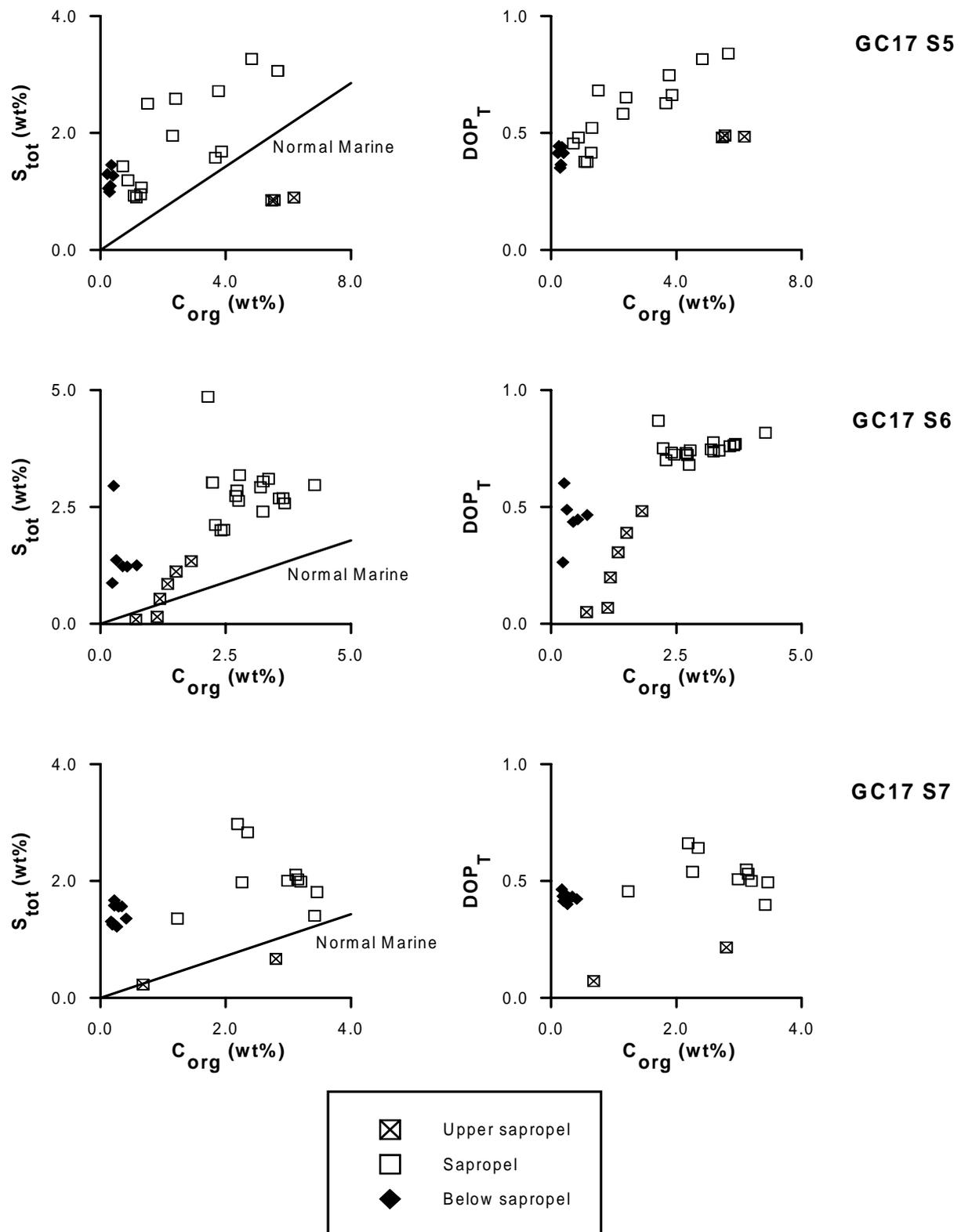$$DOP_T = \frac{0.5 \times S_{total}}{Fe_{total}}$$

Figure 2.5 *Plots of S_{tot} and DOP_T (=(0.5 × S_{tot})/Fe_{tot}) vs. C_{org} in sapropel S5, S6 and S7 in core GC17.*

The term '$0.5 \times S_{total}$' represents pyrite Fe (mol cm^{-3}), FeS$_2$ being the ideal formula for pyrite. By using Fe$_{total}$ (indicated by the subscript T in DOP_T), we will overestimate the quantity of reactive Fe and underestimate DOP. Note that concentrations are not corrected for porewater SO$_4^{2-}$ concentrations, because this does not affect DOP_T values significantly.

Samples from sapropels plot above the normal marine regression line in C-S plots as compiled by Berner (1984), as is generally the case for euxinic sediments. Samples from the S-enriched zone below the sapropels are extremely S-rich, yet C$_{org}$-poor. This suggests a postdepositional sulphidisation of these sediments with a HS$^-$ source that is not located in the sulphidized sediment itself, as has been described in detail by Boesen and Postma (1988), Middelburg (1991), and Leventhal (1995).

DOP_T values are about 0.5 in the S-rich horizons below sapropels. Values in the lower part of the sapropels are the highest, about 0.75. DOP_T values in the upper sapropel range from 0.1 to 0.5. Raiswell and Berner (1985) reported DOP values that represent the degree of pyritisation based on total Fe contents of sediment and rock samples (DOP_T). The mean DOP_T value in the Black Ven Marls, Lower Jurassic, England is 0.39 and DOP_T ranges from 0.1 to 0.5 in modern sediments of the Black Sea. DOP_T values found in the lower part of the sapropels studied in this paper are higher. The high DOP_T values are likely the result of enhanced Fe mobility and availability in these cyclic sediments. At the beginning of sapropel formation upward diffusing Fe^{2+} meets HS$^-$ at the site of SO$_4^{2-}$ reduction, which is in the sapropel, in the top of the sediment. Pyrite formation resulting from Fe^{2+} diffusion towards the sapropel yields abnormally high DOP_T values. As sapropel accumulation continues, the downward HS$^-$ flux increases and exceeds the upward Fe^{2+} flux (Fig. 2.4) and this results in S and Fe enrichments homogeneously extending below the sapropel and intermediate DOP_T values. When, at a certain distance below the sapropel, the downward HS$^-$ flux and the upward Fe flux are in balance, a distinct Fe-enrichment (Liesegang band) forms (Fig. 2.4). In the sedimentary record this band is situated at the lower boundary of the S-enriched zone below the sapropel, and is visible as a peak in Fe and S profiles. Towards the top of a newly-formed sapropel progressively less Fe is supplied from below, the only Fe being available for pyrite formation is detrital reactive Fe. Thus, DOP_T values decrease towards the top of the sapropel and reach values usually observed in non-cyclic sediments (0.1-0.5; Raiswell and Berner, 1985).

2.4.3 Implications for the sedimentary record

During the different redox regimes that succeed sapropel formation, the sediment chemistry is significantly altered. A sapropel is deposited during a period of high organic matter accumulation and possibly consequent bottomwater anoxia. Sapropel formation ends when the input of organic matter decreases and bottomwater is reventilated. Subsequently, the redox regime at the top of the sediment changes from sulphidic to oxic. A downward oxidation front is initiated and migrates into the sediment, resulting in formation of a metal-rich layer above the sapropel (de Lange et al., 1989; van Os et. al., 1991; Pruysers et al., 1991 and 1993; Higgs et al., 1994; Thomson et al., 1995). Cyclicity implies that this period of downward oxidation is followed by a timespan with increasing organic matter accumulation and renewed bottomwater

anoxia. Another sapropel is then deposited on top of the sequence causing a downward flux of reduced S.

Several situations involving postdepositional alteration of oxidized sediments by overlying reduced sediments have been reported in literature. Reduction haloes have been found in pelagic clays underlying turbiditic layers in the sediments of the Nares Abyssal Plain (Thomson et al., 1989). Sulphidisation of brackish/ freshwater sediments by HS$^-$ originating from organic-rich marine sediments deposited on top of a non-marine sequence has been observed in the Black Sea, the Baltic and Kau Bay (Boesen and Postma, 1988; Middelburg, 1991;
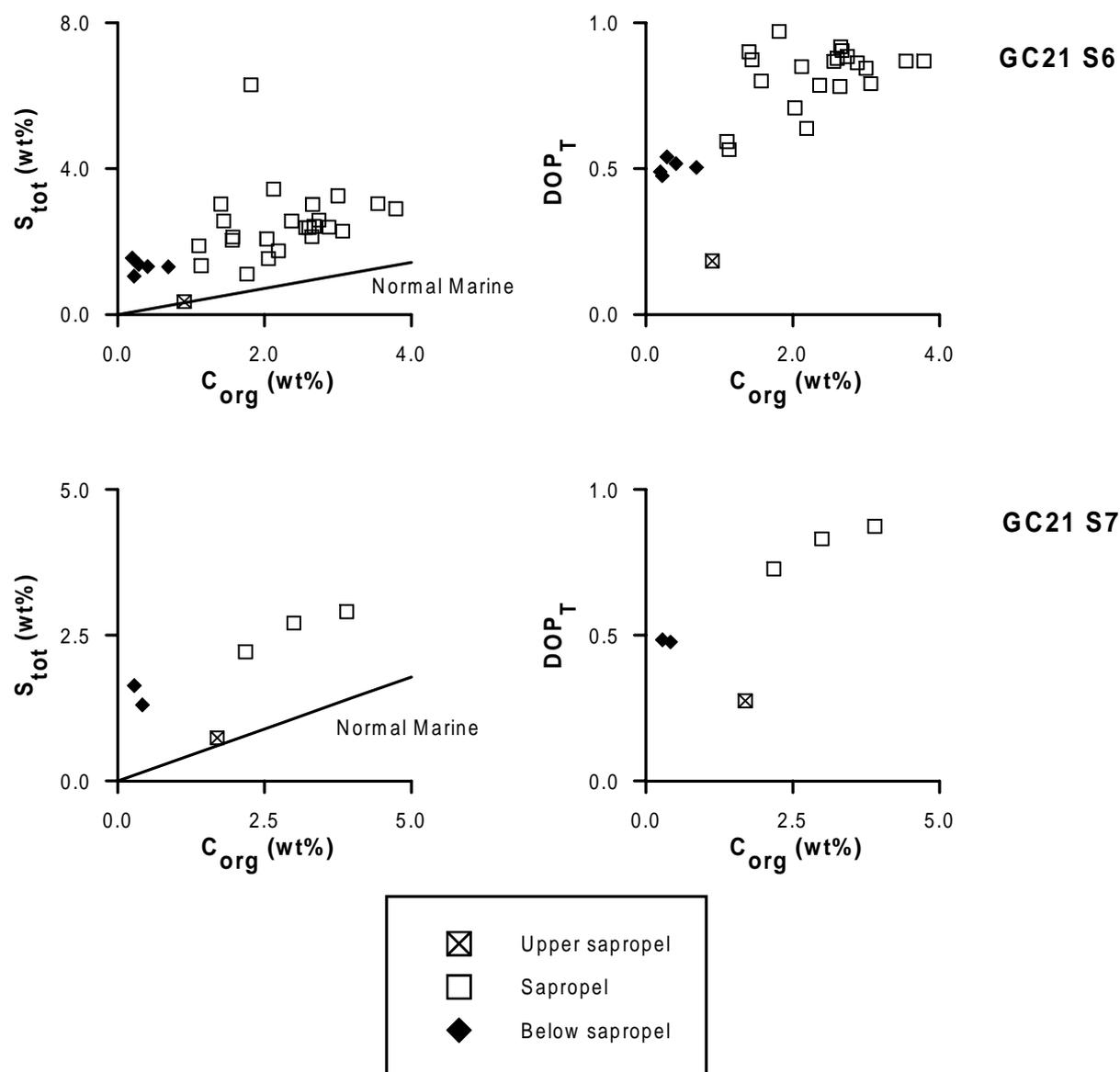

Figure 2.6 *Plots of S_{tot} and DOP_T vs. C_{org} in sapropel S6 and S7 in core GC21.*

Middelburg et al., 1991). Lyons et al. (1993) have reported formation and successive

sulphidisation of Fe and Mn oxyhydroxides during a past oxycline shoaling event in the Black Sea. These examples indicate that downward reductant fluxes are an important aspect of diagenesis in cyclic sediments.

A noteworthy feature in the sedimentary records studied here is that the types of S-enrichment below sapropels are basin-wide, i.e., they are found in the Bannock (ABC 27) as well in the Diapiric Belt Area (GC17 and GC 21). In both areas, sapropel S5 has an associated S-enriched horizon without distinct Fe and S peaks at the bottom, whereas sapropels S6 and S7 have distinct Fe and S peaks at the bottom of the S-rich zone. Higgs et al. (1994) presented data on S-enrichment below sapropel S1 for two sites, 470 km apart, that are very similar to the enrichments observed here (Fig. 2.1). These S-rich zones below sapropels are usually grey and discernible from the overlying black sapropels and underlying beige ooze. The grey-coloured horizon under sapropels has been termed the protosapropel zone (Muerdter et al., 1984) and can be easily correlated over the whole eastern Mediterranean (e.g. Murat and Got, 1987).

A final implication of this downward sulphidisation is that an additional sink for reduced S is created in these intermittent organic-poor and organic-rich sediments, compared to fully anoxic organic-rich sediments or to fully oxic organic-poor marine sediments. The amount of S preserved in the entire S-rich zone is up to twice that preserved in the sapropel alone (Table 2.4).

34

Chapter 3

Sedimentary sulphur and iron chemistry in relation to the formation of eastern Mediterranean sapropels

Abstract Detailed analyses of total S, pyritic S, humic S, NaCl-extractable S, elemental S, acid-volatile sulphide (AVS), and organic polysulphide in and around the most recent sapropel S1 (maximum C_{org} = 2.3%) and two other sapropels recovered during Ocean Drilling Program (ODP) Leg 160 (maximum C_{org} = 7.4% and 23.5%), show that the main S species in and immediately below each sapropel is pyrite. Directly above each sapropel S is hardly present in the solid phase, but occurs as porewater sulphate (SO_4^{2-}). Microbial SO_4^{2-} reduction took place in the sapropels during sapropel formation. Addition of reactive Fe to sapropel layers occurred via upward diffusion of Fe^{2+} from underlying sediments and/or through water-column Fe sulphide precipitation. All reactive Fe that was available in the sediments was used for pyrite formation. As a result, diffusion of sulphide out of the sapropels, and sulphidisation of the sediments underlying each sapropel has occurred. Only in the most C_{org}-rich sapropel did large scale uptake of reduced S by organic molecules occur, and SO_4^{2-} reduction probably still continues.

3.1 Introduction

Bacterial SO_4^{2-} reduction is a common feature in organic-rich sediments in the marine environment (e.g. Canfield, 1989; Mossmann et al.,1991; Calvert and Karlin, 1991). It is part of the complex redox system related to the oxidation of organic matter (Froelich et al., 1979). The S enrichments in the recurrent organic-rich layers (sapropels) in the eastern Mediterranean prove that these have been subject to bacterial SO_4^{2-} reduction (van Os et al., 1991; Pruysers et al., 1993; Passier et al., 1996a/Chapter 2).

The sequence of alternating organic-rich and organic-poor layers in the sedimentary record of the eastern Mediterranean provides a unique setting to study the different paleo-environmental and diagenetic signals. During sapropel formation, bacterial SO_4^{2-} reduction dominated the anoxic sediment at the sediment/water interface, whereas the organic matter oxidation in underlying sediments was dominated by reduction of Fe (hydr)oxides. The classic downward succession of oxic, suboxic, and anoxic sediment (Froelich et al., 1979) does not apply to this dynamic system. Relicts of the different redox regimes can be found in the sediment column. For example, enrichments in reduced S species indicate episodes of SO_4^{2-} reduction, and Fe (hydr)oxide-enriched layers indicate boundaries of oxic and suboxic sediments (e.g. van Santvoort et al., 1996).

A striking feature is that most of the diagenetic alteration of eastern Mediterranean sediments takes place during and relatively shortly after their formation. Most diagenetic features

inferred from S and Fe chemistry of Pleistocene sapropels recovered by gravity-coring techniques are also present in the sediments in and around the most recent Holocene sapropel S1 (5-9 kyr) (Higgs et al., 1994; Passier et al., 1996a/Chapter 2; van Santvoort et al., 1996). In this study we compare the S and Fe chemistry of two sapropels of Pliocene age recovered during ODP Leg 160 with the most recent sapropel S1, to gain insight into the factors that determine the diagenetic history of these sapropels.

3.2 Materials and methods

Three sapropels were studied. Sapropel S1 in boxcore UM26 (33°23.6'N, 25°0.9'E, water depth 2160 m, Fig. 1.1) was recovered 200 km south of Crete during the 1994 *Palaeoflux* cruise of *Urania*. The sapropel, at about 0.24 metres below seafloor (mbsf), is 4 cm thick. Light grey sediments lie beneath the sapropel; orange-brown sediments lie above it. Part of UM26 was sampled at a resolution of 0.5 to 1 cm aboard ship inside an N_2-filled glovebox and stored under N_2 in airtight containers at 4°C.

Two sapropels, recovered during ODP Leg 160, were sampled in detail directly after core- splitting aboard *JOIDES Resolution*. One of the Leg 160 sapropels was recovered in section 160-969E-6H-6. Site 969E (33°50.5'N, 24°53.0'E, water depth 2201 m, Fig. 1.1) is located on the Mediterranean Ridge, close to the UM26 site. Hole 969E contains 80 sapropel beds of early Pliocene to Holocene age. The sampled interval contains a 12-cm-thick black sapropel at 50.7 mbsf (at 27 cm in the section), surrounded by light grey sediments. This sapropel (2.943 Ma, L. Lourens, personal communication) belongs to a group of black sapropels of Pliocene age with high organic C contents (up to 30%) in a grey interval. The dark sapropel has a fine bedding-parallel parting, which may be the result of primary lamination (Emeis, Robertson, Richter, et al., 1996). The other Leg 160 sapropel originates from section 160-967C-6H-2. Site 967C (34°4.3'N, 32°43.5'E, water depth 2553 m, Fig. 1.1) is located on a small ridge near the foot of the northern slope of the Eratosthenes Seamount, about 70 km south of Cyprus. At this site, 80 sapropels of early Pliocene to Holocene age were recovered. The sampled interval contains a 14-cm-thick sapropel at 49.3 mbsf (at 30 cm in the section). The sapropel is brownish black and surrounded by grey sediments. It is of Pliocene to Pleistocene age (1.808 Ma, L. Lourens, personal communication) and appears bioturbated. Ten samples 1.5 cm thick were taken over intervals of 50 and 30 cm in sections 967C-6H-2 and 969E-6H-6, respectively. The samples were stored under N_2 in airtight containers at 4°C.

Subsamples were dried at 40°C (UM26) or freeze-dried (Leg 160) and ground in an agate mortar before dissolution in an $HClO_4$-HNO_3-HF acid mixture. The dried residue was dissolved in 1 M HCl for analysis of total S (S_{tot}), total Fe (Fe_{tot}) and total Al (Al_{tot}) with a Perkin Elmer OPTIMA 3000 inductively coupled plasma atomic emission spectrometer (ICP-AES). Organic C contents were determined with a Fisons Instruments NA-1500 NCS analyser after removal of carbonate in 1 M HCl. S_{tot}, Fe_{tot}, Al_{tot}, and C_{org} measurements were performed according to standard laboratory procedures and have standard deviations < 5%. International and in-house standards were used to check the procedures.

Dried subsamples were extracted with acetone for several hours to remove elemental S (including elemental S formed during drying from AVS and organic polysulphides, and

elemental S originally present) before pyrite extraction. Pyrite S (S_{pyr}) was extracted with the Cr(II) reduction method (Zhabina and Volkov, 1978; Canfield et al., 1986; Cutter and Oatts, 1987; Henneke, 1993; Henneke et al., 1997). AVS (consisting of Fe monosulphides) was extracted from wet subsamples in 6 M HCl under an N_2 or Ar atmosphere. Sulphide that evolved in the pyrite and AVS extractions was stripped from reaction solutions with N_2 or Ar and trapped in 1 M NaOH. The NaOH solution was analysed for HS^- by square-wave voltammetry (SWV) with a Princeton Applied Research Model 384B-4 polarographic analyser system equipped with a Model 303A static mercury drop electrode (SMDE).

A sequential extraction procedure (Henneke, 1993; Henneke et al., 1997, based on Francois, 1987a, and Ferdelman et al., 1991) was applied to wet subsamples under an N_2 atmosphere. First, easily removable S (S_{NaCl}, mostly porewater S) was extracted by 0.5 M NaCl. Then, elemental S (S_{elem}; including low-molecular-weight organic S) was extracted by methanol:toluene (3:1); pure methanol was used for UM26. Subsequently, organic polysulphides (S_{orgpol}) were broken down to elemental S in 1 M HCl and extracted by methanol:toluene (3:1); pure methanol was used for UM26. After rinsing the sample with demineralized water, humic S (S_{NaOH}) was extracted by 0.5 M NaOH. Elemental-S-containing-extracts were evaporated and SO_3^{2-} was added to convert elemental S to $S_2O_3^{2-}$, which was determined by (cathodic stripping (CS)) SWV. NaCl and NaOH extracts were analysed for major elements by ICP-AES.

The residue of the sequential extraction was dissolved in an $HClO_4$-HNO_3-HF acid mixture, dried, and dissolved in 1 M HCl for analysis of S by ICP-AES. The residual phases of the sequential extraction are pyrite and non-extractable organic S.

The reproducibility of S species analyses appeared dependent of the content and the amount of material available for measurement. Reproducibility was poor for measurements of S_{orgpol} in samples from Leg 160 sapropels below 1-2 μmol/g dry, of S_{elem} in Leg 160 samples below 0.1-0.2 μmol/g dry, and of AVS in all samples below 0.01 μmol/gdry. These poorly reproducible data showed relative deviations from the mean of 40% to 145%. All other measurements were satisfactory reproducible. The average relative deviations from the mean in duplicate measurements were 10% for pyrite and AVS, 8% for residual S, 12% for S_{elem} and S_{orgpol}, 5% for S_{NaCl}, and 9% for S_{NaOH}.

Reactive Fe was extracted from wet subsamples in dithionite (acetate/citrate buffer, pH = 4.8, 4 h, 60°C) under an N_2 atmosphere following the procedure of Kostka and Luther (1994). Dithionite is thought to extract amorphous Fe (hydr)oxides, crystalline Fe (hydr)oxides, and AVS. The Fe concentration in the dithionite extracts was measured by ICP-AES and spectrophotometrically (Köster, 1979). The average relative deviation from the mean in duplicate measurements of reactive Fe was 10%.

The water contents of the samples were determined by differences in weight before and after drying.

3.3 Results

Sapropel samples are relatively rich in S and organic C (C_{org}) (Fig. 3.1, Table 3.1). The predominant S phase in and below each sapropel is S_{pyr} (Fig. 3.1, Table 3.1). Above sapropels, however, humic S (S_{NaOH}) and S_{NaCl} are the most important S species (Fig. 3.1, Table 3.1). The C_{org} contents of the three sapropels differ significantly: the maxima are 2.3, 7.4, and 23.5 wt% for the sapropel samples from core UM26, and sections 967C-6H-2, 30 cm, and 969E-6H-6, 27 cm, respectively. The C_{org} content in non-sapropel samples ranges from 0.1 wt% to 0.6 wt% (Fig. 3.1, Table 3.1).

S_{NaCl} is fairly constant in samples from core UM26 and section 967C-6H-2, 30 cm, and both cores have similar contents. At the bottom of the sapropel in section 969E-6H-6, 27 cm, however, the S_{NaCl} is 1 order of magnitude higher (Fig. 3.1, Table 3.1).

S_{NaOH} is enriched in all three sapropel layers: the maximum contents are 27, 71, and 121 µmol/g dry for sapropel samples UM26, 967C-6H-2, 30 cm, and 969E-6H-6, 27 cm, respectively (Fig. 3.1, Table 3.1). S_{NaOH} below the sapropels is slightly higher than above them. In the NaOH extraction a small amount of pyrite may be co-extracted. Deduced from the Fe contents of the humic extract, less than 15% of the S extracted by NaOH in pyrite-rich samples may be pyritic S. This is a maximum percentage, because Fe phases other than pyrite dissolve in 0.5 M NaOH as well.

The main residual S phases of the sequential extraction are pyrite and non-extractable organic S. In most samples, the amount of residual S of the sequential extraction is comparable to or slightly smaller than the amount of pyritic S. Minor losses may have occurred during the sequential extraction procedure. In 969E-6H-6, 27 cm, however, the residual S is larger than pyritic S (Fig. 3.2). Accordingly, non-extractable organic S may be present.
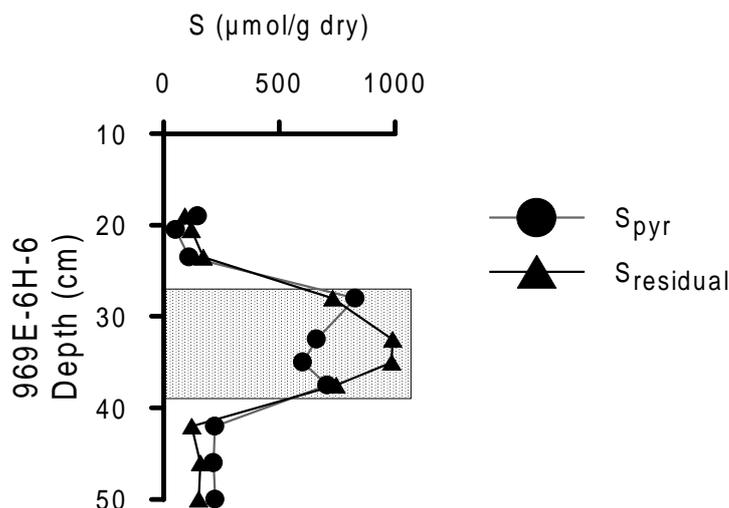

Figure 3.2 *Content vs. depth profiles of S_{pyr} (pyritic S determined by Cr(II)reduction) and $S_{residual}$ (residual amount of S of the sequential extraction) in section 969E-6H-6, 19-50 cm. The difference between the two species indicates the presence of non-extractable organic S. The shaded band indicates the position of the sapropel.*

S$_{elem}$ contents are smaller than 0.06 µmol/g dry in core UM26 and there is no apparent trend with depth. In contrast, S$_{elem}$ is enriched to 0.6 µmol/g dry in 967C-6H-2, 30 cm, and to 23 µmol/g dry in 969E-6H-6, 27 cm, and it correlates positively with the C$_{org}$ content (Fig. 3.1,
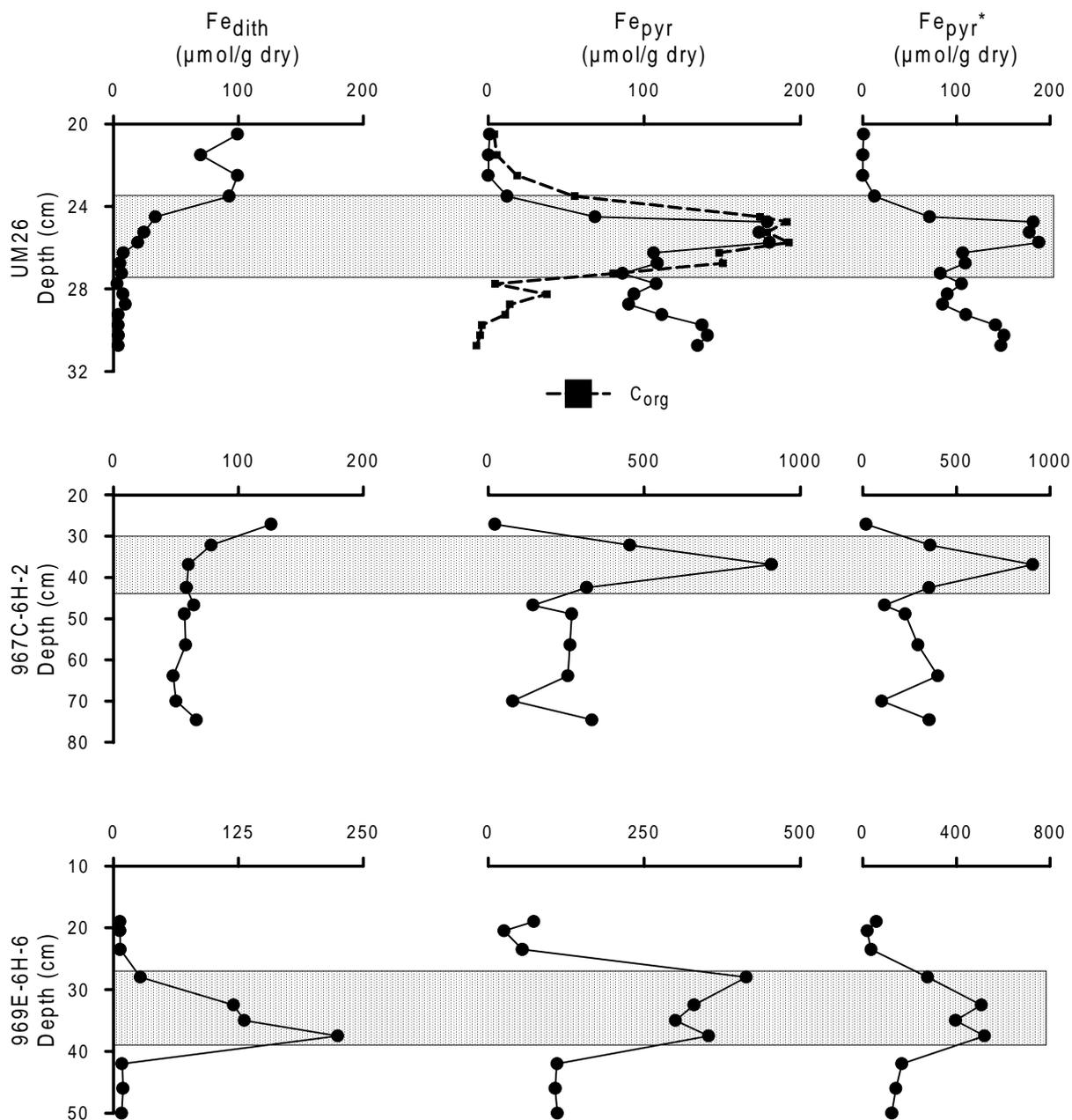
Figure 3.3 *Content vs. depth profiles of Fe$_{dith}$ (dithionite-extractable Fe), Fe$_{pyr}$ (0.5 × S$_{pyr}$, with S$_{pyr}$ determined by Cr(II) reduction), and Fe$_{pyr}$* (average Al$_{tot}$ × Fe$_{pyr}$/Al$_{tot}$ [normalisation to Al]) in core UM26, and sections 967C-6H-2, 26-75 cm, and 969E-6H-6, 19-50 cm. The shape of the C$_{org}$ profile in core UM26 is also included (for exact contents see Fig. 3.1). The shaded bands indicate the positions of the sapropels.*

Table 3.1). S_{orgpol} contents are smaller than 2 µmol/g dry in 967C-6H-2, 30 cm, and core UM26, and there is no noticeable trend with depth. In 969E-6H-6, 27 cm, though, the S_{orgpol} content correlates positively with the C_{org} content and is 4.3 µmol/g dry at maximum (Fig. 3.1, Table 3.1). AVS contents are low: 0 to 0.4 µmol/g dry in core UM26, 0.03 to 0.9 µmol/g dry in 967C-6H-2, 30cm, and 0.02 to 0.7 µmol/g dry in 969E-6H-6, 27 cm (Fig. 3.1, Table 3.1). AVS contents in samples from sapropel S1 measured directly aboard after sampling inside an N_2-filled glovebox were in the same range.

Because the AVS contents are relatively small, all dithionite-extractable Fe may be considered to represent Fe (hydr)oxides. Iron (hydr)oxides (Fe_{dith}, Fig. 3.3, Table 3.1) are relatively enriched above the sapropels in section 967C-6H-2, 30 cm and in core UM26, and at the base of the sapropel in section 969E-6H-6, 27 cm.

Independently determined total S contents (S_{tot}, Fig. 3.1, Table 3.1) compare well with the sum of all S species recovered in the sequential extraction (Table 3.2).

Table 3.2 *Comparison between the total S content of the sediments and S_{sum} (the sum of the S species measured in the sequential extraction, including residual S).*

Samples	Total sulphur (µmol/g dry)	S_{sum} (µmol/g dry)	Yield (%)
S1, UM26			
Above	56.6	46.4	82
Within	281.2	227.5	81
Below	256.1	178.1	70
967C-6H-2, 30 cm			
Above	53.7	49.9	93
Within	1079.1	986.1	91
Below	368.2	344.2	93
969E-6H-6, 27 cm			
Above	216.3	192.9	89
Within	1256.2	1164.3	93
Below	282.8	245.3	87

Note: the values are averages of samples grouped according to position
relative to sapropel.

3.4 Discussion

3.4.1 Sulphur species

3.4.1.1 NaCl-extractable S

In view of the good correlation with the water content (Fig. 3.4), the NaCl-extracted S is largely attributable to porewater SO_4^{2-}. The average porewater SO_4^{2-} concentration, calculated from the water contents and S_{NaCl}, is 34 mM (standard deviation 4%), without any trend with
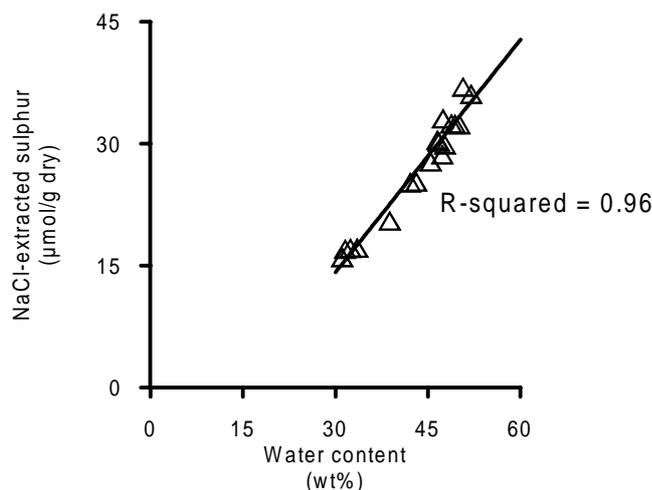

**Figure 3.4** *NaCl-extracted S vs. water content in core UM26.*

depth. This is close to the concentration of SO_4^{2-} in Mediterranean seawater (32 mM). The water contents of the Leg 160 samples could not be accurately determined, as the samples had been subject to evaporation aboard ship. Compared to the S_{NaCl} values of core UM26 and to the SO_4^{2-} porewater concentration measured aboard (Sites 969 and 967, at 50 mbsf: 32 mM), S_{NaCl} in 967C-6H-2, 30 cm, can entirely be attributed to porewater SO_4^{2-}. At the bottom of the sapropel in section 969E-6H-6, 27 cm, however, the amount of S_{NaCl} is excessive compared with porewater SO_4^{2-}. A tentative conclusion (see following discussion) from the 1:1 ratio of Ca and S in the NaCl extracts of section 969E-6H-6, 27 cm (Fig. 3.5) is that this enrichment is probably gypsum ($CaSO_4.2H_2O$). There is no correlation between S and Ba, K, Sr, and Fe in the NaCl extracts of section 969E-6H-6, 27 cm.

3.4.1.2 Organic polysulphide S, elemental S, and AVS

Insignificant amounts of AVS, S_{elem} and S_{orgpol}, all of which are possible intermediates in pyrite formation (e.g. Luther and Church, 1992) were found in core UM26 (Fig. 3.1). Because long-term accumulation of intermediate species is not likely in these marine sediments, the intermediates are indicators for active SO_4^{2-} reduction. This indicates that no substantial SO_4^{2-} reduction and no pyrite formation presently occur in these sediment. The contents of S_{orgpol} and S_{elem} in 969E-6H-6, 27 cm, and S_{elem} in 967C-6H-2, 30 cm, correlate with the C_{org} contents (Fig. 3.1). These enrichments have formed at places where the sulphide concentrations were high, resulting from in situ SO_4^{2-} reduction, within the sapropel. Elemental S forms from partial

oxidation of sulphide, and organic polysulphides form by incorporation of sulphide in organic matter. The contents of AVS, elemental S and organic polysulphide S are in general higher in 969c#6H06, 27 cm, and 967e#6H02, 30 cm, than they are in core UM26, albeit they are still at relatively low levels. This indicates that relatively more SO_4^{2-} reduction occurs, although still at a low level, at present in the older sapropels than in the youngest sapropel. In addition, low-molecular-weight organic S compounds are included in S_{elem}; these compounds may be significantly present in the sapropel in section 969c#6H06, 27 cm.

A remarkable feature is the enrichment of NaCl-extractable S, probably gypsum (see following discussion), at the base of the sapropel in section 969c#6H06, 30 cm (Fig. 3.1). This presumed gypsum enrichment is associated with an enrichment of Fe (hydr)oxides (Fe_{dith}, Fig. 3.3), indicating possible oxidation of Fe sulphides within the sapropel layer. The oxidation is most likely the result of oxygen contamination during or after sampling. The Fe sulphides prone to rapid oxidation are Fe monosulphides. Gypsum may be formed as a consequence of oxidation of Fe monosulphides (FeS_x, in which x is close to 1) and dissolution of carbonate tests, according to the following reaction:

$$4FeS_x + (3 + 6x)O_2 + (2 + 12x)H_2O + 8xCaCO_3$$
$$4FeOOH + 4xCaSO_4.2H_2O + 4xCa^{2+} + 8xHCO_3^-. \qquad (1)$$
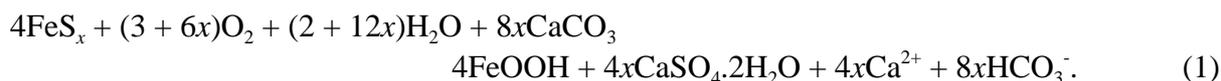
The ratio of Fe (hydr)oxide to SO_4^{2-} in gypsum is $4:4x = 1:x$. Assuming that all SO_4^{2-} is extracted with NaCl, the 1:x ratio can be obtained from the ratio of excess dithionite-extracted Fe to excess NaCl-extracted S. The observed ratio is 1:1.07 (Fig. 3.6), which yields a mean formula for Fe sulphide of $Fe_{0.93}S$. This corresponds to a mixture of mackinawite ($Fe_{0.995-1.023}S$, Ward, 1970) and greigite ($Fe_{0.75}S$), which is the most common association of Fe monosulphide minerals found in sediments (Berner, 1967). Moreover, shipboard paleomagnetic measurements of three discrete samples taken immediately after core-splitting from the base of the sapropel in section 969E-6H-6, 27 cm, show a reduction in both magnetic remanence and susceptibility with time. The time-
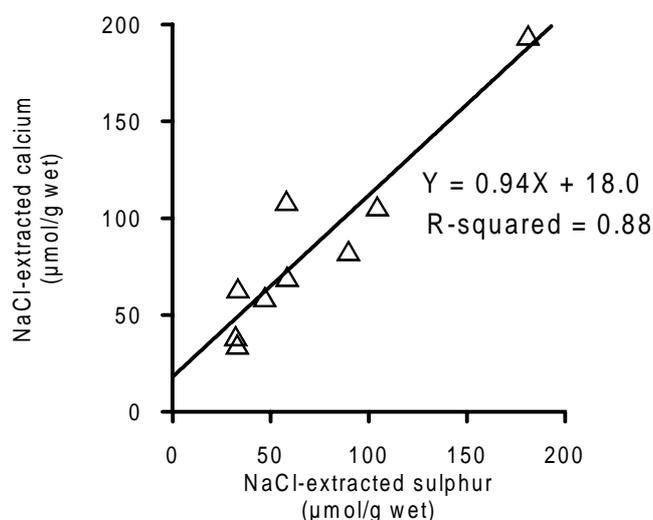

Figure 3.5 *NaCl-extracted calcium vs. NaCl-extracted S in section 969#6H06, 19-50 cm.*
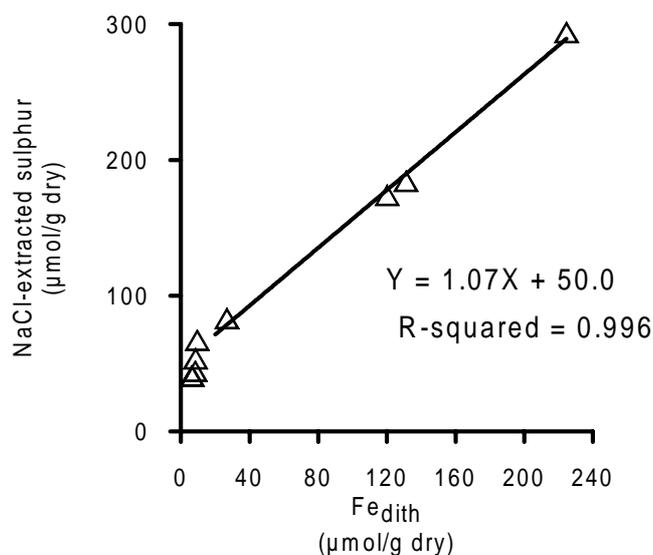
Figure 3.6 *NaCl-extracted S vs. Fe$_{dith}$ (dithionite extracted Fe) in section 969#6H06, 19-50 cm.*

dependent decay in magnetic properties (10%/day) is consistent with oxidation of a metastable ferrimagnetic Fe sulphide (Roberts et al., 199_).

Oxidation of Fe monosulphides results in the addition of Ca^{2+} and SO_4^{2-} to the sediment samples and interstitial waters. Ca^{2+} and SO_4^{2-}, which cannot have escaped by diffusion because the cores were sampled within a few hours after core-splitting, and the samples are isolated in vials, will be extracted with NaCl. On the basis of reaction (1) one would expect to find a ratio of Ca^{2+}: $SO_4^{2-} = (4x + 4x):4x = 2:1$ in these NaCl extracts. Nonetheless, the amount of Ca^{2+} that dissolves will be controlled by the dynamic equilibria of the carbonate system and not just by the stoichiometry of reaction (1). Therefore, detailed mass balance calculations were performed. These calculations predict a linear correlation between Ca^{2+} and SO_4^{2-} in NaCl extracts with a slope of 1 (i.e., Ca^{2+}: $SO_4^{2-} = 1:1$; see Appendix). In fact, the correlation between Ca^{2+} and SO_4^{2-} in NaCl extracts of the sapropel in section 969E-6H-6, 27 cm, has a slope of 0.94 (i.e., Ca^{2+}: SO_4^{2-} 1:1; Fig. 3.5). Hence, the observed correlation between Ca^{2+} and SO_4^{2-} are most likely due to the oxidation of Fe monosulphides.

Summarizing, the Fe (hydr)oxide and S_{NaCl} enrichments at the base of the sapropel in section 969E-6H-6, 27 cm, indicate the original presence of Fe monosulphides (FeS$_{1.07}$, AVS). This appearance of AVS indicates that active SO_4^{2-} reduction may still occur within this sapropel. SO_4^{2-} reduction either never stopped inside this extremely C_{org}-rich layer or started again after some time. Assuming that porewater data for Hole 969A are comparable to those of Hole 969E, the porewater profile of SO_4^{2-} indicates that SO_4^{2-} reduction may only take place at very low rates (Emeis, Robertson, Richter, et al., 1996).

3.4.1.3 Pyritic S, humic S, and non-extractable organic S

Most of the sulphide that was formed in the sapropel and retained in the sediment has reacted with Fe, and formed pyrite in and below the sapropel (Fig. 3.1), whereas another portion of the sulphide was incorporated in organic matter. The uptake of reduced S in organic matter

results in the fractions humic S (S_{NaOH}, Fig. 3.1) and non-extractable organic S (deduced from the residual fraction of the sequential extraction). Only in the central part of the sapropel in section 969E-6H-6, 27 cm, non-extractable organic S is detectable. In sediments with low reactive Fe contents, reduced S may be incorporated in the organic fraction of the sediments during early diagenesis (e.g. Sinninghe Damsté and de Leeuw, 1990).

The main S compound below each sapropel is pyrite. The pyrite has been formed as a result of downward diffusion of HS^- from the sapropel during formation of the sapropel (Passier et al., 1996a/Chapter 2). Most of the sulphide that diffused to below the sapropel has reacted with Fe (hydr)oxides in the underlying sediments or with upward-diffusing Fe^{2+}. Sediments below the sapropels, however, are also enriched in humic S (S_{NaOH}, Fig. 3.1) as compared with sediments above the sapropels. This implies that the humic substances below the sapropels may have incorporated S, during the downward diffusion of HS^-.

3.4.2 Storage of reduced S and Fe
3.4.2.1 Carbon-sulphur relationships

The C_{org} content of the sapropels differs significantly. The 23.5 wt% C_{org} found in the sapropel in section 969E-6H-6, 27 cm, is among the highest found in eastern Mediterranean sediments (Emeis, Robertson, Richter, et al., 1996). The amount of reduced S in sediments is closely related to the C_{org} content. This is due to the fact that with increasing amounts of C_{org} a larger amount of organic matter is metabolizable and more sulphide is produced (e.g. Berner and Raiswell, 1983; Berner, 1984; Leventhal, 1987). In normal marine sediments the relation between S and C contents has a slope of 1/2.8 (S_{tot}/C_{org} ratio, wt%/wt%) and passes through the origin (assuming that S fractions other than reduced S are relatively negligible). In euxinic marine environments, however, sulphide is omnipresent (independent of local C_{org} contents) and Fe sulphide formation can take place in the water column or at the sediment/water interface. In addition, even slowly reacting Fe compounds may react with sulphide in euxinic environments. Consequently, positive intercepts on the S axis are obtained in S vs. C plots for euxinic sediments, and only weak correlations may be observed (e.g. Leventhal, 1983; Berner, 1984). Additionally, postdepositional sulphidisation of C_{org}-poor sediments may result in extremely high S/C ratios (Boesen and Postma, 1988; Middelburg, 1991; Leventhal, 1995; Passier et al., 1996a/Chapter 2).

In S_{tot} vs. C_{org} plots of the discussed sapropels (Fig. 3.7), most samples plot above the normal marine regression line, pointing to euxinic features and postdepositional sulphidisation of C_{org} -poor sediments below the sapropels (Passier et al., 1996a/Chapter 2). The samples with extremely high C_{org} values from the sapropel in section 969E-6H-6, 27 cm, however, plot below the normal marine line. Reduced S formation and/or uptake in the sediment seems more limited for this part of the sapropel. There are several factors that determine the S content of sediments in which S is predominantly pyrite. Sulphate reduction and subsequent pyrite formation can be limited by (1) the availability of SO_4^{2-}, (2) amount and reactivity of organic matter, and (3) content and reactivity of Fe minerals (e.g. Berner, 1984).
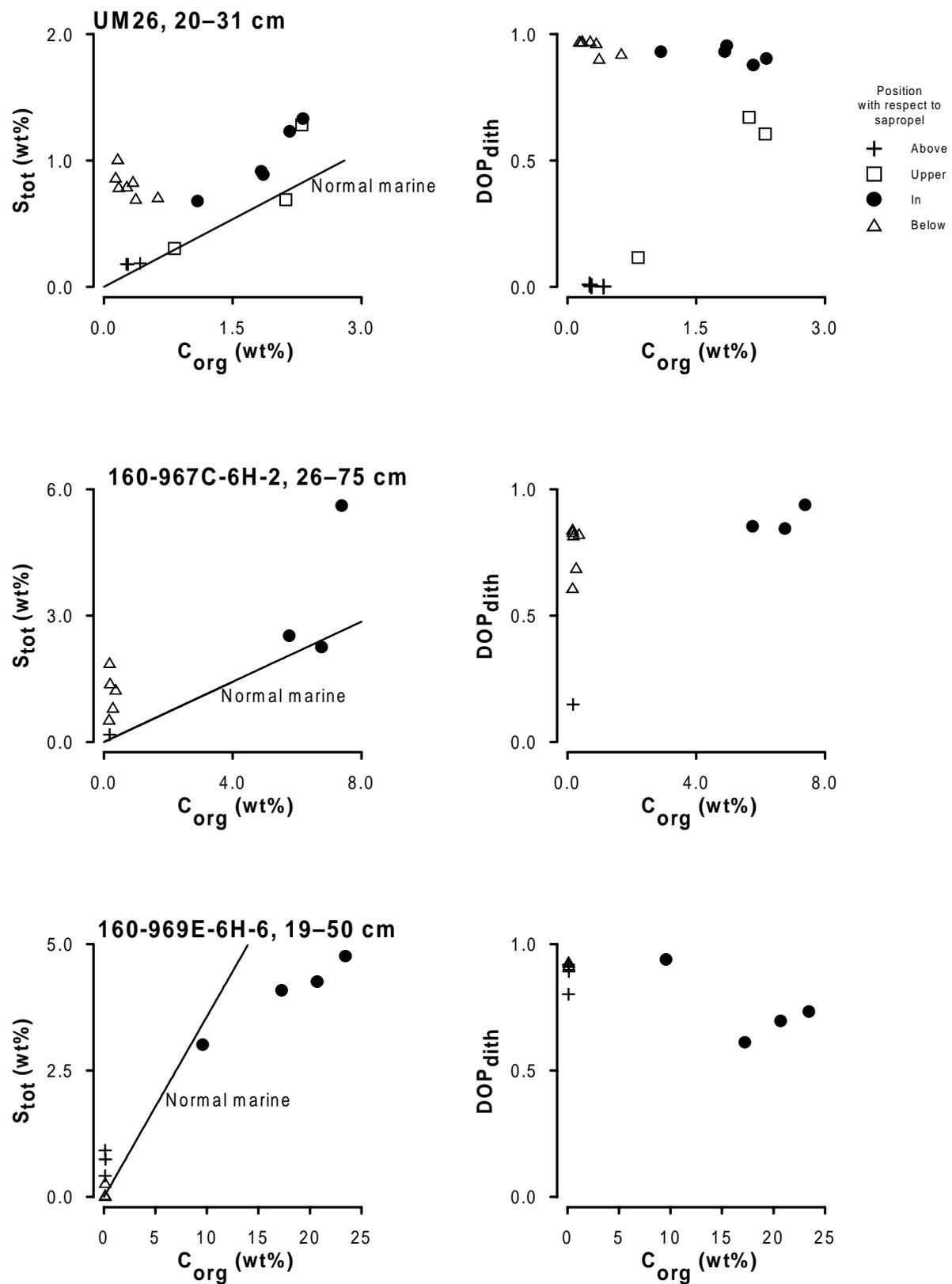
Figure 3.7 *S_{tot} and DOP_{dith} vs. C_{org} in core UM26, 20-31 cm, and sections 967C-6H-2, 26-75 cm, and 969E-6H-6, 19-50 cm.*

Availability of SO$_4^{2-}$–The first factor, the availability of SO$_4^{2-}$, is neither the limiting factor in the marine environment where sapropels are formed nor in the present-day interstitial waters of the eastern Mediterranean. Most of the porewater profiles of SO$_4^{2-}$ in the eastern Mediterranean demonstrate a downward increase owing to the dissolution of underlying evaporites, like the profiles at Sites 967 and 969 (Emeis, Robertson, Richter, et al., 1996). Preliminary S isotope data and other sedimentary data show that the SO$_4^{2-}$ concentration was not limiting for sulphide formation in the past either.

Reactivity of organic matter–The second factor, the availability of metabolizable organic matter, may be important in the sapropels. Apparently, the organic matter left over after intensive remineralisation during and shortly after sapropel formation is no longer sufficiently labile to sustain a SO$_4^{2-}$-reducing environment in most of the sapropels.

   Furthermore, the relatively low S content in the organic-rich samples of section 969E-6H-6, 27 cm (Fig. 3.7), may be in part related to a lower reactivity of the organic matter. The humic S and non-extractable organic S contents in section 969E-6H-6, 27 cm, are relatively high. Because of the incorporation of S into organic substances, organic matter may become less labile (e.g. Sinninghe Damsté and de Leeuw, 1990). However, the C$_{org}$ content is much higher in section 969E-6H-6, 27 cm, than in section 967C-6H-2, 30 cm, and core UM26. Therefore, it seems unlikely that the uptake of S into organic compounds has significantly affected the total reactivity of organic matter, and thus its reactivity for SO$_4^{2-}$ reduction.

   In summary, it seems that the reactivity of organic matter is presently limiting SO$_4^{2-}$ reduction and pyrite formation in most sapropels, but the reason for this is not clear. The mechanisms that determined the extent of pyrite formation in each sapropel during the periods that SO$_4^{2-}$ reduction was not limited by the reactivity of the organic matter, are discussed subsequently.

Content and reactivity of Fe minerals–The third limiting factor for pyrite formation, the availability of Fe, is usually inferred from plots of the degree of pyritisation (*DOP*) vs. C$_{org}$ (Raiswell and Berner, 1985). The parameter *DOP* was proposed by Berner (1970):

$$DOP \quad \frac{pyritic\ Fe}{pyritic\ Fe \quad reactive\ Fe}\ .$$

We have taken reactive Fe as equal to dithionite-extractable Fe, as recommended by Raiswell et al. (1994); *DOP* values based on dithionite-extractable Fe are *DOP*$_{dith}$ values.

   The high *DOP*$_{dith}$ values inside the sapropels, independent of C$_{org}$ content, suggest that pyrite formation in the sapropels was Fe-limited (Fig. 3.7). However, as we explain later, the observed *DOP*$_{dith}$ values indicate only that all Fe that was supplied to the sediment was stored as pyrite.

   Slightly lower *DOP*$_{dith}$ values are found for the C$_{org}$-rich samples at the base of the sapropel in section 969E-6H-6, 27 cm. These deviations are artificial, and they originate from the Fe (hydr)oxide enrichment that formed as a result of Fe sulphide oxidation, as discussed

earlier (Fig. 3.3). If the oxidized S had diffused out of the system, this would have evoked a deviation in the S_{tot} vs. C_{org} plot toward the C_{org} axis. Assuming that all oxidized S has been retained in the sediment as gypsum, oxidation of Fe sulphides does not influence the S_{tot} vs. C_{org} plot. Consequently, the relatively low S/C ratios in the C_{org}-rich part of section 969E-6H-6, 27 cm, cannot be explained by this oxidation.

High DOP_{dith} values and high S/C ratios are acquired in C_{org}-poor sediments below the sapropels, as a result of postdepositional sulphidisation (Fig. 3.7). This sulphidisation developed as soon as the sulphide production exceeded the Fe availability for pyrite formation in the sapropel (Passier et al., 1996a/Chapter 2). In core UM26 and section 967C-6H-2, 30 cm, this sulphidisation has affected only the sediments underlying the sapropels and not the overlying sediments. This indicates that only small amounts of HS^- may have diffused out of the C_{org}-rich layers after sapropel formation. In section 969E-6H-6, 27 cm, however, DOP_{dith} values and pyrite contents of the sediments overlying the sapropel are slightly higher than above the other sapropels (Fig. 3.7). Probably postdepositional or syndepositional sulphidisation of the sediments overlying the sapropel in 969E-6H-6, 27 cm, has occurred. It is not clear from these data whether the sulphide source is upward sulphidisation from the sapropel in section 969E-6H-6, 27 cm, or downward HS^- diffusion from a younger sapropel.

Relatively low DOP_{dith} values at low C_{org}-contents are found above the sapropels in core UM26 and section 967C-6H-2, 30 cm. In the eastern Mediterranean, sapropel formation is usually followed by a period of downward oxidation of the sediment. C_{org} and pyrite are oxidized at the oxidation front, and the front is marked by an Fe (hydr)oxide enrichment (de Lange et al., 1989; Pruysers et al., 1993; van Santvoort et al., 1996). Above the sapropels in core UM26 and section 967C-6H-2, 30 cm, such enrichments of Fe (hydr)oxides are present (Fig. 3.3). The Fe enrichment above sapropel S1 in core UM26 indicates active oxidation of the sapropel (van Santvoort et al., 1996), whereas the Fe enrichment above section 967C-6H-2, 30 cm, is thought to be the relict of such a front. No Fe (hydr)oxide enrichment is present above section 969E-6H-6, 27 cm. Either an oxidation front has never been present above this sapropel or any oxidized Fe has subsequently been reduced and diffused out of the sediment. It could have been used for pyrite formation elsewhere in the sediment or reacted to pyrite in situ. Accordingly, sediments above section 969E-6H-6, 27 cm, do not have anomalously low DOP_{dith} values and the low DOP_{dith} values above the other two sapropels are caused by oxidation of pyrite and C_{org} and the precipitation of Fe (hydr)oxides. The high-resolution samples from core UM26 (Fig. 3.3) show that the Fe (hydr)oxide-layer "invades" into the top of sapropel S1; this means that pyrite is more readily oxidized than C_{org}. Consequently, the sediments from this upper sapropel region have relatively low DOP_{dith} values at relatively high C_{org} contents. Although the oxidation of pyrite results in SO_4^{2-} formation (Moses et al., 1987), the oxidation at the oxidation front has not led to an enrichment of SO_4^{2-} (S_{NaCl}, Fig. 3.1) above the sapropels. This indicates that the oxidation is a slow process relative to diffusion of oxidized species away from the front.

The DOP_{dith} values lead to the conclusion that the availability of Fe has been controlling the amount of pyrite stored within the sapropels. In the next section, we discuss the mechanisms that rule the storage of pyrite in the different sapropels in more detail.

3.4.2.2 Iron source, mobility and fixation

Iron enrichments Iron (hydr)oxides are not depleted in the sapropels relatively to the underlying sediments (Fig. 3.3), although the sulphide concentration must have been higher inside the sapropels (sulphide source) than in the underlying sediments, where sulphide has diffused. In addition, DOP_{dith} values and (Al-normalized) silicate Fe contents ($Fe_{silicate} = Fe_{tot} - Fe_{pyr} - Fe_{dith}$, and $Fe_{silicate}* = $ average $Al_{tot} \times Fe_{silicate}/Al_{tot}$) within the sapropels are as high as those below the sapropels (Fig. 3.7, Table 3.3). This indicates that Fe from slowly reacting Fe-bearing silicates has not been detectably used as an extra source for pyrite formation inside the sapropel, where all reactive Fe was incorporated in pyrite. If Fe from silicates were used more extensively within the sapropel, $Fe_{silicate}$ would have been lower and DOP_{dith} values would have been higher within the sapropel. The pyrite enrichments are not due to any sedimentary dilution effect, as follows from normalisation to Al content (Fig. 3.3). As a consequence, because more pyrite has formed within than below the sapropels, there must have been an additional input of Fe to the sapropel sediment.

Table 3.3 *Range of contents of $Fe_{silicate}$ (= Fe_{tot} - Fe_{pyr} - Fe_{dith}) and $Fe_{silicate}*$ (= average $Al_{tot} \times Fe_{silicate}/Al_{tot}$).*

Samples	$Fe_{silicate}$ (µmol/g dry)	$Fe_{silicate}*$ (µmol/g dry)
S1, UM26		
Within	247 265	255 265
Below	212 259	220 254
160 967C 6H 2, 30 cm		
Within	328 421	333 368
Below	229 456	281 698
160 969E 6H 6, 27 cm		
Within	107 379	158 543
Below	180 551	202 727

Note: the values are grouped according to position
relative to sapropel.

Iron-C_{org} relationships In a plot of the sum of pyritic Fe and dithionite-extractable Fe vs. C_{org} in the sapropel samples, two groups of data points appear (Fig. 3.8). It is not important for the interpretation whether $Fe_{pyr} + Fe_{dith}$ or just Fe_{pyr} is used (Fig. 3.8). To study the limits of pyrite formation, we used a plot of Fe_{pyr} vs. C_{org} instead of S_{tot} vs. C_{org} because organic S is also included in S_{tot}. The first group of data points is situated at relatively low C_{org} contents, including samples from core UM26 and section 967C-6H-2, 30 cm; and the second group at relatively high

C_{org} contents represents section 969E-6H-6, 27 cm (Fig. 3.8). Sedimentary dilution may be an

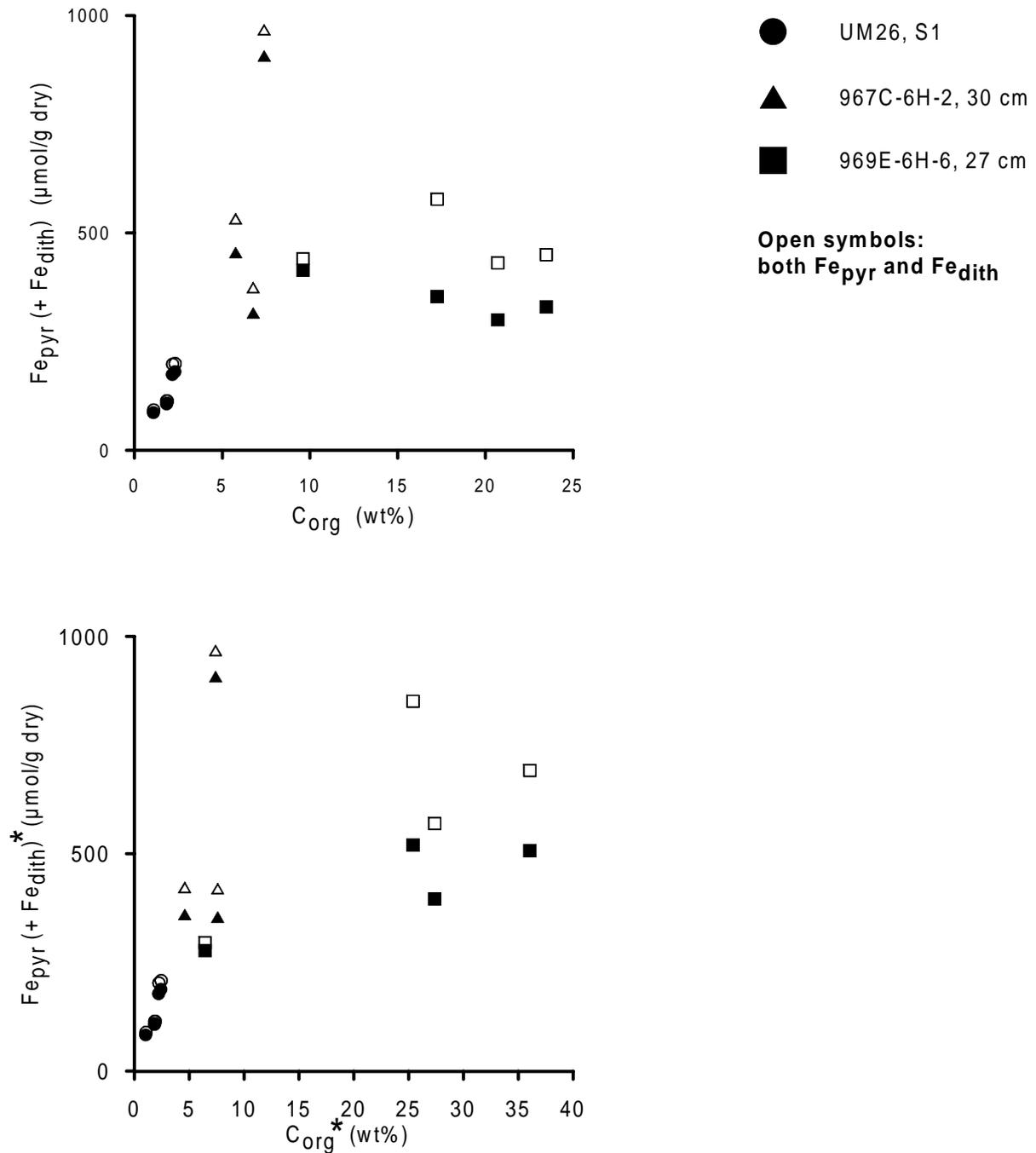**Figure 3.8** *Fe_{pyr} (+ Fe_{dith}) vs. C_{org} in sapropel samples from core UM26, and sections 967C-6H-2, 26-75 cm, and 969-6H-6, 19-50 cm. $Fe_{pyr} = 0.5 \times S_{pyr}$, S_{pyr} is determined by Cr(II) reduction, and Fe_{dith} is dithionite-extractable Fe. Asterisks indicate that the data have been normalized to Al content, for example: $C_{org}* = average\ Al_{tot} \times C_{org}/Al_{tot}$.*

important factor in the interpretation of enrichments in sediments. Therefore, the data were normalized with respect to Al_{tot}, assuming that Al to the sediment have remained constant. Plots of Al-normalized values of Fe_{pyr} (+ Fe_{dith}) vs. Al-normalized values of C_{org} yield the same general distinction between samples from core UM 26 and section 967C-6H-2, 30 cm, on one hand and samples from section 969E-6H-6, 27 cm, on the other (Fig. 3.8). The uppermost sample, with the lowest C_{org} content, from the sapropel in section 969E-6H-6, 27 cm, is separated from the C_{org}-rich samples of this sapropel, and plots in the same area as samples from core UM26 and section 967C-6H-2, 30 cm. For the first group a positive correlation between C_{org} contents and Fe is discernable. The second group has a lower Fe content, relative to C_{org}, and the Fe content is independent of C_{org}.

Positive correlations between C_{org} and the sum of pyritic and reactive Fe have been observed in previous studies of organic-rich sediments (Raiswell and Berner, 1985; Raiswell and Al-Biatty, 1989). This correlation may be either a diagenetic or a depositional feature.
The input of detrital Fe to sediments may vary as a result of climate-related changes in weathering and erosion (Raiswell and Al-Biatty, 1989). However, the most extremely C_{org}-rich sapropel (section 969E-6H-6, 27 cm), which is probably related to the most extreme climate changes, contains relatively little amounts of Fe (Figs. 3.3 and 3.8). Accordingly, an increase in detrital Fe input does not seem to be an important additional Fe source during sapropel formation. Assuming that the input of detrital reactive Fe is constant, there are two additional sources of Fe during sapropel formation: (1) diffusion of Fe^{2+} from the underlying sediment to the sediment/water interface and (2) Fe sulphide formation from dissolved Fe^{2+} and sulphide in the water column.

In these situations the supply of Fe may be coupled to the C_{org} content via sulphide production. Positive Fe vs. C_{org} correlations indicate that more SO_4^{2-} reduction has occurred and more pyrite has formed because more C_{org} is present. The mechanisms of pyrite enrichment and the correlation to the C_{org} content are discussed below.

Iron addition via diffusion from underlying sediments A mechanism to explain the addition of Fe and coupling between Fe and C_{org} is that upward-diffusing Fe^{2+} is used for pyrite formation within the sapropel at times of relatively low sulphide production. Any diffusing Fe^{2+} that is not scavenged by pyrite formation in the sapropel may be oxidized near the sediment/water interface or may escape into the water column. In sediments with a higher C_{org} content, more metabolizable organic matter was originally present. Consequently, more SO_4^{2-} reduction and fixation of sulphide as pyrite was possible, leading to a positive correlation between Fe_{pyr} and C_{org}. In this situation, sulphide production, and thus indirectly the reactivity of organic matter toward SO_4^{2-} reduction determines the extent of pyrite formation, and sulphide consumes all available Fe. The fixation of upward-diffusing Fe^{2+} as pyrite within the sapropel is possible only when the sulphide production is relatively small. When sulphide production is larger than the sum of the upward Fe^{2+} flux and detrital reactive Fe input, sulphide will diffuse out of the sapropel and will meet upward-diffusing Fe^{2+} below it. Pyrite formation takes place below the sapropel, and the upward Fe^{2+} flux does not reach the sapropel. In that case, pyrite formation within the sapropel is limited by the amount of detrital reactive Fe.

For sapropel S1, recent porewater fluxes of Fe^{2+} have been compared to the amount of Fe fixed as pyrite within and below the sapropel (Passier et al., 1997/Chapter 4). This comparison indicates that upward diffusion of Fe^{2+} during sapropel formation and detrital Fe combined could have supplied all fixed Fe. Similar calculations for older sapropels are difficult, because Fe^{2+} fluxes, detrital Fe inputs, and duration of periods of sapropel formation are not known.

The amounts of Fe fixed as pyrite in sections 967C-6H-2, 30 cm and 969E-6H-6, 27 cm, are higher than in core UM26 (Fig. 3.8). Preliminary S isotope measurements indicate that pyrite formation was probably not significant after burial of the sapropels. A similar conclusion was drawn for Pleistocene and Holocene sapropels (Passier et al., 1996a/Chapter 2; Passier et al., 1997/Chapter 4). Hence, significant Fe addition via diffusion from underlying sediments probably also stopped after burial, with the possible exception of the Fe fixed as AVS and maybe some of the pyrite at the base of the sapropel in section 969E-6H-6, 27 cm. The larger fixation of Fe in sections 967C-6H-2, 30 cm, and 969E-6H-6, 27 cm, compared with core UM26 may also arise from a larger input of detrital reactive Fe and/or a larger upward flux of Fe^{2+}. Within and below the sapropel in section 967C-6H-2, 30 cm, Fe_{dith} is higher than within and below the other sapropels (Fig. 3.3). This site is close to Cyprus, consequently, the detrital input and flux of Fe^{2+} may have been larger here. However, there is no reason to assume a larger detrital Fe input in section 969E-6H-6, 27 cm, than in core UM26, as the sites are close to each other. In addition, Fe and C_{org} are not coupled in section 969E-6H-6, 27 cm. Moreover, it was argued previously that the input of detrital Fe did not increase significantly during sapropel formation. The scenario described here (i.e., pyrite enrichment via addition of upward-diffusing Fe^{2+}) may yield only an uncoupled Fe and C_{org} situation in the sapropel when downward sulphidisation occurs: in this case, detrital reactive Fe is the only available Fe for pyrite formation, and the absolute pyrite enrichment in this sapropel cannot be explained. Another mechanism of pyrite formation seems to be important in the sapropel in section 969E-6H-6, 27 cm, which is discussed in the following.

Iron addition via Fe sulphide formation in the water column Iron addition may also arise from the precipitation of Fe sulphides in a euxinic water column. This mechanism was recently proposed for the Black Sea, where a large part of the water column contains sulphide and Fe may be liberated from sediments in suboxic zones along the basin margins (Canfield et al., 1996). This process may result in the coupling of Fe and C_{org}: the more C_{org} rains down, the more sulphide will be present in the water column, and the more Fe sulphides can precipitate in the water column, thus inducing a positive correlation between C_{org} and Fe_{pyr} in the sediment. However, the water-column Fe sulphide that is added to the sediments in euxinic basins is usually independent of the C_{org} content, because sulphide is omnipresent and not necessarily related to the local C_{org} content. In addition, the amount of Fe sulphide that is formed in the water column may be limited by the thickness of the sulphidic layer in the water column (e.g. Leventhal, 1983 and 1987). In the sapropel in section 969E-6H-6, 27 cm, Fe_{pyr} (+Fe_{dith}) is higher within the sapropel than below the sapropel and independent of the C_{org} content (Fig. 3.8). Thus, addition of Fe from the water column may have resulted in the relative pyrite enrichment inside

the sapropel in section 969E-6H-6, 27 cm. No coupling of Fe and C_{org} is visible; so, no significant pyrite was formed from upward-diffusing Fe^{2+} in the sapropel. Apparently, upward-diffusing Fe^{2+} could not reach the sapropel because downward sulphidisation occurred permanently during sapropel formation, implying a constantly high sulphide production. This observation is in agreement with the occurrence of Fe sulphide formation in the water column, and the implicit presence of sulphide in the bottomwater: when downward sulphide diffusion occurs out of a sapropel, sulphide is also expected to diffuse upward to the bottomwater. Sulphide may be oxidized at the sediment/water interface or in the bottomwater, but when the sulphide flux is relatively large, sulphidic bottomwaters may develop. Furthermore, when downward sulphidisation takes place, pyrite formation within the sapropel is Fe-limited and uptake of S in organic substances may be important (e.g. Sinninghe Damsté and de Leeuw, 1990). Hence, the presence of high amounts of organic S in section 969E-6H-6, 27 cm, can be explained.

3.4.2.3 Consequences of the imbalance between sulphide production and addition of Fe

In summary, in these sediments with predominantly syngenetic pyrite, the absence or presence of a positive correlation between Fe_{pyr} (+ Fe_{dith}) and C_{org} may indicate the site of pyrite formation: in the water column (absence of correlation) or at the sediment/water interface (positive correlation).

Because mechanisms such as sulphidisation of adjacent sediments and Fe addition to the sediments are possible in the alternating C_{org}-rich and C_{org}-poor sediments in the eastern Mediterranean, the site of SO_4^{2-} reduction does not necessarily coincide with the location of pyrite formation. Although Fe sulphide formation may be (temporarily) limited within a sapropel, sulphide production within this layer may result in the formation of Fe sulphides in the water column or below the sapropel. As the sulphidisation of organic-poor sediments below sapropels invokes high S/C ratios, the sediments from where the S originates will have lower S/C ratios when sulphide diffuses out of the source sediment (sapropel). Downward sulphidisation has been important during the formation of the sapropel in section 969E-6H-6, 27 cm, as a result of the extremely high C_{org} content. This may explain the apparent S deficiency in these sediments (Fig. 3.7). In contrast, as long as downward sulphidisation does not occur, the supply of Fe^{2+} to the sapropel results in a higher fixation capacity for sulphide within the sapropels, and thus in higher S_{tot} contents. This is expressed by the fact that many sapropel samples lie far above the normal marine regression line in S_{tot} vs. C_{org} plots (e.g. section 967C-6H-2, 30 cm and core UM26, Fig. 3.7).

3.5 Conclusions

The elevated C_{org} contents of sapropels have induced anoxic, SO_4^{2-}-reducing sedimentary conditions and the fixation of reduced S. Pyrite is the main S species in the sediments in and below the sapropels. The presence of AVS in the extremely-organic-rich (up to 23.5%) sapropel in section 969E-6H-6, 27 cm, indicates that detectable, but slow, SO_4^{2-} reduction still occurs in that interval.

Two postdepositional changes are important in the cyclic sediments in the eastern

Mediterranean: (1) sulphidisation of sapropel-underlying sediments during sapropel formation, and (2) oxidation of sapropel and overlying sediments after sapropel burial. The sulphidisation results in elevated pyrite contents, and, to a lesser extent, in elevated humic S contents below each sapropel. Furthermore sulphidisation of the sediments both underlying and overlying a sapropel may happen around extremely-organic-rich sapropels, where SO_4^{2-} reduction continues after sapropel formation.

The Fe sources for pyrite formation may comprise (1) Fe^{2+} diffusing upward from underlying sediments, (2) detrital Fe, and (3) water-column Fe through Fe sulphide formation in the water column. Syngenetic pyrite formation during sapropel development takes place at the sediment/water interface or in the water column. Water-column Fe sulphide formation has probably been important in the most organic-rich (up to 23.5%) sapropel (in section 969E-6H-6, 27 cm), implying that the bottomwaters contained sulphide during a substantial part of the formation of this sapropel. During the formation of sapropels with lower C_{org} contents, Fe sulphide formation in the water column, and thus sulphidic bottomwaters, were probably not as important.

Addition of Fe to the site of sulphide production, the sapropel, results in higher S fixation relative to the C_{org} content in sapropels, whereas downward sulphidisation results in a lower fixation of S relative to C_{org} content within the sapropels. Although S fixation is enhanced below a sapropel, S may also escape upward into the bottomwater during periods of downward sulphidisation. This escaped reduced S may either oxidize at the chemocline or form Fe sulphide in the water column.

The enrichment of Fe_{pyr} in the sediments is controlled primarily by the amount of Fe that is added to the sediment interval and fixed by direct Fe sulphide formation, rather than by the amount of detrital Fe: when more Fe is added by diffusion from underlying sediments or by precipitation of Fe sulphides in the water column, more pyrite is found in the sediments. The extent of the Fe_{pyr} enrichment within sapropels depends on the relative magnitudes of the sulphide production in the sapropel and the addition of Fe to the sapropel during its formation.

Appendix

Oxidation of sedimentary FeS_x, in which x is close to one, and consequent changes in Ca, SO_4, and Fe chemistry were modeled. The net oxidation reaction is:

$$4FeS_x + (3 + 6x)O_2 + (2 + 4x)H_2O \quad 4FeOOH + 8xH^+ + 4xSO_4^{2-}. \qquad (A1)$$

Reaction (A1) corresponds to the formation of sulphuric acid in the calcareous sediment. As a result, carbonate dissolves, and Ca^{2+} is liberated. The addition of sulphuric acid to the sediment can be modeled as the addition of an amount of acid to a calcite suspension, using the basic interpretation of the alkalinity as a balance of charges (e.g. Morel and Hering, 1993):

$$Alk \quad = excess\ negative\ charge\ from\ weak\ acids$$
$$= excess\ positive\ charge\ from\ strong\ base, \qquad (A2)$$

we obtain:

$$Alk \quad = [OH^-] - [H^+] + [HCO_3^-] + 2[CO_3^{2-}] +$$
$$= [Na^+] + [K^+] + 2[Ca^{2+}] + 2[Mg^{2+}] - [Cl^-] - 2[SO_4^{2-}] + \quad . \qquad (A3)$$

In the "acid-addition" experiment, all terms om the right-hand side, except $[Ca^{2+}]$ and $[SO_4^{2-}]$, are constant. Consequently,

$$[Ca^{2+}] = [SO_4^{2-}] + \tfrac{1}{2} \times ([OH^-] - [H^+] + [HCO_3^-] + 2[CO_3^{2-}]) + constant. \qquad (A4)$$

Even when we use the exact definition of alkalinity (e.g. Morel and Hering, 1993) and take into account the formation of carbonate complexes, which comprise about 35% of the total dissolved carbonate in seawater (e.g. $NaCO_3^-$ and $CaCO_3^0$), the same equation (i.e., A4) is obtained. According to Equation (A4), $[Ca^{2+}] : [SO_4^{2-}] = 1:1$, on the condition that the second term on the right-hand side ("TERM", half the alkalinity, neglecting carbonate complexes) is relatively constant.

To study the response of this term to the addition of sulphuric acid, chemical equilibrium calculations on a simple model system were done. This model system closely resembles the sedimentary situation at Hole 969A at 51.34 mbsf from which porewaters were analysed (Emeis, Robertson, Richter, et al., 1996). This sedimentary environment is assumed to be present in the sapropel in section 160-969E-6H-6, 27 cm, before FeS_x is oxidized. This model system consists of an inert electrolyte at 0.72 M, 31.8 mM SO_4^{2-}, 38.7 mM acid, and calcite (solid); from this system 18.9 mM CO_2 has been withdrawn; the temperature is $25^{\circ}C$ and the pressure is 1 atm. In this system equilibrium with atmospheric CO_2 is not taken into account, because the porewaters were analysed and sediment samples were stored in closed vials only a few hours after core-splitting, whereas the CO_2 gas-solution equilibration times are in the order of days (FeS_x oxidation takes place between core-splitting and storage). The vials have minimal headspace;

therefore, equilibrium with CO_2 (gas) can be neglected as well. For this system, neglecting the formation of complexes, the following values were calculated: $[Ca^{2+}] = 19.7$ mM, $[SO_4^{2-}] = 31.8$ mM, and $[OH^-] - [H^+] + [HCO_3^-] + 2[CO_3^{2-}] = 0.760$ mM. The shipboard measurements of these parameters at 51.34 mbsf in Hole 969A are $[Ca^{2+}] = 21.7$ mM, $[SO_4^{2-}] = 31.8$ mM, and alkalinity = 1.882-meq/L (Emeis, Robertson, Richter, et al., 1996). Regarding the fact that in seawater about 90% of Ca is present as free Ca^{2+} and the $([OH^-] - [H^+] + [HCO_3^-] + 2[CO_3^{2-}])$ contributes approximately 65% of the alkalinity (Whitfield, 1974), this model can be considered reasonable for the sediment samples before oxidation.

The addition of sulphuric acid, representing the oxidation of FeS_x, to the initial system described previously was modeled. The variation in the second term on the right-hand of equation (A4) ("TERM"), as a function of the total SO_4^{2-} concentration (which is proportional to the amount of acid added), is given in Figure 3.A1. Compared to the changes in $[Ca^{2+}]$ and $[SO_4^{2-}]$, this term appears to be practically constant, resulting in a linear relationship, with a slope of 1, between $[SO_4^{2-}]$ $([H_2SO_4]_{added})$ and $[Ca^{2+}]$ (Fig. 3.A1). In these calculations it was assumed that CO_2 (gas), possibly evolved during oxidation, was conserved in the system. However, when the loss of CO_2 (gas), which occurs during transfer of the sample to an N_2 atmosphere, is included in the calculations, the linear relationship between $[Ca^{2+}]$ and $[SO_4^{2-}]$ is maintained.

The pH variation is also shown in Figure 3.A1. Because the pH decreases to below the
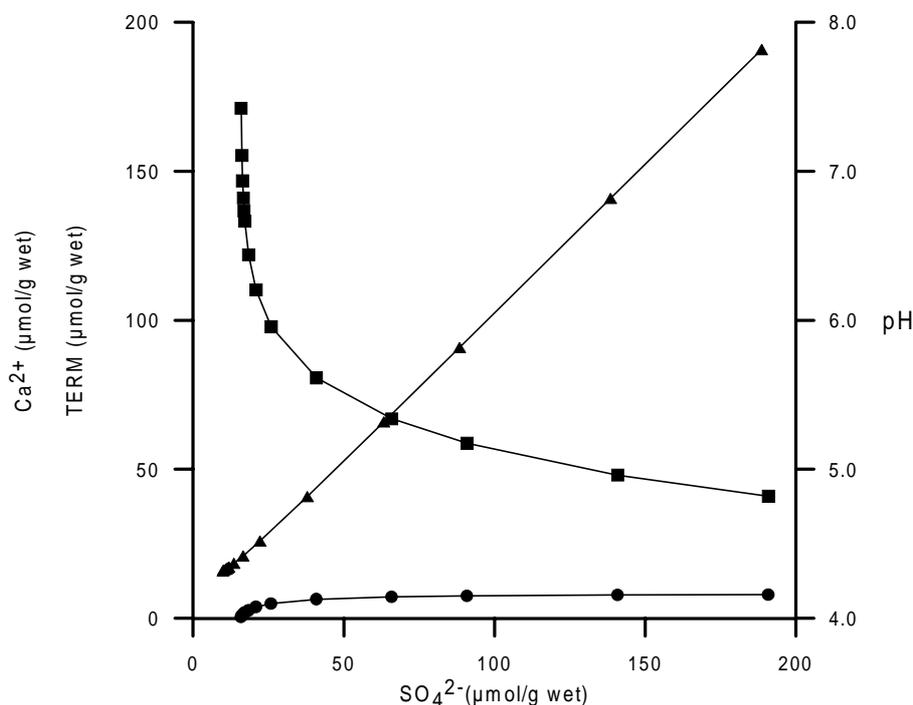
Figure 3.A1 *The calculated values of ½ × ([OH⁻] - [H⁺] + [HCO₃⁻] + 2[CO₃²⁻]) ("TERM",), [Ca²⁺] ( ), and pH ( ) as a function of the total concentration of SO₄²⁻ (initial [SO₄²⁻] + added sulphuric acid). The data are expressed in contents in wet sediment (μmol/g wet), enabling direct comparison to the data depicted in Figure 3.5. A water content of 50% is assumed (y mM = 0.5 × y μmol/g wet).*

pK_a value (6.15 for seawater) of the H_2CO_3/HCO_3^- equilibrium, the linear correlation between $[Ca^{2+}]$ and $[SO_4^{2-}]$ can easily be seen when reaction (1) (see "3.4 Discussion") is rewritten with H_2CO_3 as the principal component, rather than HCO_3^-.

Chapter 4

Pyrite contents, microtextures, and sulphur isotopes in relation to formation of the youngest eastern Mediterranean sapropel*

Abstract–Pyrite within and below sapropels in the eastern Mediterranean is a result of microbial SO_4^{2-} reduction within the sapropel, and the subsequent reaction of sulphide (HS^-) with detrital Fe and Fe^{2+} diffusing upward from underlying sediments. Below the youngest Mediterranean sapropel, S1, pyrite (up to 281 µmol pyritic S/g) is mostly present as euhedral crystals, whereas within the sapropel only framboidal pyrite (up to 360 µmol pyritic S/g) has been detected. Framboidal microtextures indicate pyrite formation at the site of HS^- production within the sapropel. Euhedral pyrite, below the sapropel, forms when SO_4^{2-} reduction in the sapropel outcompetes iron liberation and supply, and HS^- diffuses out of the sapropel. Sulphur isotope values of pyrite are extremely light in the sapropel (-37.3‰ to -38.2‰) as well as below the sapropel (-45.6‰ and -49.6‰), indicating that HS^- has formed in a system with abundant SO_4^{2-} and in the presence of oxidants.

4.1 Introduction

In marine sediments pyrite occurs as micron-sized euhedral crystals and micron-sized crystals in a raspberry-like morphology (framboidal pyrite) (e.g. Sweeney and Kaplan, 1973). Framboidal textures are the result of rapid pyrite formation from aqueous solutions highly supersaturated with both Fe monosulphides and pyrite, in which reaction kinetics favour the formation of Fe monosulphides before pyrite. By contrast, euhedral pyrite forms more slowly at saturation levels that are below those of Fe monosulphides (e.g.Sweeney and Kaplan, 1973; Goldhaber and Kaplan, 1974; Raiswell, 1982; Rickard, 1997), as confirmed by pyrite synthesis experiments (Wang and Morse, 1996) which show that pyrite morphology changes from cubic to octahedral to spherulitic with increasing degree of supersaturation. Raiswell (1982) argued that the texture of pyrite in pyritiferous carbonate concretions in ancient sedimentary rocks depends on the relative rates of HS^- generation and Fe supply. Bisulphide generation is determined by the rate of SO_4^{2-} reduction, and Fe supply by the in situ availability of reactive iron. In these concretions, framboidal pyrite apparently formed during early stages of diagenesis. During later stages of diagenesis, euhedral pyrite with higher $^{34}S/^{32}S$ isotope signatures formed because in situ Fe sources and porewater SO_4^{2-} became depleted, and the SO_4^{2-} reduction rate decreased. Wilkin et al. (1996) proposed that size distributions of framboids are indicative of formation conditions: framboids found in sediments underlying euxinic water columns are smaller than those in sediments underlying oxic or dysoxic water columns.

In this study, we assess the relation between the content, microtexture, and sulphur isotope composition of pyrite within and below the most recent eastern Mediterranean sapropel S1. We integrate the well-characterized pyrite formation conditions known from laboratory studies (Sweeney and Kaplan, 1973; Rickard, 1997; Wang and Morse, 1996), the inferred formation pathways of pyrite in sediments and sedimentary rocks (Raiswell, 1982; Wilkin et al., 1996), and recent insights into sulphur isotope fractionation during the oxidative part of the sulphur cycle (Canfield and Thamdrup, 1994). These complementary approaches provide a new insight into the conditions of pyrite formation and related redox conditions in eastern Mediterranean sediments during sapropel formation.

4.2 Eastern Mediterranean sediments

Sediments in the eastern Mediterranean are characterized by the presence of organic-rich layers, sapropels, in a hemipelagic sediment sequence. The origin of sapropels is still a matter of debate. Climate-induced enhanced productivity (e.g. Calvert, 1983) and preservation due to oxygen depletion in the bottomwaters (e.g. Rossignol-Strick et al., 1982) are thought to be involved in sapropel formation. The youngest sapropel, S1, formed between 5 and 9 ka (e.g. van Santvoort et al., 1996).

Sapropels are enriched in Fe and S as a result of bacterial SO_4^{2-} reduction within the sapropels and pyrite formation during and shortly after sapropel deposition, but SO_4^{2-} reduction is no longer active within recent sapropels (Passier et al., 1996a/Chapter 2). The sapropels are usually underlain by grey sediments, the so-called "protosapropel" zone (Maldonado and Stanley, 1976). Iron and S are also enriched in this zone, whereas C_{org} is not. Pyrite formed below sapropels, causing the grey color of the "protosapropel" zone, as a result of diffusion of HS^- out of the HS^- source (sapropel) (Passier et al., 1996a/Chapter 2). Thus the protosapropel did not form before sapropel deposition, but as a result of downward sulphidisation during and shortly after sapropel deposition, in this context "synsapropel" would be a better term.

4.3 Material and methods

Boxcore UM26 (lat 33°23.6'N, long 25°0.9'E, water depth 2160 m) was recovered 200 km south of Crete (Fig. 1.1), during the 1994 Palaeoflux cruise of R.V. *Urania*, and contains sapropel S1. A subcore of UM26 was subsampled at a resolution of 0.5 to 1 cm aboard ship inside a N_2-filled glovebox and stored under N_2 in air-tight containers at 4°C.

Pyrite and C_{org} contents were measured according to methods described by Passier et al. (1996a/Chapter 2). For pyrite sulphur isotope ($\delta^{34}S_{pyr}$) analysis, H_2S evolved during Cr(II) reduction was trapped in a Cd-acetate solution as CdS, $AgNO_3$ was subsequently added, and Ag_2S was reprecipitated. Ag_2S precipitates were measured for their stable S isotope composition ($^{34}S/^{32}S$) relative to the Vienna-Canyon Diablo troilite (V-CDT) by means of C-irmMS. Six subsamples (positions in Fig. 4.1) of about 2 g of wet sediment were rinsed with demineralized water, dried inside a desiccator in vacuum, gently crushed, and moulded in resin. Thin sections of this resin were examined, and pyrite identified and photographed, with an electron microprobe-scanning electron microscope (JEOL 8600) and a CamScan series 4 scanning electron microscope.

4.4 Pyrite content and iron availability

The most important S species in sapropel S1 is pyrite as follows from the comparison between S_{tot} and S_{pyr} (Fig. 4.1). Detailed analysis of other S species, such as acid-volatile sulphide, organic S, and elemental S, revealed that these fractions were insignificant compared to pyrite (Passier et al., 1996b; Passier and de Lange, 199_/Chapter 3). Pyrite and C_{org} are enriched in the sapropel. Pyrite is also enriched in a zone below the sapropel (Fig. 4.1). The
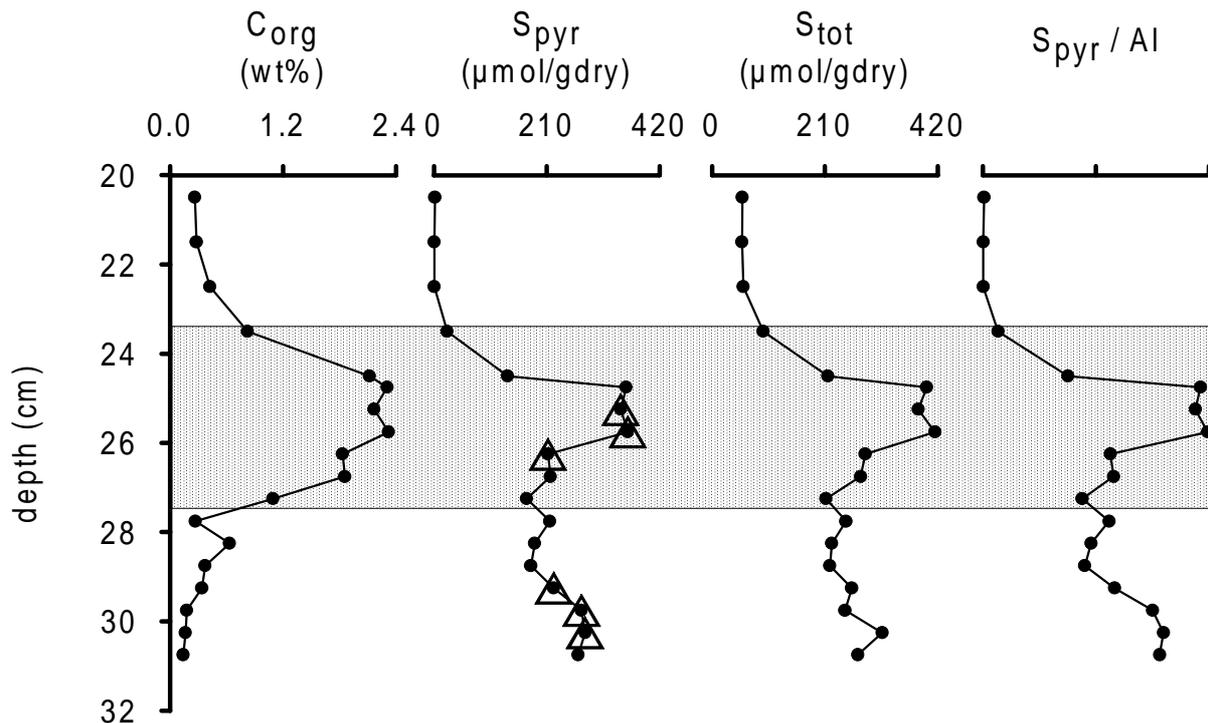
Figure 4.1 *Content vs. depth profiles of organic carbon (C_{org}), pyritic sulphur (S_{pyr}), and total sulphur (S_{tot}). Pyritic sulphur normalized to the Al content (S_{pyr}/Al) shows that relative pyrite enrichment is not due to any dilution effect. Triangles indicate positions of samples that were studied with electron microscopy. The sapropel is indicated by the shaded area.*

pyrite below the sapropel is formed from HS⁻ that diffused downward out of the sapropel during sapropel deposition (Fig. 4.2b; Passier et al., 1996a/Chapter 2). The pyrite maximum, however, is situated inside the sapropel (Fig. 4.1); this means that Fe has been relatively enriched in the sapropel. Thus, when the majority of the pyrite inside the sapropel formed (Fig. 4.2a), HS⁻ did not diffuse down out of the sapropel, but Fe^{2+} could diffuse into the sapropel from below and hence result in enhanced pyrite formation (Fig. 4.2a). This happens when SO_4^{2-} reduction rates are low relative to the rate of Fe liberation, as in the iron-dominated system described by Berner (1969). The band-like enrichment of pyrite emphasizes the importance of pyrite formation in this sediment.
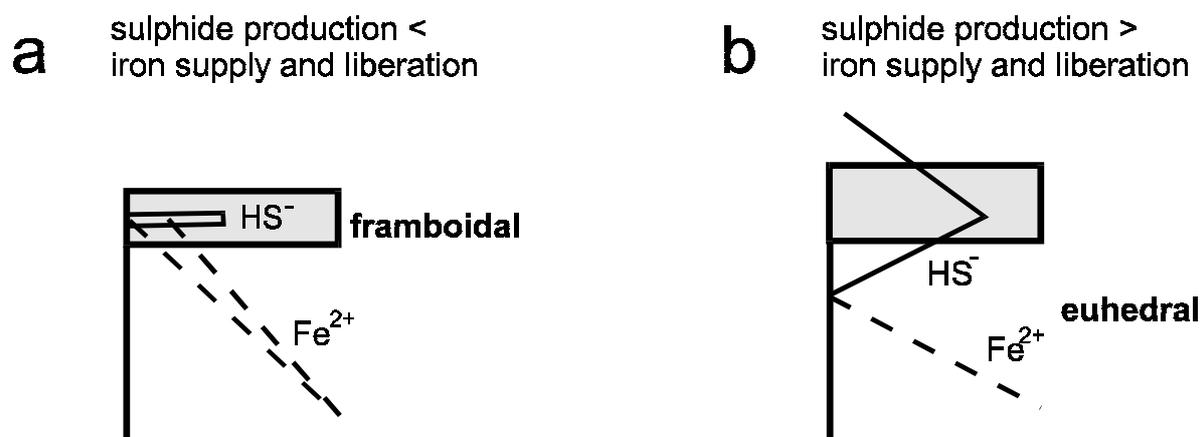
Figure 4.2 *Schematic representation of inferred pyrite formation conditions and concentration gradients of HS⁻ and Fe²⁺: a. during periods of rapid formation of framboidal pyrite within the sapropel; b. during periods of slow formation of euhedral pyrite below the sapropel.*

The HS⁻ source for pyrite formation is bacterial SO_4^{2-} reduction inside the sapropel. The Fe source comprises two pools: detrital Fe within the sapropel and Fe diffusing from underlying sediments (Passier et al., 1996a/Chapter 2 and 1996b). The amount of pyritic Fe within and below the sapropel minus a constant amount of reactive detrital iron, can be used to estimate the input of upward-diffusing Fe during sapropel deposition (note that the pyrite present in the upper, now oxidized, part of the sapropel, and that present in the unrecovered part of the S-enriched zone below the sapropel are included). This flux is 0.07 µmol cm⁻² yr⁻¹, which can be compared to the upward Fe flux of 0.089 µmol cm⁻² yr⁻¹ in sapropel S1 at site UM26, as estimated from the porewater profile (van Santvoort et al., 1996). These two fluxes are in reasonable close agreement, which suggests that the described scenario is plausible, and that pyrite formation and/or Fe oxidation were able to act as traps for upward-diffusing Fe²⁺.

4.5 Pyrite microtextures

Within sapropel S1 pyrite occurs as framboids that have mean diameters of 5 to 10 µm, and consist of cubic microcrystals that are smaller than 1 µm (Table 4.1, Fig. 4.3). Most pyrite within the sapropel is associated with shells, the dimensions of the shells clearly influenced the shape of the framboids (Fig. 4.3). Below the sapropel, however, pyrite is mostly present as euhedral (octahedral and cubic) crystals with diameters of 2 to 10 µm, and clusters (often with hexagonal crosscuts) of euhedral crystals (Table 4.1, Fig. 4.4). Furthermore, massive pyrite shell infillings and large irregular pyrite aggregates are present below the sapropel, and there is also pyrite which is not associated with shells. In the intermediate sample DD01301, both framboids consisting of microcrystals < 1 µm and framboidal aggregates of euhedral crystals as large as 5 µm are found (Table 4.1). Bioturbation probably occurred during the onset of sapropel deposition, so that both organic-rich sapropel sediment and organic-poor sediment are present in sample DD01301.

The size distribution of the framboids in sapropel S1 (5-10 µm and occasionally larger)

is typical for formation of pyrite in sediments near the sediment-water interface below an oxic or dysoxic water column (Wilkin et al., 1996).

Our observations of framboidal pyrite in the sapropel and euhedral pyrite below the sapropel are consistent with the mechanism proposed by Raiswell (1982) and experimental results of Sweeney and Kaplan (1973), Rickard (1997), Wang and Morse (1996). During the deposition of sapropel S1, Fe was supplied by liberation from in situ sources and diffusion from suboxic sediments directly underlying the sapropel. As long as the supply of Fe could keep pace with the production of HS^-, HS^- reacted in situ with Fe (i.e., at the site of SO_4^{2-} reduction), where HS^- was continuously produced. This situation resulted in rapid formation of framboidal pyrite (Fig. 4.2a). At times of increased HS^- production relative to Fe liberation and/or supply, HS^- diffused out of the C_{org}-rich layer, titrating reactive Fe present below the sapropel and reacting with upward-diffusing Fe^{2+}, to form pyrite (Passier et al., 1996a/Chapter 2). Below sapropel S1, at the site of pyrite formation, the concentration of HS^- was never as high as in the sapropel (the HS^- source) itself; the iron was less reactive, because the most reactive Fe oxides had been reduced before, and slow diffusive pyrite formation occurred. This led to the growth of euhedral pyrite below the sapropel (Fig. 4.2b).

4.6 Stable sulphur isotopes

The $\delta^{34}S$ values of pyrite ($\delta^{34}S_{pyr}$) in UM26 are -37.3‰ to -38.2‰ in the sapropel, and -45.6‰ and -49.6‰ below the sapropel (Table 4.1). The $\delta^{34}S_{pyr}$ reflects $\delta^{34}S$ of sulphide formed, because limited fractionation occurs when reduced S is transformed into pyrite (Price and Shieh, 1979). Mediterranean seawater SO_4^{2-} has a $\delta^{34}S$ value of +20.6‰ (de Lange et al., 1990), thus fractionations of 57.9‰ to 70.2‰ occurred. These fractionations are very high: maximum isotopic fractionations of 40‰ to 70‰ between SO_4^{2-} and reduced S are usually observed in sediments (e.g. Goldhaber and Kaplan, 1974; Chambers and Trudinger, 1979). The observed fractionations of 57.9‰ to 70.2‰ imply that SO_4^{2-} reduction took place in an open system, where exchange with seawater readily occurred, and thus no depletion of the SO_4^{2-} pool arose. Depletion would cause the remaining SO_4^{2-} (and the reduced S formed from it) to become progressively heavier ("reservoir effect," e.g. Jørgensen, 1979). This exchange with seawater is possible close to the sediment-water interface during sapropel deposition. However, the maximum fractionation between sulphide and SO_4^{2-} observed in laboratorium studies with SO_4^{2-} respiring bacteria is 4 to 46‰, where the highest fractionations occurred at the lowest SO_4^{2-} reduction rates (e.g. Chambers and Trudinger, 1979). Further fractionation has been reported to occur during bacterial HS^- oxidation to elemental S (or other intermediate oxidized S species such as thiosulphate), followed by bacterial disproportionation (Canfield and Thamdrup, 1994). Extensive, repeated HS^- oxidation results in lighter isotopic values ($\delta^{34}S$ values) of reduced S. If reoxidation invoked the high fractionations, oxidants must have been able to reach the HS^- that was formed in the sapropel. This may have been nitrate and oxygen from the bottomwater or sedimentary Fe and Mn oxides. At times that HS^- production is high relative to Fe liberation and supply (Fig. 4.2b), HS^- will diffuse downward and sulphidize sediments below the sapropel. Bisulphide may also move into the bottomwaters, diffuse upward, and reach the chemocline, where reoxidation

occurs. Subsequently, evolved elemental S settles back to the sediment and disproportionates, inducing more negative S isotope values in the sediment. A similar scenario was proposed for the present Black Sea (Canfield and Thamdrup, 1994). The HS^- produced during these periods of Fe limitation in the sapropel (Fig. 4.2b), will be incorporated into pyrite forming below the sapropel. When less HS^- is incorporated in pyrite at the site of HS^- production, i.e., the sapropel, more HS^- can participate in the reoxidation cycle, and $\delta^{34}S$ of pyrite forming below the sapropel will become even more negative. This might explain that $\delta^{34}S_{pyr}$ values below the sapropel are more negative than within the sapropel. Moreover, pyrite within the sapropel might also have been overprinted by relatively heavy reduced S that formed from porewater SO_4^{2-} after burial of the sapropel due to a reservoir effect.

Note that part of the pyrite is formed in the absence of external oxidants at the site of pyrite formation. Most pyrite reaction mechanisms include an external oxidant; however, direct pyrite formation with sulphide itself acting as an oxidant has recently been made plausible (e.g. Drobner et al., 1990; Rickard,1997), but the consequences for S isotope fractionation are not yet known.

4.7 Implications

The complementary information obtained from pyrite contents, microtextures, and sulphur isotopes defines the conditions of pyrite formation within and below sapropel S1 in the eastern Mediterranean. All observed variations in the properties of pyrite can be related to fluctuations in the production of HS^- relative to the supply of reactive Fe. When HS^- production in the sapropel is relatively low, Fe reaches the source of HS^- inside the sapropel, a pyrite enrichment forms, and pyrite formation is rapid, resulting in a framboidal texture. When HS^- production is relatively high, HS^- breaks out of the sapropel, and forms the euhedral pyrite below the sapropel, in the so-called "synsapropel." During periods of high HS^- production, bottomwaters may eventually become sulphidic. Nevertheless, on the basis of the size classification of framboidal pyrite of Wilkin et al. (1996) the water column has been predominantly oxic to dysoxic during sapropel formation.

As opposed to the system described by Raiswell (1982), the $\delta^{34}S$ of the euhedra is not heavier than the $\delta^{34}S$ value of the framboids, because the source of HS^- is the open SO_4^{2-} reduction system close to the sediment-water interface for both textures, and there is no distinction between early diagenetic pyrite formed close to the sediment-water interface and pyrite formed during later diagenesis far below the sediment-water interface.

Chapter 5

Modes of sapropel formation in the eastern Mediterranean: some constraints based on pyrite properties∗

Abstract–Pyrite formation within and directly below sapropels in the eastern Mediterranean was gouverned by the relative rates of sulphide production and Fe liberation and supply to the organic-rich layers. At times of relatively high SO_4^{2-} reduction, sulphide could diffuse downward from the sapropel and formed pyrite in underlying sediments. The sources of Fe for pyrite formation comprised detrital Fe and diagenetically liberated Fe(II) from sapropel-underlying sediments. In organic-rich sapropels, input of Fe from the water column via Fe sulphide formation in the water may have been important as well. Rapid pyrite formation at high saturation levels resulted in the formation of framboidal pyrite within the sapropels, whereas below the sapropels slow euhedral pyrite formation at low saturation levels occurred. $\delta^{34}S$ values of pyrite are -33‰ to -50‰. Below the sapropels $\delta^{34}S$ is lower than within the sapropels, as a result of increased sulphide reoxidation at times of relatively high sulphide production and concentration when sulphide could escape from the sediment. The percentage of initially formed sulphide that was reoxidized was estimated from organic carbon fluxes and burial efficiencies in the sediment. It ranges from 34% to 80%, varying significantly between sapropels. Increased paleoproductivity as well as enhanced preservation contributed to magnified accumulation of organic matter in sapropels.

5.1 Introduction

The sedimentary record of the eastern Mediterranean is characterized by the occurrence of organic-rich layers, sapropels, of centimetres to decimetres thickness. The origin of sapropels is related to paleoclimatic changes. Sapropels are thought to form during wet climate caused by precession-induced insolation variations and concomitant enhanced precipitation over parts of Africa and the Mediterranean borderlands. During these wet periods, increased input of fresh water caused a higher stability of the water column and perhaps even a circulation reversal from anti-estuarine circulation to estuarine circulation (e.g. Rossignol-Strick, 1982; Rohling and Hilgen, 1991; Fontugne and Calvert, 1992). Furthermore, increased input of nutrients in freshwater or via upwelling of deep water to the surface waters of the eastern Mediterranean caused enhanced productivity of organic matter. Increased productivity in the surface waters and/or enhanced preservation due to oxygen depletion in the bottomwaters were reported to be possible causes of increased accumulation of organic carbon and sapropel formation (e.g. Olausson, 1961; Rossignol-Strick et al., 1982; Calvert et al., 1992).

The sequence of alternating organic-rich and organic-poor layers in the sedimentary record of the eastern Mediterranean provides a unique setting to study the different paleoenvironmental signals and their diagenetic modification. During sapropel formation, bacterial SO_4^{2-} reduction dominated the sediment at the sediment/water interface, whereas organic matter oxidation in the sediments directly below the sapropel was dominated by reduction of Fe (hydr)oxides (Passier et al., 1996a/Chapter 2). The classic downward succession of oxic, suboxic, and anoxic sediment (e.g. Froelich et al., 1979) does not apply to this dynamic system. Pyrite is present in and immediately below each sapropel as a result of microbial SO_4^{2-} reduction and subsequent reaction of reduced S with Fe, mainly during the formation of the sapropel (Passier et al., 1996a/Chapter 2; 1997/Chapter 4).

This paper addresses the information on sapropel formation that can be deduced from pyrite contents, pyrite microtextures, and the isotopic composition of pyrite. Moreover, these pyrite data are used to put some constraints on the burial efficiency of organic carbon in sapropels.

5.2 Materials and methods

Three sapropels were selected for detailed investigation. Boxcore UM26 (33°23.6'N, 25°0.9'E, water depth 2160 m) was recovered 200 km south of Crete during the 1994 *Palaeoflux* cruise of RV *Urania* (Fig. 1.1); it contains a 4-cm-thick sapropel at about 0.24 m below seafloor (mbsf). Light grey sediments lie beneath the sapropel, orange-brown sediments lie above it. This sapropel is known as sapropel S1, which formed between 9 and 5 kyr ago (Higgs et al., 1994). A subcore of UM26 was subsampled at a resolution of 0.5 to 1 cm aboard ship inside an N_2-filled glovebox and stored under N_2 in airtight containers at 4°C.

Two sapropels, recovered during ODP Leg 160 with Drilling Vessel *JOIDES Resolution* were sampled in detail directly after core-splitting aboard ship. Sapropel 969 was recovered in Section 160-969E-6H-6. Site 969E (33°50.5'N, 24°53.0'E, water depth 2201 m) is located on the Mediterranean Ridge, 30 miles NW of the UM26-site (Fig. 1.1). Hole 969E contains 80 sapropel beds from early Pliocene to Holocene age. The sampled interval contains a 12 cm-thick black sapropel at 50.7 mbsf, with the top at 27 cm in the section, surrounded by light grey sediments. This sapropel is time equivalent to insolation cycle i-282, with an age of 2.943 Ma, as revealed by astronomical tuning of the ODP sapropels (L. Lourens, personal communication). It belongs to a group of black sapropels of Pliocene age with high organic carbon contents (up to 30%) embedded in a grey interval. The dark sapropel has a fine horizontal internal structure, which may be the result of primary lamination (Emeis, Robertson, Richter, et al., 1996). The other Leg 160 sapropel, 967, originates from Section 160-967C-6H-2. Site 967C (34°4.3'N, 32°43.5'E, water depth 2553 m) is located on a small ridge near the foot of the northern slope of the Eratosthenes seamount, about 70 km south of Cyprus (Fig. 1.1). At this site 80 sapropels from early Pliocene to Holocene age were recovered. The sampled interval contains a 14 cm-thick sapropel at 49.3 mbsf, starting at 30 cm section-depth. The sapropel is brownish black and surrounded by grey sediments. It was deposited at the end of the Pliocene and appears bioturbated. The sapropel is time equivalent to insolation cycle i-176, which has an age of 1.808

Ma, as followed from astronomical tuning of the ODP sapropels (L. Lourens, personal communication). About fifteen samples of 1.5 cm thickness each were taken over an interval of 70 and 50 cm for 967 and 969 respectively. The samples were stored under N_2 in airtight containers at 4°C.

Subsamples were dried at 40°C (UM26) or freeze-dried (Leg 160) and ground in an agate mortar before dissolution in an $HClO_4$-HNO_3-HF acid mixture. The dried residue was dissolved in 1 M HCl for analysis of total S (S_{tot}), Ba and Al with a Perkin Elmer OPTIMA 3000 inductively coupled plasma atomic emission spectrometer (ICP-AES). Organic carbon (C_{org}) contents were determined with a Fisons Instruments NA-1500 NCS-analyser after removal of carbonate with 1 M HCl. S_{tot}, Ba, Al and C_{org} measurements were performed according to standard laboratory procedures and have standard deviations < 5%. International and in-house standards were used to check the procedures and the accuracy.

Dried subsamples were extracted with acetone for several hours to remove elemental S (including elemental S formed from acid-volatile sulphides (AVS) and organic polysulphides during drying, and elemental S initially present) before pyrite extraction. Pyritic S (S_{pyr}) was extracted with the Cr(II) reduction method (Zhabina and Volkov, 1978; Canfield et al., 1986; Henneke et al., 1997). Sulphide that evolved in the pyrite extraction was stripped from reaction solutions with N_2 or Ar, and trapped in 1 M NaOH. The NaOH solution was analysed for sulphide by square wave voltammetry (SWV) with a Princeton Applied Research Model 384B-4 polarographic analyser system equipped with a Model 303A static mercury drop electrode (SMDE). $S_{reduced}$ is the sum of all significant reduced S phases, comprising S_{pyr} below the sapropels, and S_{pyr}, organic S, and acid-volatile sulphide (AVS) within the sapropels (Passier and de Lange, 199_/Chapter 3).

For pyrite isotope analysis ($\delta^{34}S_{pyr}$) H_2S, evolved during Cr(II) reduction, was trapped in a Cd-acetate solution as CdS, $AgNO_3$ was added, and Ag_2S was precipitated. The precipitate was washed in demineralized water, separated from the solution by centrifugation and dried. Ag_2S precipitates were analysed for their stable S isotope composition by means of combustion isotope ratio monitoring mass spectrometry (C-irmMS; Böttcher et al., 199_a) with an Elemental Analyser (Carlo Erba EA 1108) coupled to a Finnigan Mat 252 Mass Spectrometer via a Finnigan Mat Conflo II Split Interface. The isotope values were corrected for a -0.3‰ difference between a standard pyrite and the Ag_2S that was made from it. The SO_4^{2-} extracted from the sediments of the lower part of 969 with 0.5 M NaCl was precipitated as barite, and the stable S isotopic composition was measured by C-irmMS. $^{34}S/^{32}S$ ratios are given in the δ-notation relative to the Vienna-Canyon Diablo Troilite (V-CDT) standard.

Subsamples of sapropels 969 and 967 (positions in Table 5.1) were rinsed with demineralized water, dried inside a desiccator under vacuum, gently crushed, and moulded in resin. Thin sections of this resin were examined, and pyrite identified and photographed with an electron microprobe-scanning electron microscope (JEOL 8600).

5.3 Results and discussion

5.3.1 Two scenarios for pyrite formation

Pyritic S is the predominant S phase within and below the sapropels (Fig. 5.1). The S_{pyr} and S_{tot} profiles in and below sapropels show three major features. Firstly, pyrite is relatively enriched within the sapropel, as is C_{org} (Fig. 5.1). Secondly, a broad pyrite enrichment is present in a zone below the sapropel, whereas C_{org} is not (Fig. 5.1). Thirdly, a distinct pyrite peak often marks the lower boundary of the pyrite enrichment below the sapropel. These features were first recognized in the total S profiles of the Holocene and Pleistocene sapropels (Passier et al., 1996a/Chapter 2). The Holocene and Pliocene sapropels presented in this paper show the same features (Fig. 5.1): there are pyrite peaks within the sapropels, and pyrite enrichments below the sapropels. A sharp pyrite peak is present at the lower end of the pyrite enrichment in 969, a broader peak marks the end of the enrichment in 967. The lower boundary of sapropel S1 was not recovered in boxcore UM26, therefore, UM26 is compared to core MT1, that has a similar S_{tot} profile (Fig. 5.2) and was recovered close to site UM26 (Fig. 1.1; 33°18.4'N, 25°10.9'E, water depth 2217 m, recovered during the 1993 *Marflux*-5 cruise of R.V. Tyro). The lower boundary of the S enrichment below the sapropel is recovered in MT1 (Fig. 5.2).
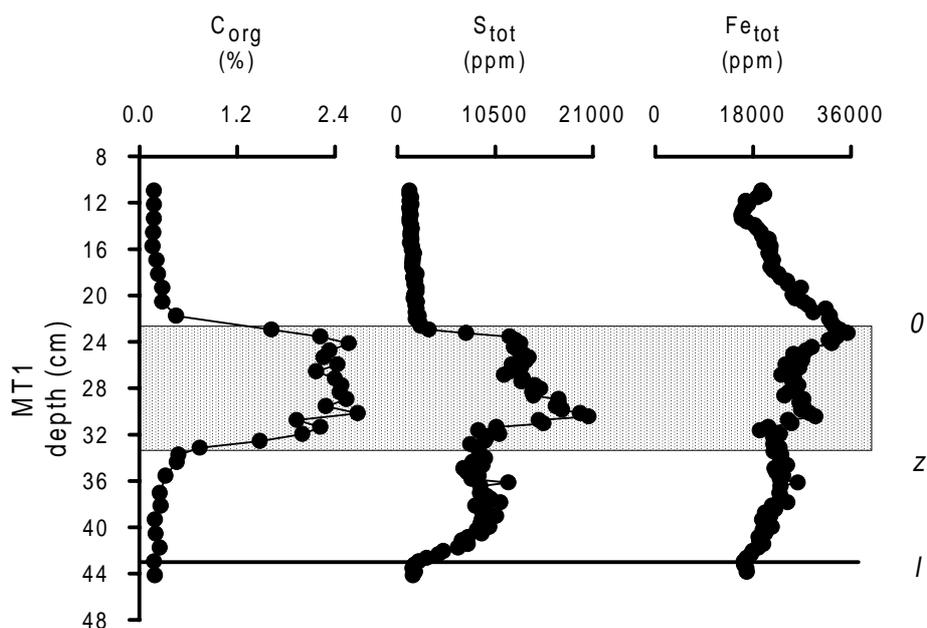
Figure 5.2 *Content vs. depth profiles of C_{org}, S_{tot} (total S), and Fe_{tot} (total Fe) in sapropel S1 in boxcore MT1. The shaded band is the visible sapropel interval between 0 and z. l is the lower boundary of the S-rich zone below the sapropel.*

The formation of these pyrite enrichments can be explained in terms of Fe and sulphide supply and mobility during sapropel formation. The mobility of Fe and sulphide in sediments with a C_{org}-rich layer was studied experimentally by Berner (1969). Depending on the relative amounts of reactive Fe and dissolved ΣH_2S, he identified three scenarios: low-Fe-content, high-

Fe-content and intermediate-Fe-content, the last being termed a Liesegang situation. In the low-Fe-content model, dissolved ΣH_2S produced by SO_4^{2-}-reducing bacteria diffuses downward out of a C_{org}-rich layer until it reacts with immobile solid-phase reactive Fe to form Fe sulphides. In the high-Fe-content model Fe(II) migrates upward to the sulphide-rich organic layer, where Fe sulphides are formed subsequently. In the intermediate situation, dissolved sulphide migrates downward and Fe(II) migrates upward.

We propose that the pyrite enrichments in and below the sapropels are the result of two different endmember-scenarios of sulphide production and Fe liberation and supply, that are analogues of the models of Berner (1969) (Fig. 5.3). The first scenario (A) applies when sulphide production within the sapropel is smaller than the Fe liberation and supply to the sapropel (high-Fe-content model). The second scenario (B) applies when sulphide production within the sapropel exceeds Fe liberation and supply to the sapropel (low-Fe-content model) (Passier et al., 1996a/Chapter 2; Passier et al., 1997/Chapter 4; Passier and de Lange, 199_/Chapter 3).

Figure 5.3 *Two scenarios of sapropel formation: a. scenario A: sulphide production is low relative to iron liberation and supply; b. scenario B: sulphide production is high relative to iron liberation and supply.*

5.3.1.1 Scenario A: sulphide production within sapropel smaller than Fe liberation and supply to sapropel

In this scenario (Fig. 5.3a) reduced S is fixed as pyrite within the sapropel by reaction with detrital Fe (hydr)oxides and with upward-diffusing Fe(II) (high-Fe-content model). This upward-diffusing Fe is liberated from Fe(hydr)oxides during suboxic diagenesis in sapropel-underlying sediments (Passier et al., 1996a/Chapter 2). Upward-diffusing Fe(II) reacts with sulphide, any Fe(II) that is not trapped by sulphide will be reoxidized and precipitate, and consequently be trapped as Fe(hydr)oxides at the sediment surface, remaining available for Fe

sulphide formation. As a consequence pyrite formation is enhanced and pyrite enrichments are peak-shaped within the sapropels. Sulphide can be reoxidized at the sediment-water interface by nitrate and oxygen from the bottomwater or by sedimentary Fe and Mn (hydr)oxides. Such oxidation affects the isotopic composition of reduced S (see later discussion).

5.3.1.2 Scenario B: sulphide production within sapropel exceeding Fe liberation and supply to sapropel

In this scenario (Fig. 5.3b) sulphide migrates into sediments below the sapropel (Passier et al., 1996a/Chapter 2), and into bottomwaters overlying the sapropel. The only possible Fe source in the sapropel sediment is detrital Fe, and pyrite formation is Fe-limited within the sapropel (low-Fe-content model). Upward-diffusing Fe does not reach the sapropel, but reacts to pyrite when it encounters downward-diffusing sulphide which also sulphidizes Fe oxides below the sapropel. This leads to pyrite enrichments below the sapropels, for example below sapropels S1, 967, and 969 (Fig. 5.1). At a certain point below the sapropel, a balance between upward Fe flux and downward sulphide flux may result in a Liesegang situation (intermediate-Fe-content model) and in the accumulation of Fe sulphides in distinct peaks (Fig. 5.1; Passier et al., 1996a/Chapter 2). Sulphide may accumulate in the water column, where it may be reoxidized at the chemocline, which has consequences for the isotopic composition of pyrite that forms (see later discussion), or it may form Fe sulphides in the water column. Additional Fe might be liberated at the margins of the basin in response to a fluctuating oxycline, as was proposed for the present-day euxinic Black Sea (Canfield et al., 1996). This Fe reacts with sulphide in the water column, or settles to the sediments as Fe (hydr)oxides after reoxidation. Another consequence of Fe limitation within a sapropel is possible uptake of reduced S into organic compounds (e.g. Sinninghe Damsté and de Leeuw, 1990), which may have happened in organic-rich sapropel 969 (Passier and de Lange, 199_/Chapter 3). In theory, sulphide could also migrate out of a sapropel after burial, and thus sulphidize sapropel-overlying as well as sapropel-underlying sediments. Isotopic compositions of pyrite, however, indicate that this is not the case, and that sulphide does not migrate out of the sapropel after it has been buried. Sediments overlying older sapropels can of course be influenced by downward migration of sulphide out of younger sapropels (see later discussion).

5.3.1.3 Pyrite microtextures in relation to the two scenarios

Sedimentary pyrite occurs as micron-sized euhedral crystals, micron-sized crystals in a raspberry-like morphology (framboidal pyrite), and as more massive forms such as aggregates, overgrowths, and infillings (e.g. Love and Amstutz, 1966; Rickard, 1970; Sweeney and Kaplan, 1973). The framboids and euhedral crystals appear to be the earliest forms, whereas the more massive forms are secondary (e.g. Love and Amstutz, 1966; Wilkin et al., 1996). Framboidal textures are thought to result from rapid pyrite formation from aqueous solutions highly supersaturated with respect to both Fe monosulphides and pyrite, in which reaction kinetics favour the formation of Fe monosulphides prior to pyrite. By contrast, euhedral pyrite seems to form more slowly at saturation levels below those of Fe monosulphides (e.g. Sweeney and

Kaplan, 1973; Goldhaber and Kaplan, 1974; Raiswell, 1982). Recent pyrite synthesis experiments deepened these observations: Wang and Morse (1996) showed that pyrite morphology changed from cubic to octahedral to spherulitic with increasing degree of supersaturation. Wilkin and Barnes (1996) argued that fast conversion rates of Fe monosulphides to pyrite, possible when oxygen is present, play a key role in framboid formation. Rickard (1997) reported that rapid pyrite formation by sulphide oxidation of Fe monosulphides resulted in the formation of framboidal pyrite. These results can be summarized in a general rule of thumb that is useful for field studies: fast pyrite formation at high saturation levels yields framboidal pyrite, whereas slow pyrite formation at low saturation levels yields euhedral pyrite.

Within the sapropels 969 and 967 pyrite is predominantly present as framboids (Table 5.1, Fig. 5.4a,b), whereas below the sapropels, pyrite is mainly present as euhedral forms (Table 5.1): irregular euhedral aggregates (Fig. 5.4c), euhedral shell infillings and overgrowths (Fig. 5.4d), and euhedral crystals (Fig. 5.4e). The same distinction has been observed for the microtextures of pyrite within and below sapropel S1 in UM 26 (Passier et al., 1997/Chapter 4). The different microtextures within and below the sapropels reflect the different formation scenarios of pyrite formation (Passier et al., 1997/Chapter 4). Framboids are the result of rapid pyrite formation within the sapropels, when Fe liberation and supply was sufficient to trap sulphide in the sapropel, where it was continously produced (scenario A, Fig. 5.3a). At times of pyrite formation below the sapropels (scenario B, Fig. 5.3b) diffusive supply of sulphide and Fe resulted in slow formation of euhedral pyrite. The concentration of sulphide was never as high as in the sapropel (the sulphide source) itself. The Fe was less reactive, because the most reactive Fe (hydr)oxides had been reduced before, and slow diffusive pyrite formation occurred. Thus, the framboids are primary forms of pyrite, which formed in the sapropel layers during their deposition, and the euhedral pyrite is a secondary feature for the sediments below the sapropels, that were post-depositionally sulphidized. The uniform size of microcrystals (<1 to 1.5 µm) within single framboids suggests that all microcrystals aggregated at the same time, and that no microcrystals were added with progressive burial (Wilkin et al., 1996). In addition to framboidal pyrite, euhedral crystals are present within sapropels 967 and 969 (Fig. 5.4a,b), and some framboids in sapropels 967 and 969 have slightly angular outlines. This illustrates that secondary pyrite formation at slow rates has occurred in these sapropels after burial. After burial the concentrations of sulphide and Fe were low, because the most reactive Fe minerals had already been reduced and SO_4^{2-} reduction rates were no longer as high as with recently-deposited organic matter. The euhedral-shaped framboid-like aggregates in sapropel 967 (Fig. 5.4f) might be the result of secondary overgrowth on framboids. It is remarkable that no euhedral crystals were observed within sapropel S1, indicating that post-burial SO_4^{2-} reduction and post-burial pyrite formation have not (yet) been significant in this sapropel.

The exceptional large groups of framboids (2 to 15 µm), floating in a mass (30 to 300 µm) of small microcrystals (<<1 µm), that we call "veiled" framboids, in the upper part of 969 (Fig. 5.4g) might be replacement structures in now dissolved carbonate microfossil shells. The size and form are comparable to some of the shells found in other samples, for example below sapropel 969 (Fig. 5.4d). Furthermore, almost no shells were observed in the upper sapropel sample examined by microprobe and the carbonate content is only 27 wt%, as determined from

the weight-loss of the samples as a result of 1 M HCl extraction. In comparison, the lower sapropel sample examined by microprobe has a carbonate content of 48 wt%. This suggests that enhanced dissolution of carbonate may have occurred in the upper part of sapropel 969.

Wilkin et al. (1996 and 1997) related the size distribution of pyrite framboids to the redox state of the overlying water column: the framboids of sediments underlying euxinic water columns are on average smaller and less variable in size than those of sediments underlying oxic or dysoxic water columns. The dataset of framboid sizes in the sapropels discussed here is not large enough to extract statistically significant information on the size distribution. However, the largest observed framboid was only 20 µm in sapropels 967 and 969, and the major size range of the framboids was 2 to 10 µm. When compared to the results of Wilkin et al. (1996 and 1997), this size range does not preclude that some fraction of the pyrite originated in a euxinic water column. In contrast, the framboids are slightly larger in samples of sapropel S1 in UM26 (Passier et al., 1997/Chapter 4), where the dominant size range of framboids is 5 to 10 µm and framboids up to 25 µm have been observed. This suggests that oxic to dysoxic rather than euxinic conditions existed in the water column during formation of sapropel S1.

5.3.1.4 Pyrite enrichment within the sapropels in relation to the two scenarios

From the scenarios A and B it follows that the pyrite peaks within the sapropels may have formed when sulphide production in the sapropel was low relative to Fe availability and supply, when Fe(II) could diffuse into the sapropel from below and hence this resulted in enhanced pyrite formation. Another reason for enrichment of pyrite within the sapropel could be extensive Fe sulphide formation in the water column during sapropel formation, as was proposed to be important in anaerobic/euxinic environments in the Black Sea, Cariaco Trench and Framvaren fjord (Canfield et al., 1996; Raiswell and Canfield, 199_). In this situation additional Fe could be supplied through liberation of Fe in suboxic zones along the basin margins. An Fe budget may be used to distinguish between these two possibilities.

The reactive Fe source for pyrite in and below the sapropels may comprise three pools: (1.) detrital Fe within the sapropel, (2.) Fe diffusing from underlying sediments, and (3.) Fe from the water column, transferred to the sediment via Fe sulphide formation in the water column (Passier et al., 1997/Chapter 4; Passier and de Lange, 199_/Chapter 3). The input of detrital reactive Fe from the continents likely did not increase during sapropel formation, because this input in the central parts of the eastern Mediterranean is thought to be associated with dust input (Medinets, 1996) whereas sapropels formed during relatively wet climate conditions (e.g. Rohling and Hilgen, 1991), when dust formation is minimal. Moreover, Fe from silicates has not contributed more to the formation of pyrite within than below the sapropel, as follows from the fact that contents of silicate-bound Fe are constant throughout the sapropels and sapropel-underlying sediments (Pruysers et al., 1993; Passier and de Lange, 199_/Chapter 3). The relative importance of an additional Fe source from the water column can be estimated: the total integrated amount of pyritic Fe in and below the sapropel (Fe_{int}, µmol cm^{-2}) minus the amount of reactive detrital Fe used in pyrite formation (Fe_{detr}, µmol cm^{-2}), divided by the duration of sapropel formation (t, yr) yields an estimate of the flux of Fe needed from other sources than

detrital (Flux $_{Fe\,add}$, µmol cm^{-2} yr^{-1}):

$$\text{Flux}_{Fe\,add} = \frac{Fe_{int} - Fe_{detr}}{t} ,$$

where

$$\text{Fe}_{int} = \int_{0}^{l} \left(\frac{S_{pyr}}{2} \times \rho\right)\cdot dx ,$$

$$\text{Fe}_{detr} = Fe_{background} \times \rho \times \Delta x ,$$

and

$$\text{t} = \frac{sapropel\ thickness}{\omega} .$$

ρ is the dry bulk density [g/cm^3], S_{pyr} is the pyritic S content [µmol/gdry], Fe$_{background}$ is the Fe from detrital input, here assumed to be constant and estimated to be 100 µmol g^{-1}, as follows from preliminary Fe extractions from recent non-sapropelic, oxic eastern Mediterranean surface sediments (A. Rutten, personal communication), ω is the sediment accumulation rate [cm yr^{-1}]. Sediment parameters are taken from Emeis, Robertson, Richter, et al. (1996). Δx [cm] is the length from the top of the sapropel (position *0*, Fig. 5.2) to the lower boundary of the pyrite-enriched zone below the sapropel (position *l*, Fig. 5.2). Whereby the pyrite peaks below the sapropels in 969 and 967 are taken to be the lower boundaries of the pyrite-enriched zone (*l*), since the zone to which sulphide migrates out of a sapropel often is bounded by a pyrite peak (Passier et al., 1996a/Chapter 2). Position *l* for S1 has been estimated from S$_{tot}$ measurements in core MT1 (Fig. 5.2). For sapropel S1, the upper, now oxidized, part of the sapropel has been included in the calculation as well, assuming that half of the sapropel has been oxidized (van Santvoort et al., 1996). Based on the Ba profiles in sapropel 967 and 969, post-depositional oxidation has not been as important in these sapropels. Barium is thought to indicate the original position of the sapropel before partial oxidation (van Santvoort et al., 1996), and Ba is enriched only within 967 and 969, whereas it is enriched both within and above S1 in UM26 (Fig. 5.1; Passier and de Lange, 199_/Chapter3).

The additional Fe flux (Flux$_{Fe\,add}$) is 0.07 µmol cm^{-2} yr^{-1} for S1, which can be compared to the upward Fe flux of 0.089 µmol cm^{-2} yr^{-1}, as estimated from the present-day porewater profile at site UM26 (van Santvoort et al., 1996). These two fluxes are in reasonable close agreement, which suggests that the detrital and upward-diffusing Fe were the only two important Fe inputs for sapropel S1 (Passier et al., 1997/Chapter 4), and that scenario A (Fig. 5.3a) was

important for the formation of pyrite peaks within this relatively organic-poor sapropel. For sapropels 967 and 969 the additional Fe fluxes are 2.4 and 1.1 µmol cm^{-2} yr^{-1}, respectively. The latter fluxes are much higher than the estimates of present-day upward Fe fluxes based on porewater profiles in the eastern Mediterranean, being 0.089 to 0.15 µmol cm^{-2} yr^{-1} (Pruysers et al., 1993; van Santvoort et al., 1996). It could be that the detrital reactive Fe inputs were higher for these older sapropels, especially at site 967 which is close to the Cypriotic coast, but there is no reason to assume a larger detrital Fe input for sapropel 969 compared to sapropel S1 given their proximity. Therefore, additional Fe inputs from the water column are required especially for organic-rich sapropel 969 and likely for 967, and thus scenario B (Fig. 5.3b) was important. It appears that pyrite contents as in sapropel S1 (up to 400 µmol g^{-1} pyritic S) are the maximum contents for comparable systems in which only detrital and upward-diffusing Fe sources are important, while sapropels with higher pyrite contents likely received Fe sulphide input from the water column.

5.3.1.5 Alternation of the two scenarios, lateral and temporal variations

The balance between sulphide production and Fe availability and supply may vary with time and place within one sapropel and in between sapropels. At the onset of sapropel formation, during transition from suboxic to sulphidic sedimentary conditions, C_{org} mineralisation initially is not very high, because the C_{org} content is still relatively low, and thus bacterial sulphide production can be expected to be relatively low. Moreover, an upward flux of Fe(II) to the sediment-water interface likely exists, with accumulation of Fe (hydr)oxides at the sediment surface. Thus, this initial situation may lead to a high-Fe-content model, and pyrite formation as described in scenario A. During the next stage of sapropel formation, the SO_4^{2-} reduction rate is likely to increase as a result of higher C_{org} accumulation rates to the sediments. Reactive Fe (hydr)oxides present in the sediments become transformed to Fe sulphides. Sulphide production may then start to outcompete Fe liberation and supply, and a low-Fe-content model, scenario B, applies. This may be followed by a period in which the input of fresh organic matter may vary periodically, on seasonal scales or on longer timescales. Therefore, scenario A and B may alternate. The step-wise profiles of pyrite, with a pyrite peak within the sapropels and a broad, but lower, enrichment below the sapropels (Fig. 5.1), indicate that the switch from a scenario A dominated system to a scenario B dominated system was relatively rapid. If not, a more gradual transition between the pyrite contents in the peak and those below the sapropels would be present. These rapid changes are possible, because the position of the sulphidize-down front can rapidly adjust, as diffusion time t over a distance x of 10 to 50 cm is on the scale of weeks to a year for the sulphide ion with a diffusion coefficient D in the order of $7*10^{-6}$ cm^{2}s^{-1} (Passier et al., 1996a/Chapter 2), estimated using $t = x^2/10D$ (e.g. Crank et al., 1981). The rate of the front migration depends mainly on the relative magnitudes of downward sulphide and upward Fe fluxes, and the content of reactive Fe below the sapropel.

Thus, the pyrite profiles are the result of a dynamic system of temporal variations of sulphide production relative to Fe liberation and supply during sapropel deposition. Two steady-state situations are the end-members of this system: the first results in pyrite peaks within the

sapropels, and the second results in pyrite peaks below the sapropels.

Apart from these temporal variations in relative sulphide and Fe availability, there are also lateral variations in pyrite formation in sapropels. The background reactive Fe content that reacts with S to form pyrite is 100 µmol g^{-1}, about 0.5 wt%. Berner (1969) somewhat arbitrarily defined marine sediments with >1.4 wt% reactive Fe as high-Fe-content systems, therefore, it can be concluded that the eastern Mediterranean sapropels are potentially low-Fe-content systems, so that downward sulphidisation below each sapropel can occur. However, Pruysers et al. (1993) reported S1 sapropels without pyrite enrichments in the sediments below the sapropels. These sapropels were recovered at about 600 m water depth, near Crete. Compared to the pyrite contents in the lateral equivalent sapropel S1 in UM26 (S_{pyr} up to 400 µmol g^{-1}), the maximum S_{tot} contents are low (only 150 to 250 µmol g^{-1}). Moreover, reactive Fe contents are still high in these sapropels (Pruysers et al., 1993). Perhaps the bottomwaters overlying these shallow sapropels have been reventilated more often and more extensively than the bottomwaters in the deeper parts of the basin, which resulted in more oxic and suboxic degradation of organic matter, and less SO_4^{2-} reduction and sulphide production. This distinction between the shallower and the deeper parts of the basin was also suggested by several investigators to explain increasing C_{org} contents with increasing depth of deposition (Béthoux, 1993; Rohling, 1994). Additionally, upward-diffusing Fe(II) not trapped by sulphide or oxygen may have escaped from the sediments and migrated into the bottomwater. Elsewhere in the basin this Fe could have been included in Fe sulphide formation. As opposed to this example of shallow water sapropels that are continuously in the high-Fe-content mode (relative to sulphide production), sapropel 969 seems to be an example for an extreme low-Fe-content mode (relative to sulphide producton) (Passier and de Lange, 199_/Chapter 3). The extreme Fe limitation in this sapropel resulted not only in diffusion of sulphide out of the sapropel but also in accumulation of dissolved sulphide and consequently in organic S formation (Passier and de Lange, 199_/Chapter 3).

5.3.1.6 Stable S isotope composition of pyrite in relation to the two scenarios

Bulk sediment δ^{34}S values in Pleistocene sapropel S7 and in the S-enriched zone below are about -40‰ (Passier et al., 1996a/Chapter 2). Whereas our previous study focussed on total sediment S-isotopes, we now have data for stable S isotopes of pyrite δ^{34}S$_{pyr}$ for the three sapropels discussed in this paper (Fig. 5.1). The δ^{34}S$_{pyr}$ reflects δ^{34}S of sulphide formed, because limited fractionation occurs when reduced S is transformed into pyrite (Price and Shieh, 1979). The δ^{34}S$_{pyr}$ values associated with the sapropels are relatively light (-36.7‰ to -49.6‰ in S1, -37.1‰ to -47.7‰ in 967, and -33.1‰ to -48.0‰; Fig. 5.1; Table 5.1). This implies that fractionations of at least 53.7‰ to 70.2‰ occurred relative to present Mediterranean seawater (δ^{34}S ≈ +20.6‰, de Lange et al., 1990). Isotopic fractionations of 40‰ to 70‰ between SO_4^{2-} and reduced solid S are usually observed in marine sediments (e.g. Goldhaber and Kaplan, 1974; Chambers and Trudinger, 1979). The observed high fractionations indicate that SO_4^{2-} reduction took place in an open system, where exchange with seawater readily occurred, so that SO_4^{2-} supply via diffusion or advection was large relative to the SO_4^{2-} reduction rates, and SO_4^{2-} was never depleted. Such a setting is possible close to the sediment-water interface during sapropel

deposition or in the water column. Barium, mainly present as barite (Bishop, 1988; Thomson et al., 1995), does not seem to be significantly remobilized in the sapropels of this study (Fig. 5.1), giving additional evidence that SO_4^{2-} was never significantly depleted in the sapropel layers. A maximum $^{34}S/^{32}S$ fractionation of 46‰ between sulphide and SO_4^{2-} has been observed in experimental studies on microbial dissimilatory SO_4^{2-} reduction (e.g. Chambers and Trudinger, 1979). Further isotope fractionation, however, may result from reoxidation of sulphide to intermediate S species such as elemental S or thiosulphate, followed by the bacterial disproportionation into isotopically lighter sulphide and heavier SO_4^{2-} (Canfield and Thamdrup, 1994; Cypionka et al., 199_). Extensive, repeated HS$^-$ oxidation and disproportionation of intermediate oxidized S species result in lighter isotopic values ($\delta^{34}S$ values) of reduced S. The oxidation of sulphide required supply of oxidants during sapropel formation. Like the openness of the SO_4^{2-} reduction system, reoxidation of HS$^-$ is therefore most intense close to the sediment/water interface or in the water column.

Oxidants may have been nitrate and oxygen from the bottomwater or sedimentary Fe and Mn (hydr)oxides. In scenario A (Fig. 5.3a), these oxidants are available from sedimentary Fe and Mn (hydr)oxides, or by diffusion from the bottomwater to the sediment. Sapropel S1(UM26) is bioturbated, therefore, additional supply of oxidants was possible via porewater irrigation and solid-phase mixing. Sapropel 967, however, is not as bioturbated as S1, and sapropel 969 is even laminated (Emeis, Robertson, Richter, et al., 1996). In scenario B (Fig. 5.3b), where a variable part of the water column may be anoxic extending from the bottom into the water column, sulphide may be reoxidized at the chemocline. Subsequently, evolved elemental S settles back to to sediment and disproportionates, causing more negative S isotope values in the water column and in the sediment. Moreover, Fe sulphides may form at or just below the chemocline. A similar scenario was proposed for the present-day euxinic Black Sea (Canfield and Thamdrup, 1994). Apart from relatively light sulphide, relatively heavy SO_4^{2-} forms during disproportionation, this heavy SO_4^{2-} is taken up in the large SO_4^{2-} pool which has an open connection with the bottomwater, so that the pool as a whole will not become significantly heavier.

5.3.1.7 $\delta^{34}S_{pyr}$ values within sapropels vs. $\delta^{34}S_{pyr}$ values below sapropels

The $\delta^{34}S_{pyr}$ values below the sapropels are lighter than those within the sapropels. This difference may be the result of the two different scenarios in which pyrite forms. In scenario A sulphide is rapidly consumed by Fe, whereas in scenario B sulphide is not directly trapped as Fe sulphide. Therefore, the sulphide pool in scenario B is more subject to reoxidation and disproportionation and it will become lighter. Pyrite formation from this sulphide pool is predominantly below the sapropel, and thus pyrite below the sapropel has more negative $\delta^{34}S_{pyr}$ values than pyrite within the sapropel. During extreme scenario B-conditions, isotopically light Fe sulphides may also form in the water column. In contrast, pyrite that forms within the sapropel in scenario A, in periods with low sulphide production rates, is heavier.

Another reason for the difference in $\delta^{34}S_{pyr}$ values within and below sapropels may arise when SO_4^{2-} reduction proceeds on a relatively low level after burial of the sapropel. Then porewater SO_4^{2-} could become depleted and become progressively heavier with depth ("reservoir

effect," e.g. Jørgensen, 1979). Consequently, heavier sulphide and pyrite would form within the sapropel. Porewater SO_4^{2-} concentrations at ODP sites 967 and 969 do not show a decrease with depth. In contrast, there is even an increase with depth as a result of diffusion of SO_4^{2-} from underlying Messinian salt deposits (Emeis, Robertson, Richter, et al., 1996). $\delta^{34}S$ values of SO_4^{2-} increase with depth, for example from bottomwater values at the top of 969 to + 25.8 ‰ at 50 mbsf (Böttcher et al., 199_a), due to a diffusive supply of SO_4^{2-} derived from Messinian evaporites ($\delta^{34}S$ = +23‰, Böttcher et al., 199_a) superimposed on bacterial SO_4^{2-} reduction at relatively low rates.

It could be argued that the relatively light $\delta^{34}S_{pyr}$ below the sapropels is caused by reoxidation of downward-diffusing sulphide by Fe (hydr)oxides present below the sapropel, and subsequent disproportionation. Depending on the relative magnitudes of the downward sulphide flux and the upward Fe flux, the sulphidisation front moves downward and thus new oxidants are included in the reaction. Whenever the sulphidisation front remains at one level for a longer period, or passes a certain level again, the accumulating pyrite will not be as light as the first pyrite, because pyrite is formed from Fe(II) rather than from Fe (hydr)oxides. However, this cannot be the explanation of the decreasing $\delta^{34}S_{pyr}$ with depth below each sapropel, for the decrease in $\delta^{34}S_{pyr}$ coincides with an increase in pyrite content, and thus a larger portion of pyrite formed without Fe (hydr)oxides.

Part of the pyrite below each sapropel is formed in the absence of external oxidants at the site of pyrite formation, whereas the sulphide pool (in the sapropel) from which it forms may be significantly influenced by reoxidation-disproportionation. Most pyrite reaction mechanisms include an external oxidant at the site of pyrite formation. Recently, direct pyrite formation with sulphide itself acting as an oxidant has been suggested (e.g. Drobner et al., 1990; Rickard, 1997). Although S isotope fractionation upon this reaction has not yet been investigated, it is expected that only minor isotope effects should occur in analogy to the experimental results of Price and Shieh (1979).

5.3.1.8 The sulphide reoxidation index

A measure for the proportion of reduced S that formed during times of intensive reoxidation ("the sulphide reoxidation index") can be established using the following isotopic balance, assuming that the pyrite consists of two end-members, one formed at times of minimal sulphide reoxidation, and another formed at times of maximum sulphide reoxidation:

$$\delta^{34}S_{pyr} = (1-a) \times \delta^{34}S_{min} + a \times \delta^{34}S_{max} \, ,$$

where $\delta^{34}S_{min}$ is an estimate of the $\delta^{34}S_{pyr}$ values resulting from minimal reoxidation of sulphide, $\delta^{34}S_{max}$ from maximum reoxidation. After rearranging the equation, the sulphide reoxidation index (a) is:

$$a = \frac{\delta^{34}S_{pyr} - \delta^{34}S_{min}}{\delta^{34}S_{max} - \delta^{34}S_{min}} \, .$$

sulphide reoxidation index
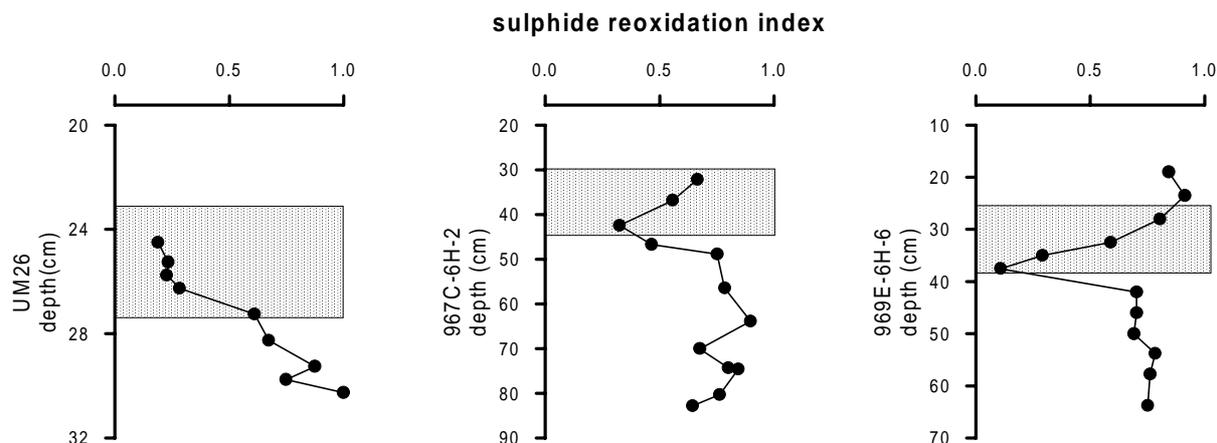
Figure 5.5 *Sulphide reoxidation indices in sapropels S1 in boxcore UM26, ODP-160-967C-6H-2, 30-44 cm and ODP-969E-6H-6, 27-39 cm.*

The assumption that there are only two S isotopic components in the pyrite pool is a rough generalisation. It is not known how much depletion was achieved during each oxidation-disproportionation cycle, therefore this index only yields a rough estimate and is not sufficient to indicate the exact extent of reoxidation. However, the index is illustrative as a comparison of the proportions of pyrite that formed from a highly reoxidized S pool.

$\delta^{34}S_{max}$ is taken to be -49.6‰, which is the lowest $\delta^{34}S_{pyr}$ value measured in the three studied sapropels. $\delta^{34}S_{min}$ has been calculated from the $\delta^{34}S$ value of Fe monosulphides that are present in the lower part of sapropel 969. These Fe monosulphides are thought to have formed from sulphide originating from present-day slow SO_4^{2-} reduction in the sapropel. The Fe monosulphides were oxidized during sampling, forming gypsum, which has been extracted with 0.5 M NaCl (Passier and de Lange, 199_/Chapter 3). $\delta^{34}S$ of the NaCl extractable S in the lower part of 969 is -22.0‰. This value has been corrected for the fraction of porewater SO_4^{2-} present in the sample, with a $\delta^{34}S$ value of +25.8‰ (Böttcher et al., 199_a). The resulting $\delta^{34}S$ value for the oxidized Fe monosulphides is -31.1‰, and the fractionation with respect to average $\delta^{34}S$ of porewater SO_4^{2-} is -54.3‰ in sapropels 967 and 969. Hereby, the $\delta^{34}S$ value of SO_4^{2-} is assumed to be the mean of bottomwater $\delta^{34}S$ values (+20.6‰) and the present-day $\delta^{34}S$ of porewater SO_4^{2-} in sapropel 969 (+25.8‰). For 969 and 967 $\delta^{34}S_{min}$ is thus -31.1‰. For S1, which has not been influenced (yet) by heavier SO_4^{2-} than bottomwater SO_4^{2-}, $\delta^{34}S_{min} = +20.6 -54.3 = -33.7‰$.

The calculated sulphide reoxidation indices (Fig. 5.5) are the highest below the sapropels and in the top of sapropels 967 and 969, where 60 to 90% of the pyrite formed at times of extreme sulphide reoxidation. A downward oxidation front has removed pyrite from the top of sapropel S1 in UM26 (e.g. van Santvoort, 1996), thus no indices are available for the top of S1. The pyrite below the sapropels formed at times of scenario B. Consequently, the sulphide reoxidation indices below each sapropel are high. The sulphide in the top of the sapropels may have formed in the water column from the relatively light sulphide pool at times of scenario B. The relatively high pyrite contents above sapropel 969, and its extremely negative $\delta^{34}S_{pyr}$, indicate that these sediments could have received sulphide from younger, overlying sapropels during a period of relatively high sulphide production. This might also have influenced the

extremely negative $\delta^{34}S_{pyr}$ in the top of sapropel 969.

The sulphide reoxidation indices within the lower part of the three sapropels (Fig. 5.5) show that only 10 to 30% of the reduced S in pyrite in these sediments has formed at times of high sulphide reoxidation. Low sulphide reoxidation indices mean that either the majority of Fe sulphides formed *in situ* within the sapropel during its deposition, or that slow SO_4^{2-} reduction and pyrite formation took place after burial of the sapropel. The first option is most likely in S1. The latter option may apply to sapropel 969, because pyrite formation was extremely Fe-limited during its formation as indicated by the uptake of reduced S in organic compounds. Moreover, the occurrence of Fe monosulphides at the base of sapropel 969 (see difference between S_{pyr} and $S_{reduced}$ (Fig. 5.1)) suggests ongoing SO_4^{2-} reduction within this organic-rich layer (Passier and de Lange, 199_/Chapter 3). In sapropel 967 both *in situ* pyrite formation during sapropel formation and after burial may have been important.

5.3.2 Sulphide reoxidation and paleo carbon burial efficiencies

Canfield and Teske (1996) proposed that the isotopic composition of reduced S in sediments can be related to the fraction of sulphide that is reoxidized and lost from the system (Fig. 5.6). The isotopic composition of pyrite in and below the sapropels is -30 to -50 ‰, this means that it is depleted by 50 to 70 ‰ relative to seawater SO_4^{2-}. Compared to the positive correlation between ^{34}S sulphide depletion and sulphide reoxidation percentage for marine sediments compiled by Canfield and Teske (1996), the oxidation percentage for sulphide in these sediments would be over 85%. This means that the reduced S in the sediment represents only
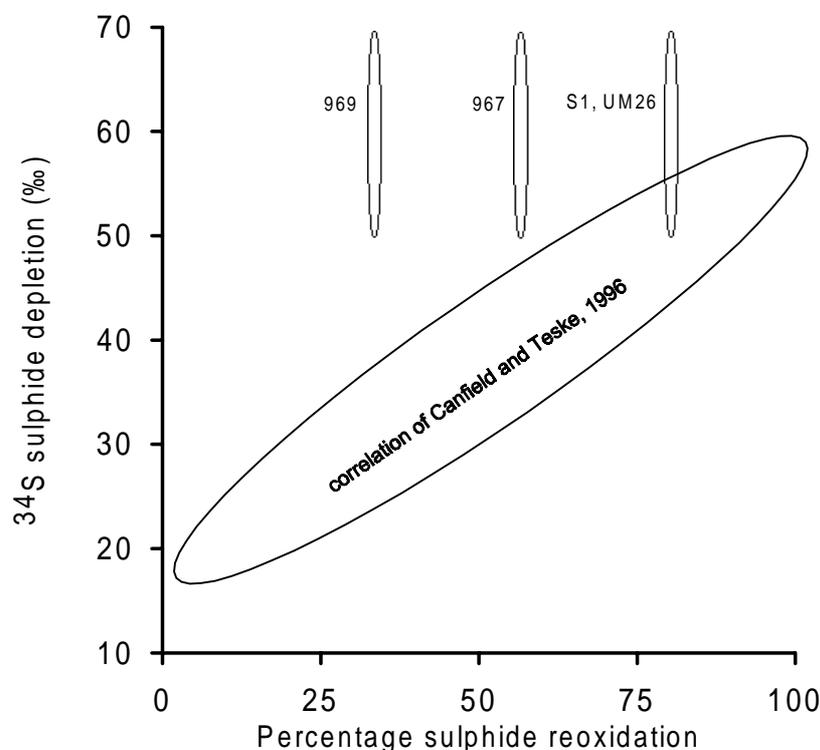
Figure 5.6 *^{34}S sulphide depletion vs. reoxidation percentage of initially produced sulphide.*

15% of the reduced S formed initially. This has large consequences for organic matter mineralisation and burial estimates that are based on the amount of reduced S found in the solid phase of the sediment.

The basis for calculation of the burial efficiency of C_{org} is the generalized SO_4^{2-} reduction reaction:

$$2CH_2O + SO_4^{2-} \rightarrow H_2S + 2HCO_3^- .$$
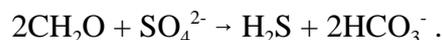
The burial efficiency for C_{org} in the sapropel can be calculated using:

$$BE_S = (\frac{C_{int}}{2 \times S_{int} + C_{int}}) \times 100\%.$$

Where C_{int} (mol/cm^2) and S_{int} (mol/cm^2) are depth integrated amounts of C_{org} and reduced S respectively, calculated as follows:

$$S_{int} = \int_0^l S \cdot dx = \int_0^l (S_{reduced} \times \rho) \cdot dx,$$

and

$$C_{int} = \int_0^z C \cdot dx = \int_0^z (C_{org} \times \rho) \cdot dx .$$

Where ρ is the dry bulk density (gdry/cm^3), C_{org} is the organic carbon content (mol/gdry), and $S_{reduced}$ (Fig. 5.1) is the reduced S content (mol/gdry). Position *0* is the top of the organic-rich layer, whereas *z* is at the bottom. Position *z* is also the top of the pyrite-enriched zone below the sapropel, whereas *l* is the lower boundary of this zone (Fig. 5.2). The pyrite peaks below the sapropels in 969 and 967 are taken to be the lower boundaries of the pyrite-enriched zone (*l*). Position *l* for S1 has been estimated using S_{tot} measurements in core MT1 (Fig. 5.2). The key assumption was made that S_{int} calculated in this way originates from the sapropel itself (Passier et al., 1996a/Chapter 2).

BE_S ranges from 55 to 80% (Table 5.2). Similarly calculated burial efficiencies reported by Passier et al. (1996a) (Chapter 2) in Holocene and Pleistocene sapropels range from 20 to 45%. These calculations are based on the assumptions that all organic matter mineralisation after burial took place by SO_4^{2-} reduction, and that 100% of reduced S is retained within the sediment. As discussed above, the latter assumption is not very realistic, since sulphide may escape from the sediment and may be reoxidized. Therefore, it is necessary to include all reoxidized sulphide in the calculation of the burial efficiency (BE_{Sox}):

$$BE_{Sox} = \frac{C_{int}}{2 \times f \times S_{int} + C_{int}} \times 100\%,$$

where:

$$f = \frac{100}{100-b},$$

where b is the percentage of initially produced sulphide that was reoxidized. Deduced from the correlation between ^{34}S sulphide depletion and percentage sulphide reoxidation, the reoxidation percentage is higher than 85% (Fig. 5.6). At 85% sulphide reoxidation BE_{Sox} values are 15 to 37%, and at 90% BE_{Sox} values are 11 to 29% (Table 5.2).

Canfield (1989) observed higher burial efficiencies for C_{org} in euxinic and semi-euxinic sediments compared to oxic sediments. The burial efficiencies that he calculated from actual SO_4^{2-} reduction rates, range from 13 to 48% for sites with sediment accumulation rates of 1.7 to 5 cm kyr^{-1}. These burial efficiencies compare favorably with the burial rates for the sediments discussed here (sediment accumulation rate = 3 cm kyr^{-1}) that were obtained while taking into account extensive oxidation of sulphide (BE_{Sox}, Table 5.2).

Table 5.2 *Calculated organic carbon burial efficiencies and sulphide reoxidation percentages in sapropels S1 in UM26, ODP-160-967C-6H-2, 30-44 cm and ODP-969E-6H-6, 27-39 cm. BE_s is the burial efficiency of organic carbon assuming no sulphide reoxidation, $BE_{Sox, 85\%}$ and $BE_{Sox, 90\%}$ are the burial efficiencies assuming 85% and 90% of sulphide reoxidation, respectively. The "sulphide reoxidation % at best fit" is the percentage calculated from comparison of paleoproductivities.*

sapropel	BE_S	$BESox, 85\%$	$BE_{Sox, 90\%}$	sulphide reoxidation percentage at best fit
S1	59	18	12	80
967	55	15	11	54
969	80	37	29	34

5.3.2.1 Enhanced preservation leading to higher organic carbon contents in sapropel 969

The computed BE_S and BE_{Sox} values are similar for S1 and 967, but those for 969 are higher (Table 5.2). Enhanced preservation in 969 might have been (partly) responsible for the extremely high C_{org} content in 969. The hypothetical amount of C_{org} that would be present in sapropel 969, if the burial efficiency was smaller, can be calculated using:

$$C_{int\ hypothetical} = \frac{(BE_{hypothetical})}{BE} \times C_{int}.$$

Organic carbon contents would be only 0.38 times of the contents observed now, when the same low burial efficiencies that occur in S1 and 967 are applied to the exceptionally organic-rich sapropel 969: $C_{int\,hypothetical} = 0.38 * C_{int}$ for $BE_{hypothetical} = 11\%$ instead of $BE = 29\%$ (90% sulphide reoxidation). A factor of 0.69 is found for $BE_{hypothetical} = 55\%$ instead of $BE_{hypothetical} = 80\%$ (when no sulphide reoxidation is assumed). This relates to maximum C_{org}-contents of only 9 to 16 wt% compared to the observed 23.5 wt%.

It should be realized that a possible underestimation of S_{int} in 969 also results in a higher burial efficiency of C_{org}. If the length of the S-rich zone below the sapropel is longer than assumed, S_{int} is underestimated. However, S_{int} would have to be 3.3 times larger to get $BE = 55\%$ instead of 80% and the S-rich zone below the sapropel should be longer than 1 m, an underestimation of this magnitude is unlikely.

Uptake of S into organic compounds might lead to the enhanced preservation of organic matter (Sinninghe Damsté and de Leeuw, 1990). Organic S compounds are relatively abundant in 969, these compounds formed as a result of extreme Fe limitation within the sapropel. S1 and 967 do not contain abundant organic S (Passier and de Lange, 199_/Chapter 3). It may also be possible that anoxicity in the water column resulted in a decreased degradation of organic matter, by the diminished ability of anaerobic bacteria to oxidize a full suite of sedimentary organic compounds (Canfield, 1989), or by the absence of meio- and macrofauna.

5.3.2.2 Checking the sulphide reoxidation percentage via estimates of paleoproductivity

Sapropels are reported to form at times of elevated productivity in the surface waters (e.g. Rossignol-Strick et al., 1982, Calvert et al., 1992). Estimates of the export paleoproductivity (the organic carbon that is exported from the photic zone into the deep sea) can be obtained through empirical formulas based on Ba contents of sediments ($P_{exp,\,Dym}$, Dymond et al., 1992), and organic carbon accumulation rates ($P_{exp,\,Sarn}$, Sarnthein et al., 1992). These calculations were performed as described in van Os et al. (1994). The mean calculated export productivities for sediments within the sapropels are 35 to 151 $gCm^{-2}yr^{-1}$ (Table 5.3). It should be realized that a lot of pittfalls and limitations are associated with the calculation of paleoproductivities from sediment parameters (Sarnthein et al., 1992; Dymond and Collier, 1996) especially because the empirical formulas were determined in oxic environments, which may not represent the eastern Mediterranean during sapropel deposition, and because of the fact that a lot of parameters in the empirical relationships cannot be directly measured in ancient environments. In spite of all these pitfalls and limitations, $P_{exp,\,Dym}$ and $P_{exp,\,Sarn}$ show a general good agreement (Table 5.3), therefore the calculations are probably yielding reasonable first-order estimates.

The mean export productivities during sapropel formation $P_{exp,\,Sarn}$ and $P_{exp,\,Dym}$ of 35 to 151 $gCm^{-2}yr^{-1}$ (Table 5.3), can be transformed into primary productivities in the surface waters (Eppley and Peterson, 1979), yielding values of 118 to 302 $gCm^{-2}yr^{-1}$. These values for the primary production during sapropel deposition are much higher than the present-day primary production in the eastern Mediterranean of 26 $gCm^{-2}yr^{-1}$ (Béthoux, 1989). In fact, they are comparable to primary productivities in recent high productivity areas, such as the Atlantic

Table 5.3 *Export productivities during sapropel formation calculated according to Sarnthein ($P_{exp, Sarn}$) and Dymond ($P_{exp, Dym}$) in sapropels S1 in UM26, ODP-160-967C-6H-2, 30-44 cm and ODP-969E-6H-6, 27-39 cm.*

sapropel	$P_{exp, Sarn}$ (gCm^{-2}yr^{-1})		$P_{exp, Dym}$ (gCm^{-2}yr^{-1})	
	max	mean	max	mean
S1	73	64	51	35
967	119	116	103	80
969	163	150	236	151

Ocean off North West Africa (50 to 250 gCm^{-2}yr^{-1}, Müller and Suess (1979)), and the Peru continental margin (330 gCm^{-2}yr^{-1}, Müller and Suess, 1979). For a Pliocene sapropel in a land section in Sicily van Os et al. (1994) calculated a maximum export productivity in the sapropel of about 50 gCm^{-2}yr^{-1}, thus in the same range as the export productivity in sapropel S1 in UM26.

Another estimate of the export paleoproductivity from the surface waters can be made from accumulation rates and burial efficiencies of C$_{org}$ using empirical relationships of Betzer et al. (1984) and Eppley and Peterson (1979). The burial efficiency of C$_{org}$ can be estimated from the reduced S content of the sediments and a certain sulphide reoxidation percentage. By comparing these values of export productivity with other estimates such as $P_{exp, Sarn}$ and $P_{exp, Dym}$, we can assess which oxidation percentage for sulphide is reasonable in this context.

The paleoproductivity calculations for the sapropels were repeated at different sulphide reoxidation percentages, and the obtained values were compared with $P_{exp, Sarn}$, by means of the residual sum of squares. The sulphide reoxidation percentages are 34 to 80% (Table 5.2) when the residual sum of squares is the smallest. These values are considerably lower than the sulphide reoxidation percentages (>85%) inferred from the relation between sulphide isotopic composition and sulphide reoxidation of Canfield and Teske (1996). Consequently, sulphide reoxidation might be less than one may conclude from this correlation. Nonetheless, it seems that substantial loss of sulphide occurred (Fig. 5.6). The sulphide reoxidation percentage for 969 is lower than the sulphide reoxidation percentage for 967. This is consistent with a lower sulphide reoxidation index (see earlier discussion) for 969 than for 967 (Fig. 5.5). Consequently, relatively more SO$_4^{2-}$ reduction without extensive reoxidation must have occurred after burial in 969 than in 967. The sulphide reoxidation index in S1 is lower than in 967, however, whereas the oxidation percentage calculated here is higher. This could result from $P_{exp, Sarn}$ being too high in S1, which also follows from the discrepancy between $P_{exp, Sarn}$ and $P_{exp, Dym}$ for this sapropel. The reoxidation in S1, therefore, could be much lower than 80%. Burial efficiencies associated with the calculated sulphide reoxidation percentages for the best fit are 16 to 73%, again, the highest burial efficiency is observed for 969 (Table 5.2).

5.3.2.3 Implications of the variations in paleoproductivity and burial efficiencies

Pyrite characteristics are determined by the relative magnitudes of sulphide production in the sapropels and Fe liberation and supply to the sapropels. The production of sulphide depends on the rate of SO_4^{2-} reduction and this in turn depends on input of reactive organic matter to the sediments. The input of organic matter is gouverned by the export productivity in the surface waters of the eastern Mediterranean, which is related to climate changes (Fig. 5.7; e.g. Rohling and Hilgen, 1991). The pyrite characteristics in and around the sapropels suggest that the sulphide production during deposition of each sapropel was subject to temporal (seasonal or climatic) and lateral variations.

climate   →   enhanced primary productivity   →   increased settling OM
                                                                                ↓
          ←←←←←←←←←←←←enhanced OM accumulation
       ↓

   sulphate reduction   →   reduced reactivity OM in sulphate reduction
                                                                (due to formation of organic S compounds;
                                                                disability of anaerobic bacteria to oxidize all
                                                                organic matter and absence of meio- and
                                                                macrobenthos in anoxic bottomwater (?))

       ↓   ↓

   reduced OM accumulation   enhanced OM accumulation
   pyrite formation relatively high   pyrite formation relatively low
   examples: S1, 967   example: 969

Figure 5.7 *Schematic representation of the effect of productivity and burial efficiency of organic carbon on the organic carbon accumulation and pyrite formation in sapropels.*

The mean calculated export productivities (Table 5.3) during sapropel formation were the highest for the most organic-rich sapropel (969) and the lowest for the least organic-rich sapropel (UM26). Moreover, burial efficiencies, and thus preservation, of organic matter for the sapropels increase with increasing organic matter accumulation. Thus, high C_{org} contents originate from both increased productivity in the surface waters as well as enhanced preservation (Fig. 5.7). A reason for this enhanced preservation in sapropel 969 could be that high sulphide production resulted in Fe limitation for pyrite formation and uptake of S into organic compounds. The formation of organic S compounds may have reduced the reactivity of the organic matter. Furthermore, anoxia in the bottomwaters may have resulted from the high sulphide production, initiating a decreased degradation of organic matter by the diminished ability of anaerobic bacteria to oxidize a full suite of sedimentary organic compounds (Canfield, 1989) or by preventing meio- and macrofauna to consume carbon. The reduced reactivity of organic matter may have acted as a feedback mechanism to slow down sulphide production (Fig. 5.7). A diminished sulphide production as well as the escape of sulphide from the sapropel causes the

lower pyrite contents relative to the high C_{org} contents in sapropel 969, compared to the other sapropels (Fig. 5.7). It is noteworthy that the sapropel with the highest C_{org} burial efficiency (969), also shows the most extensive SO_4^{2-} reduction after burial, indicating that reactive organic matter that was buried, became available for decomposition again.

5.4 Conclusions

(1.) The pyrite characteristics within and directly below each sapropel are determined by the relative magnitudes of sulphide production in the sapropels and Fe liberation and supply to the sapropel. Pyrite below the sapropels formed at times that sulphide production is high relative to Fe liberation and supply. Pyrite within the sapropel formed at times of low sulphide production relative to Fe liberation and supply.

(2.) Iron budgets show that sources of Fe for pyrite formation comprised only detrital and upward-diffusing Fe in sapropel S1, whereas in more organic-rich sapropels an additional input of Fe via water-column Fe sulphide formation likely occurred.

(3.) The pyrite microtextures within sapropels are mainly framboidal, resulting from fast pyrite formation at high saturation levels, whereas pyrite below sapropels is mostly euhedral, resulting from slow pyrite formation at low saturation levels.

(4.) The S isotopes in pyrite are depleted in ^{34}S relative to ^{32}S by 54 to 70 ‰ with respect to seawater SO_4^{2-}. Pyritic S below the sapropels is even more depleted than within the sapropels. This is due to more pronounced reoxidation of sulphide when sulphide production outcompeted Fe supply.

(5.) The estimated reoxidation percentages of sulphide in the different sapropels ranges from 34 to 80%, based on organic carbon fluxes and burial efficiencies.

(6.) Export productivity of organic matter from the surface waters was an order of magnitude higher during sapropel formation than at present. The highest productivity was found for the most organic-rich sapropel.

(7.) Enhanced preservation of organic matter is increasingly important in organic-rich sapropels.

Table 5.1 *Pyrite microtextures and stable isotope values of pyrite ($\delta^{34}S_{pyr}$) in samples within and below sapropels ODP-160-967C-6H-2, 30-44 cm and ODP-160-969E-6H-6, 27-39 cm.*

Sample ID	Position	Forms of pyrite, in order of importance	Size of majority of framboids	Diameter range of pyrite	Fig. 5.4	$\delta^{34}S_{pyr}$ (‰)
967C-6H-2, 36-38 (9671)	sapropel	framboids	5 to 10 µm	2 to 16 µm	b	-41.1
		euhedral crystals		2 to 10 µm	b	
		groups of euhedral shaped framboid-like aggregates		2 to 20 µm	f	
967C-6H-2, 63-65 (9672)	below sapropel	irregular euhedral aggregates		20 to 150 µm	e	-47.7
		euhedral crystals		2 to 30 µm	e	
		massive euhedral shell infilling and overgrowth		130 µm		
967C-6H-2, 74-75 (9673)	below sapropel, pyrite peak	massive euhedral shell infillings and overgrowths		several hundred µm		-45.9
		irregular euhedral aggregates		20 to 100 µm		
		euhedral crystals		10 to 16 µm		
969E-6H-6, 27-29 (9691)	upper sapropel	groups of "veiled" framboids	2 to 10 µm	groups: 30 to 300 µm, framboids: 2 to 15 µm	g	-46.0
		framboids		2 to 20 µm	a	
		euhedral crystals		<1 to 7 µm	a	
969E-6H-6, 37-38 (9692)	lower sapropel	framboids	5 to 10 µm	2 to 17 µm		-33.1
		euhedral crystals		1 to 10 µm		
969E-6H-6, 57-59 (9693)	below sapropel, pyrite peak	irregular euhedral aggregates		20 to 80 µm	c	-45.2
		massive euhedral shell infillings and overgrowths		up to 300 µm	d	
		euhedral crystals		2 to 10 µm		

Chapter 6

Sulphur enrichment in organic matter of eastern Mediterranean sapropels: a study of sulphur isotope partitioning*

Abstract–Eastern Mediterranean sediments containing three different sapropels (S1 in Core UM26, i-176 in ODP Core 967C, and i-282 in ODP Core 969E) were analysed in detail for δ^{34}S values and S/C ratios of organic matter by combustion-isotope ratio monitoring mass spectrometry (C-irmMS). The organic sulphur in the sediments is a mixture of sulphur derived from (1) incorporation of inorganic reduced sulphur produced by dissimilatory microbial sulphate reduction, and (2) biosynthetic sulphur. Organic sulphur is enriched within the sapropels where pyrite formation was Fe-limited for certain periods of time. During these periods, the surplus of sulphide diffused out of the sapropels, which caused pyrite formation below the sapropels and sulphide reoxidation in the water column above the sapropels. At the same time a significant excess of dissolved sulphide was present within the sapropels and reactive Fe was no longer competing with organic matter for the uptake of reduced sulphur.

6.1 Introduction

Abundant inorganic reduced S is present in eastern Mediterranean organic-rich sediment layers (sapropels). The predominant S compound in the sapropels is pyrite (FeS_2). Pyrite formed from Fe and from sulphide that was produced by dissimilatory bacterial SO_4^{2-} reduction. Sulphate reduction took place during and shortly after sapropel formation. After burial of the sapropels SO_4^{2-} reduction has not been important, in view of the SO_4^{2-} concentrations and SO_4^{2-} isotopic compositions of the porewaters (Böttcher, 199_a; Passier et al., 199_/Chapter 5). Pyrite formation within the organic-rich layers has been Fe-limited during sapropel deposition (Passier et al. 1996a/Chapter 2). Organic substances compete with reactive Fe for reduced S in sediments, especially when the amount of reactive Fe is limited. In that case bisulphide (HS⁻) concentrations in the porewaters rise, and organic matter can become a significant sink for reduced S (Kaplan et al., 1963; Nissenbaum and Kaplan, 1972; Francois, 1987a and 1987b; Bein et al. 1990; Mossmann et al. 1990 and 1991; Ferdelman et al. 1991; Raiswell et al., 1993; Henneke et al., 1997; Hartgers et al., 1997). In sediments, this uptake of reduced S into organic matter is assumed to take place via reactions of sulphide and/or polysulphides with reactive sites on organic molecules (Casagrande et al., 1979; Mango, 1983; Francois, 1987a and 1987b; Kohnen et al., 1989; Sinninghe Damsté and de Leeuw, 1990; Philip et al., 1992).

Sulphur that is present in the organic fraction of marine anoxic sediments mainly originates from the uptake of reduced inorganic S during early diagenetic processes. In addition,

---

biosynthesized S, present in labile fractions of organic tissues, may be incorporated in residual organic matter after liberation from the original labile tissues during decomposition at the earliest stages of diagenesis (Anderson and Pratt, 1995; Brüchert and Pratt, 1996). Analysis of stable S isotopes can reveal the origin of S in organic matter. Reduced S produced by dissimilatory bacterial SO_4^{2-} reduction has a relatively light, negative, isotopic composition. In contrast, biosynthetic S incorporated in living tissues has an isotopic composition similar to seawater SO_4^{2-} (e.g. Kaplan et al., 1963). The sulphidisation of organic matter can reduce the lability and thus enhance the overall preservation of organic matter (e.g. Sinninghe Damsté and de Leeuw, 1990).

In this paper, we report on the contents and isotopic composition of the organic S compounds in eastern Mediterranean sapropels. We propose a model for organic S formation and constrain the timing with respect to pyrite formation.

6.2 Materials and methods

6.2.1 Samples

Three sapropels were selected for detailed investigation. Sapropel S1 in boxcore UM26 (33°23.6'N, 25°0.9'E, water depth 2160 m) was recovered 200 km south of Crete during the 1994 *Palaeoflux* cruise of R/V *Urania* (Fig. 1.1). The sapropel, at about 0.24 metres below seafloor (mbsf), is 4 cm thick and appears bioturbated. The age of sapropel S1 is 5 to 9 kyr (Higgs et al., 1994). Light grey sediments lie beneath the sapropel, orange-brown sediments lie above it. A subcore of UM26 was sampled at a resolution of 0.5 to 1 cm aboard ship inside an N_2-filled glovebox and stored under N_2 in airtight containers at 4°C, another subcore was divided into cm-thick slices from which porewaters were extracted in Reeburgh-type sediment squeezers inside an N_2-filled glovebox (de Lange, 1992); the residual sediments were stored at 4°C. Two sapropels, recovered during ODP Leg 160 with Drilling Vessel *JOIDES Resolution* were sampled in detail directly after core-splitting aboard ship. Sapropel 967 originates from Section 160-967C-6H-2. Site 967C (34°4.3'N, 32°43.5'E, water depth 2553 m) is located on a small ridge near the foot of the northern slope of the Eratosthenes seamount, about 70 km south of Cyprus (Fig. 1.1). At this site 80 sapropels from early Pliocene to Holocene age were recovered. The sampled interval contains a 14 cm-thick sapropel at 49.3 mbsf, starting at 30 cm section-depth. The sapropel is brownish black and surrounded by grey sediments. It was deposited at the end of the Pliocene (age: 1.808 Ma; i-cycle 176; L. Lourens, personal communication) and appears bioturbated. The other Leg 160 sapropel, 969, was recovered in Section 160-969E-6H-6. Site 969E (33°50.5'N, 24°53.0'E, water depth 2201 m) is located on the Mediterranean Ridge, 30 miles NW of the UM26-site (Fig. 1.1). Hole 969E contains 80 sapropel beds from early Pliocene to Holocene age. The sampled interval contains a 12 cm-thick black sapropel at 50.7 mbsf, with the top at 27 cm in the section, surrounded by light grey sediments. This sapropel belongs to a group of black sapropels of Pliocene age (2.943 Ma; i-cycle 282; L. Lourens, personal communication) with high organic C contents (up to 30%) imbedded in a grey interval. The dark sapropel has a fine horizontal internal structure, which may be the result of primary lamination (Emeis, Robertson, Richter, et al., 1996). About fifteen samples of 1.5 cm thickness each were taken over an interval of 70 and 50 cm for 967 and 969, respectively. The samples were stored

under N_2 in airtight containers at $4^{\circ}C$.

Table 6.1 *Isotopic compositions of humic acids ($\delta^{34}S_{hum}$), fulvic acid fractions ($\delta^{34}S_{ful\,I}$ and $\delta^{34}S_{ful\,II}$), and Cr(II) residues ($\delta^{34}S_{org}$) in UM26.*

Core	sample ID	depth in section (cm)	position wrt sapropel	$\delta^{34}S_{hum}$ (‰)	$\delta^{34}S_{ful\,I}$ (‰)	$\delta^{34}S_{ful\,II}$ (‰)	$\delta^{34}S_{org}$ (‰)
UM26	D0025	11.5	above	+14.0	+14.7	+11.6	+4.3
UM26	D0031	21.5	oxidized	+14.2	+14.0	+15.4	+12.4
UM26	D0033	23.5	within	-6.0	-18.6	-	-
UM26	D0035	25.5	within	-10.0	-3.6	-6.8	-6.9
UM26	D0038	28.5	below	+11.5	+5.1	+3.6	+5.9
UM26	D0040	30.5	below	+10.4	+13.0	+0.9	+11.4

-: no data

wrt: with respect to

6.2.2 Total S and organic C

Subsamples were dried at 40°C or freeze-dried and ground in an agate mortar before dissolution in an $HClO_4$-HNO_3-HF acid mixture. The dried residue was dissolved in 1 M HCl for analysis of total S (S_{tot}) with a Perkin Elmer OPTIMA 3000 inductively coupled plasma atomic emission spectrometer (ICP-AES). Organic carbon (C_{org}) contents were determined with a Fisons Instruments NA-1500 NCS analyser after removal of carbonate in 1 M HCl. S_{tot} and C_{org} measurements were performed according to standard laboratory procedures and have standard deviations < 5%. International and in-house standards were used to check the procedures.

6.2.3 Pyrite, humic S and non-extractable organic S

Pyritic S (S_{pyr}) was extracted with the Cr(II) reduction method (Zhabina and Volkov, 1978; Canfield et al., 1986; Passier and de Lange, 199_/Chapter 3). Dried subsamples were extracted with acetone for several hours to remove elemental S (including elemental S formed during drying from acid-volatile sulphides (AVS) and organic polysulphides, and elemental S initially present), before pyrite extraction with 20 ml of 1 M HCl/1 M $CrCl_2$ solution for 2.5 h in an N_2 atmosphere at room temperature. Sulphide that evolved in the pyrite extraction was stripped from reaction solutions with N_2 or Ar, and trapped in 1 M NaOH. The NaOH solution was analysed for sulphide by square wave voltammetry (SWV) with a Princeton Applied Research Model 384B-4 polarographic analyser system equipped with a Model 303A static mercury drop electrode (SMDE).

A sequential extraction procedure for quantitative analysis of sedimentary S species (Passier and de Lange, 199_/Chapter 3, based on work by Francois, 1987a and 1987b; Ferdelman et al., 1991; Henneke et al., 1997), was applied to wet subsamples under an N_2 atmosphere. During this extraction humic substances were extracted from the sediments with 0.5 M NaOH after removal of porewater S, elemental S, low-weight organic S, acid-volatile sulphides and

organic polysulphides. NaOH extracts containing humic S (S_{hum}) were analysed for S by ICP-AES. Subsequently, the residue of this extraction was dissolved in an $HClO_4$-HNO_3-HF acid mixture, dried, and dissolved in 1 M HCl for analysis of residual S (S_{res}) by ICP-AES. The residual phases of the sequential extraction are pyrite and non-extractable organic S. The content of non-extractable organic S (S_{orgres}) was calculated from the difference between S_{res} and S_{pyr}. The average relative deviations from the mean in duplicate measurements were 10% for S_{pyr}, 8% for S_{res}, and 9% for S_{NaOH}.

For the analysis of stable S isotopes of pyrite ($\delta^{34}S_{pyr}$; Passier et al., 199_/Chapter 5), H_2S evolved from pyrite during Cr(II) reduction was trapped in a Cd-acetate solution as CdS, $AgNO_3$ solution was added and Ag_2S precipitated. The Ag_2S precipitates were washed with demineralized water and measured for their stable S isotope composition (see below).

Table 6.2 *S/C ratios calculated from S_{org} and C_{org} (($S/C)_{org}$) and from direct measurements of the S and C contents of the Cr(II) residues (($S/C)_{res}$) in samples from sapropel 969.*

sample ID	depth in section (cm)	$(S/C)_{org}$	$(S/C)_{res}$
160-969E-6H-6, 27-29	28	0.021	0.021
160-969E-6H-6, 32-33	32.5	0.026	0.029
160-969E-6H-6, 34-36	35	0.023	0.025
160-969E-6H-6, 37-38	37.5	0.025	0.019

6.2.4 Combustion-isotope ratio monitoring mass spectrometry (C-irmMS)

Sulphur isotope ratios ($^{34}S/^{32}S$) of the different separated fractions described in this paper were analysed by combustion-isotope ratio monitoring mass spectrometry (C-irmMS) as described by Böttcher et al. (199_a). Samples were combusted in an elemental analyser (Carlo Erba EA 1108) connected to a Finnigan MAT 252 mass spectrometer via a Finnigan MAT Conflo split interface. The liberated SO_2 gas was transported in a continuous stream of He (5.0 grade). Pure Sn cups (99.9 % Sn, Luedi) used for combustion were carefully precleaned (Böttcher et al., 1997) to minimize blank variations. For all samples containing organic C, the helium dilution option of the Conflo II was used to reduce the entry of CO_2 into the ion source of the mass spectrometer. $^{34}S/^{32}S$ ratios are given in the δ-notation ($\delta^{34}S$) relative to the Vienna-Canyon-Diablo Troilite (V-CDT) standard. Replicate measurements of $\delta^{34}S$ agreed within +/- 0.2‰, except for fractions with extremely low S contents (<0.01 wt% S) where the reproducibility was estimated to be better than +/- 1‰. Additionally, the mass spectrometric signal on mass 64 was used to quantify the S contents of some fractions (Böttcher et al., 199_b). The total organic carbon (TOC) content was analysed in selected samples using the mass spectrometric signal on mass 44.

Table 6.3a *Organic C (C_{org}), organic S (S_{org}), ($S/C)_{org}$, isotopic compositions of organic S ($\delta^{34}S_{org}$), and isotopic composition of pyritic S ($\delta^{34}S_{pyr}$) in and around sapropel S1 in UM26. Additional $\delta^{34}S_{pyr}$ and C_{org} values were taken from Passier et al., 199_/Chapter 5.*

Sample ID	depth in section (cm)	position wrt sapropel	C_{org} (wt%)	S_{org} (wt%)	$(S/C)_{org}$	$\delta^{34}S_{org}$ (‰)	$\delta^{34}S_{pyr}$ (‰)
D0025	11.5	above	0.12	0.0073	0.022	+4.3	-
D0031	21.5	oxidized	0.27	0.014	0.020	+12.4	-
D0033	23.5	within	1.7	-	-	-	-
DD01291	24.5	within	2.1	-	-	-	-36.7
DD01293	25.3	within	2.2	0.050	0.009	-5.8	-37.4
D0035	25.5	within	2.0	0.061	0.011	-6.9	-38.5
DD01294	25.8	within	2.3	0.24	0.038	-4.8	-37.3
DD01295	26.3	within	1.8	-	-	-	-38.2
DD01297	27.3	within	1.1	-	-	-	-43.4
DD01299	28.3	below	0.63	-	-	-	-44.4
D0038	28.5	below	0.38	0.014	0.014	+5.9	-47.4
DD01301	29.3	below	0.34	-	-	-	-47.6
DD01302	29.8	below	0.17	-	-	-	-45.6
DD01303	30.3	below	0.16	-	-	-	-49.6
D0040	30.5	below	0.16	0.0085	0.020	+11.4	-48.3

-: no data

wrt: with respect to

6.2.5 Isolation of organic S compounds for stable S isotope analysis

In order to get a complete extraction of humic substances, an extraction scheme based on Poutanen and Morris (1983) and Fengler et al. (1989) was applied to a set of samples from core UM26 from which porewaters had been removed: 4 to 8 gram of freeze-dried sediment was extracted with 40 ml of 0.1 M NaOH/0.1 M $Na_2P_2O_7$. The solution was purged with N_2 to remove oxygen. The extraction tubes were placed in the dark in an ultrasonic bath for 1 h and subsequently in a shaker for 23 h, then the extracts were separated from the residue by centrifuging and decanting. This extraction was repeated until the extract was colourless (8 repetitions). The 8 extracts were combined, filtered (1 µm glasfiber) and acidified with HCl to pH 1-2. By acidification the part of the humic substances that are base soluble, but acid insoluble

Table 6.3b *Organic C (C_{org}), organic S (S_{org}), $(S/C)_{org}$, isotopic compositions of organic S ($\delta^{34}S_{org}$), and isotopic composition of pyritic S ($\delta^{34}S_{pyr}$) in and around sapropel 967. Additional $\delta^{34}S_{pyr}$ and C_{org} values were taken from Passier et al., 199_/Chapter 5.*

Sample ID	depth in section (cm)	position wrt sapropel	C_{org} (wt%)	S_{org} (wt%)	$(S/C)_{org}$	$\delta^{34}S_{org}$ (‰)	$\delta^{34}S_{pyr}$ (‰)
160-967C-6H-2, 12-13	13.7	above	0.18	0.0041	0.009	+5.3	-
160-967C-6H-2, 31-33	32.2	within	5.8	-	-	-	-43.4
160-967C-6H-2, 36-38	36.9	within	7.4	0.32	0.016	-26.0	-41.4
160-967C-6H-2, 42-43	42.5	within	6.8	-	-	-	-37.1
160-967C-6H-2, 46-47	46.7	below	0.27	-	-	-	-39.7
160-967C-6H-2, 48-50	48.9	below	0.36	-	-	-	-45.0
160-967C-6H-2, 56-57	56.4	below	0.19	-	-	-	-45.6
160-967C-6H-2, 63-65	63.9	below	0.16	-	-	-	-47.7
160-967C-6H-2, 69-71	70	below	0.16	-	-	-	-43.6
160-967C-6H-2, 74-75	74.3	below	0.29	0.004	0.005	+15.8	-45.9
160-967C-6H-2, 74-76	74.6	below	0.17	-	-	-	-46.7
160-967C-6H-2, 80-81	80.3	below	0.18	-	-	-	-45.2
160-967C-6H-2, 82-84	82.8	below	0.39	-	-	-	-43.0

-: no data

wrt: with respect to

are precipitated (humic acids), while the substances that are both base and acid soluble (fulvic acids) remain in solution. Humic acids were allowed to precipitate for 48 h in a shaker in the dark, after which the mixtures were centrifuged and decanted. The residues were dialysed against demineralized water for 6 days and dried in a desiccator. The yield of humic acids was 0.02 to 0.48% of the original dry sediment. The solution containing fulvic acids was evaporated in a water bath at 80 to 90°C to a volume of about 30 ml. During evaporation, precipitates formed in the extracts, it is not clear whether these were humic or fulvic acids. These precipitates were separated from the solution by centrifuging, dialysed against demineralized water and dried. This "fulvic acid I" fraction was 0.03 to 0.38 wt% of the original sediment. The remaining solution was dialysed and totally evaporated in a desiccator, the "fulvic acid II" fraction was 0.05 to 0.19 wt% of the original sediment. The residual sediments were subsequently extracted with 0.5 M NaOH, there was no yield, however. Thus, the 0.1 M NaOH/0.1 M $Na_2P_2O_7$ extraction removed the humic substances quantitatively.

Table 6.3c *Organic C (C_{org}), organic S (S_{org}), (S/C)$_{org}$, isotopic compositions of organic S ($\delta^{34}S_{org}$), and isotopic composition of pyritic S ($\delta^{34}S_{pyr}$) in and around sapropel 969. Additional $\delta^{34}S_{pyr}$ and C_{org} values were taken from Passier et al., 199_/Chapter 5.*

Sample ID	depth in section (cm)	position wrt sapropel	C_{org} (wt%)	S_{org} (wt%)	(S/C)$_{org}$	$\delta^{34}S_{org}$ (‰)	$\delta^{34}S_{pyr}$ (‰)
160-969E-6H-6, 18-20	19	above	0.11	-	-	-	-46.7
160-969E-6H-6, 23-24	23.5	above	0.14	-	-	-	-48.0
160-969E-6H-6, 27-29	28	within	9.6	0.54	0.022	-29.0	-46.0
160-969E-6H-6, 32-33	32.5	within	23.5	1.65	0.026	-29.5	-42.0
160-969E-6H-6, 34-36	35	within	20.7	1.29	0.023	-29.0	-36.5
160-969E-6H-6, 37-38	37.5	within	17.3	1.13	0.025	-29.2	-33.1
160-969E-6H-6, 41-43	42	below	0.13	-	-	-	-44.1
160-969E-6H-6, 45-47	46	below	0.13	-	-	-	-44.1
160-969E-6H-6, 49-51	50	below	0.12	-	-	-	-43.9
160-969E-6H-6, 53-55	53.8	below	0.11	-	-	-	-45.6
160-969E-6H-6, 57-59	57.8	below	0.14	0.0053	0.014	-3.9	-45.2
160-969E-6H-6, 63-65	63.8	below	0.14	0.0030	0.008	+2.2	-45.0

-: no data

wrt: with respect to

This rather elaborate isolation scheme using base extractions, was compared with the isolation of organic S compounds in the residue of the pyrite extraction. Pyrite was removed from ca. 50 mg of acetone extracted sediment with the Cr(II) reduction method and the H_2S evolved from pyrite was precipitated as Ag_2S (see above). The residues of the Cr(II) reduction and the Ag_2S precipitates were washed with demineralized water. The residues only contain organic bound S, because SO_4^{2-}, elemental S, polysulphides and acid-volatile sulphide were removed during drying, acetone extraction and demineralized water washes.

The fractions recovered during the humic extractions and Cr(II) reduction were analysed for their stable S isotope composition by C-irmMS, yielding $\delta^{34}S_{hum}$, $\delta^{34}S_{ful\ I}$, $\delta^{34}S_{ful\ II}$, for the humic acids, fulvic acids I, and fulvic acids II, respectively, $\delta^{34}S_{org}$ for the Cr(II) residue, and $\delta^{34}S_{pyr}$ for Ag_2S.

Most of the isotopic compositions of the fractions from the base extraction were comparable to the values measured in the Cr(II) reduction residues ($\delta^{34}S_{org}$) (Table 6.1), only for D0025 $\delta^{34}S_{org}$ is remarkably lower than the $\delta^{34}S$ values of the base extractable S. In addition, the

stable S isotope compositions of the organic fraction were not influenced or contaminated during the Cr(II) reduction by pyritic S. This is clearly reflected by the positive values of organic S below sapropel S1, where only little organic S is present, but a large content of extremely negative pyrite is found (Table 6.1, Fig. 6.1). Therefore, we decided to use the Cr(II) reduction method to investigate the incorporation of S into organic matter within and around the eastern Mediterranean sapropels S1, 967 and 969. This method offers the advantage that both base-extractable and non-extractable organic matter are analysed, instead of a structurally ill-defined fraction of organic matter. Moreover, organic S and pyritic S can be analysed isotopically from the same small amount of sample, allowing a high downcore resolution of measurements. The average relative deviation from the mean in independent duplicate measurements of S contents in Cr(II) residues of sediment samples was 14%, the absolute deviations in independent isotope measurements were smaller than 2‰.
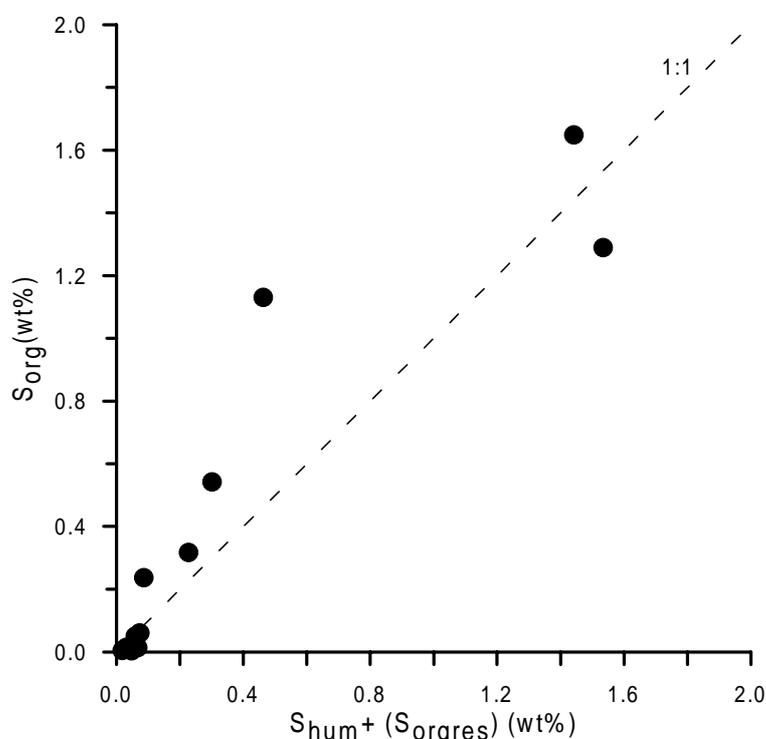
Figure 6.2 *Organic S measured in the residue of Cr(II) reduction (S_{org}) versus the sum of humic S and residual organic S of the sequential extraction (S_{hum} + (S_{orgres})) for samples within and around S1 in UM26, 967 and 969. Given is the 1:1 correlation line, the actual best fit is y = 1.00 x + 0.07, R-squared = 0.85.*

The S contents of the Cr(II) residues were corrected for the weight loss during Cr(II) extraction arising from loss of pyrite and acid-soluble phases (carbonates, oxides) to calculate the total organic S content of the sediments (S_{org}). The weight loss of acid-soluble phases is known from the determination of organic C. Atomic ratios of organic S to organic C in the sediments were calculated in two ways: from S_{org} and C_{org} (($S/C)_{org}$) and directly from the S and

C contents of the Cr(II) residues (($S/C)_{res}$), for the four samples where C contents of the residues were available. Comparison of the results showed that the S/C ratios calculated from S_{org} and C_{org} (($S/C)_{org}$) are reliable (Table 6.2).

S_{org} contents in the Cr(II) residue were compared to the sum of S_{hum} and S_{orgres} from the quantitative sequential extraction (Fig. 6.2); it appears that there is a good agreement between the two methods.

6.3 Results

The investigated sapropels contained significant amounts of organic C (C_{org}), with maxima of 2.3, 7.4, and 23.5 wt% for S1, 967 and 969, respectively (Fig. 6.1). Total S (S_{tot}) and pyritic S (S_{pyr}) contents were relatively high both within and below the sapropels (Fig. 6.1). Humic S (S_{hum}) was also enriched in the sapropels, and slightly elevated below the sapropels (Fig. 6.1). Sapropel 969 contained a significant amount of non-extractable organic S (S_{orgres}), whereas sapropel S1 and 967 did not (Fig. 6.1). Atomic ($S/C)_{org}$ ratios ranged from 0.005 to 0.022 above and below the sapropels, and from 0.009 to 0.038 within the sapropels (Table 6.3a, b, c). Isotopic compositions of organic S in Cr(II) residues ($\delta^{34}S_{org}$) ranged from -3.9‰ to +15.8‰ above and below the sapropels, and from -29.5‰ to -4.8‰ within the sapropels, the most negative values were found in sapropel 969 (Fig. 6.1; Table 6.3a, b, c). $\delta^{34}S$ values of coexisting pyrite ranged from -48.3‰ to -33.1‰ within and below the sapropels (Passier et al. 199_/Chapter 5; Fig. 6.1; Table 6.3a, b, c).

Figure 6.3 *Organic S contents (S_{org}) versus organic C contents (C_{org}), and ($S/C)_{org}$ versus C_{org} for samples within and around sapropels S1 in UM26, 967 and 969.*
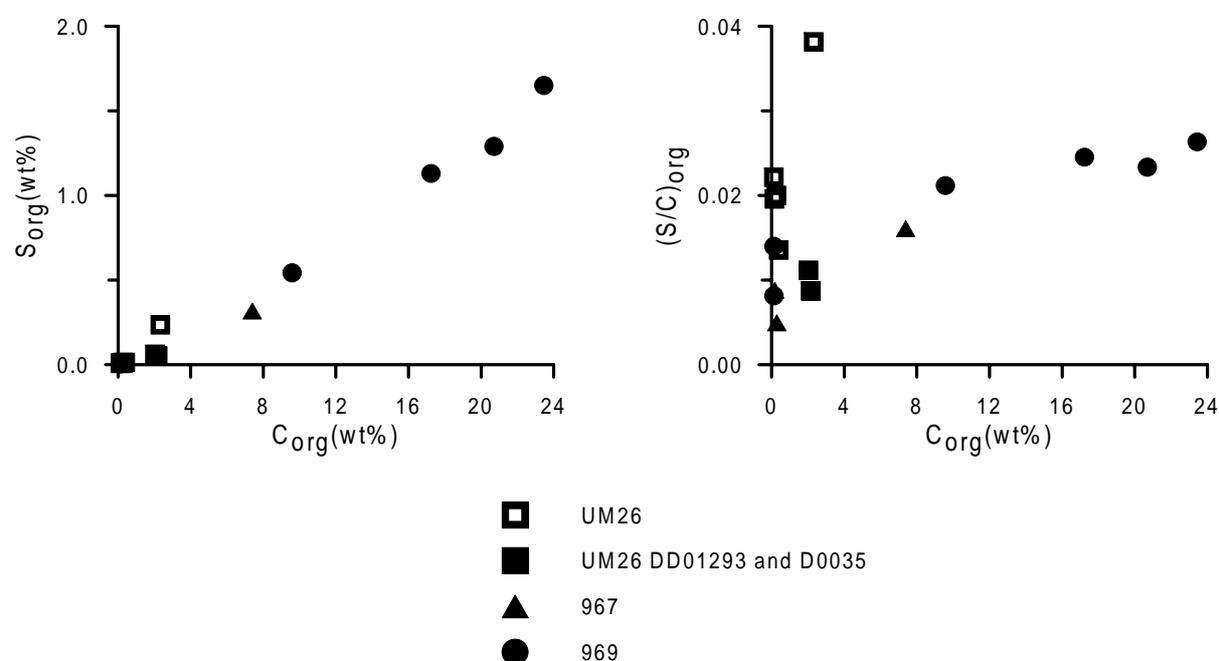
6.4 Discussion

Both the S_{org} contents and $(S/C)_{org}$ ratios of the sediments correlate positively with the C_{org} contents (Fig. 6.3). Published atomic $(S/C)_{org}$ ratios in several marine sediments and sedimentary rocks range from 0.006 to 0.38 (Table 6.4), overlapping the range observed in the present study (0.005 to 0.038; Tables 6.3 and 6.4). The facts that $(S/C)_{org}$ ratios increase with the C_{org} content (Fig. 6.3) and that they are larger than the algal ratios in marine plankton (0.004 to 0.010; Table 6.4), indicate uptake of S into organic matter, or preferential mineralisation of C over S within the organic-rich sediments. The organic matter in organic-poor non-sapropelic sediments is likely to be decomposed to a larger extent than the organic matter within the sapropels (Passier et al., 199_/Chapter 5), however, so preferential mineralisation of C over S would invoke larger increases in $(S/C)_{org}$ in organic-poor sediments. Therefore, preferential mineralisation of C over S cannot be the dominating mechanism. Moreover, most of the initial biosynthesized organic S compounds (proteins, amino acids) are relatively labile, and will be degraded rapidly after deposition. The uptake of reduced S into the organic matter during periods of high porewater sulphide concentrations in the sapropels is a more likely option, because the highest $(S/C)_{org}$ are found in the sediments where reactive reduced S compounds were most abundant during early diagenesis (Passier et al., 199_/Chapter 5). This hypothesis is supported by the decrease of $\delta^{34}S_{org}$ values with increasing $(S/C)_{org}$ ratios (Fig. 6.4).

6.4.1 Uptake of reduced S into organic matter

Sulphur that is biosynthesized by marine organisms has $\delta^{34}S$ values close to the $\delta^{34}S$ of seawater SO_4^{2-} from which it formed (e.g. Kaplan et al., 1963). Reduced S, produced during bacterial dissimilatory SO_4^{2-} reduction within the sapropel layers, is highly depleted in ^{34}S relative to ^{32}S. The isotopic composition of this reduced S, as deduced from the $\delta^{34}S$ values of pyrite associated with the sapropels, was between -33‰ and -50‰ (Passier et al., 1997 and 199_/Chapters 4 and 5).
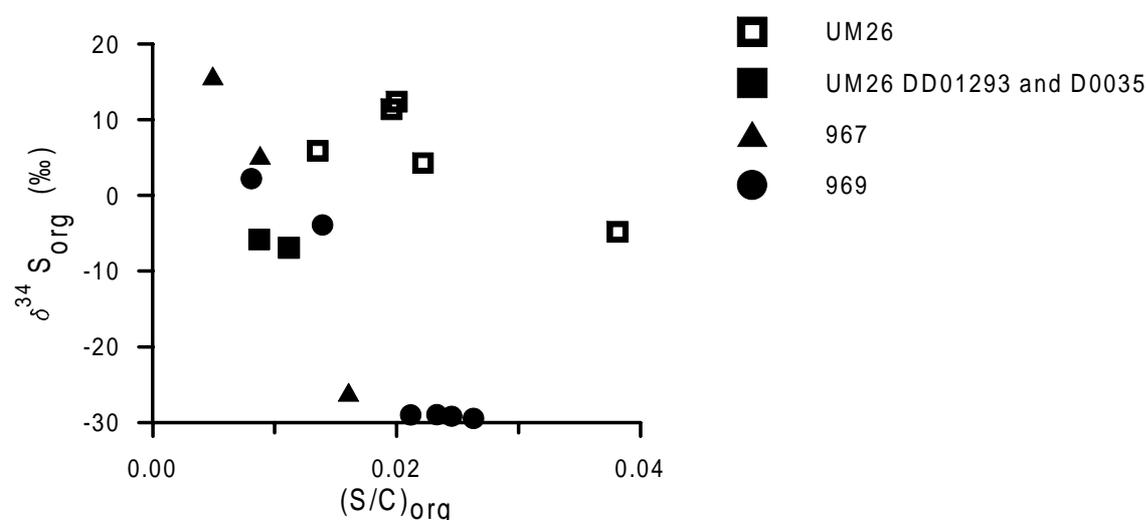

Figure 6.4 *Isotopic compositions of organic S ($\delta^{34}S_{org}$) versus $(S/C)_{org}$ within and around sapropels S1 in UM26, 967 and 969.*

Table 6.4 *Atomic S/C ratios in organic matter from marine plankton, marine sediments, and marine sedimentary rocks.*

Material	Atomic S/C range	Reference
Marine planktonic material	0.004 - 0.010	Francois, 1987b
Basins off California	0.006 - 0.015	Nissenbaum and Kaplan, 1972
Jervis Inlet, British Columbia	0.011- 0.019	Francois, 1987b
Peru Margin	0.011 - 0.056	Mossmann et al., 1991
Cretaceous carbonates	0.04 - 0.38	Bein et al., 1990
Jurassic marine shales	0.012 - 0.019	Raiswell et al., 1993
Eastern Mediterranean anoxic basins	0.038 - 0.204	Henneke et al., 1997
Eastern Mediterranean sapropel containing sediments	0.005 - 0.038	this study

Reduced S is thought to be incorporated into organic matter without any fractionation of S isotopes (Mossmann et al., 1991; Raiswell et al., 1993), since reactions involving uptake of reduced S seem to proceed with small sulphur isotopic fractionations (Fry, 1988). The uptake of ^{34}S-depleted reduced S into organic matter which initially had a more positive δ^{34}S value, can explain the decrease in $\delta^{34}S_{org}$ within the sapropel layers (Fig. 6.1). This hypothesis is supported by the linear correlation between $(S/C)_{org}$ ratios and $\delta^{34}S_{org}$ in sapropels 967 and 969 (Fig. 6.4). This linear correlation suggests a binary mixing model for S isotopes in the organic matter, with one endmember with δ^{34}S of biosynthesized S, close to seawater SO_4^{2-} (+20.6‰ eastern Mediterranean, de Lange et al., 1990), and another endmember with one single constant negative δ^{34}S value, such as reduced S produced by bacterial SO_4^{2-} reduction. The fact that the negative endmember has a constant δ^{34}S value, suggests that the SO_4^{2-} pool from which reduced S was formed also had a constant δ^{34}S value, indicating that there was no depletion of SO_4^{2-} in the system. This linear correlation between $\delta^{34}S_{org}$ and $(S/C)_{org}$ (Fig. 6.4), however, is not present in S1 (see later discussion).

If this hypothesis of uptake of reduced S with a negative δ^{34}S into organic matter is valid, then the increase in $(S/C)_{org}$ ratios ($\Delta(S/C)_{org} = (S/C)_{org\ measured} - (S/C)_{org\ origin}$) should be the same as the amount of reduced S that has to be added to the organic matter (S_{added}/C_{org}) in order to explain the decrease in $\delta^{34}S_{org}$ (Francois, 1987b):

$$\Delta(\frac{S}{C})_{org} \stackrel{?}{=} \frac{S_{added}}{C_{org}} .$$

In this comparison, the ratio S_{added}/C_{org}, which is the amount of S that should be added according to the hypothesis, is calculated from:

$$\frac{S_{added}}{C_{org}} = \frac{\delta^{34}S_{org} \times (\frac{S}{C})_{org\,measured} - \delta^{34}S_{origin} \times (\frac{S}{C})_{org\,origin}}{\delta^{34}S_{added}} ,$$

where $\delta^{34}S_{org}$ and $(S/C)_{org\,measured}$ (Table 6.5) are the average values of all Cr(II) residues of sapropel samples. $\delta^{34}S_{origin}$ and $(S/C)_{org\,origin}$ (Table 6.5) are the original values in the sediments before addition of an amount of reduced S to the organic matter, estimated as the average $\delta^{34}S$ and S/C values of all Cr(II) residues of non-sapropel samples (Table 6.3a, b, c). Hereby it was assumed that these original values were comparable for non-sapropel and sapropel sediments. $\delta^{34}S_{added}$ (Table 6.5) is the average of $\delta^{34}S$ of pyrite within and below the sapropels (Table 6.3a, b, c; Passier et al., 199_/Chapter 5). The main assumption in this calculation is that degradation of organic matter does not affect S/C ratios of the organic matter by preferential degradation of one element over the other. The comparison of S_{added}/C_{org} to $\Delta(S/C)_{org}$ (Table 6.5) reveals that the hypothesis of addition of reduced S is reasonable and can explain the observed increases in the S content of organic matter in sapropel 967 and 969, however there is a large discrepancy between S_{added}/C_{org} and $\Delta(S/C)_{org}$ in sapropel S1 (see later discussion). The fact that values of S_{added}/C_{org} are slightly larger than $\Delta(S/C)_{org}$ in 967 and 969 (Table 6.5) could be due to a small isotopic re-equilibration between inorganic reduced S and organically bound S (Francois, 1987b).

Table 6.5 *Parameters for isotope balance calculations, see text for explanation of parameters, and BE (burial efficiencies) of organic matter (Passier et al., 199_/Chapter 5) in sapropels S1, 967, and 969.*

Sapropel	$\delta^{34}S_{org}$ (‰)	$(S/C)_{org\,measured}$ ($\times10^{-3}$)	$\delta^{34}S_{origin}$ (‰)	$(S/C)_{org\,origin}$ ($\times10^{-3}$)	$\delta^{34}S_{added}$ (‰)	$\Delta(S/C)_{org}$ ($\times10^{-3}$)	S_{added}/C_{org} ($\times10^{-3}$)	BE (%)
S1	-5.8	19.34	+7.2	18.43	-42.9	0.9	5.5	59
967	-26.0	16.05	+10.6	6.87	-43.7	9.2	11.2	55
969	-29.2	23.83	-0.85	11.03	-42.6	15.1	16.1	80

The original isotopic compositions of organic matter ($\delta^{34}S_{origin}$; Table 6.5) are relatively heavy, but not as heavy as published values for biosynthesized S, which forms from seawater (+20.6‰) with a fractionation of about -1‰ to -2‰, yielding marine organic matter with $\delta^{34}S_{org}$ of about +19‰ (Peterson and Howarth, 1987; Fry, 1988). Probably some reduced S has been incorporated in the "original" organic material or exchanged between reduced S and biosynthesized organic S occurred in and around anoxic microniches (Francois, 1987b). This uptake may be more important below sapropels than above sapropels, because downward sulphide diffusion out of the sapropels occurred (Passier et al., 1996a/Chapter 2, Passier and de Lange, 199_/Chapter 3). The amount of biosynthetic S can be estimated from:

$$F_{bio} = \frac{\delta^{34}S_{org} - \delta^{34}S_{added}}{+19 - \delta^{34}S_{added}} \times 100\%,$$

where F_{bio} is the biosynthetic fraction of organic S, and +19 the hypothetical isotopic value (in ‰) of this biosynthetic S. In the non-sapropelic ("origin") sediments 68 to 87% of the organic S could be biosynthetic (Table 6.6) as calculated from average $\delta^{34}S_{org}$ values in non-sapropelic sediments ($\delta^{34}S_{origin}$) and estimated $\delta^{34}S_{added}$ values (Table 6.5). Within the sapropels the calculated biosynthetic fraction of organic S is 60, 28 and 22%, for sapropel S1, 967, and 969, respectively (Table 6.6). It is unlikely that the biosynthetic S has been directly incorporated into the organic sedimentary matter, because most biosynthetic S compounds are relatively labile. However, it has been suggested that during the breakdown of S biomolecules, reactive S species are formed which may be rapidly and efficiently incorporated into the residual organic matter so that at least a part of the originally biosynthetic S is preserved in the sediments (Anderson and Pratt, 1995; Brüchert and Pratt, 1996).

Table 6.6 *Calculated biosynthetic S fraction (F_{bio}) in non-sapropel and sapropel sediments of S1, 967, and 969.*

Sapropel	F_{bio} (%) non-sapropel	F_{bio} (%) sapropel
S1	81	60
967	87	28
969	68	22

$\delta^{34}S_{org}$ and $(S/C)_{org}$ values in sample D0031 are comparable to the other non-sapropel samples in UM26 (Table 6.3a). This is remarkable because this sample originates from the upper, oxidized part of sapropel S1 (van Santvoort et al., 1996). Postdepositional oxidation of the top of the sapropel removed organic C and pyrite from the sediments and it is likely that the sediments once contained as much reduced S as the sapropel samples of UM26. Thus, organic S in the oxidized zone is expected to have been influenced by more negative isotopic compositions, and relatively light S could have been taken up into the organic matter. Probably this added part of the S is more sensitive to reoxidation than the fraction of S that reached the sediments in organic matter that settled through the water column. The similar $\delta^{34}S_{org}$ and $(S/C)_{org}$ values in non-sapropel and oxidized sapropel sediments suggest that the values for $\delta^{34}S_{origin}$ and $(S/C)_{org \, origin}$ were comparable for non-sapropel and sapropel sediments, as was assumed in the calculations.

Summarizing, the hypothesis of uptake of reduced S with a relatively light isotopic composition seems to be correct for 967 and 969. For S1 in UM26, however, there are some complications. The correlations between $(S/C)_{org}$, C_{org} and $\delta^{34}S_{org}$ of samples of UM26 are

dissimilar to those for 967 and 969 (Figs. 6.3, 6.4). In UM26, samples from all zones of the sediment have exceptionally high $(S/C)_{org}$ ratios, while $\delta^{34}S_{org}$ values are not atypical (Fig. 6.1; Table 6.3a,b,c). Only two adjacent samples (DD01293 and D0035; Table 6.3a) within sapropel S1 fit into the datasets of 967 and 969 (Figs. 6.3, 6.4). It may be that the organic matter in the sediments of UM26, with exception of the zone around samples DD01293 and D0035, differs from that in 969 and 967, containing relatively more S, both biosynthetic S and added reduced S. The discrepancy between S_{added}/C_{org} and $\Delta(S/C)_{org}$ in sapropel S1 (Table 6.5) can also be explained from this difference in organic matter: the two samples with lower $(S/C)_{org}$ ratios (DD01293 and D0035) are relatively important for estimating the average $(S/C)_{org\ measured}$ ratios in sapropel S1, causing $\Delta(S/C)_{org}$ to be small compared to S_{added}/C_{org}. Whether possible differences in organic matter are indeed the cause of the anomalous data in UM26, however, requires a more detailed organic geochemical investigation, which is in progress.

6.4.2 Iron limitation as the cause of organic S formation

The uptake of reduced S into organic matter is most pronounced in sapropel 969 and least pronounced in sapropel UM26. This can be explained from the Fe availability for pyrite formation relative to sulphide production within the sapropel layers. Relative high sulphide production resulted in Fe limitation for pyrite formation within the sapropel, where the sulphide was produced. As a consequence, sulphide concentrations within the sapropel rose and sulphide migrated out of the organic-rich layers into the bottomwater and into the sediments underlying the sapropel, where pyrite was formed (Passier et al., 1997 and 199_/Chapters 4 and 5). Increased sulphide concentrations and the absence of reactive Fe that is competing for sulphide with organic matter, cause the uptake of reduced S species into organic substances (Ferdelman et al., 1991; Raiswell et al., 1993). Therefore, simultaneously with Fe limitation within the sapropel, reduced S could have been incorporated into the organic matter within the sapropel. Moreover, the uptake of S into organic matter seems to be favoured by the presence of partially-oxidized S species (Francois, 1987b; Raiswell et al., 1993). During Fe limitation within the sapropel, sulphide that escaped into the bottomwater reoxidized to elemental S, and settled back to the sediment, resulting in the presence of more partially-oxidized S species in the sapropel. Whereas during periods when pyrite formation is not limited within the sapropel, sulphide is rapidly taken up in pyrite formation, so that little sulphide is reoxidized (Passier et al., 199_/Chapter 5). For the sapropels discussed here, the Fe limitation has been most extreme in the organic-rich sapropel 969 (Passier et al., 199_/Chapter 5), this concords with the most pronounced organic S formation in sapropel 969.

The uptake of S into organic matter may cause enhanced preservation of organic matter (e.g. Sinninghe Damsté and de Leeuw, 1990). Indeed, when comparing the three investigated sapropels, more organic matter seems to be preserved in sapropel 969 (Passier et al., 199_/Chapter 5), where both the burial efficiency of organic matter (Passier et al., 199_/Chapter 5; Table 6.5) and the atomic $(S/C)_{org}$ ratio (Table 6.5) are the highest. In sapropel 967 the burial efficiency as well as the $(S/C)_{org}$ ratio are the lowest (Passier et al., 199_/Chapter 5, Table 6.5). In sapropel S1, both parameters are intermediate (Passier et al., 199_/Chapter 5). However, other

factors, such as anoxicity in the water column, may also contribute to a decreased degradation of organic matter, by the diminished ability of anaerobic bacteria to oxidize a full suite of sedimentary organic compounds (Canfield, 1989), or by the absence of meio- and macrofauna (Passier et al., 199_/Chapter 5). The exact influence of the S containing organic compounds on the preservation of organic matter in the sapropels is to be assessed by detailed organic geochemical analyses of these compounds.

6.5 Conclusions

The S contents and S isotopic compositions of organic matter in eastern Mediterranean sapropel containing sediments can be easily analysed in the residue of sediments after drying, acetone-extraction and Cr(II) reduction by C-irmMS. Organic S in and around sapropels is a mixture of S derived from (1) incorporation of inorganic reduced S produced by microbial SO_4^{2-} reduction and (2) biosynthetic S. The uptake of reduced S into organic matter within sapropels was controlled by the availability of reactive Fe relative to the sulphide production within sapropels.

Chapter 7

Eastern Mediterranean photic zone euxinia during Pliocene sapropel formation∗

7.1 Introduction and summary

Sapropels (organic matter (OM)-rich layers) are common in the eastern Mediterranean Neogene sedimentary record. Their formation is thought to have been initiated by climate-related enhanced productivity that led to higher settling rates of OM on the seafloor (Rossignol-Strick et al., 1982; Calvert et al., 1992) and/or to increased OM preservation due to oxygen depletion in stagnant bottomwaters (Rossignol-Strick et al., 1982). Some exceptionally OM-rich Pliocene sapropels were recovered during Leg 160 of the Ocean Drilling Program (Emeis, Robertson, Richter et al., 1996). These sapropels were found to contain molecular fossils derived from photosynthetic green sulphur bacteria, proving that during Pliocene sapropel formation euxinic (sulphidic) conditions in the water column extended into the photic zone. The sapropels also have a high content of trace elements. This must be due to the fact that metal sulphides in the water column scavenged these trace elements very efficiently. In addition, the abundance of pyrite and its isotopic composition are consistent with Fe sulphide formation in the water column during sapropel deposition. This study provides the first evidence for water column euxinia over substantial periods during Pliocene sapropel formation in the eastern Mediterranean, and proves that euxinic conditions must have existed throughout the eastern Mediterranean at that time.

7.2 Materials and methods

Geochemical analyses were performed on seven upper Pliocene sapropels obtained from several eastern Mediterranean ODP Leg 160 sites (Table 7.1; Fig. 1.1). The sediment samples (0.5 to 1 cm resolution) were freeze-dried and ground in an agate mortar. Organic carbon contents (C_{org}) were determined with an NCS-analyser after carbonate had been removed with 1 M HCl. Sediment was dissolved in an $HClO_4$-HNO_3-HF acid mixture. The dried residue was dissolved in 1 M HCl for analysis with ICP-AAS (Mo, Ni, V, Ba), Zeeman AAS (Cd), and FIAS (Se) (Nijenhuis et al., 199_). Pyritic S (S_{pyr}) was extracted using the Cr(II) reduction method after removal of elemental S with acetone (Passier et al., 199_/Chapter 5). The evolved sulphide was trapped in 1 M NaOH and measured polarographically. Pyritic S for isotopic analysis was extracted with the same reduction method, trapped as Ag_2S, and measured for the stable S isotope composition ($\delta^{34}S_{pyr}$, ‰) relative to the V-CDT standard by means of C-irmMS: $\delta^{34}S_{pyr} = 1000 \times [(^{34}S/^{32}S)_{pyr} - (^{34}S/^{32}S)_{V\text{-}CDT}]/((^{34}S/^{32}S)_{V\text{-}CDT}$ (Passier et al., 199_/Chapter 5). Samples for organic geochemical analysis (Bosch et al., 199_) were ultrasonically extracted with mixtures of

---

methanol and dichloromethane. Elemental S was removed with activated Cu. The apolar fractions were separated from the extracts on an activated Al_2O_3 column, and analysed by GC and GC-MS.

7.3 Discussion and conclusions

Astronomical tuning of the sapropels revealed that these sapropels are time equivalent to three grey layers and/or sapropels of the Punta Piccola section (Sicily, Italy), i-292, i-290, and i-282, and sapropel i-176 of the Vrica and Singa sections (Calabria, Italy), which have ages of 3.058, 3.036, 2.943, and 1.808 Ma, respectively (Lourens et al., 1996). The sapropels are distinct, dark grey to black sediment layers with a thickness ranging from centimetres to decimetres, embedded in light grey to brown hemipelagic carbonate oozes. Fine lamination of the sapropels points to the absence of bioturbation and anoxia of the bottomwaters (Emeis, Robertson, Richter et al., 1996). The sapropels contain significant amounts of isorenieratene derivatives, trace elements and pyrite (Table 7.1; Fig. 7.1).
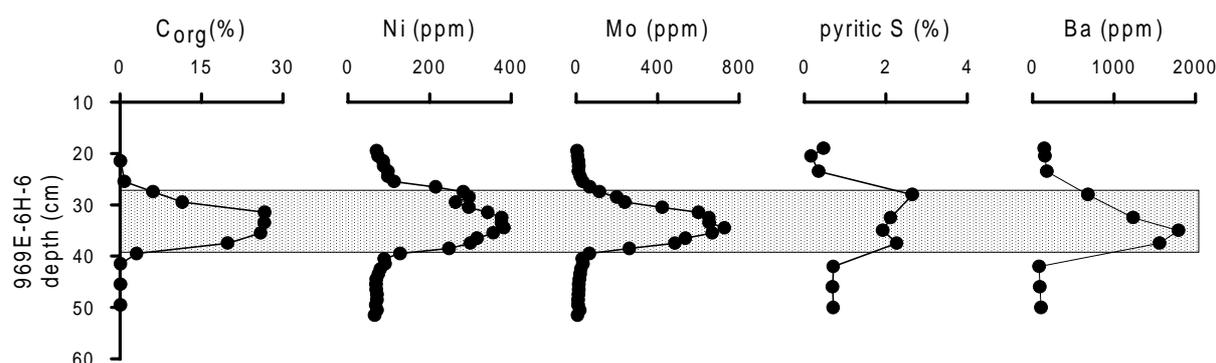

Figure 7.1 *Content vs. depth profiles of C_{org}, Ni, Mo, pyritic S, and Ba in and around ODP sapropel 160-969E-6H-6, 27-39 cm; the shaded area indicates the position of the sapropel.*

The occurrence of isorenieratene derivatives in the sapropels analysed (Table 7.1) indicate a periodic overlap of the photic and euxinic zones in Pliocene Mediterranean waters during sapropel formation. Isorenieratene is a carotenoid biosynthesized exclusively by the brown strain of photosynthetic green sulphur bacteria (Chlorobiaceae) (Liaaen-Jensen, 1978). These bacteria use the reverse tricarboxylic acid cycle to fix CO_2, resulting in a biomass anomalously enriched in [13]C (Quandt et al., 1977). The ^{13}C contents of the isorenieratene derivatives are indeed 13-14‰ enriched relative to algal-derived biomarkers, which confirms that they originate from green sulphur bacteria (Summons and Powell, 1986; Kohnen et al., 1992; Sinninghe Damsté et al., 1993; Hartgers et al., 1994). Since Chlorobiaceae are phototrophic, and require free sulphide as an electron donor to fix CO_2, their occurrence is restricted to euxinic waters in the photic zone. The presence of ^{13}C-enriched isorenieratene-derived compounds in the Pliocene sapropels, therefore, provides unambiguous evidence that the photic zone contained sulphide over substantial periods of time during sapropel formation. This situation is comparable to the present-day euxinic Black Sea, where green sulphur bacteria occur at the base of the photic zone (Repeta

et al., 1989) and isorenieratene derivates are found in the sediment (Sinninghe Damsté et al., 1993).

The presence of euxinic conditions in the water column during sapropel deposition explains the exceptionally high contents in the sapropels of trace elements (Table 7.1, Fig. 7.1) scavenged by metal sulphide precipitation in a euxinic water column. These trace element enrichments cannot be explained by increased planktonic and detrital inputs or diagenetic remobilisation (Nijenhuis et al., 199_). The same scavenging mechanism is also thought to have played an important role in transferring trace metals to the sediments of Cretaceous black shales (Arthur et al., 1990), whose trace element contents are comparable to those of the studied sapropels (Table 7.1).

The enrichment of pyrite (FeS_2) in the sapropels (Fig. 7.1, Table 7.1) is attributed to the decomposition of OM via microbial sulphate reduction and subsequent reaction of the reduced S with Fe during sapropel formation (Passier et al., 1996a/Chapter 2; Passier et al., 199_/Chapter 5). The amount of Fe supplied to the sapropels from detrital sources and its diffusion toward the sapropels cannot adequately explain the amount of pyrite found in the sapropels. The integrated pyrite content of sapropel i-282C is 6 mmol cm^{-2}, whereas the total supply of detrital Fe and upward Fe diffusion from underlying sediments during sapropel formation is only 2 mmol cm^{-2} (as calculated at site UM26 (Passier et al., 1997/Chapter 4) near Site 969). A euxinic water column, however, provides an additional Fe source as a result of the formation of Fe sulphides in the water column. Additional Fe and trace elements for metal sulphide formation in the water column can be supplied after their liberation from (hydr)oxides at the margins of a euxinic basin in response to a fluctuating oxycline. This is occurring at present in the Black Sea (Kempe et al., 1991; Canfield et al., 1996). Isotopic compositions of pyritic S ($\delta^{34}S_{pyr}$) are also consistent with a euxinic water column. Values of $\delta^{34}S_{pyr}$ in the sapropel samples are about -40 ‰ (Table 7.1), indicating that reduced S was depleted by about 60‰ compared to sea water sulphate (present day value: + 20.6 ‰ (de Lange et al., 1990). To achieve S isotopic fractionations between sulphate and pyrite of this magnitude, sulphate reduction must take place under continuous supply of dissolved sulphate (open system) and must be followed by further ^{34}S depletion in the sulphide pool by reoxidation and disproportionation processes in the sulphur cycle (Canfield and Thamdrup, 1994). In the present-day Black Sea (Fry et al., 1991; Canfield and Thamdrup, 1994), sulphide oxidation occurs at the oxic/anoxic chemocline, which results in lighter isotopic compositions of sulphide in the euxinic water column. The enrichment of pyrite directly below sapropel i-282C (Fig. 7.1) indicates that sulphide diffused into the non-sapropelic sediment below as a result of Fe limitation for pyrite formation within the sapropel (Passier et al., 1996a/Chapter 2; Passier et al., 199_/Chapter 5).

Depletion of oxygen and consequent formation of euxinia over substantial periods of time during Pliocene sapropel formation in the eastern Mediterranean may have resulted from increased primary productivity of OM, in turn leading to a higher demand for oxygen, or from the development of stagnant conditions, resulting in reduced replenishment of oxygen. The well-documented climate-induced (Rossignol-Strick, 1985; Hilgen, 1991) increase in freshwater and nutrient inputs from Africa and Europe during sapropel formation induced both higher primary production and stagnation of the water column (Rossignol-Strick et al., 1982; Rossignol-Strick,

1985). An anoxic water column will probably enhance the preservation of OM. In the sediment of anoxic basins like the Black Sea about 3 to 10 % of the primary productivity is preserved (Bralower and Thierstein, 1987). If the average present-day primary productivity in the eastern Mediterranean of 26 gC m^{-2} yr^{-1} (Béthoux, 1989) settles through an anoxic water column, this would mean that 1 to 3 gC m^{-2} yr^{-1} is buried in the sediments. However, the accumulation of OM is larger in the Pliocene sapropels studied here, e.g. 7 gC m^{-2} yr^{-1} in i-282C. Thus, the primary productivity must have increased during sapropel formation.

This assumed increase in primary productivity is supported by the enrichment of barium, which may serve as a paleoproductivity indicator (Dymond et al., 1992; van Os et al., 1994) in the sapropels (Fig. 7.1). The depletion of oxygen in the water column resulting from OM decomposition during sapropel deposition can be estimated from the magnitude of the new OM production (the export flux, which is part of the primary production of OM, from the photic zone to deep waters) during sapropel formation, the amount of OM that accumulated in the sediment, and the amount of reduced S that was stored in the sediment without having been reoxidized. The average new production during deposition of the sapropels calculated on the base of the Ba contents (Fig. 7.1) as a paleoproductivity indicator (Dymond et al., 1992; van Os et al., 1994) is 150 gC m^{-2} yr^{-1} for sapropel i-282C, the accumulation of organic matter is only 7 gC m^{-2} yr^{-1} and the stored reduced S corresponds to 2 gC m^{-2} yr^{-1}. The difference between newly produced and stored OM yields an oxygen demand of 3×10^{13} mol O$_2$ yr^{-1} in the water column during sapropel deposition. The present-day new production is only 6 to 12 gC m^{-2} yr^{-1} (Béthoux, 1989), and the supply of oxygen to the eastern Mediterranean through deep water formation in the Levantine and Adriatic basins is only 1×10^{13} mol O$_2$ yr^{-1} (Béthoux, 1989). In the present-day eastern Mediterranean, the amount of oxygen used for organic matter decomposition is less than the amount supplied; the surplus oxygen is exported to the western Mediterranean (Béthoux, 1989). In contrast, the new production during Pliocene sapropel formation was so high that oxygen in the water column was entirely depleted.

These calculations suggest that water column euxinia could have been achieved through increased OM production during sapropel formation without there being any reduction of the oxygen supply to deep waters through stagnation of the water column. Moreover, continued circulation provided yet another input of trace elements from the western Mediterranean to the eastern Mediterranean during the formation of the sapropels. Mass balance calculations of the trace elements in the sapropels indicate that trace elements could not all have been supplied by rivers. For example, the total amount of nickel sequestered in sapropel i-282C, assuming that it covers two thirds of the eastern Mediterranean, is 65×10^{12} g, whereas rivers can supply only 5-12×10^{12} g during sapropel formation over a period from 3 to 7 kyr, and a stagnant water column can deliver only 2×10^{12} g (Nijenhuis et al., 199_), assuming that all trace elements are trapped. Thus, our data suggest that euxinic conditions in the eastern Mediterranean during deposition of the exceptionally OM-rich Pliocene sapropels were not necessarily the result of stagnation of the water column.

The geochemical characteristics and water column specifications that demonstrate that the water column of the eastern Mediterranean must have been euxinic from the bottom up into the photic zone over substantial periods during Pliocene sapropel formation, are comparable to

those of the present-day Black Sea. However, euxinia in the Black Sea is caused mainly by water column stagnation, whereas during Pliocene sapropel formation in the eastern Mediterranean enhanced productivity played an important role in oxygen depletion. Although some of our observations might be explained to some extent by the combination of an extreme oxygen minimum zone (OMZ) and bottomwater anoxia, our results clearly indicate a sulphidic photic zone. Present-day OMZs, however, are not completely devoid of oxygen and do not contain H_2S (Summerhayes et al., 1992). Deep marine black shales (Arthur et al., 1990) are believed to form under almost the same conditions as the sapropels in the Pliocene eastern Mediterranean. These OM-, trace element, pyrite-rich, and ^{13}C-rich isorenieratene derivatives-containing sapropels can therefore be considered as analogues of deep marine black shales.

Table 7.1 *The sapropels studied, their age, water depth and depth in sediment. The average (avg) trace element contents and average organic carbon (C_{org}) contents in the studied sapropels and Cretaceous Black shales, enrichment factors with respect to average non-sapropel sediments around the sapropels are indicated in brackets. Organic carbon contents (C_{org}), pyritic sulphur contents (S_{pyr}) and the stable sulphur isotopic composition of pyrite ($\delta^{34}S_{pyr}$) of specific subsamples and presence of isorenieratene derivatives in these subsamples.*

sapropel code	ODP sapropel[a] (cm)	Age (Ma)	Water depth (m)	Depth (mbsf[b])	avg Cd (ppm)	avg Mo (ppm)	avg Ni (ppm)	avg Se (ppm)	avg V (ppm)	avg C_{org} (wt%)	sample (cm)	C_{org} (wt%)	S_{pyr} (wt%)	$\delta^{34}S_{pyr}$ (‰)	isoren. deriv.[e]
i-176	160-967C-6H-2, 30-44	1.808	2553	48.4	n.d.[c]	98 (32)	190 (2)	13 (121)	430 (5)	5.0 (37)	36-37.7	7.4	5.8	-41.4	++
i-282A	160-964D-10H-1, 103-110	2.943	3660	80.2	34 (130)	195 (16)	317 (9)	29 (131)	1317 (13)	15.3 (149)	107.5-108	21.1	2.4	-36.1	+
i-282B	160-967C-8H-4, 114-130	2.943	2553	72.2	3 (45)	202 (6)	183 (4)	22 (52)	555 (6)	8.4 (63)	122.5-123	14.5	2.8	-37.4	+
i-282C	160-969E-6H-6, 27-39	2.943	2201	50.7	31 (270)	407 (26)	299 (4)	24 (17)	1937 (19)	17.7 (81)	32-33	23.5	2.1	-42.0	++
i-290A	160-964E-6H-5, 77-103	3.036	3661	82.9	6 (61)	45 (6)	291 (9)	n.d.[c]	304 (5)	5.0 (76)	99-100	23.6	3.6	-39.5	+
i-292A	160-966C-5H-3,4, 148-13	3.058	926	42.6	1 (9)	133 (21)	101 (3)	n.d.[c]	340 (4)	6.0 (24)	10-11	11.6	1.1	-39.1	-
i-292B	160-967C-8H-6, 40-57	3.058	2553	74.5	8 (51)	224 (18)	174 (4)	n.d.[c]	918 (7)	13.2 (64)	46-47	20.3	1.9	-37.3	+
Cretaceous Black Shales[d]					14	163	145	n.d.[c]	647	9.3					

[a] gives the stratigraphic position of the complete sapropel.

[b] mbsf: metres below seafloor

[c] n.d.: no data

[d] Arthur et al., 1990, Brumsack, unpublished results

[e] isorenieratene derivatives, ++ abundant, + trace, -not detected

Chapter 8

Sediment chemistry and magnetic properties in an anomalously reducing core from the eastern Mediterranean Sea∗

Abstract–In Core KC19C (19.6 m long), recovered in the abyssal plain between Crete and Cyprus in the eastern Mediterranean, a large number of organic-rich layers (sapropels) occur, which correlate to maxima in the insolation curve. In contrast to comparable sites in the eastern Mediterranean, porewaters contain sulphide down from a few metres below seafloor (mbsf). Geochemical analyses were performed on the porewaters (ammonium, alkalinity, sulphate, manganese, iron, bisulphide, chloride) and sediments (organic carbon, barium, total sulphur, total iron, manganese, pyrite, dithionite-extractable iron). In addition, a series of magnetic parameters and ratios (NRM, ARM, IRM, χ_{in}, ARM/IRM, S-ratio, ARM_{20mT}/ARM_{in}) were determined. In the top of the sediments, Fe and Mn (hydr)oxides occur at the oxic-suboxic boundary just above the youngest sapropel Si2 (S1 at 0.4 mbsf); these (hydr)oxides appear to be more easily demagnetized by means of alternating fields than the (hydr)oxides further down which presumably are of detrital origin. The transition from suboxic to anoxic sediments is located at ~2 mbsf. Sulphide is produced, possibly in sulphate reduction by methane oxidation, at ~17.5 mbsf. From 17.5 mbsf sulphide migrates upward, titrating reactive Fe, resulting in pyrite formation in the entire sediment column up to 2 mbsf. At this depth, the upward sulphide flux has been totally consumed by reaction with solid phase Fe and dissolved Fe(II) diffusing downward from the suboxic zone above. From ~2 mbsf downward magnetic intensities are significantly reduced, indicating reductive dissolution of Fe-oxide minerals and pyrite formation. As a consequence no reliable NRM data can be obtained in the lower half of the core.

8.1 Introduction

In the present-day eastern Mediterranean, SO_4^{2-} reduction is not important for at least the upper 100 metres below seafloor in most hemipelagic sediments (Pruysers et al., 1991; Emeis, Robertson, Richter et al., 1996). Suboxic diagenesis is dominant in these sediments. Notable exceptions are the anoxic conditions found in sediments of so-called mud volcanoes (Robertson et al., 1996) and in sediments underlying brine-filled basins (Henneke et al, 1997). The suboxic diagenesis is characterized by reductive dissolution of Mn and Fe (hydr)oxides, and upward diffusion of Mn^{2+} and Fe^{2+}. At 20 to 30 cmbsf (centimetres below seafloor) in the sediment the reduced Fe and Mn species meet downward diffusing oxygen resulting in the precipitation of Mn and Fe (hydr)oxides at the oxidation front above the youngest sapropel (Thomson et al., 1995; van Santvoort et al, 1996), which is sapropel Si2 (S1; Si numbering after Lourens et al., 1996; Langereis et al., 1997). Hence, it is surprising that sulphide is present in the porewaters of the

---

19.6 m-long piston core KC19C (33°47.85' N, 28°36.50 E, water depth 2750 m; Fig. 1.1) from a hill in the Herodotus Abyssal Plain between Crete and Cyprus. This exceptional core was therefore selected for a detailed biogeochemical study. In addition, KC19C contains a large number of sapropels. These recurrent organic-rich layers in the eastern Mediterranean sedimentary record are related to astronomically forced climatic variations (e.g. Hilgen, 1991). Accordingly, the time scales of sapropel sequences can be ideally calibrated with astronomical cyclicity records. As KC19C contained an extraordinarily complete series of sapropels, the core is very useful to reconstruct a time frame. Moreover, the time-span of the sediments in this core is long enough to potentially detect the Brunhes/Matuyama geomagnetic reversal and short reversal excursions in the Brunhes chron. These geomagnetic features were found in 37 m-long piston core KC01B (36°15.25'N, 17°44.34'E, water depth 3643 m; Fig. 1.1) from the Ionian Sea (Dekkers et al., 1994; Langereis et al., 1997). This core is representative for the eastern Mediterranean and it has been successfully used for the astronomical calibration of sapropels based on magnetostratigraphy and geochemical properties (Dekkers et al., 1994; Langereis et al., 1997). In core KC01B the reversal of the Earth's magnetic field at the transition from the Brunhes to the Matuyama chron is recorded at almost 30 mbsf which was calculated to be at 812 ka, i.e. with a delay of ca. 30 kyr (Langereis et al., 1997). The sapropel layers in core KC01B are enriched in organic C and Ba, related to enhanced productivity during sapropel formation (van Santvoort et al., 1997). Enrichments of Fe and S are present in the sapropels in core KC01B as a result of bacterial SO_4^{2-} reduction and subsequent pyrite formation. Sediments in between the sapropels do not contain significant pyrite, except for distinct zones below each sapropel, where Fe and S are enriched as a result of pyrite formation following diffusion of sulphide out of a sapropel during its deposition (Passier et al., 1996a/Chapter 2). Although past depositional and diagenetic regimes are recorded in the sediments, present-day diagenetic processes may continuously change the chemistry of the entire sedimentary record. In the present contribution, we use detailed geochemical and magnetic analyses of core KC19C to demonstrate the profound consequences of present-day diagenetic processes, in particular that of SO_4^{2-} reduction, on the chemistry of sediments that were deposited up to hundreds of thousands of years ago. We will show that these geochemical processes can obscure and destroy geological information stored in the sedimentary record.

8.2 Materials and methods

8.2.1 Core

Long Kullenberg Core KC19C (19.6 metres of sediment) was recovered in the eastern Mediterranean Sea on a hill in the Herodotus Abyssal Plain (Fig. 1.1) during the 1991 MD69-Marflux expedition with R.V. Marion Dufresne. The core contained a succession of sapropels with an anomalously high number of sapropels below sapropel Si20 (S8; Si numbering after Lourens et al., 1996; Langereis et al., 1997). The olive green to brownish black sapropels were embedded in homogeneous grey to white carbonate oozes. A strong H_2S smell came out of all the sections of the core below 4 mbsf upon splitting onboard ship. The lowermost two sections (122 cm) of the core were characterized by highly fluctuating P-wave velocities, while the other

sections showed smooth P-wave velocity patterns. In addition, expansion cracks were observed in the deepest section.

8.2.2 Porewater

Immediately after core-splitting, one half of the core sections was transferred into an N_2-filled (oxygen always below 0.001%) glove box system at the *in situ* bottomwater temperature. Porewater extraction was started within 24 h of core collection. Portions of wet sediment were put into Reeburgh-type sediment squeezers mounted inside the glovebox. Appoximately five sediment samples of about 10 cm length were squeezed per meter of core. The porewaters were extracted under a N_2 pressure of up to 1×10^3 kPa (Reeburgh, 1967; de Lange, 1992). After the sediment samples for porewater extraction were taken, Eh and pH punch-in measurements were taken as closely to the sampled intervals as possible. Eh equipment consisted of a reference electrode, an Ingoldt Pt electrode, and a Knick portamess 651 mV meter. The electrode assembly was allowed to stabilize for three minutes. A Zobell solution was used for calibration of the potential difference measurements, these were recalculated to values relative to a standard H_2 electrode. For pH a combination of glass/reference electrode was used, the electrode was allowed to stabilize for 30 seconds and recalibrated in between measurements of each 1 m core section. Porewater samples were subsampled inside a glove box for onboard analysis of ammonium (NH_4^+), bisulphide (HS^-), and alkalinity (Alk). Ammonium and bisulphide were analysed on a TRAACS-800 auto analyser system (Grasshoff, 1976). The error in nutrient measurements was $< 4\%$. Bisulphide measurements below the top six metres of KC19C showed an enormous scatter (20 to 400 µmol/l), probably as a result of oxidation or degassing before analysis. Therefore, no measurements were done below 9 mbsf. Bisulphide was present in all the core sections below, however, as concluded from the strong H_2S smell. The detection limit for bisulphide was 2 µmol/l. Alkalinity was determined by automatic titration. In Utrecht chloride (Cl^-) was analysed by potentiometric titration with a deviation of $<1\%$ using a 0.06 M $AgNO_3$ solution (van Santvoort and de Lange, 1996).

A set of subsamples was acidified to pH 0-1 inside a glovebox onboard ship. The samples were stored at $4°C$ until analysis of total Mn, total Ba, and total S by inductively coupled plasma atomic emission spectrometry (ICP-AES, ARL 34000). Total S is equal to the SO_4^{2-} content of the porewaters, because sulphide was removed by acidification. Total dissolved Fe in the porewaters of KC19C was determined by Zeeman atomic absorption spectrometry (Perkin Elmer 4100 ZL Zeeman AAS). Relative deviations from the mean in duplicate measurements for porewater Mn, Ba, S, and Fe were $< 5\%$. For Fe and Mn detection limits were meaningful, these were 0.4 and 0.1 µmol/l, respectively.

8.2.3 Solid phase

The core sections were stored at $4°C$ and sampled in Utrecht with 10-cm resolution. However, from 10 cm above to 10 cm below each sapropel, continuous sampling with a resolution of 0.5 cm was applied. Samples were freeze-dried and ground in an agate mortar. Subsamples were dissolved in an $HClO_4$-HNO_3-HF acid mixture. The dried residue was

dissolved in 1 M HCl for analysis of total S (S_{tot}), total Ba, total Fe (Fe_{tot}), total Mn (Mn) and total Al (Al) with a Perkin Elmer OPTIMA 3000 inductively coupled plasma atomic emission spectrometer (ICP-AES). Organic C (C_{org}) contents were determined with a Fisons Instruments NA-1500 NCS-analyser after removal of carbonate with 1 M HCl. The results of S_{tot}, Ba, Fe_{tot}, Mn, Al and C_{org} have standard deviations < 5%. International and in-house standards were used to check the procedures.

Pyrite was extracted from a selection of dried subsamples, after extraction of elemental S (including elemental S formed during drying from AVS (acid-volatile sulphides) and organic polysulphides, and elemental S originally present) with acetone. Pyritic S (S_{pyr}) was extracted with the Cr(II) reduction method (Zhabina and Volkov, 1978; Canfield et al., 1986; Henneke et al. 1997). Sulphide that evolved from pyrite during the extraction was stripped from reaction solution with Ar, and trapped in 1 M NaOH. The NaOH solution was analysed for sulphide by square wave voltammetry (SWV) with a Princeton Applied Research Model 384B-4 polarographic analyser system equipped with a Model 303A static mercury drop electrode (SMDE). The average relative deviations from the mean in duplicate measurements for pyrite were 10%.

Reactive Fe was extracted from a selection of dried subsamples in dithionite (Fe_{dith}) (50 g/l sodium dithionite in acetate/citrate buffer, pH = 4.8, 4 h, 60°C) under an N_2 atmosphere following the procedure of Kostka and Luther (1994). Dithionite is thought to extract amorphous Fe (hydr)oxides, crystalline Fe (hydr)oxides, and AVS. The Fe concentration in the dithionite extracts was measured by ICP-AES. The average relative deviation from the mean in duplicate measurements of reactive Fe was 10%.

8.2.4 Paleomagnetic and rock-magnetic measurements

Samples for paleomagnetic and rock-magnetic analyses were collected with a resolution of 10 cm throughout the core, with the exclusion of intervals within 10 cm around sapropels. This resolution implies one sample per ~2200 years. The samples are cylindrical with an outer diameter of 25 mm and a height of 22 mm; the sample volume is 8 cm^3. For all samples the natural remanent magnetisation (NRM) was progressively demagnetized by stepwise alternating field (AF) demagnetisation up to peak fieldstrength of 80 mT in 8 steps with 10 mT increments. The characteristic remanent magnetisation (ChRM) is the NRM intensity after AF demagnetisation at 20 mT. In the top of the core fieldstrengths of up to 120 mT were needed to completely demagnetize the specimens; 20 mT increments were used above 80 mT. The stationary three axes AF demagnetisation method was employed. NRMs were measured with a 2G Enterprises SQUID (superconducting quantum interference device) magnetometer, model 740R with a noise level of 10^{-11} A m^2 (corresponding to 1.25 µA m^{-1} for a 8 cm^3 sample). Low-field or initial magnetic susceptibility (χ_{in}) was measured (at room temperature) with a KLY-2 susceptometer (AGICO corporation, Brno, Czech Republic). Operating conditions of the instrument are a measuring frequency of 920 Hz with a rms fieldstrength of 0.37 mT (300 A m^{-1}). The noise level of the instrument is 4×10^{-8} SI. Values are based on three readings in orthogonal directions of the samples and corrected for the diamagnetic contributions of the sample holder

and sample cups. Anhysteretic remanent magnetisation (ARM) was induced with a peak alternating field of 100 mT and a direct current bias field of 29 µT. Subsequently the ARM was AF demagnetized at a field of 20 mT (three orthogonal directions) to remove its soft viscous part. Isothermal remanent magnetisation (IRM) was induced with a PM4 pulse magnetizer. IRM values are based on a fieldstrength of 1 T, which completely saturated the samples. To determine the S-ratio ($-IRM_{-0.3T}/IRM_{1T}$) a back field of 0.3 T was induced. Intensities were measured with a digitized spinner magnetometer based on the Jelinek JR3 drive unit (noise level 5×10^{-9} A m^2) or with a JR5A spinner magnetometer (noise level 5×10^{-10} A m^2; both manufactured by AGICO). The samples proved to be sufficiently solid to withstand the spinning.
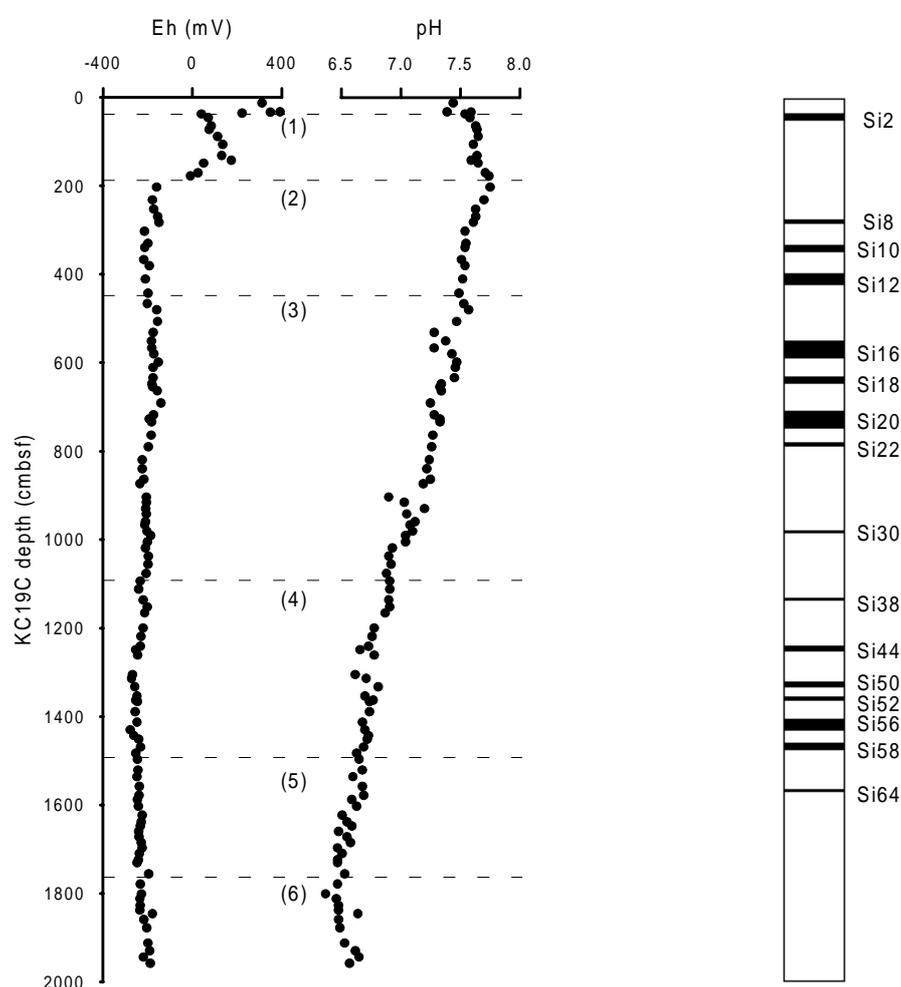

Figure 8.1 *Eh and pH punch-in measurements vs. depth in KC19C. The horizontal lines indicate the most important changes in present-day chemistry: (1) Mn, Fe (hydr)oxide precipitation, (2) Eh shift, (3) end of the zone of maximum dissolved Mn concentrations (4) end of detectable Mn^{2+} concentrations, (5) onset of barite dissolution, (6) minimum SO_4^{2-} concentration. Sapropel numbering after Lourens et al. (1996).*

8.3 Results

8.3.1 Eh and pH punch-in measurements

Eh (Fig. 8.1) shows a sharp shift from oxic (maximum 393 mV at 33 cmbsf) to anoxic conditions in the top of the core at 180 cmbsf, further down, the Eh gradually decreases to a minimum of -277 mV at 1430 cmbsf. At the bottom of the core Eh slightly increases. The values of pH (Fig. 8.1) gradually decrease with depth, from pH 7.8 to pH 6.6, before slightly increasing at the bottom of the core.

8.3.2 Porewater

Ammonium (Fig. 8.2) shows a downward increase from a minimum of about 10 µmol/l in the top of KC19C to a maximum of 1695 µmol/l at the lower end of KC19C. Alkalinity (Fig. 8.2) increases downward from 2 to 14 meq/l at 1550 cmbsf, and decreases again towards the end of the core. Porewater SO_4^{2-} (Fig. 8.2) is the mirror image of alkalinity, it decreases downward from 32 mmol/l in the top of KC19C to 1 mmol/l at 1750 cmbsf, and increases again further down. Porewater Mn (Fig. 8.2) sharply increases with depth in the top of KC19C, is subsequently enriched in the top 550 cmbsf, with a maximum of 17 µmol/l at 190 cmbsf; below 600 cmbsf Mn is around 2 µmol/l. Porewater Fe (Fig. 8.2) is also enriched in the top of KC19C, with a maximum concentration of 7 µmol/l. The scatter in the Fe data may be caused by oxidation of Fe species before subsampling and acidification. Bisulphide concentrations (Fig. 8.2) are below limit of detection in the top of KC19C, and rise above the detection limit (2 µmol/l) at 390 cmbsf. Around 700 cmbsf the bisulphide concentration sharply increases towards maxima of 380 µmol/l, below 900 cmbsf no bisulphide measurements were carried out. Dissolved Ba (Fig. 8.2) is hardly present in the top of KC19C, at 1300 cmbsf, it starts increasing towards a maximum of 10 µmol/l. Chloride (Fig. 8.2) concentrations increase gradually with depth from 606 mmol/kg in the top of KC19C to a maximum of 704 mmol/kg at the lower end of the core (van Santvoort and de Lange, 1996).

8.3.3 Solid phase

Solid phase enrichments of C_{org} and Ba (Fig. 8.3) reflect the positions of the sapropels. Fe_{tot} and S_{tot} (Fig. 8.3) are enriched in these layers, and also in a distinct zone below each
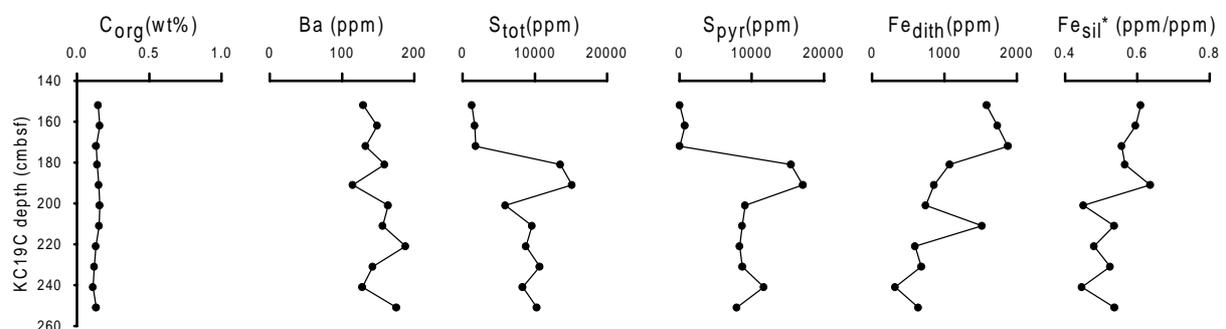

Figure 8.4 *Contents of organic C (C_{org}), Ba , total S (S_{tot}), pyritic S (S_{pyr}), dithionite-extractable Fe (Fe_{dith}) and silicate Fe divided by Al (Fe_{sil}*) in sediments of KC19C vs. depth around 2 mbsf.*

sapropel, where C_{org} and Ba are not enriched. Manganese (Fig. 8.3) peaks above some of the sapropels, as well as Fe_{tot}. The base level of S_{tot} increases sharply at 180 cmbsf, at the same depth the pyrite content increases (Fig. 8.4). From the comparison between S_{tot} and S_{pyr} follows that pyrite is the most important S phase around 180 cmbsf (Fig. 8.4). Fe_{dith} (Fig. 8.4) decreases over this interval around 180 cmbsf.
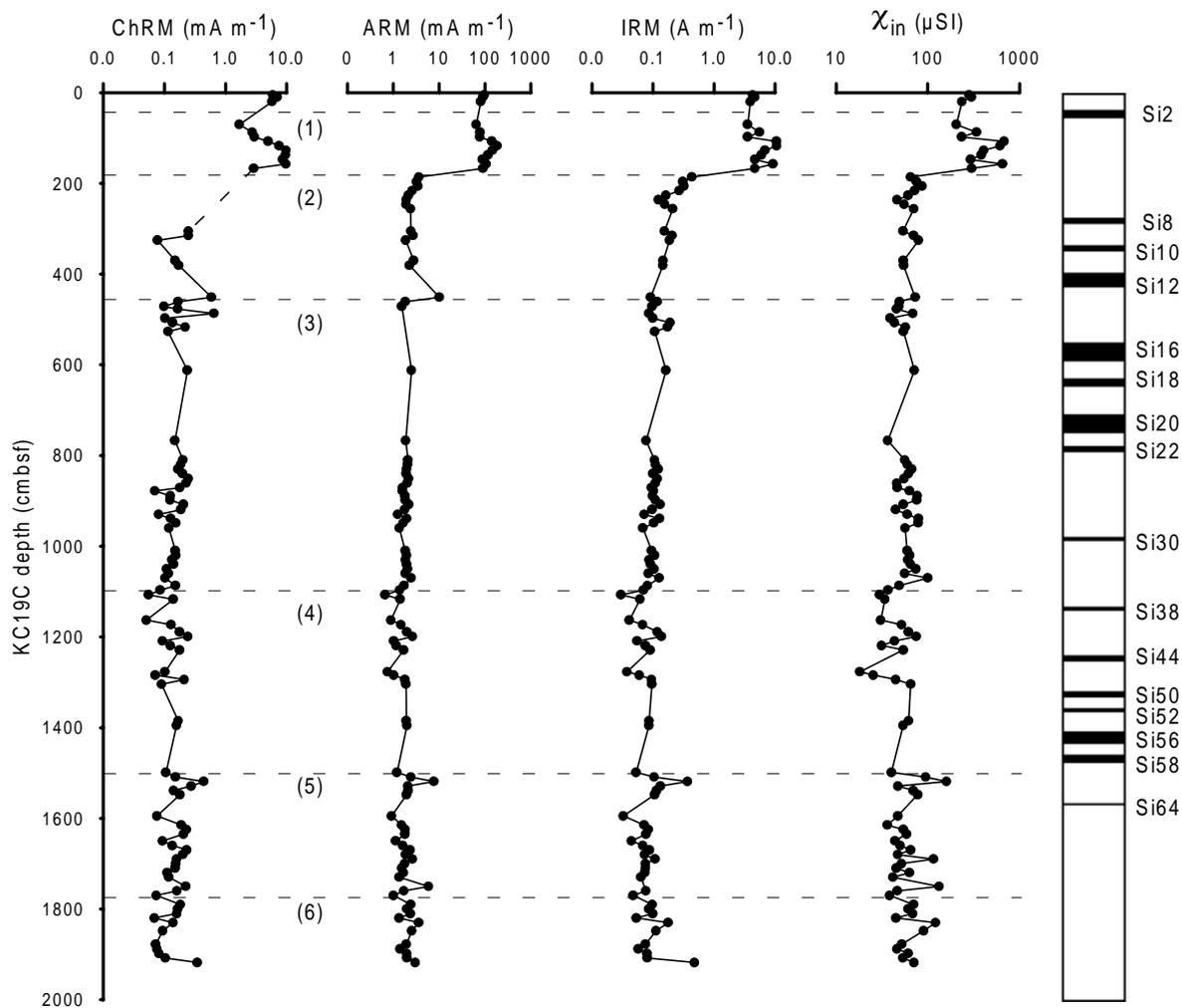

Figure 8.5 *Rock-magnetic parameters ChRM, ARM, IRM and χ_{in} vs. depth in core KC19C, the data are plotted on a logaritmic scale. Sapropel numbering after Lourens et al. (1996). For meaning of the horizontal lines see caption of Fig. 8.1.*

8.3.4 Rock-magnetic results

Rock-magnetic parameters ARM, IRM and χ_{in} (Fig. 8.5) all show the same changes with depth. Relative values are fairly high in the top 20 cm of the core, and decrease slightly in the next 50 cm to a minimum at 70 cmbsf. Below they increase to a maximum around 110 to 120 cmbsf. The maxima at this depth are 180 mA m^{-1}, 11 A m^{-1}, and 680 µSI for ARM, IRM, and χ_{in} respectively. Below 120 cmbsf the intensities decrease, there is a local maximum around 160

cmbsf. From 160 to 190 cmbsf the intensities decrease rapidly. Below 190 cmbsf, intensities of ARM range from 1 to 10 mA m^{-1} with an average value of 2 mA m^{-1}, IRM intensities range from 0.03 to 0.48 A m^{-1} with an average of 0.12 A m^{-1}, and χ_{in} ranges from 20 to 160 µSI, with an average of 60 µSI.

8.3.5. Paleomagnetic results

ChRM intensities (Fig. 8.5) show the same pattern as the other magnetic parameters. There is a local maximum of 7 mA m^{-1} in the top 20 cmbsf. The absolute maximum around 120 cmbsf is 10 mA m^{-1}. Below 2 mbsf the intensities decrease sharply, and they range from 50 to 650 µA m^{-1} with an average of 160 µA m^{-1}. Usually, ca. 50% of the NRM is demagnetized at 20 mT AF. Demagnetisation diagrams (Fig. 8.6) are good in the upper 5 metres with a well-defined ChRM component (Fig. 8.6a,b,c). The quality of the diagrams is poorer in the uppermost core segment of 80 cm (Fig. 8.6a). The quality of the diagrams degrades with depth down from 8 mbsf, defining the NRM components worse (Fig. 8.6d through i). Below 10 mbsf the components cannot be properly defined, in the sediments above only normal polarities are recorded. Sediments below 12 mbsf show erratic demagnetisation behaviour which is not interpretable (Fig. 8.6g through i). In some samples, at high AF levels the NRM tends to move away from the origin in the horizontal plain (Fig. 8.6g), this could be a consequence of the acquisition of gyroremanent magnetisation (GRM; e.g. Stephenson, 1993).

8.4 Discussion

8.4.1 Astronomical time frame for KC19C

The quality of the paleomagnetic data in the lower half of the core is insufficient to establish the presence of the Brunhes/Matuyama (B/M) boundary in this core, or any reversal excursion in the Brunhes. This is rather unfortunate because the B/M boundary would have been a convenient calibration point in the lower part of the core for the reconstruction of a time frame, keeping in mind that delayed NRM acquisition is not uncommon in this type of sediment (Langereis et al., 1997). No oxygen isotope stratigraphy is available either. A reliable depth to age conversion, however, can still be made by correlating sapropels to the insolation curve. The occurrence of an exceptionally large number of sapropels in KC19C facilitates this correlation (Fig. 8.7a). For comparison, both core KC19C and KC01B (Langereis et al., 1997) are shown in Fig. 8.7a. The procedure of Lourens et al. (1996) was followed to reconstruct the time frame. In this method, the sapropel record is correlated to the 65°N summer insolation target curve calculated from the astronomical solution La90 (Laskar, 1990; Laskar et al., 1993) with present-day values of dynamical ellipticity of the Earth and tidal dissipation by the Sun and Moon. A time-lag of 3 kyr between maxima in summer insolation and sapropel midpoints is adopted. The maxima and minima in the insolation curve are numbered starting from the Recent. Maxima are even-numbered, while minima are odd-numbered, sapropels are named after the insolation peak at which they appear, preceded by "Si" (Lourens et al., 1996; Langereis et al., 1997). This nomenclature provides a more complete series of sapropel designations than the conventional "S" nomenclature.

Table 8.1 *Calibration points used for the reconstruction of the time frame for core KC19C. 'Lagged by 3 kyr' means that the sapropel-midpoints are 3 kyr younger than the corresponding insolation maxima.*

Sapropel "Si"	Sapropel "S"	Midpoint (cmbsf)	Age (lagged by 3 kyr) (ka)
Si2	S1	41.5	8
Si8	S3	277	81
Si10	S4	340	102
Si12	S5	409	124
Si16	S6	563	172
Si18	S7	637	195
Si20	S8	726.5	217
Si22	S9	782	240
Si30	S10	981	331
Si38	S11	1134.5	407
Si44	S12	1245	461
Si50	Sa	1325.5	529
Si52		1358	553
Si56	Sb	1425	597
Si58		1466	618
Si64		1566	690

The calibration points used for the correlation of the sapropels to the insolation curve are given in Table 8.1. Si56 consists of a well-developed sapropel with two thin sapropelitic layers a few cms above; the midpoint of the well-developed sapropel is used as a calibration point. Si58 is a double sapropel layer (like Si16 and Si20). There are no sedimentological indications of hiatuses in the core; so in the depth-to-time conversion continous sedimentation was assumed. This results in a smooth depth versus age plot (Fig. 8.7b) strongly supporting the assumption of absence of hiatuses. The lowermost sample with the oldest sediment is calculated by linear extrapolation from the Si58-Si64 interval. A decreasing sedimentation rate with increasing depth may be related to initial compaction as a consequence of increasing sediment load.

The lowermost sample corresponds to an age of 943 ka, this sediment is deposited well within the Matuyama chron, but it is younger than the deepest sapropels in KC01B. The absence of sapropels in the lowermost part of KC19C suggests that the linear extrapolation from the Si58-Si64 interval does not overestimate the age of the core (in fact linear extrapolation from the Si50-Si64 interval would yield an age of 926 ka for the lowermost sample). Of course calculated ages in the interval below Si64 (690 ka) are less reliable than above. The B/M boundary (780 ka)

would occur at ~1690 cmbsf. Demagnetisation diagrams, however, do not indicate any meaningful reversed directions in the interval of interest.

8.4.2 The present-day diagenetic system at site 19C deduced from porewater data

The solid phase of marine sediments reflects both past and present diagenesis, whereas porewaters just reflect ongoing processes. We will first discuss the present-day diagenetic system in KC19C revealed by the porewater chemistry. The most important early diagenetic process in marine sediments is the oxidation of organic matter by micro-organisms using a sequential series of oxidants in decreasing order of thermodynamic energy yield (e.g. Froelich et al., 1979, de Lange, 1986). The order of oxidants is oxygen, nitrate, Mn (hydr)oxides, Fe (hydr)oxides and SO_4^{2-}. It should be realized that not only the presence or absence of certain oxidants determines the diagenetic reactions but also their reactivity and availability. The Eh value is an important indicator of the redox state in the sediment. Eh decreases rapidly in the top of the sediment towards Si2 (Fig. 8.2). Below Si2 Eh increases again, but at 180 cmbsf, it decreases to negative values, indicating anoxic conditions. The presence of sulphide in the porewaters and the decrease of the porewater SO_4^{2-} concentration (Fig. 8.2) confirm that SO_4^{2-} reduction is going on in the sediments.

The increasing ammonium and alkalinity concentrations and decreasing pH with depth (Fig. 8.2) show that organic matter degradation is important in these sediments. Ammonium reacts with oxygen or Mn (hydr)oxides to nitrate (Murray et al., 1995); the high concentration of ammonia therefore indicates that these oxidants (oxygen and Mn (hydr)oxides) are depleted in a large part of the core. In fact, the top 30 cmbsf of the core are similar to average eastern Mediterranean surface sediments, where oxygen and nitrate penetrate to about 25 cmbsf. The depth of penetration is determined by the position of the youngest sapropel Si2. At the top of this sapropel, the oxidative species oxygen and nitrate react with organic C and pyrite in sapropel Si2, and with upward-diffusing Mn and Fe to form Mn and Fe (hydr)oxides (burndown of the sapropel; van Santvoort et al., 1996). Below 30 cmbsf, reduction of Mn and Fe (hydr)oxides dominates the sediments (suboxic diagenesis) releasing Mn^{2+} and Fe^{2+} to the porewaters. Manganese and Fe (hydr)oxides may be present above buried sapropels as relicts of burndown of these sapropels; in KC19C this occurs especially above sapropel Si8 at 275 to 280 cmbsf (Fig. 8.3).

In most eastern Mediterranean sediments on abyssal sites suboxic decomposition of organic matter remains the most important diagenetic process in at least the upper 100 metres of sediment; SO_4^{2-} reduction and consequent sulphide production are not prominent (e.g. Emeis, Robertson, Richter, et al., 1996). It is therefore remarkable that in KC19C sulphide is present in the porewaters, its concentration steadily increasing with depth (Fig. 8.2).

The porewater Mn profile shows that reductive dissolution of Mn (hydr)oxides is most pronounced between 100 and 300 cmbsf (Fig. 8.2). Mn^{2+} diffuses out of this zone, both upward and downward. Mn^{2+} diffuses upward to the level where Mn (hydr)oxides precipitate above sapropel Si2. Mn^{2+} diffuses downward into the sediment, the decreasing concentration of Mn^{2+} with depth indicates that there must a sink for reduced Mn in the sediment. This sink could be

precipitation of Mn carbonates, chemisorption on or coprecipitation with calcium carbonates (e.g. Aller et al., 1986; Middelburg et al., 1987; Sternbeck and Sohlenius, 1997) or the incorporation of Mn into pyrite or a Mn sulphide phase (Huerta-Diaz and Morse, 1992; Böttcher and Huckriede, 1997). If Mn carbonates precipitate, the alkalinity will be affected, which is not clear from the alkalinity profile (Fig. 8.2). It should be realized, however, that Mn concentrations are low relative to alkalinity, so that possible Mn carbonate precipitation does not significantly influence the alkalinity profile. Porewater profiles of Mn as found in KC19C, with a distinct porewater enrichment in the suboxic zone of the sediment are characteristic of many anaerobic sediments all over the world; for example the Amazone shelf (Aller et al., 1986) and the South Atlantic (Schultz et al., 1994; Pruysers, unpublished results). In addition to Mn^{2+}, Fe^{2+} is liberated to the porewaters in the upper part of KC19C by reductive dissolution of Fe (hydr)oxides (Fig. 8.2). A sink for Fe is present in the top of the core, namely the formation of Fe (hydr)oxides above sapropel Si2, and another sink is present between 200 and 400 cmbsf, which is likely the formation of Fe sulphides. Bisulphide could originate from bacterial reduction of SO_4^{2-} at 17.5 mbsf. Sulphate diffuses from the bottomwater to 17.5 mbsf, where its concentration is minimal (see Section 8.4.8). At the lower end of the core, SO_4^{2-} concentrations in the porewaters have decreased in such a way, that barite is undersaturated, and dissolves. Consequently, Ba is released to the porewaters (Fig. 8.2). The Ba that is released to the porewaters diffuses upward and barite reprecipitates where SO_4^{2-} concentrations are higher. This process causes the the extreme solid phase enrichment of Ba around 1500 cmbsf (Figs. 8.3, 8.8). Other solid phase Ba enrichments are related to sapropels (see 8.4.3).

8.4.3 Solid phase expressions of the present-day diagenetic system

Examples of present-day diagenesis are the solid phase Mn and Fe enrichments above sapropel Si2 (Fig. 8.3) and solid phase Ba enrichment at 1500 cmbsf (Figs. 8.3, 8.8); these enrichments are coupled to the porewater chemistry as it is observed in the sediment at present. The most anomalous feature in the solid phase of core KC19C, as compared to other eastern Mediterranean cores, is the nearly continuous pyrite enrichment which is present from 180 cmbsf
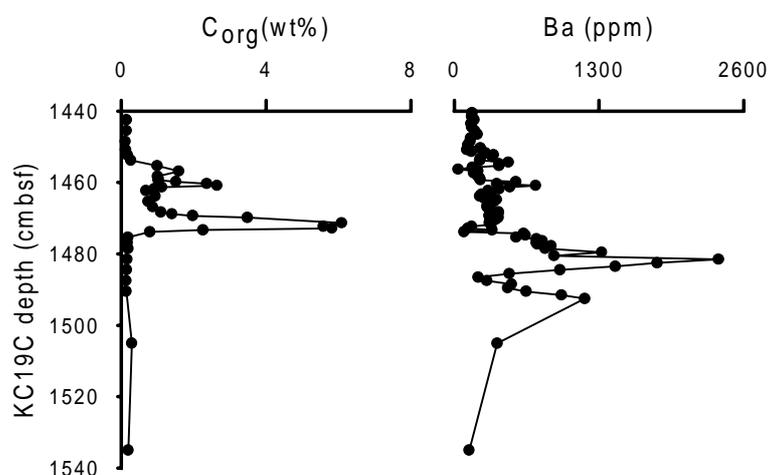

Figure 8.8 *Contents of organic C (C_{org}) and Ba in the sediments of KC19C vs. depth around 1500 cmbsf.*

downward (Fig. 8.4). The base level of S (Fig. 8.3) increases at this depth and does not return to the low levels typical of the top of the core. This sudden increase in pyrite coincides with the transition from positive to negative Eh values (Fig. 8.2) and thus indicates the present boundary between suboxic and anoxic conditions in the sediment. The interval of the abrupt increase in pyrite at 180 cmbsf is unrelated to a possible sapropel, because it does not coincide with an enrichment of organic C or of solid phase Ba (Fig. 8.4). These compounds could indicate the presence of a sapropel or entirely oxidized sapropel ("ghost sapropel", Langereis et al., 1997; van Santvoort et al, 199_).

8.4.4 Solid phase expressions of past diagenetic systems
8.4.4.1 Sapropels

Examples of relicts of past diagenetic systems are the S and Fe enrichments within and below each sapropel (Fig. 8.3) that formed as a result of SO_4^{2-} reduction and subsequent Fe sulphide formation during sapropel deposition or shortly after burial of the sapropels (Passier et al., 1996a/Chapter 2). Solid phase Ba enrichments (Fig. 8.3) are also associated with the sapropels, as barite is an indicator of increased productivity in the surface waters during sapropel formation (van Os et al., 1994; van Santvoort et al., 199_; Passier et al., 199_/Chapter 5). Diagenetic remobilisation of Ba out of sapropels may cause peaks in solid phase Ba just above and just below sapropels and disturbance of the Ba profile within a sapropel (van Os et al., 1991), such features are observed in and around Si16 (Fig. 8.9), Si18, Si20, Si22, Si30, and Si44 in KC19C (Fig. 8.3). Enrichments of Ba that occur directly above organic-C enrichments, indicate the partly oxidation of a sapropel layer (van Santvoort et al., 1996 and 199_), such as above Si2, Si8 (Fig. 8.10), and Si10 in KC19C (Fig. 8.3).
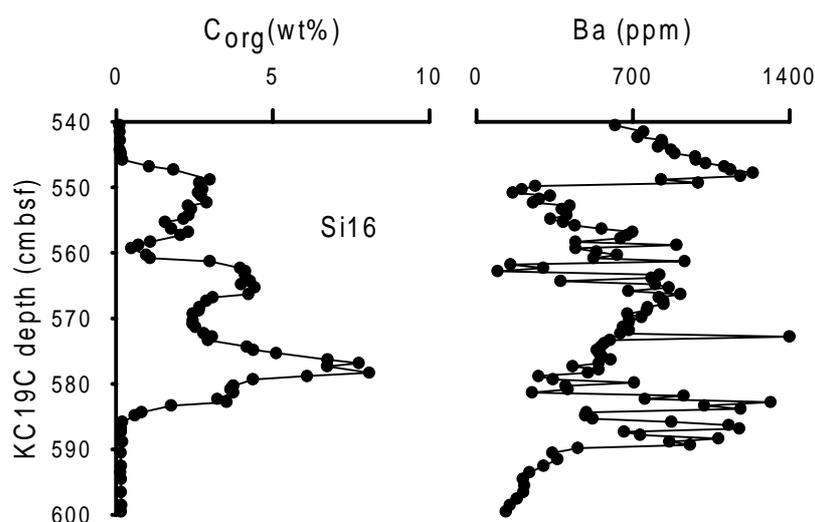

Figure 8.9 *Contents of organic C (C_{org}) and Ba within and around sapropel Si16 in sediments of KC19C.*
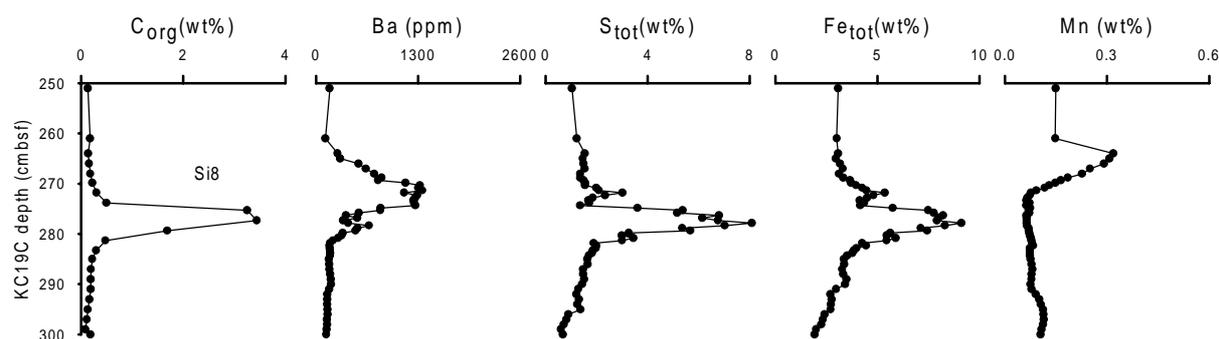
Figure 8.10 *Contents of organic C (C_{org}), Ba, total S (S_{tot}), total Fe (Fe_{tot}) and Mn within and around sapropel Si8 in sediments of KC19C.*

8.4.4.2 Oxidation fronts

Other relicts of past diagenetic systems are the distinct Mn enrichments directly above sapropels (Fig. 8.3), which are most pronounced above Si8 (Fig. 8.10), Si16, Si30 and Si38, these enrichments are indicators of initial precipitation of Mn (hydr)oxides during past nonsteady-state oxidation of the top of a sapropel shortly after its deposition, such as the precipitates that have formed recently above sapropel Si2 (van Santvoort et al., 1996). The Mn (hydr)oxides formed at ancient oxidation fronts are being dissolved in the suboxic and anoxic environments that have been present in the sediments after the precipitation of the (hydr)oxides. This is reflected by the progressively decreasing peak-heights of the Mn enrichments above sapropels with depth. The Mn enrichments above sapropels are accompanied by Fe enrichments above sapropels, which are also relicts of past oxidation fronts above sapropels, these Fe enrichments appear to have been pyritized, as follows from the S enrichment at the same level (Fig. 8.10). The Mn enrichment between 800 and 900 cmbsf may be a relict of the position of a past oxidation front, which was not associated with a sapropel. In this interval of the sediment "violet fronts" are visible. This Mn enrichment is associated with an Fe enrichment just below. The Fe enrichment likely formed at the same oxidation front as the Mn enrichment. These Fe oxides appear to have been sulphidized, so that there is also an enrichment in solid phase S at this level.

8.4.5 Relation between sediment diagenesis and magnetic properties

The magnetic parameters ChRM, ARM, χ_{in}, IRM, (Fig. 8.5) all show the same pattern with depth in core KC19C (Fig. 8.11). Above sapropel Si2, the magnetic intensities are relatively high. Just below sapropel Si2 the magnetic intensities are relatively low (note that no samples for magnetic measurements were taken in and 10 cm around the sapropels). In between the sulphidized zone below sapropel Si2 and the suboxic/anoxic boundary at about 2 mbsf the magnetic intensities show an absolute maximum. Below the suboxic/anoxic boundary, the magnetic intensities are at very low levels ranging from 1% to ~10% of the maximum.

The features in the top of core KC19C above the suboxic/anoxic boundary, are identical to those in KC01B (Dekkers et al., 1994; Langereis et al., 1997). Typically, directly above sapropels high magnetic intensities are present as a result of precipitation of magnetic minerals, as occurs at present above the youngest sapropel Si2 (van Santvoort et al., 1996). This yields high
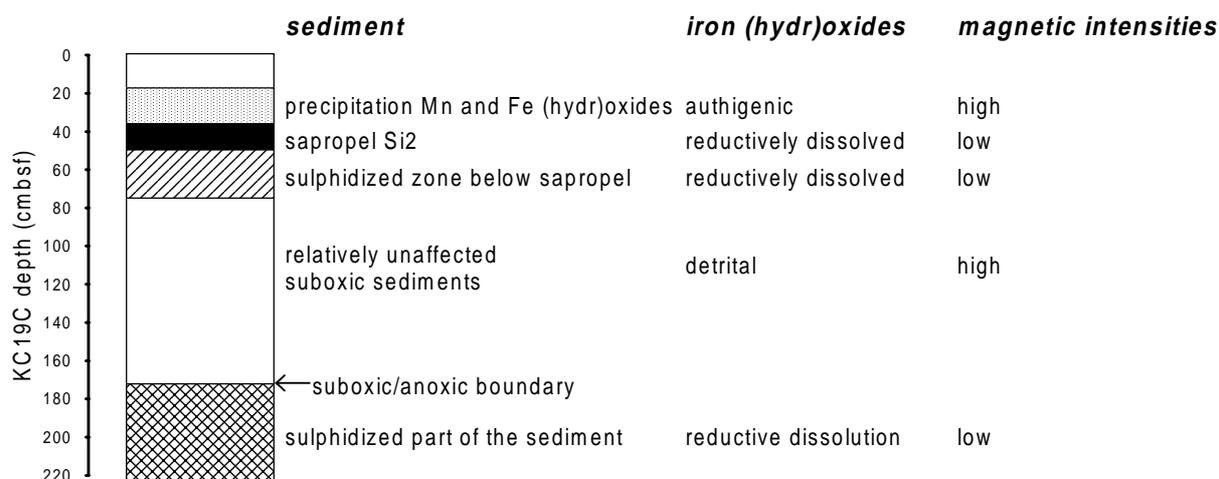
| | *sediment* | *iron (hydr)oxides* | *magnetic intensities* |

Figure 8.11 *Different diagenetic zones and consequences for the Fe (hydr)oxide minerals and magnetic intensities in the top of core KC19C. These authigenic Fe oxides above Si2 are formed at the level where upward-diffusing Fe(II) meets with downward diffusing oxidants (oxygen and nitrate). In the sapropel and the sulphidized zone below the sapropel, where detrital Fe oxides were originally present, reductive dissolution and transformation into pyrite has removed these magnetic minerals, resulting in low magnetic intensities (Langereis et al., 1997). In between the sulphidized zone below Si2 and the suboxic/anoxic boundary at ~2 mbsf, detrital Fe oxides are still present and are only slowly dissolving in the suboxic environment, below the suboxic/anoxic boundary Fe oxides (both detrital and authigenic) have been removed by reductive dissolution and pyrite formation, and consequently the magnetic intensity is minimal.*

intensities in the upper 20 cmbsf. Low values of ARM and NRM just below sapropels, as recorded below Si2 in KC19C, can be associated with the dissolution of magnetic minerals as a result of downward sulphidisation of sapropel-underlying sediments (Passier et al., 1996a/Chapter 2) during sapropel formation. Values of χ_{in} in KC01B have less distinct minima below sapropels than ARM and NRM, this is also observed below Si2 in KC19C, and is attributed to the fact that changes in (ferrimagnetic) susceptibility are buffered by the paramagnetic contribution of clay minerals.

The change to the low intensities in the lower, anoxic, part of the core is the result of reductive dissolution of magnetic Fe (hydr)oxide minerals (magnetically predominantly magnetite) and the reaction of these Fe (hydr)oxides to pyrite. These reactions have influenced all sediments older than ~50 ka. The dissolution and pyritisation of magnetite is common in anoxic marine sediments (e.g. Canfield and Berner, 1987). Several investigators (Karlin and Levi, 1985; Channell et al., 1990; Karlin, 1990a and 1990b; Leslie et al., 1990a and 1990b; Robinson, 1990; Bloemendal et al., 1993) have found that anoxic diagenesis affects magnetic parameters, and that it is important to identify such influence before drawing paleomagnetic and paleoclimatic conclusions from magnetic properties in nearshore as well as in pelagic sediments.

8.4.6 Details of magnetic mineralogy

The decrease of ARM/IRM with depth between 0 and 2 mbsf (Fig. 8.12) indicates a slight decrease of the single domain magnetite fraction, indicating a possible preferential dissolution of smaller grains (e.g. Leslie et al., 1990a). This sediment interval coincides with the suboxic zone in which Mn and Fe are actively released to the porewaters (Fig. 8.2) as a result of reductive dissolution of Fe and Mn (hydr)oxides. The subsequent shift to higher ARM/IRM from 2 to 8 mbsf (Fig. 8.12) in the sulphidic part of the sediment may indicate breakup of larger multidomain grains, making them look like single domain grains, or the increased importance of magnetic grains that are resistant to dissolution, for example inclusions in silicate grains (Leslie et al., 1990a).

The Fe (hydr)oxides above sapropel Si2 are of dominantly authigenic origin, whereas the Fe (hydr)oxides below the sulphidized zone under Si2 are of detrital origin (Fig. 8.11). This difference is reflected in the low ratio of ARM after demagnetisation in 20 mT vs. initial ARM (ARM_{20mT}/ARM_{in}; Fig. 8.12), which indicates that the authigenic Fe (hydr)oxides above Si2 can be easily demagnetized suggesting that grain-size distribution in the authigenic Fe (hydr)oxides
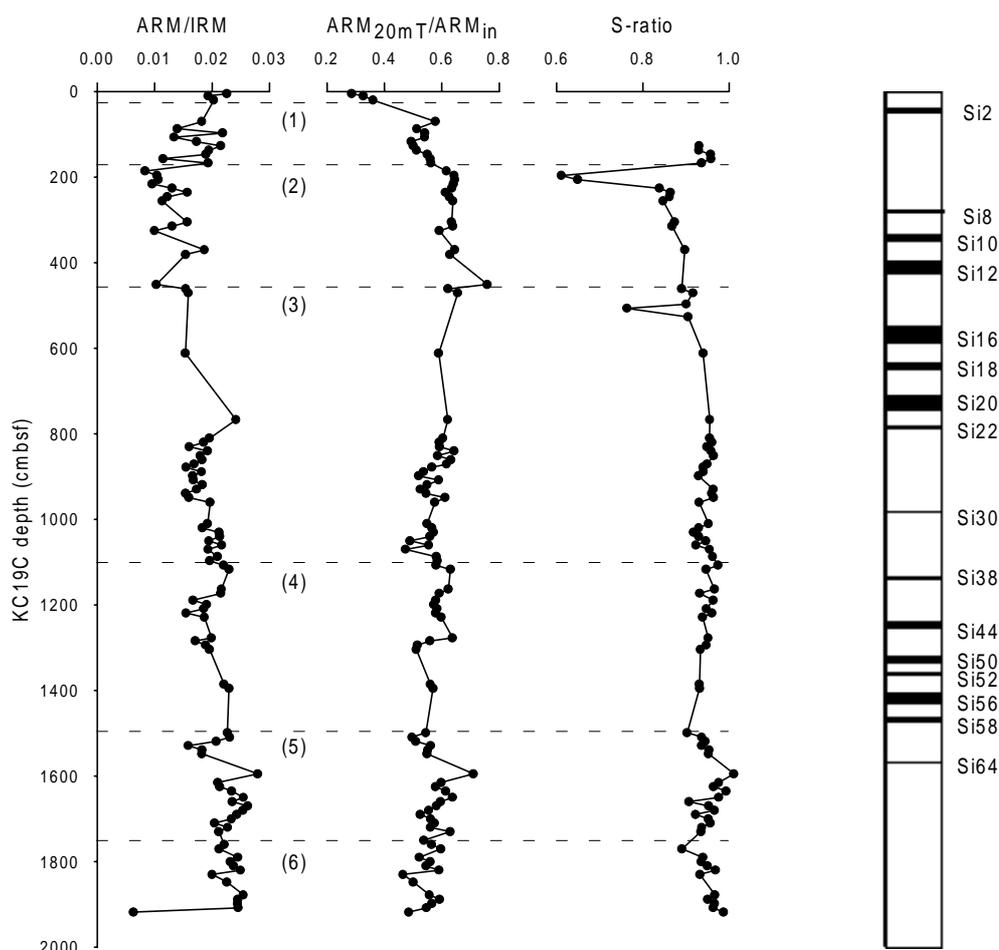

Figure 8.12 *ARM/IRM, ARM_{20mT}/ARM_{in} and S-ratio, vs. depth in core KC19C. Sapropel numbering after Lourens et al. (1996). For meaning of the horizontal lines see caption of Fig. 8.1.*

is slightly shifted towards smaller grains (< 30 nm; "semi" superparamagnetic (SP) grains) compared to the detrital grain-size distribution.

The S-ratio (-IRM$_{-0.3T}$/IRM$_{1T}$; Fig. 8.12) increases slightly with depth down from 2 to 8 mbsf, implying that relatively unoxidized magnetite becomes increasingly important with depth in the anoxic zone relative to hematite and goethite. Preferential dissolution of hematite and goethite is likely, because the half-lifes with respect to consumption by sulphide for hematite and goethite are orders of magnitude smaller than that for magnetite (Canfield et al., 1992). A remarkable step to higher ARM/IRM and S-ratio values below 15 mbsf (Fig. 8.12) may be related to changes in the detrital input to the sediment.

The sharp dip in the S-ratio just above 2 mbsf (Fig. 8.12) seems related to the suboxic/anoxic boundary, where intermediate Fe (mono)sulphides may have formed at the level where upward-diffusing sulphide and downward diffusing Fe meet. The dip may represent either these intermediate Fe (mono)sulphide phases or the products of oxidation of these phases after core recovery. The Fe (hydr)oxides resulting from oxidation of Fe sulphides such as greigite would yield even lower S-ratios than the original Fe sulphides (Dekkers and Schoonen, 1996). Additionally, this dip in the S-ratio just above 2 mbsf coincides with a spike in Fe$_{dith}$ (Fig. 8.4), which may represent the same Fe minerals.

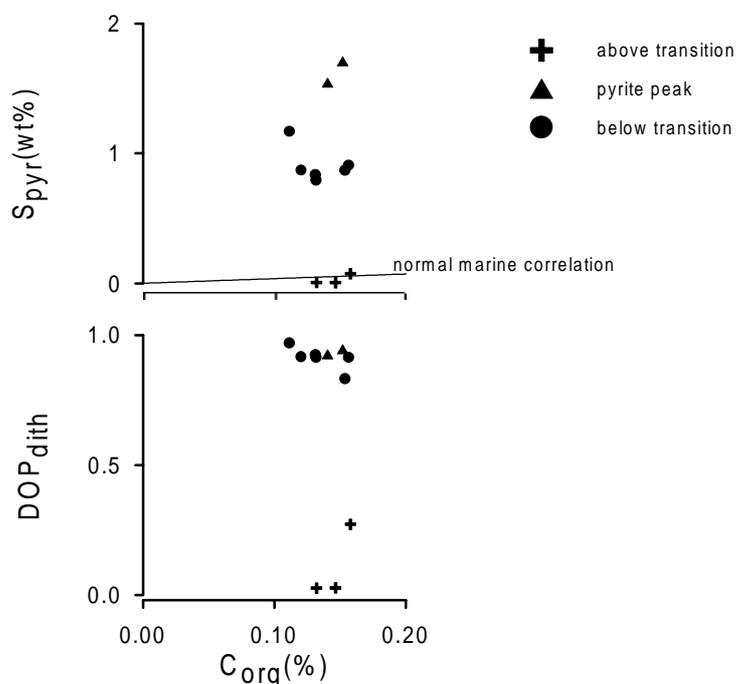### 8.4.7 Sulphidisation of the sediments

The most intriguing feature in KC19C is the rapid shift from positive to negative Eh values at 180 cmbsf, indicating the transition from an oxic to a sulphidic environment. The shift coincides with an increase in pyrite contents and an abrupt loss of magnetic minerals. Clearly, the sediments at site 19C are sulphidized by some upward input of sulphide. To study this sulphidisation more thoroughly, the Fe and S chemistry has been investigated.

The content of Fe that is available for pyrite formation, reactive Fe (Fe$_{dith}$), decreases with depth in the zone around 180 cmbsf (Fig. 8.4). The level of 6 to 34 µmol/g dry sediment is comparable with the Fe$_{dith}$ contents within and below sapropels where reactive Fe availability limited pyrite formation (Passier and de Lange, 199_/Chapter 3). Accordingly, pyrite formation is likely to be Fe-limited in the sediments around 180 cmbsf as well. The ratio between pyritic Fe and the sum of reactive Fe and pyritic Fe (the degree of pyritisation, *DOP*), can provide a better insight into the availability of Fe and the formation of pyrite in sediments (Berner, 1970). *DOP* based on dithionite-extractable Fe can be expressed as follows:

$$DOP_{dith} = \frac{pyritic\ Fe}{pyritic\ Fe\ +\ reactive\ Fe}\ .$$

We have taken reactive Fe to be equal to dithionite-extractable Fe, as recommended by Raiswell et al. (1994). The amount of reduced S in sediments is usually closely related to the C$_{org}$ content, because with increasing C$_{org}$ a larger amount of organic matter is metabolizable resulting in more sulphide production (e.g. Berner and Raiswell, 1983; Berner, 1984; Leventhal, 1987). In 'normal' marine sediments the regression line in S vs. C plots has a slope of 1/2.8 (S$_{tot}$/C$_{org}$ ratio,

wt%/wt%) and passes through the origin (assuming that S fractions other than reduced S are negligible). In euxinic (sulphidic) marine environments, however, sulphide is omnipresent (independent of local C_{org} contents) and Fe sulphide formation can take place in the water column or at the sediment/water interface. Even slowly reacting Fe compounds may react with sulphide in euxinic environments. Consequently, positive intercepts on the S axis are obtained in S vs. C plots for euxinic sediments, and only weak correlations may be observed (e.g. Leventhal, 1983; Berner, 1984). Postdepositional sulphidisation of C_{org}-poor sediments may result in extremely high S/C ratios (Boesen and Postma, 1988; Middelburg, 1991; Leventhal, 1995; Passier et al., 1996a/Chapter 2). Plots of the pyrite contents versus C_{org} contents in the transitional interval around 180 cmbsf in core KC19C (Fig. 8.13) illustrate that this pyrite is not supported by the presence of organic C, as in the 'normal marine' correlation (e.g. Raiswell and Berner, 1985). Consequently, it is likely that the reduced S present in the sediments below 180 cmbsf does not originate from SO_4^{2-} reduction of sedimentary organic matter at the interval of pyrite formation, but that sulphide has been added to the sediment from another source. The pyrite content is distinctly higher in the two samples from the pyrite peak between 180 and 200 cmbsf (Figs. 8.4 and 8.13). In contrast, DOP_{dith} values are all close to one and independent of C_{org} (Fig. 8.13), indicating that pyrite formation has been Fe-limited for all samples. This distinct pyrite peak, therefore, is thought to have formed by the downward diffusion of additional Fe. The source for this Fe(II) is reductive dissolution of Fe (hydr)oxides in the suboxic part of the sediment in the top of the upper sediment. In order to form a distinct pyrite peak, the site (front) where sulphide and Fe meet must have been at the same level for some time. The Fe limitation for pyrite formation suggests that all reactive Fe has been sulphidized almost completely below 180 cmbsf, which is the present suboxic/anoxic boundary.

Figure 8.13 *Pyritic S (S_{pyr}) vs. organic C (C_{org}), and DOP_{dith} vs. organic C (C_{org}) around 200 cmbsf in KC19C.*

The less reactive Fe phases, such as silicate bound Fe(III), may also be used in pyrite formation to some extent (Canfield et al., 1992). In fact, silicate bound Fe ($Fe_{sil} = Fe_{tot} - Fe_{dith} - Fe_{pyr}$, where $Fe_{pyr} = S_{pyr}/2$), divided by the Al content ($Fe_{sil}^* = Fe_{sil}/Al$) decreases with depth over the interval around 180 cmbsf (Fig. 8.4). This indicates that more Fe from silicates has been used for pyrite formation in the sulphidized part of the sediment below 180 cmbsf.

The atypical sulphidisation in the sediments of core KC19C compared to core KC01B is also clear from comparison of S_{tot} vs. C_{org} for non-sapropel samples at 10 cm resolution in core KC19C and the same plot for core KC01B (Fig. 8.14; Dekkers et al., 1994; van Santvoort et al, 1997). This comparison reveals that the S contents in relatively C_{org}-poor sediments are much higher in KC19C than in KC01B, indicating again the sulphidisation of organic poor sediments in KC19C.

8.4.8 Source of reduced S

The source of the reduced S that sulphidized the sediments in KC19C below 180 cmbsf is not SO_4^{2-} reduction of sedimentary organic matter at the site of pyrite formation. The linear SO_4^{2-} profile concentrations in the upper 17.5 mbsf of sediment suggests that the SO_4^{2-} concentration is controlled by diffusion from the bottomwater to 17.5 mbsf. At 17.5 mbsf SO_4^{2-} is used, apparently in bacterial SO_4^{2-} reduction, whereby sulphide is formed. This sulphide, in turn, diffuses away from the site of sulphide formation, and titrates all Fe available for pyrite formation. This titration has resulted in the nearly complete consumption of magnetic minerals up to 180 cmbsf. The depth to which sulphide reaches from below, is not only controlled by the amount of solid phase Fe available for pyrite formation but also by the diffusive flux of Fe(II)
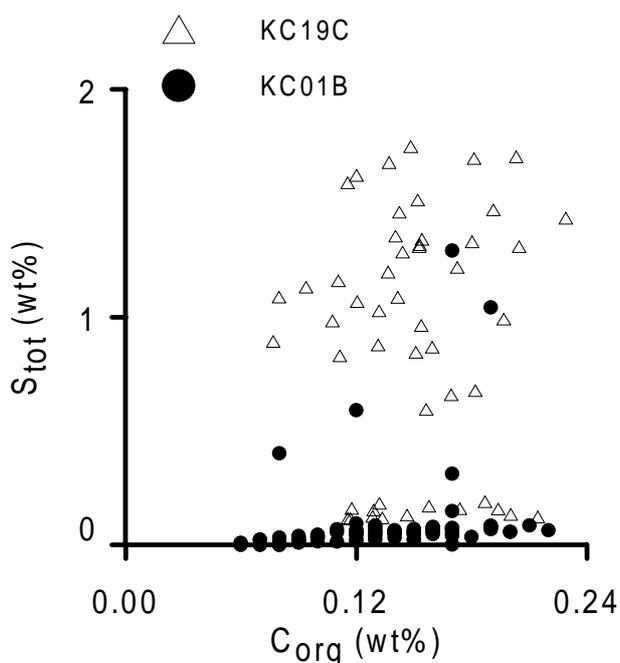

Figure 8.14 *Total S (S_{tot}) vs. organic C (C_{org}) in non-sapropel samples at a resolution of 10 cm in cores KC19C and KC01B.*

from above.

It is not clear from the geochemical data why SO_4^{2-} reduction is occurring at 17.5 mbsf. At 17.5 mbsf there is no organic C enrichment to support significant SO_4^{2-} reduction. Another striking feature is that below 17.5 mbsf, porewater SO_4^{2-} increases again in a linear way, suggesting the upward diffusion of SO_4^{2-}. Underlying Messinian salts are the likely source of SO_4^{2-}, as indicated by the increasing concentrations of chloride with depth (Fig. 8.2) (van Santvoort and de Lange, 1996). Sulphate reduction is situated in a confined zone around 17.5 m. Considering the highly fluctuating P-wave velocities below 18.5 mbsf and the presence of expansion cracks, that suggest that these sediments are disturbed, a possible explanation for SO_4^{2-} reduction in the lower end of the core could be a lateral input of methane, and subsequent methane oxidation in bacterial SO_4^{2-} reduction. To resolve whether SO_4^{2-} reduction occurs via oxidation of methane or via oxidation of sedimentary organic matter, the amounts of used SO_4^{2-} and produced bicarbonate, which equals alkalinity in marine porewaters, have been compared.

The simplified reaction for SO_4^{2-} reduction of sedimentary organic matter is:

$$2\,CH_2O + SO_4^{2-} \rightarrow 2\,HCO_3^- + HS^- + H^+, \tag{1}$$

and the ratio between the amount of SO_4^{2-} that is consumed in the reaction and the amount of bicarbonate that is produced can be expressed as: $R = |\Delta SO_4^{2-}/\Delta HCO_3^-| = 0.5$. Whereas the reaction for coupled methane oxidation and SO_4^{2-} reduction is:

$$CH_4 + SO_4^{2-} \rightarrow HCO_3^- + HS^- + H_2O, \tag{2}$$

where $R = |\Delta SO_4^{2-}/\Delta HCO_3^-| = 1$. The consumption of SO_4^{2-} and the production of bicarbonate can be quantified from the slopes in the porewater profiles of SO_4^{2-} and alkalinity. The main assumption in this quantification is that transport by other processes than one-dimensional diffusion affects both slopes in the same way, so that this transport does not affect the ratio between the slopes in the SO_4^{2-} and the alkalinity profile. The diffusive transport of SO_4^{2-} to the presumed site of SO_4^{2-} reduction is:

$$\left| J_{diff,SO_4} \right| = \phi\, D_{j,sed,SO_4}\, \left(\left| \frac{\Delta[SO_4^{2-}]}{\Delta x} \right|_{above} + \left| \frac{\Delta[SO_4^{2-}]}{\Delta x} \right|_{below} \right), \tag{3}$$

and the diffusive transport of bicarbonate away from the site of SO_4^{2-} reduction is:

$$\left| J_{diff,HCO_3} \right| = \phi\, D_{j,sed,HCO_3}\, \left(\left| \frac{\Delta[HCO_3^-]}{\Delta x} \right|_{above} + \left| \frac{\Delta[HCO_3^-]}{\Delta x} \right|_{below} \right), \tag{4}$$

where ϕ is the porosity, $D_{j,sed,SO4}$ is the diffusion coefficient of SO_4^{2-} in the sediment, $D_{j,sed,HCO3}$ is the diffusion coefficient for bicarbonate in the sediment, and *above* and *below* designate the gradients above the presumed site of SO_4^{2-} reduction and below this site, respectively. These

equations yield:

$$R = \frac{|J_{diff,SO_4}|}{|J_{diff,HCO_3}|} = \frac{D_{j,sed,SO_4}}{D_{j,sed,HCO_3}} \frac{(|\frac{\Delta[SO_4^{2-}]}{\Delta x}|_{above} + |\frac{\Delta[SO_4^{2-}]}{\Delta x}|_{below})}{(|\frac{\Delta[HCO_3^{-}]}{\Delta x}|_{above} + |\frac{\Delta[HCO_3^{-}]}{\Delta x}|_{below})} \tag{5}$$

$D_{j,sed,SO4}/D_{j,sed,HCO3} = 0.915$, calculated according to Li and Gregory (1974), at $12°C$, which is the ambient temperature. The sums of the slopes of the porewater profiles (Fig. 8.15) are 0.049 and 0.034 mmol l^{-1} cm^{-1} for SO_4^{2-} and bicarbonate, respectively. Thus, R = 1.3, which indicates that SO_4^{2-} reduction by oxidation of methane (R = 1) is more likely than SO_4^{2-} reduction by oxidation of sedimentary organic matter (R = 0.5). The fact that R is larger than 1 may be related to some uptake of bicarbonate into carbonate formation. In addition, it may be that partly reduced S phases are included in the S-pool that is being reduced by methane oxidation, this would mean that less bicarbonate is produced for every sulphide produced than suggested in reaction (2). If methane input is gouverning SO_4^{2-} reduction, this process does not have to be constant in time, for methane may build-up and migrate up in the sediments during distinct events.

The situation of SO_4^{2-} reduction by methane oxidation, and upward diffusion of salt is similar, although on a smaller scale, to the processes observed in mud volcanoes along the Mediterranean Ridge (Robertson et al., 1996). The mud volcanoes are mud domes on the hemipelagic seafloor where mud debris is extruded.The domes are characterized by the occurrence of salt-saturated porewaters, as a result of dissolution of nearby Messinian salt. Furthermore, extensive SO_4^{2-} reduction and venting of hydrocarbon gas are observed in mud volcanoes. It may be possible that the unusual features observed in the sediments of core KC19C are the first signal for the initial stages of mud volcano formation at this site.
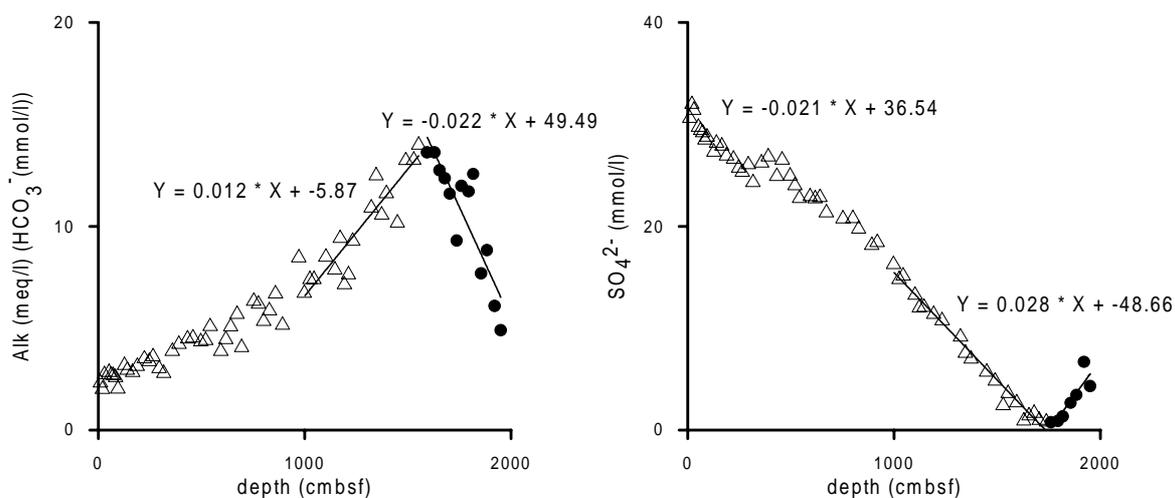

Figure 8.15 *Porewater alkalinity (Alk) and SO_4^{2-} concentrations vs. depth in core KC19C, and the fitted linear profiles in the lower part of the core.*

8.5 Conclusions

Anomalous present-day sulphide formation due to bacterial SO_4^{2-} reduction at 17.5 mbsf in the sediment (age ~800 ka) at site 19C in the eastern Mediterranean has invoked reductive dissolution of reactive Fe minerals and consequent pyrite formation in the entire sediment column up to about 2 mbsf (age ~50 ka). At this depth the suboxic to anoxic transition is situated. Sulphide penetrates from below to this level at about 2 mbsf. This depth is controlled by the relative magnitudes of the upward sulphide flux and the downward Fe(II) flux in the suboxic sediments above the transition. The entire cored interval below, i.e. until 19.6 mbsf (age ~950 ka), has been severely influenced by this reductive dissolution of Fe (hydr)oxides, therefore only low magnetic intensities can be obtained below 2 mbsf, and no paleomagnetic information can be obtained below 10 mbsf at this site in the eastern Mediterranean.

130

References

Aller R.C., Mackin J.E., and Cox R.T. Jr. (1986) Diagenesis of Fe and S in Amazon inner shelf muds: apparent dominance of Fe reduction and implications for the genesis of ironstones. *Cont. Shelf Res.* **6**, 263–289.

Anderson T.F. and Pratt L.M. (1995) Isotopic evidence for the origin of organic sulfur and elemental sulfur in marine sediments. In *Geochemical Transformations of Sedimentary Sulfur* (ed. M.A Vairavamurthy and M.A.A. Schoonen); *Amer. Chem. Soc. Symp. Series* **612**, 378–396.

Arthur M.A., Brumsack H.-J., Jenkyns H.C., and Schlanger S.O. (1990) Stratigraphy, geochemistry, and paleoceanography of organic carbon-rich Cretaceous sequences. In *Cretaceous resources, events and rhythms* (ed. R.N. Ginsburg and B. Beaudoin), pp. 75–119. Elsevier.

Bein A., Almogi-Labin A., and Sass E. (1990) Sulfur sinks and organic carbon relationships in Cretaceous organic-rich carbonates: implications for evaluation of oxygen-poor depositional environments. *Amer. J. Sci.* **290**, 882–911.

Berner R.A. (1967) Thermodynamic stability of sedimentary iron sulfides. *Amer. J. Sci.* **265**, 773–785.

Berner R.A. (1969) Migration of iron and sulfur within anaerobic sediments during early diagenesis. *Amer. J. Sci.* **267**, 19–42.

Berner R.A. (1970) Sedimentary pyrite formation. *Amer. J. Sci.* **268**, 1–23.

Berner R.A. (1978) Sulfate reduction and the rate of deposition of marine sediments. *Earth Planet. Sci. Lett.* **37**, 492–498.

Berner R.A. (1980) *Early Diagenesis. A theoretical approach.* Princeton University Press.

Berner R.A. (1984) Sedimentary pyrite formation: An update. *Geochim. Cosmochim. Acta* **48**, 605–615.

Berner R.A. and Canfield D.E. (1989) A new model for atmospheric oxygen over Phanerozoic time. *Amer. J. Sci.* **289**, 333–361.

Berner R.A. and Raiswell R. (1983) Burial of organic carbon and pyrite sulfur in sediments over Phanerozoic time: a new theory. *Geochim. Cosmochim. Acta* **47**, 855–862.

Bertrand P. and Lallier-Vergès E. (1993) Past sedimentary organic matter accumulation and degradation controlled by productivity. *Nature* **364**, 786–788.

Béthoux J.P. (1989) Oxygen consumption, new production, vertical advection and environmental evolution in the Mediterranean Sea. *Deep-Sea Res.* **36**, 769–781.

Béthoux, J.P. (1993) Mediterranean sapropel formation, dynamic and climatic viewpoints. *Oceanol. Acta* **16**, 127–133.

Betzer R.R., Showers W.J., Laws E.A., Winn C.D., DiTullio G.R., and Kroopnick P.M. (1984) Primary productivity and particle fluxes on a transect of the equator at 153°W in the Pacific Ocean. *Deep-Sea Res* **31**, 1–11.

Bishop J.K.B. (1988) The barite-opal-organic carbon association in oceanic particulate matter. *Nature* **332**, 341–343.

Bloemendal J., King J.W., Hunt P.B., DeMenocal P.B., and Hayashida A. (1993) Origin of the sedimentary magnetic record at Ocean Drilling Program Sites on the Owen Ridge, Western Arabian Sea. *J. Geophys. Res.* **98**, 4199–4219.

Boesen C. and Postma D. (1988) Pyrite formation in anoxic environments of the Baltic. *Amer. J. Sci.* **288**, 575–603.

Bosch H.-J., Sinninghe Damsté J.S., and de Leeuw J.W. (199_) Molecular paleontology of Eastern Mediterranean sapropels: evidence for photic zone euxinia. In *Proc. ODP, Sci. Results, 160* (ed. A.H.F. Robertson et al.). College Station, TX, ODP. In press.

Böttcher M.E. and Huckriede H. (1997). First occurrence and stable isotope composition of authigenic γ-MnS in the central Gotland Deep (Baltic Sea). *Mar. Geol.* **137**, 201–205.

Böttcher M.E., Rusch A., Höpner T., and Brumsack H.-J. (1997) Stable sulfur isotope effects related to local intense sulfate reduction in a tidal sandflat (Southern North Sea): results from loading experiments. *Isotopes Environm. Health Stud.* **33**, 109–129.

Böttcher M.E., Brumsack H.-J., and de Lange G.J. (199_a) Sulfate reduction and related stable isotope (^{34}S, ^{18}O) variations in interstitial waters from the Eastern Mediterranean (Leg 160). In *Proc. ODP, Sci. Results, 160* (ed. A.H.F. Robertson et al.). College Station, TX, ODP. In press.

Böttcher M.E., Oelschläger B., Höpner T., Brumsack H.-J., and Rullkötter J. (199_b) Sulfate reduction related to the early diagenetic degradation of organic matter and black spot formation in tidal sand flats: Stable isotope (^{13}C, ^{34}S, ^{18}O) and compositional results. *Org. Geochem.* Submitted.

Bottrell S. and Raiswell R. (1989) Primary versus diagenetic origin of Blue Lias rhythms (Dorset, UK): evidence from sulphur geochemistry. *Terra Nova* **1**, 451–456.

Bralower T.J. and Thierstein H.R. (1987) Organic carbon and metal accumulation rates in Holocene and mid-Cretaceous sediment: palaeoceanographic significance. In *Marine Petroleum and Source Rocks* (ed. J. Brooks and A.J. Fleet); *Geol. Soc. Spec. Publ.* **26**, 345–369.

Brüchert V. and Pratt L.M. (1996) Contemporaneous early diagenetic formation of organic and inorganic sulfur in estuarine sediments from St. Andrew Bay, Florida, USA. *Geochim. Cosmochim. Acta* **60**, 2325–2332.

Buckley H.A., Easton A.J., and Johnson L.R. (1974) Iron and manganese encrustations in Recent sediments. *Nature* **249**, 436–437.

Calvert S.E. (1983) Geochemistry of Pleistocene sapropels and associated sediments from the Eastern Mediterranean. *Oceanol. Acta* **6**, 255–267.

Calvert S.E. and Karlin R.E. (1991) Relationships between sulfur, organic carbon, and iron in the modern sediments of the Black Sea. *Geochim. Cosmochim. Acta* **55**, 2483–2490.

Calvert S.E., Nielsen B., and Fontugne M.R. (1992) Evidence from nitrogen isotope ratios for enhanced productivity during formation of eastern Mediterranean sapropels. *Nature* **359**, 223–225.

Canfield D.E. (1989) Sulfate reduction and oxic respiration in marine sediments: implications for organic carbon preservation in euxinic environments. *Deep-Sea Res.* **36**, 121–138.

Canfield D.E. (1994) Factors influencing organic carbon preservation in marine sediments. *Chem. Geol.* **114**, 315–329.

Canfield D.E. and Berner R.A. (1987) Dissolution and pyritization of magnetite in anoxic marine sediments. *Geochim. Cosmochim. Acta* **51**, 645–659.

Canfield D.E. and Teske A. (1996) Late Proterozoic rise in atmospheric oxygen concentration inferred from phylogenetic and sulphur-isotope studies. *Nature* **382**, 127–132.

Canfield D.E. and Thamdrup B. (1994) The production of [34]S-depleted sulfide during bacterial disproportionation of elemental sulfur. *Science* **266**, 1973–1975.

Canfield D.E., Raiswell R., Westrich J.T., Reaves C.M., and Berner R.A. (1986) The use of chromium reduction in the analysis of reduced inorganic sulfur in sediments and shales. *Chem. Geol.* **54**, 149–155.

Canfield D.E., Raiswell R., and Bottrell S. (1992) The reactivity of sedimentary iron minerals toward sulfide. *Amer. J. Sci.* **292**, 659–683.

Canfield D.E., Lyons T.W., and Raiswell R. (1996) A model for iron deposition to euxinic Black Sea sediments. *Amer. J. Sci.* **296**, 818–834.

Casagrande D.J., Idowu G., Friedman A., Rickert P., Siefert K., and Schlenz D. (1979) H_2S incorporation in coal precursors: origins of organic sulphur in coal. *Nature* **282**, 599–600.

Chambers L.A. and Trudinger P.A. (1979) Microbiological Fractionation of Stable Sulfur Isotopes: A Review and Critique. *Geomicrobiol. J.* **1**, 249–293.

Channell J.E.T., Hawthorne T., and Torii M. (1990) Contrasting magnetic properties in Leg 107 sediments: preservation and alteration of titanomagnetite at adjacent sites. In *Proc. ODP*, *Sci. Results, 107* (ed. K.A. Kastens et al.), pp. 113–128. College Station, TX, ODP.

Cita M.B. (1989) Evidence of relief inversion in satellite-basins (rim-syncline) of Bacino Bannock. First results of the BAN-88 cruise. In *Anoxic Basins of the eastern Mediterranean. Results of the Third Conference, Bergamo (Italy) December 14–16 1988,* (ed. M.B. Cita et al.); *Ric. suppl.* **72**, 16–19.

Cita M.B., de Lange G.J., and Olausson E. (1991) Anoxic basins and sapropel deposition in the Eastern Mediterranean: Past and Present. *Mar. Geol.* **100**, 1–4.

Colley S., Thomson J., Wilson T.R.S., and Higgs N.C. (1984) Post-depositional migration of elements during diagenesis in brown clay and turbidite sequences in the North East Atlantic. *Geochim. Cosmochim. Acta.* **48**, 1223–1235.

Crank J., McFarlane N.R., Newby J.C., Paterson G.D., and Pedley J.B. (1981) *Diffusion processes in environmental systems.* Macmillan.

Cutter G.A. and Oatts Th.J. (1987) Determination of dissolved sulfide and sedimentary sulfur speciation using gas chromatography photoionization detection. *Anal. Chem.* **59**, 717–721.

Cypionka H., Smock A.S., Boettcher M.E. (199_) A combined pathway of sulfur compound disproportionation in a sulfate reducing bacterium. *Science*. Submitted.

Dekkers M.J. and Schoonen M.A.A. (1996) Magnetic properties of hydrothermally synthesized greigite (Fe$_3$S$_4$)–I. Rock magnetic parameters at room temperature. *Geophys. J. Int.* **126**, 360–368.

Dekkers M.J., Langereis C.G., Vriend S.P., van Santvoort P.J.M., and de Lange, G.J. (1994) Fuzzy *c*-means cluster analysis of early diagenetic effects on natural remanent magnetisation acquisition in a 1.1 Myr piston core from the Central Mediterranean. *Phys. Earth Planet. Inter.* **85**, 155–171.

de Lange G.J. (1986) Early diagenetic reactions in interbedded pelagic and turbiditic sediments in the Nares Abyssal Plain (western North Atlantic): Consequences for the composition of sediment and interstitial water. *Geochim. Cosmochim. Acta* **50**, 2543–2561.

de Lange G.J. (1992) Shipboard routine and pressure-filtration system for pore-water extraction from suboxic sediments. *Mar. Geol.* **109**, 77–81.

de Lange G.J., Jarvis I., and Kuijpers A. (1987) Geochemical characteristics and provenance of late Quaternary sediments from the Madeira Abyssal Plain, N Atlantic. In *Geology and Geochemistry of Abyssal Plains* (ed. P.P.E. Weaver and J. Thomson); *Geol. Spec. Publ.* **31**, 147–165.

de Lange G.J., Middelburg J.J., and Pruysers P.A. (1989) Discussion: Middle and Late Quaternary depositional sequences and cycles in the eastern Mediterranean. *Sedimentology* **36**, 151–156.

de Lange G.J., Middelburg J.J., van der Weijden C.H., Catalano G., Luther G.W. III, Hydes D.J., Woittiez J.R.W., and Klinkhammer G.P. (1990) Composition of anoxic hypersaline brines in the Tyro and Bannock Basins, eastern Mediterranean. *Mar. Chem.* **31**, 63–88.

Drobner E., Huber H., Wächtershäuser G., Rose D., and Stetter K.O. (1990) Pyrite formation linked with hydrogen evolution under anaerobic conditions. *Nature* **346**, 742–744.

Dymond J. and Collier R. (1996) Particulate barium fluxes and their relationships to biological productivity. *Deep-Sea Res.* **43**, 1283–1308.

Dymond J., Suess E., and Lyle M. (1992) Barium in deep-sea sediment: a geochemical proxy for paleoproductivity. *Paleoceanography* **7**, 163–181.

Emeis K.-C., Robertson A.H.F, Richter C., et al. (1996) *Proc. ODP, Init. Repts., 160*. College Station, TX, ODP.

Eppley R.W. and Peterson B.J. (1979) Particulate organic matter flux and planktonic new production in the deep ocean. *Nature* **282**, 677–680.

Erba E. (1988) Tyro-87 - "ABC" cruise; Quaternary calcareous nannofossil biostratigraphy of the "ABC" cores from the eastern Mediterranean.

Fengler G., Haupt E.T.K., and Liebezeit G. (1989) Humic substances in Holocene sediments of the Skagerrak (NE North Sea) and the Elbe river. *The Science of the Total Environment* **81/82**, 335–342.

Ferdelman T.G., Church Th.M., and Luther G.W. III (1991) Sulfur enrichment of humic substances in a Delaware salt marsh sediment core. *Geochim. Cosmochim. Acta* **55**, 979–988.

Fontugne M.R. and Calvert S.E. (1992) Late Pleistocene variability of the carbon isotopic composition of organic matter in the eastern Mediterranean: monitor of changes in carbon sources and atmospheric CO_2 concentrations. *Paleoceanography* **7**, 1–20.

Francois R. (1987a) A study of the extraction conditions of sedimentary humic acids to estimate their true in situ sulphur content. *Limnol. Oceanogr.* **32**, 964–972.

Francois R. (1987b) A study of sulphur enrichment in the humic fraction of marine sediments during early diagenesis. *Geochim. Cosmochim. Acta* **51**, 17–27.

Froelich P.N., Klinkhammer G.P., Bender M.L., Luedtke N.A., Heath G.R., Cullen D., Dauphin P., Hammond D., Hartman B., and Maynard V. (1979) Early oxidation of organic matter in pelagic sediments of the eastern equatorial Atlantic: suboxic diagenesis. *Geochim. Cosmochim. Acta* **43**, 1075–1090.

Froelich P.N., Arthur M.A., Burnett W.C., Deakin M., Hensley V., Jahnke R., Kaul L., Kim K.-H., Roe K., Soutar A., and Vathakanon C. (1988) Early diagenesis of organic matter in Peru continental margin sediments: phosphorite precipitation. *Mar. Geol.* **80**, 309–343.

Fry B. (1988) Food web structure on Georges Bank from stable C, N, and S isotopic compositions. *Limnol. Oceanogr.* **33**, 1182–1190.

Fry B., Jannasch H.W., Molyneaux S.J., Wirsen C.O., Muramoto J.A., and King S. (1991) Stable isotope studies of the carbon, nitrogen and sulfur cycles in the Black Sea and the Cariaco Trench. *Deep-Sea Res.* **38**, 1003–1019.

Goldhaber M.B. and Kaplan I.R. (1974) The sulfur cycle. In *The Sea* (ed. E.D. Goldberg), Vol. 5, Chap. 17, pp. 569–655. Wiley.

Grasshoff K. (1976) *Methods of seawater analysis*. Verlag Chemie.

Hartgers W.A., Sinninghe Damsté J.S., Requejo A.G, Allan J., Hayes J.M., and de Leeuw J.W. (1994) Evidence for only minor contributions from bacteria to sedimentary organic carbon. *Nature* **369**, 224–227.

Hartgers W.A., Lòpez J.F., Sinninghe Damsté J.S., Reiss C., Maxwell J.R., and Grimalt J.O. (1997). Sulfur-binding in recent environments: II. Speciation of sulfur and iron and implications for the occurrence of organo-sulfur compounds. *Geochim. Cosmochim. Acta* **61**, 4769–4788.

Henneke E. (1993) Early diagenetic processes and sulphur speciation in pore waters and sediments of the hypersaline Tyro and Bannock Basins, eastern Mediterranean. Ph.D. dissertation, Utrecht University. *Geologica Ultraiectina* **108**.

Henneke E., Luther G.W. III, and de Lange G.J. (1991) Determination of inorganic sulphur speciation with polarographic techniques: Some preliminary results for recent hypersaline anoxic sediments. *Mar. Geol.* **100**, 115–123.

Henneke E., Luther G.W. III, de Lange G.J., and Hoefs J., (1997) Sulphur speciation in anoxic hypersaline sediments from the eastern Mediterranean Sea. *Geochim. Cosmochim. Acta* **61**, 307–321.

Higgs N.C., Thomson J., Wilson T.R.S., and Croudace I.W. (1994) Modification and complete removal of eastern Mediterranean sapropels by postdepositional oxidation. *Geology* **22**, 423–426.

Hilgen F.J. (1991) Astronomical calibration of Gauss to Matuyama sapropels in the Mediterranean and implication for the geomagnetic polarity time scale. *Earth Planet. Sci. Lett.* **104**, 226–244.

Huerta-Diaz M.A. and Morse J.W. (1992) Pyritization of trace metals in anoxic marine sediments. *Geochim. Cosmochim. Acta* **56**, 2681–2702.

Jarvis I. and Higgs N. (1987) Trace-element mobility during early diagenesis in distal turbidites: late Quaternary of the Madeira Abyssal Plain, N Atlantic. In *Geology and Geochemistry of Abyssal Plains* (ed. P.P.E. Weaver and J. Thomson); *Geol. Spec. Publ.* **31**, 1057–1069.

Jørgensen B.B. (1979) A theoretical model of the stable sulfur isotope distribution in marine sediments. *Geochim. Cosmochim. Acta* **43**, 363–374.

Kaplan I.R., Emery K.O., and Rittenberg S.C. (1963) The distribution and isotopic abundance of sulphur in recent marine sediments off southern California. *Geochim. Cosmochim. Acta* **27**, 297–331.

Karlin R. (1990a) Magnetite diagenesis in marine sediments from the Oregon Continental Margin. *J. Geophys. Res.* **95**, 4405–4419.

Karlin R. (1990b) Magnetic mineral diagenesis in suboxic sediments at Bettis Site W-N, NE Pacific Ocean. *J. Geophys. Res.* **95**, 4421–4436.

Karlin R. and Levi S. (1985) Geochemical and sedimentological control of the magnetic properties of hemipelagic sediments. *J. Geophys. Res.* **90**, 10373–10392.

Kempe S., Diercks A.-R., Liebezeit G., and Prange A. (1991) Geochemical and structural aspects of the pycnocline in the Black Sea (R/V Knorr 134-8 Leg 1, 1988). In *Black Sea Oceanography* (ed. E. Idzar and J.W. Murray), pp. 89–110. Kluwer Academic Publishers.

Kidd R.B., Cita M.B., and Ryan W.B.F. (1978) Stratigraphy of eastern Mediterranean sapropel sequences recovered during DSDP Leg 42A and their paleoenvironmental significance. In *Init. Rep. Deep Sea Drill. Proj.* (ed. K. Hsü et al.), Vol. 42, pp. 421–443. U.S. Government Printing Office.

Kirschvink J.L. (1980) The least-squares line and plane and the analysis of palaeomagnetic data. *Geophys. J. of the Royal Astron. Soc.* **62**, 699–718.

Kohnen M.E.L., Sinninghe Damsté J.S., ten Haven H.L., and de Leeuw J.W. (1989) Early incorporation of polysulphides in sedimentary organic matter. *Nature* **341**, 640–641.

Kohnen M.E.L., Schouten S., Sinninghe Damsté J.S, de Leeuw J.W., Merrit-Dawn A., and Hayes J.M. (1992) Recognition of paleobiochemicals by a combined molecular sulphur and isotope geochemical approach. *Science* **256**, 358–362.

Köster H.M. (1979) *Die chemische Silikatanalyse*. Springer-Verlag.

Kostka J.E. and Luther G.W. III (1994) Partitioning and speciation of solid phase iron in saltmarsh sediments. *Geochim. Cosmochim. Acta* **58**, 1701–1710.

Langereis C.G., Dekkers M.J., de Lange G.J., Paterne M., and van Santvoort P.J.M. (1997) Magnetostratigraphy and astronomical calibration of the last 1.1 Myr from an eastern Mediterranean piston core and dating of short events in the Brunhes. *Geophys. J. Int.* **129**, 75–94.

Laskar J. (1990) The chaotic motion of the solar system: a numerial estimate of the size of the chaotic zones. *Icarus* **88**, 266–291.

Laskar J., Joutel F., and Boudin F. (1993) Orbital , precessional, and insolation quantities for the Earth from -20 Myr to +10 Myr. *Astron. Astrophys.* **270**, 522–533.

Leslie B.W., Lund S.P., and Hammond D.E. (1990a) Rock magnetic evidence for the dissolution and authigenic growth of magnetic minerals within anoxic marine sediments of the California continental borderland. *J. Geophys. Res.* **95**, 4437–4452.

Leslie B.W., Hammond D.E., Berelson W.H., and Lund S.P. (1990b) Diagenesis in anoxic sediments from the California continental borderland and its influence on iron, sulfur, and magnetite behavior. *J. Geophys. Res.* **95**, 4453–4470.

Leventhal J.S. (1983) An interpretation of carbon and sulfur relationships in Black Sea sediments as indicators of environments of deposition. *Geochim. Cosmochim. Acta* **47**, 133–137.

Leventhal J.S. (1987) Carbon and sulfur relationships in Devonian shales from the Appalachian Basin as an indicator of environment of deposition. *Amer. J. Sci.* **287**, 33–49.

Leventhal J.S. (1995) Carbon-sulfur plots to show diagenetic and epigenetic sulfidation in sediments. *Geochim. Cosmochim. Acta* **59**, 1207–1212.

Li Y.-H. and Gregory S. (1974) Diffusion of ions in sea water and in deep-sea sediments. *Geochim. Cosmochim. Acta* **38**, 703–714.

Liaaen-Jensen S. (1978) Chemistry of carotenoid pigments. In *Photosynthetic bacteria* (ed. R.K. Clayton and W.R. Sistrom), pp. 233–247. Plenum Press.

Lourens L.J., Hilgen F.J., Gudjonsson L., and Zachariasse W.J. (1992) Late Pliocene to early Pleistocene astronomically forced sea surface productivity and temperature variations in the Mediterranean. *Mar. Micropaleontol.* **19**, 49–78.

Lourens L.J., Antonarakou A., Hilgen F.J., van Hoof A.A.M., Vergnaud-Grazzini C., and Zachariasse W.J. (1996) Evaluation of the Plio-Pleistocene astronomical time scale. *Paleoceanography* **11**, 391–413.

Love L.G. and Amstutz G.C. (1966) Review of microscopic pyrite from the Devonian Chattanooga Shale and Rammelsberg Banderz. *Fortschr. Miner.* **43**, 273–309.

Luther G.W. III (1987) Pyrite oxidation and reduction: Molecular orbital theory considerations.

Geochim. Cosmochim. Acta **51**, 3193–3199.

Luther G.W. III and Church T.M. (1992) An overview of the environmental chemistry of sulfur in wetland systems. In *Sulfur Cycling on the Continents* (ed. R.W. Howarth et al.), Scope, pp. 125–142. John Wiley and Sons Ltd.

Lyons T.W. and Berner R.A (1992) Carbon-sulfur-iron systematics of the uppermost deep-water sediments of the Black Sea. *Chem. Geol.* **99**, 1–27.

Lyons T.W., Berner R.A., and Anderson R.F. (1993) Evidence for large pre-industrial perturbations of the Black Sea chemocline. *Nature* **365**, 538–540.

Maldonado A. and Stanley D. J. (1976) The Nile Cone: Submarine fan development by cyclic sedimentation. *Mar. Geol.* **20**, 27–40.

Mango F.D. (1983) The diagenesis of carbohydrates by hydrogen sulfide. *Geochim. Cosmochim. Acta* **47**, 1433–1441.

Medinets V.I. (1996) Shipboard derived concentrations of sulphur and nitrogen compounds and trace metals in the Mediterranean aerosol. In *The impact of desert dust across the Mediterranean* (ed. S. Guerzoni and R. Chester), pp. 359–368. Kluwer.

Middelburg J.J. (1991) Organic carbon, sulphur, and iron in recent semi-euxinic sediments of Kau Bay, Indonesia. *Geochim. Cosmochim. Acta.* **55**, 815–828.

Middelburg J.J., de Lange G.J., van der Weijden C.H. (1987) Manganese solubility control in marine pore waters. *Geochim. Cosmochim. Acta* **51**, 759–763.

Middelburg J.J., de Lange G.J., and Kreulen R. (1990) Dolomite formation in anoxic sediments of Kau Bay, Indonesia. *Geology* **18**, 399–402.

Middelburg J.J., Calvert S.E., and Karlin R. (1991) Organic-rich transitional facies in silled basins: Response to sea-level change. *Geology* **19**, 679–682.

Morel F.M.W. and Hering J.G. (1993) *Principles and Applications of Aquatic Chemistry*. John Wiley and Sons, Inc.

Moses C.O., Nordstrom D.K., Herman J.S., and Mills A.L. (1987) Aqueous pyrite oxidation by dissolved oxygen and by ferric iron. *Geochim. Cosmochim. Acta* **51**, 1561–1571.

Mossmann J.-R., Aplin A.C., Curtis C.D., and Coleman M.L. (1990) Sulfur geochemistry at Sites

680 and 686 on the Peru Margin. In *Proc. ODP, Sci. Results, 112* (ed. E. Suess et al.), pp. 455–464. College Station, TX, ODP.

Mossmann J.-R., Aplin A.C., Curtis C.D., and Coleman M.L. (1991) Geochemistry of inorganic and organic sulphur in organic-rich sediments from the Peru Margin. *Geochim. Cosmochim. Acta* **55**, 3581–3595.

Mucci A. and Edenborn H.M. (1992) Influence of an organic-poor landslide deposit on the early diagenesis of iron and manganese in a coastal marine sediment. *Geochim. Cosmochim. Acta* **56**, 3909–3921.

Muerdter D.R., Kennett J.P., and Thunell R.C. (1984) Late Quaternary Sapropel Sediments in the Eastern Mediterranean Sea: Faunal Variations and Chronology. *Quat. Res. 21,* 385–403.

Müller P.J. and Suess E. (1979) Productivity, sedimentation rate, and sedimentary organic matter in the oceans–I. Organic carbon preservation. *Deep-Sea Res.* **26**, 1347–1362.

Murat A. and Got H. (1987) Middle and Late Quaternary depositional sequences and cycles in the eastern Mediterranean. *Sedimentology* **34**, 885–899.

Murray J.W., Codispoti L.A., and Friederich G.E. (1995) Oxidation-reduction environments: the suboxic zone in the Black Sea. *Amer. Chem. Soc. Adv. Chem. Series* **244**, 157–176.

Nieuwenhuize J., Maas Y.E.M, and Middelburg J.J. (1994) Rapid analysis of organic carbon and nitrogen in particulate materials. *Mar. Chem.* **45**, 217–224.

Nijenhuis I.A., Brumsack H.-J., and de Lange G.J. (199_) The trace element budget of the Eastern Mediterranean during Pliocene sapropel formation. In *Proc. ODP, Sci. Results, 160* (ed. A.H.F. Robertson et al.). College Station, TX, ODP. In press.

Nissenbaum A. and Kaplan I.R. (1972) Chemical and isotopic evidence for the *in situ* origin of marine humic substances. *Limnol. Oceanogr.* **17**, 570–582.

Olausson E. (1961) Studies of deep-sea cores. *Rep. Swed. Deep-Sea Exped., 1947-48* **8**, 353–391.

Passier H.F. and de Lange G.J. (199_) Sedimentary sulfur and iron chemistry in relation to the formation of eastern Mediterranean sapropels. In *Proc. ODP, Sci. Results, 160* (ed. A.H.F. Robertson et al.). College Station, TX, ODP. In press. Chapter 3, this thesis.

Passier H.F, Middelburg J.J., van Os B.J.H., and de Lange G.J. (1996a) Diagenetic pyritisation under eastern Mediterranean sapropels caused by downward sulphide diffusion, *Geochim.*

Cosmochim. Acta **60**, 751–763. Chapter 2, this thesis.

Passier H.F., de Lange G.J., Middelburg J.J., and van Os B.J.H. (1996b) Sulphur appearances in and around sapropels, eastern Mediterranean. In *Proceedings of the Fourth International Symposium on the Geochemistry of the Earth's Surface* (ed. S.H. Bottrell et al.), pp. 101–104. University of Leeds.

Passier H.F., Middelburg J.J., de Lange G.J., and Böttcher M.E. (1997) Pyrite contents, microtextures, and sulfur isotopes in relation to formation of the youngest eastern Mediterranean sapropel. *Geology* **25**, 519–522. Chapter 4, this thesis.

Passier H.F., Middelburg J.J., de Lange G.J., and Böttcher M.E. (199_) Modes of sapropel formation in the eastern Mediterranean: some constraints based on pyrite properties. *Mar. Geol.* Chapter 5, this thesis. Accepted.

Pedersen T.F. (1983) Increased productivity in the eastern equatorial Pacific during the last glacial maximum (19,000 to 14,000 yr B.P.). *Geology* **11**, 16–19.

Pedersen T.F. and Shimmield G.B. (1991) Interstitial water chemistry, leg 117: Contrasts with the Peru Margin. In *Proc. ODP, Init. Repts., 117* (ed. W.L. Prell et al.), pp. 499–513. College Station, TX, ODP.

Peterson B.J. and Howarth R.W. (1987) Sulfur, carbon, and nitrogen isotopes used to trace organic matter flow in the salt-marsh estuaries of Sapelo Island, Georgia. *Limnol. Oceanogr.* **32**, 1195–1213.

Philip R.P., Suzuki N., and Galvez-Sinibaldi A. (1992) Early-stage incorporation of sulfur into protokerogens and possible kerogen precursors. In *Productivity, Accumulation, and Preservation in Recent and Ancient Sediments* (ed. J.Whelan and J.W. Farrington), pp. 264–282. Columbia University Press.

Poutanen E.-L. and Morris R.J. (1983) The occurrence of high molecular weight humic compounds in the organic-rich sediments of the Peru continental shelf. *Oceanol. Acta* **6**, 21–28.

Prahl F.G., de Lange G.J., Lyle M., and Sparrow M.A. (1989) Post-depositional stability of long-chain alkenones under contrasting redox conditions. *Nature* **341**, 434–437.

Price F.T. and Shieh Y.N. (1979) Fractionation of sulfur isotopes during laboratory synthesis of pyrite at low temperatures. *Chem. Geol.* **27**, 245–253.

Pruysers P.A., de Lange G.J., and Middelburg J.J. (1991) Geochemistry of eastern Mediterranean sediments: Primary sediment composition and diagenetic alterations. *Mar. Geol.* **100**, 137–154.

Pruysers P.A., de Lange G.J., Middelburg J.J., and Hydes D.J. (1993) The diagenetic formation of metal-rich layers in sapropel-containing sediments in the eastern Mediterranean. *Geochim. Cosmochim. Acta.* **57**, 527–536.

Quandt I., Gottschalk G., Ziegler H., and Stichler W. (1977) Isotope discrimination by photosynthetic bacteria. *FEMS Microbiol. Lett.* **1**, 125–128.

Raiswell R. (1982) Pyrite texture, isotopic composition and the availability of iron. *Amer. J. Sci.* **82**, 1244–1263.

Raiswell R. (1993) Kinetic controls on depth variations in localised pyrite formation. *Chem. Geol.* **107**, 467–469.

Raiswell R. and Al-Biatty H.J. (1989) Depositional and diagenetic C-S-Fe signatures in early Paleozoic normal marine shales. *Geochim. Cosmochim. Acta* **53**, 1147–1152.

Raiswell R. and Berner R.A. (1985) Pyrite formation in euxinic and semi-euxinic sediments. *Amer. J. Sci.* **285**, 710–724.

Raiswell R. and Canfield D.E. (199_) Sources of iron for pyrite formation in marine sediments. *Amer. J. Sci.* In press.

Raiswell R., Buckley F., Berner R.A., and Anderson T.F (1988) Degree of pyritization of iron as a paleoenvironmental indicator of bottom-water oxygenation. *J. Sed. Petrol.* **58**, 812–819.

Raiswell R., Bottrell S.H., Al-Biatty H.J., and Tan M. MD. (1993) The influence of bottom water oxygenation and reactive iron content on sulfur incorporation into bitumens from Jurassic marine shales. *Amer. J. Sci.* **293**, 569–596.

Raiswell R., Canfield D.E., and Berner R.A. (1994) A comparison of iron extraction methods for the determination of degree of pyritisation and the recognition of iron-limited pyrite formation. *Chem. Geol.* **111**, 101–110.

Reeburgh W.S. (1967) An improved interstitial water sampler. *Limnol. Oceanogr.* **12**, 163–170.

Repeta D.J., Simpson D.J., Jørgensen B.B., and Jannasch H.W. (1989) Evidence for anoxygenic photosynthesis from the distribution of bacteriochlorophylls in the Black Sea. *Nature* **342**, 69–72.

Rickard D.T. (1970) The origin of framboids. *Lithos* **3**, 269–293.

Rickard D. (1997) Kinetics of pyrite formation by the H_2S oxidation of iron (II) monosulfide in aqueous solutions between 25 and 125^0C: The rate equation. *Geochim. Cosmochim. Acta* **61**, 115–134.

Roberts A.P., Stoner J., and Richter C. (199_) Diagenetic magnetic enhancement of sapropels from the eastern Mediterranean Sea. In *Proc. ODP, Sci. Results, 160* (ed. A.H.F. Robertson et al.). College Station, TX, ODP. Submitted.

Robertson A.H.F. and Shipboard Scientific Party (1996) Mud volcanism on the Mediterranean Ridge. In *Proc. ODP, Init. Repts., 160* (ed. K.-C. Emeis et al.), pp. 521–526. College Station, TX, ODP.

Robinson S.G. (1990) Applications for whole-core magnetic susceptibility measurements of deep-sea sediments: Leg 115 results. In *Proc. ODP*, *Sci. Results, 115* (ed. R.A. Duncan et al.), pp. 737–771. College Station, TX, ODP.

Rohling E.J. (1994) Review and new aspects concerning the formation of eastern Mediterranean sapropels. *Mar. Geol.* **122**, 1–28.

Rohling E.J. and Gieskes W.W.C (1989) Late Quaternary changes in Mediterranean Intermediate Water density and formation rate. *Paleoceanography* **4**, 531–545.

Rohling E.J. and Hilgen F.J. (1991) The eastern Mediterranean climate at times of sapropel formation: a review. *Geol. Mijnb.* **70**, 253–264.

Ross D.A., Degens E.T., and MacIlvaine J. (1970) Black Sea: Recent sedimentary history. *Science* **170**, 163–165.

Rossignol-Strick M. (1985) Mediterranean Quaternary sapropels, an immediate response of the African Monsoon to variation of insolation. *Palaeogeogr., Palaeoclimatol., Palaeoecol.* **49**, 237–263.

Rossignol-Strick M., Nesterhoff W., Olive P., and Vergnaud-Grazzini C. (1982) After the deluge: Mediterranean stagnation and sapropel formation. *Nature* **295**, 105–110.

Sarmiento J.L., Herbert T., and Toggweiler J.R. (1988) Mediterranean nutrient balance and episodes of anoxia. *Global Biogeoch. Cycles* **2**, 427–444.

Sarnthein M., Pflaumann U., Ross R., Tiedemann R., and Winn K. (1992) Transfer functions to

reconstruct ocean palaeoproductivity: a comparison. In *Upwelling Systems: Evolution Since the Early Miocene* (ed. C.P. Summerhayes et al.); *Geol. Soc. Spec. Publ.* **64**, 411–427.

Schultz H.D., Dahmke A., Schinzel U., Wallmann K., and Zabel M. (1994) Early diagenetic processes, fluxes, and reaction rates in sediments of the South Atlantic. *Geochim. Cosmochim. Acta* **58**, 2041–2060.

Scranton M.I., Sayles F.L., Bacon M.P., and Brewer P.G. (1987) Temporal changes in the hydrography and chemistry of the Cariaco Trench. *Deep-Sea Res.* **34**, 945–963.

Sinninghe Damsté J.S. and de Leeuw J.W. (1990) Analysis, structure and geochemical significance of organically-bound sulfur in the geosphere: state of the art and future research. *Org. Geochem.* **16**, 1077–1101.

Sinninghe Damsté J.S., Wakeham S.G., Kohnen M.E.L., Hayes J.M., and de Leeuw J.W. (1993) A 6,000-year sedimentary molecular record of chemocline excursions in the Black Sea. *Nature* **362**, 827–829.

Stephenson A. (1993) Three-axis static alternating field demagnetization of rocks and the identification of natural remanent magnetization, gyroremanent magnetization and anisotropy. *J. Geophys. Res.* **98**, 373–382.

Sternbeck J. and Sohlenius G. (1997) Authigenic sulfide and carbonate mineral formation in Holocene sediments of the Baltic Sea. *Chem. Geol.* **135**, 55–73.

Summerhayes, C.P., Prell, W.L., and Emeis, K.C. (ed.) (1992) *Upwelling Systems: Evolution Since the Early Miocene; Geol. Soc. Spec. Publ.* **64**.

Summons R.E. and Powell T.G. (1986) Chlorobiaceae in Palaeozoic seas revealed by biological markers, isotopes and geology. *Nature* **319**, 763–765.

Sweeney R.E. and Kaplan I.R. (1973) Pyrite framboid formation: Laboratory synthesis and marine sediments. *Econ. Geol.* **68**, 618–634.

Thomson J., Higgs N.C., and Colley S. (1989) A geochemical investigation of reduction haloes developed under turbidites in brown clay. *Mar Geol.* **89**, 315–330.

Thomson J., Higgs N.C., Croudace I.W., Colley S., and Hydes D.J. (1993) Redox zonation of elements at an oxic/post-oxic boundary in deep-sea sediments. *Geochim. Cosmochim. Acta* **57**, 579–595.

Thomson J., Higgs N.C., Wilson T.R.S., Croudace I.W., de Lange G.J., and van Santvoort P.J.M. (1995) Redistribution and geochemical behaviour of redox-sensitive elements around S1, the most recent eastern Mediterranean sapropel. *Geochim. Cosmochim. Acta* **59**, 3487–3501.

Tribovillard N.P., Desprairies A., Lallier-Vergès E., Bertrand P., Moureau N., Ramdani A. and Ramanampisoa L. (1994) Geochemical study of organic-matter rich cycles from the Kimmeridge Clay Formation of Yorkshire (UK): productivity versus anoxia. *Palaeogeogr., Palaeoclimatol., Palaeoecol.* **108**, 165–181.

van Os B.J.H., Middelburg J.J., and de Lange G.J. (1991) Possible diagenetic mobilization of barium in sapropelic sediment from the eastern Mediterranean. *Mar. Geol.* **100**, 125–136.

van Os B.J.H., Visser H.J., Middelburg J.J., and de Lange G.J. (1993) Occurrence of thin, metal-rich layers in deep-sea sediments: a geochemical characterization of copper remobilization. *Deep-Sea Res.* **40**, 1713–1730.

van Os B.J.H., Lourens L.J., Hilgen F.J., de Lange G.J., and Beaufort L. (1994) The formation of Pliocene sapropels and carbonate cycles in the Mediterranean: Diagenesis, dilution, and productivity. *Paleoceanography* **9,** 601–617.

van Santvoort P.J.M. and de Lange G.J. (1996) Messinian salt fluxes into the present-day Eastern Mediterranean: implications for budget calculations and stagnation. *Mar. Geol.* **132**, 241–251.

van Santvoort P.J.M., de Lange G.J., Thomson J., Cussen H., Wilson T.R.S., Krom M.D., Ströhle K. (1996) Active post-depositional oxidation of the most recent sapropel (S1) in sediments of the eastern Mediterranean. *Geochim. Cosmochim. Acta* **60**, 4007–4024.

van Santvoort P.J.M., de Lange G.J., Langereis C.G., and Dekkers M.J. (199_) Geochemical and paleomagnetic evidence for the occurrence of 'missing' sapropels in eastern Mediterranean sediments, *Paleoceanography*. In press.

Wang Q. and Morse J.W. (1996) Pyrite formation under conditions approximating those in anoxic sediments I. Pathway and morphology. *Mar. Chem.* **52**, 99–121.

Ward J.C. (1970) The structure and properties of some iron sulfides. *Rev. Pure Appl. Chem.* **20**, 175–206.

Whitfield M. (1974) The ion-association model and the buffer capacity of the carbon dioxide system in seawater at 25^0C and 1 atmosphere total pressure. *Limnol. Oceanol.* **19**, 235–248.

Wilkin R.T. and Barnes H.L. (1996) Pyrite formation by reactions of iron monosulfides with dissolved inorganic and organic sulfur species. *Geochim. Cosmochim. Acta* **60**, 4167–4179.

Wilkin R.T., Barnes H.L., and Brantley S.L. (1996) The size distribution of framboidal pyrite in modern sediments: An indicator of redox conditions. *Geochim. Cosmochim. Acta* **60**, 3897–3912.

Wilkin R.T., Arthur M.A., Dean W.E. (1997) History of water-column anoxia in the Black Sea indicated by pyrite framboid size distributions. *Earth Planet. Sci. Lett.* **148,** 517–525.

Wilson T.R.S, Thomson J., Colley S., Hydes D.J., Higgs N.C., and Sørensen J. (1985) Early organic diagenesis: The significance of progressive subsurface oxidation fronts in pelagic sediments. *Geochim. Cosmochim. Acta* **49**, 811–822.

Wilson T.R.S., Thomson J., Hydes D.J., Colley S., Culkin F., and Sørensen J. (1986) Oxidation Fronts in Pelagic Sediments: Diagenetic Formation of Metal-Rich Layers. *Science* **232**, 972–975.

Zhabina N.N. and Volkov I.I. (1978) A method of determination of various sulfur compounds in sea sediments and rocks. In *Environmental Biogeochemistry and Geomicrobiology* (ed. W.E. Krumbein),Vol. 3, *Methods, Metals and Assessment*, pp. 735–746. Ann Arbor Sci.

Zijderveld J.D.A. (1967) A.C. demagnetization of rocks: analysis of results. In *Methods in Palaeomagnetism* (ed. D.W. Collinson et al.), pp. 254–286. Elsevier.

Samenvatting in het Nederlands

De huidige Middellandse Zee

De Middellandse Zee (Fig. 1.1) wordt omsloten door Europa, Azië en Afrika. Via de Straat van Gibraltar is deze randzee verbonden met de Atlantische Oceaan. Het bekken bestaat uit een oostelijk en een westelijk deel, gescheiden door een ondiepe drempel bij Sicilië. Op dit moment is de verdamping uit de Middellandse Zee groter dan de aanvoer van water via rivieren en neerslag. Deze negatieve waterbalans wordt gecompenseerd door een instroom van Atlantisch water via het zeeoppervlak. In het oosten van de Middellandse Zee is de saliniteit, en zodoende de dichtheid, dusdanig toegenomen dat het water naar de bodem zakt. Dit zware dieptewater stroomt het bekken uit via de drempel bij Gibraltar, resulterend in het huidige anti-estuariene stromingspatroon. De instroom van nutriënt-arm oppervlaktewater uit de Atlantische Oceaan en de uitstroom van nutriënt-rijk zout dieptewater, zorgt ervoor dat de oostelijke Middellandse Zee een "nutriëntwoestijn" is, met een lage productie van organisch materiaal (OM) in de oppervlaktewateren (e.g. Sarmiento et al., 1988; Béthoux, 1989).

Sapropelen in de oostelijke Middellandse Zee

Recente sedimenten in de oostelijke Middellandse Zee bevatten minder dan een half gewichtsprocent organische koolstof, terwijl gedurende het Neogeen een aantal donkere sedimentlagen zijn afgezet met een organische-koolstofgehalte van een paar tot zelfs 30 gewichtsprocent. Deze cyclisch voorkomende lagen met een hoog gehalte organische koolstof worden sapropelen genoemd. Ze zijn enkele centimeters tot decimeters dik en omgeven door lichtbruine tot grijze hemipelagische sedimenten. De oorzaak van het voorkomen van sapropelen is gerelateerd aan paleoklimatologische omstandigheden in het Middellandse Zeegebied. De organisch-rijke laagjes zijn afgezet gedurende perioden met relatief veel neerslag wanneer de instraling van de zon op het noordelijk halfrond maximaal was. De variaties in deze instraling worden vooral veroorzaakt door de precessiecyclus van de baan van de aarde, die een periode heeft van plusminus 21 duizend jaar (e.g. Hilgen, 1991; Lourens et al., 1992). Gedurende de afgelopen jaren zijn de redenen van sapropeelvorming uitvoerig bediscussieerd. Sapropeelvorming zou kunnen zijn geïnitieerd door een verhoging van de productie van OM in de oppervlaktewateren, die geleid heeft tot een hogere flux van OM naar de zeebodem en/of door een grotere preservatie van OM vanwege zuurstofdepletie in het bodemwater van de Middellandse Zee. Tijdens instralingsmaxima nam de hoeveelheid neerslag toe, wat een grotere toevoer van zoetwater en nutriënten vanuit Europa, Azië en Afrika veroorzaakte. Deze verhoogde toevoer van nutriënten zorgde voor een grotere productie van OM. De verhoogde instroom van zoetwater en de algehele verandering van het weer brachten ook veranderingen in het circulatiepatroon en de anatomie van de waterkolom in de oostelijke Middellandse Zee teweeg, die wellicht zowel de preservatie als de productie van OM beïnvloedden. Een van de theorieën is dat de circulatie in het bekken trager werd, wat resulteerde in een zuurstofloos milieu in het bodemwater en een betere preservatie van OM. Een andere theorie gaat ervan uit dat een verandering van het circulatiepatroon de opwelling van nutriënt-rijk water en een verhoging van

de productie van OM veroorzaakte. Daarnaast heeft de instroom van veel zoetwater de pycnocline omhoog verplaatst, waardoor nutriënten de fotische zone ingebracht werden en de productie van OM steeg (e.g. Olausson, 1961; Rossignol-Strick et al., 1982; Rossignol-Strick, 1985; Rohling and Gieskes, 1989; Calvert et al., 1992).

Een unieke sedimentafwisseling

Sapropelen zijn het gevolg van een verhoogde accumulatie van OM op de zeebodem. Deze accumulatie van OM is nauw verweven met allerlei vroeg-diagenetische processen. Het belangrijkste proces is de afbraak van OM door bacteriën, die hiervoor een reeks van oxidatoren gebruiken (zuurstof, nitraat, mangaan- en ijzer(hydr)oxiden, sulfaat) (e.g. Froelich et al, 1979). In de meeste organisch-rijke sedimenten worden zuurstof en nitraat reeds opgebruikt in de bovenste millimeters van het sediment, hieronder worden andere oxidatoren gebruikt voor de afbraak van OM. De consumptie van oxidatoren resulteert in de ontwikkeling van een aantal redoxzones in het sediment. Meestal worden sedimenten steeds reducerender met de diepte en bestaat de sedimentkolom uit achtereenvolgens oxische, suboxische en anoxische sedimenten. De afwisselende afzetting van sapropelen en organisch-arme sedimenten in de oostelijke Middellandse Zee, veroorzaakt echter een heel andere sedimentzonering, waarin unieke diagenetische interacties plaatsvinden tussen (anoxische) organisch-rijke lagen die bovenop (sub)oxische organisch-arme sedimenten liggen en vice versa.

Zwavel in organisch-rijke sedimenten

Eén van de belangrijkste diagenetische processen in organisch-rijke mariene sedimenten is de afbraak van OM in bacteriële sulfaatreductie (e.g. Canfield, 1989; Mossmann et al., 1991; Calvert and Karlin, 1991). In bacteriële sulfaatreductie wordt bisulfide (HS^-) geproduceerd. Het bisulfide kan gedeeltelijk geoxideerd worden of reageren met OM en met reactieve metaalverbindingen (e.g. Berner, 1984; Luther and Church, 1992). Al deze reacties kunnen door bacteriën beïnvloed worden. Bij de reactie van gereduceerde zwavel met opgelost ijzer of reactieve ijzermineralen worden ijzersulfiden gevormd. Het meest bekende ijzersulfide is pyriet (FeS_2). De biogeochemische kringloop van zwavel speelt een grote rol bij het reguleren van zuurstof- en kooldioxidegehalten in de atmosfeer. Begraving en oxidatie van pyriet zijn schakels tussen de biogeochemische kringlopen van zuurstof, koolstof en zwavel. Deze processen zijn zeer belangrijk in het reguleren van het zuurstofgehalte van de atmosfeer, net zoals begraving en oxidatie van OM (e.g. Berner and Canfield, 1989). Vandaar dat het gedrag van zwavel in sedimenten, met name pyrietvorming, intensief bestudeerd wordt. De eigenschappen van pyriet hangen af van de vormingsgeschiedenis van het pyriet en de omringende sedimenten. Het pyrietgehalte hangt grotendeels af van de beschikbaarheid van sulfaat, reactief OM en reactief ijzer tijdens vorming van een sediment (Berner, 1984). Ook de microtextuur van pyriet in mariene sedimenten (framboïdisch, i.e. op gelijkend op een framboos, of euhedrisch; e.g. Sweeney and Kaplan, 1973; Raiswell, 1982; Wang and Morse, 1996; Wilkin and Barnes, 1996) en de samenstelling van zwavelisotopen in pyriet (e.g. Goldhaber and Kaplan, 1974; Chambers and Trudinger, 1979; Raiswell, 1982; Canfield and Thamdrup, 1994) kunnen waardevolle informatie verschaffen over het vormingsmilieu van pyriet.

Dit proefschrift

In dit proefschrift wordt de zwavelgeochemie van sedimenten uit de oostelijke Middellandse Zee bestudeerd. De sedimentkernen die gebruikt zijn bij dit onderzoek zijn genomen tijdens de 1987 *ABC* cruise met R/V *Tyro* (kern ABC27), de 1988 *BAMO-3* expeditie van R/V *Bannock* (kernen GC17 en GC21), de 1991 *Marflux* cruise met R/V *Marion Dufresne* (kernen KC01B en KC19C), de 1993 *Marflux* cruise met R/V *Tyro* (kern MT1), de 1994 *Palaeoflux* cruise met R/V *Urania* (kern UM26) en tijdens ODP Leg 160 in 1995 (Sites 964, 966, 967, and 969) (Fig. 1.1).

Hoofdstuk 2 gaat over het meest opvallende kenmerk van de zwavelchemie rond sapropelen: behalve dat zwavel en ijzer verrijkt zijn in sapropelen, zijn deze elementen ook verrijkt onder de sapropelen, waar organische koolstof niet verrijkt is. Deze zwavel- en ijzerverrijkingen duiden op de aanwezigheid van pyriet (FeS_2). De stabiele-isotopensamenstelling van zwavel in het bulksediment in en onder sapropelen laat zien dat de gereduceerde zwavel zowel in als onder sapropelen, gevormd is dichtbij het sedimentoppervlak, dat wil zeggen, tijdens of kort na sapropeelafzetting. De pyrietvorming in sapropelen werd gelimiteerd door de hoeveelheid reactief ijzer die beschikbaar was in de sapropeel. Door ijzertekort kon bisulfide vanuit de sapropelen naar sedimenten eronder migreren. Dit resulteerde in pyrietvorming onder elke sapropeel door reactie van bisulfide met reactieve ijzermineralen en opgelost Fe(II) wat omhoog diffundeerde. Dit sulfidisatie-mechanisme heeft tot gevolg dat in de afwisselend organisch-rijke anoxische /organisch-arme suboxische sedimenten twee maal zoveel zwavel opgeslagen wordt dan in homogene organisch-rijke sedimenten.

Hoofdstuk 3 behandelt de speciatie van sedimentair zwavel en het gehalte reactief ijzer in afzettingen met sapropelen. De belangrijkste zwavelverbinding in en onder sapropelen is pyriet. Net boven sapropelen is nauwelijks zwavel aanwezig in de vaste fase van het sediment, hier domineert sulfaat in poriënwater. Organische zwavelverbindingen zijn alleen op grote schaal gevormd in de bestudeerde sapropeel met het hoogste organische-koolstofgehalte (tot 23,5 gewichtsprocent). De aanwezigheid van andere ijzersulfides dan pyriet duidt erop dat sulfaatreductie mogelijk nog steeds actief is in de meest organisch-rijke sapropeel, terwijl in sapropelen met een lager organische-koolstofgehalte geen sulfaatreductie meer plaatsvindt.

De hoofdstukken 4 en 5 beschouwen de kenmerken van pyriet in en onder sapropelen in detail, om meer inzicht te krijgen in de vormingsgeschiedenis van pyriet en sapropelen. Deze kenmerken blijken te zijn bepaald door de relatieve snelheden van bisulfideproductie en ijzertoevoer in de sapropelen. Deze snelheden hebben zowel lateraal als in de tijd gevarieerd gedurende sapropeelafzetting. Wanneer er relatief veel sulfaatreductie plaatsvond, kon bisulfide uit een sapropeel ontsnappen en vormde pyriet onder de sapropeel. De bronnen van ijzer voor pyrietvorming tijdens sapropeelvorming waren detritische reactieve ijzermineralen en opgelost Fe(II) dat vrijgemaakt werd uit sedimenten onder de sapropeel tijdens diagenese. In zeer organisch-rijke sapropelen kon ook opgelost Fe(II) in de waterkolom een bron van ijzer voor pyrietvorming zijn, via vorming van ijzersulfides in het water. Snelle pyrietvorming bij hoge verzadiging van bisulfide en ijzer in de sapropelen leverde framboïdische pyriet op, terwijl onder sapropelen langzame vorming van euhedrische pyriet bij lage verzadigingsniveaus optrad.

Zwavel in pyriet in sapropelen is sterk verrijkt in het lichte isotoop ^{32}S. Onder sapropelen is dit isotoop zelfs nog sterker verrijkt dan erin. Dit is het gevolg van een verhoogde reoxidatie van bisulfide ten tijde van relatief grote bisulfideproductie, toen het uit het sediment kon ontsnappen naar de waterkolom. Zo'n tachtig procent van de oorpronkelijk geproduceerde sulfide zou geoxideerd kunnen zijn. Het effect van deze verregaande reoxidatie van sulfide op berekeningen van de begravingsefficientie en paleoproductiviteit van OM worden behandeld in Hoofdstuk 5. De hoge accumulatie van OM in sapropelen blijkt veroorzaakt te zijn door zowel een verhoogde paleoproductiviteit van OM als een toegenomen preservatie van OM op de zeebodem.

Hoofdstuk 6 onderzoekt de oorsprong van zwavel in organische verbindingen in en rond sapropelen, door bestudering van stabiele-isotoopsamenstellingen van zwavel en de ratio tussen zwavel en koolstof in OM. De organische zwavel in de sedimenten blijkt een mengsel van zwavel afkomstig uit (1) anorganische gereduceerde zwavel gevormd bij bacteriële sulfaatreductie en (2) biosynthetische zwavel. De grootste opname van zwavel in organisch materiaal vondt plaats in sapropelen. Hier was te weinig reactief ijzer aanwezig voor vorming van ijzersulfides, zodat ijzer geen concurrent was van OM voor de opname van gereduceerde zwavel, en sulfide concentraties in de poriewaters behoorlijk stegen.

Hoofdstuk 7 combineert gegevens uit organisch-geochemische analyses, sporenelement analyses en pyrietonderzoek voor een aantal zeer organisch-rijke sapropelen uit het Plioceen. Deze gegevens bewijzen dat de waterkolom in de oostelijke Middellandse Zee euxinisch (sulfidisch) geweest is tijdens vorming van deze sapropelen.

Hoofdstuk 8 beschouwt de sedimentchemie en magnetische eigenschappen in een kern met een lengte van 19,6 meter, genomen op een uitzonderlijke locatie in de abyssale oostelijke Middellandse Zee. Deze kern bevat een groot aantal sapropelen, zodat de stratigrafie kon worden vastgesteld. Het is uitzonderlijk dat het poriewater op deze locatie vanaf een paar meter onder de zeebodem sulfide bevat, terwijl dit op de meeste vergelijkbare locaties in de oostelijke Middellandse Zee niet het geval is. Deze sulfide is mogelijk geproduceerd in bacteriële sulfaatreductie gecombineerd met de oxidatie van methaan op ongeveer 17,5 meter onder de zeebodem. De migratie van sulfide naar boven in het sediment, heeft ervoor gezorgd dat vrijwel al het reactieve ijzer in het sediment dieper dan 2 meter onder de zeebodem gepyritiseerd is. Hierdoor zijn de paleomagnetische signalen in de ijzermineralen vernietigd, en kunnen er geen betrouwbare paleomagnetische metingen gedaan worden in de onderste helft van de kern.

Dit proefschrift illustreert dat de processen in mariene sedimenten zeer dynamisch kunnen zijn, vooral wanneer verschillende redoxregimes gedwongen worden naast elkaar te bestaan. Dit kan gebeuren als sedimenten met verschillende gehalten OM bovenop elkaar afgezet worden, ten gevolge van periodieke variaties in het milieu, of wanneer processen in de ondergrond, zoals de aanvoer van methaan, het chemische systeem in de sedimenten verstoren. Ten gevolge van deze redoxverstoringen kunnen sedimenten chemisch worden omgezet na afzetting. Enerzijds verdoezelen deze omzettingen de geologische signalen die opgeslagen zitten in het sediment. Anderzijds kunnen relicten van geochemische processen ook de paleo-oceanografische en diagenetische geschiedenis van sedimenten onthullen.

Acknowledgements

Many people have supported me during the last four years and they have made this thesis into what it is now. I am indebted to all of them and I want to thank a number of people in particular.

First of all, I am grateful to Cees van der Weijden and Gert de Lange for offering me the opportunity to become a marine geochemist and to investigate the fascinating eastern Mediterranean. I greatly acknowledge the help of Jack Middelburg for introducing me to the world of scientific writing and for the stimulating discussions we had. Bertil van Os generously provided data for my first publication which gave me a perfect start. Thanks are due to Michael Böttcher for his continuous enthusiastic collaboration and stable sulphur isotope measurements. I am thankful to Mark Dekkers for introducing me to the field of rock-magnetism. The interesting discussions with Hendrik-Jan Bosch, Anke Leenders, Jan de Leeuw, Lucas Lourens, Ivar Nijenhuis, and Jaap Sinninghe Damsté about sapropel formation and the shaping of a manuscript were highly appreciated. I am grateful to Peter van der Linde for his help in tackling the aquatic geochemistry of sulphide oxidation. I thank René Alink, Mark van Alphen, Paul Anten, Tilly Bouten, Tea Broer, Pieter Kleingeld, Dineke van de Meent, Henk Meijer, Gijs Nobbe, Arnold van Dijk, Helen de Waard, and Ton Zalm for their indispensable technical assistance in the laboratory.

Furthermore, I thank all my colleagues at the Department of Geochemistry who were not directly involved in the science in this thesis, but who have made my stay at the Faculty, the field trips and the conferences we visited into unforgettable events; I especially thank Marcel Hoefs, Thomas Keijzer, Sieger van der Laan, Dorinda van der Linden, Gerben Mol, Peter Pruysers, Gert-Jan Reichart, Arrian Rutten, Patrick van Santvoort, Dick Schipper, Sjoerd Schenau, Arthur Schmidt, Gerard van den Berg, Hendrik-Jan Visser, and Mariëtte Wolthers.

Finally, I am grateful to my friends and family. Jurriaan has made the difficult episodes in the creation of this thesis easier with his love and patience. I am proud of my parents, who are very interested in my life and work. I can always count on their advice and support. Therefore, this thesis has been dedicated to them.

2

2

Voor YY:

Geef mij maar Pukapuka, wat heerlijk
is het hier. Niks school, niks algemene
vorming, maar zoals Aloeaoe zegt:
"Inzicht, doorzicht en op zijn tijd een
goede banaan."

<div align="right">

(Rob Knoppert, NRC)

</div>